Patterns of stress and strain distribution during deep mining at Boulby, N. Yorkshire

Mabeka, Ndongala

Patterns of stress and strain distribution during deep mining at Boulby, N. Yorkshire

Mabeka Ndongala

Department of Geography

Durham University

Thesis submitted for the degree of Master of Philosophy (MPhil)

2011

Declaration

I confirm that none of the material included in this thesis has been previously submitted for a degree at the Durham University or at any other University. The thesis is the result of my own work. Other sources contained herein, where relevant, have been acknowledged.

Abstract

The understanding of stress-deformation state transmission within the rock mass above deep mine workings is a key factor to the comprehension of the response of rock masses to changes of stress regime brought about by the mining activity for the safety of surface and subsurface structures. Based on monitoring data from active actual mine workings, this study numerically analyzes factors controlling stress and deformation using the 2D Fast Lagrangian Analysis of Continua (FLAC 2D) code and a strain-softening model to approximate creep behaviour of rock masses. The results show that distribution of stress and deformation at Boulby mine is primarily governed by the lithological heterogeneity of the overlying strata and the geological structure, including its nature within the undermined area. Data from a bespoke roof-to-floor monitoring closuremeter indicate that convergence of openings is a function of local variables, including the site location, geometry and age of the site. Patterns of ground subsidence are compared to the pattern of levelling-based measured ground subsidence. Furthermore, the analysis shows that the strain-softening model reasonably approximates the creep behaviour of the excavations. The results have implications for how we monitor and model subsidence due to mining deep excavations.

Contents

List of tables

Chapter 2

Chapter 3

Chapter 4

List of equations

Chapter 2

Chapter 3

List of figures

Chapter 2

Chapter 6

Chapter 7

List of plates

Chapter 2

Chapter 3

Chapter 4

Chapter 5

Acknowledgements

This research was sponsored by the Cleveland Potash Limited through the University of Durham and I am grateful for the funding provided through the studentship without it this research would not have been possible.

I would like to thank Ian Scott, Allan Williams, David Pybus at Boulby Mine and particularly Dave Potter for their assistance during the monitoring process of mine roof and also for providing me with data of roof closure partly used in this research. I am indebted to the people at Boulby Mine for their admirable constant support and enthusiasm.

My particular and sincere thanks must go to my two supervisors for their vision and guidance throughout this project. In Professor Dave Petley and Dr Nick Rosser I have found very engaging and intelligent supervisors, who helped me in crucial moments of this thesis. Throughout the three years Professor Dave Petley and Dr Nick have always made time for supervision despite their incredibly busy schedule. I am especially thankful to Dr Nick Rosser who devoted significant portion of his time especially for the analysis of data and for the completion of this thesis. And I am grateful for their patience.

I am thankful to Dr Stuart Dunning for his guidance at the beginning of this research and Dr Mike Lim for his contribution to the underground mine fieldwork. I would like to acknowledge the contributions of Mr. Ringo Tan of Mott MacDonald Ltd. London and Dr Joseph Quinn at University of Leeds for their valued assistance with FLAC 2D programming issues. Particular thanks to Dr Lubanzadio Mavatikua of BP Exploration and Operating for his inputs towards the final review of this work.

I am indebted to the technicians Allison Clark, Chris Longley and particularly Eddie Million and Mervyn Brown for their valued support and without their assistance most of the fieldwork would not have carried out. Particular thanks to Mohamed Al-Ali for the knowledge we shared and also to Natalie Beale for the two years we spent together.

There are many people to whom I owe many thanks for their encouragements during my thesis; among them is L. Mvuala, M.-D. Sopta, R. Matondo, A. Aissi, F. Lupetu, W. Nsingi, D. Mayamona, Dr M. Massamba, MD P. Tuyindi, Dr I. Chukwuemeka, Dr E. Aniah, Dr D. Amaraegbu and a special thank goes to J. K. Kasandji for his support to my wife for the completion of her nursing courses.

And finally my family, I do not have the words to convey what you mean for me for your love and support. On a more personal note, I would like to thank my wife Kashashu Sitala to who I express my sincere apologies for the reduced attention she was given from me during this research; to you I dedicate this work.

Chapter 1
Introduction to the study

1.1 Research context and motivation

Increasing use of deep underground space for Research Laboratories and the continued development of mineral resources require understanding of rock masses behaviour subjected to changes of stress regime as a result of excavation. More particularly, the propagation of geomechanical stress and deformation processes through rock masses to the surface is a key of concern in this study. An approach to understanding such referred behaviour could be achieved through stress and deformation patterns distribution analysis.

Excavation of underground openings induces stress and strain redistribution in the rock mass surrounding the excavated opening (Aguado and Gonzalez, 2009; Stiros and Kontogianni, 2009; Alkan *et al.,* 2007; Chandler, 2004). Stress provides boundary conditions of force and changes in stress affect excavation stability. This results in detrimental effects on the environment surrounding the excavation. Changes of stress regime could induce ground subsidence at the surface.

Numerical methods are effectively used to investigate stress and strain distribution within rock masses. However, most of the investigations are based on the Finite Element Method and in most of cases they are associated either with excavations for coal (Xie *et al*., 2009; Mark *et al*., 2007), tunnels (Henk, 2006; Hao and Azzam, 2005; Kontogianni and Stiros, 2002) or for Research laboratories (Chandler, 2004). Furthermore, although some finite difference analyses have been devoted to investigate stress and strain distribution in salt and potash mines (Rothenburg *et al*., 2007); the behaviour of these rocks was characterized by the commonly used long term deformation or creep model. Little or no particular attention has been given to factors

which govern the distribution of stress and strain distribution within rock masses. Henceforth, the difficulty to evaluate the effects of controlling factors such as lithological heterogeneity and geological structures on the patterns of stress and displacement distribution, particularly during deep active mining.

1.2 An approach to analysing patterns of stress and displacement distribution associated with underground active potash mining

Boulby mine is an active mine and its structure is expected to experience detrimental effect such as instability owing to changes brought to the *in situ* stress by the ongoing mining activity (Kwon and Wilson, 1999). Thus, the need to characterize the short term response of the structure to mining activity to ensure the safety of workers and any structure built underground.

The approach used in the current study is to analyze and quantify stress and displacement distribution using the Fast Lagrangian Analysis of Continua (FLAC 2D) code based on the Finite Difference Method (FDM). This will enhance understanding the deformation of rock mass and particularly the stress-displacement transmission through the overburden as a result of mining potash.

Given that the current research is more interested in stress and displacement distribution associated with the short term behaviour of the excavations at Boulby mine, the strain-softening model was applied to carnalite marl, potash and salt rocks as an approximation to the creep behaviour broadly used in most of numerical analyses of the rocks (Rothenburg *et al*., 2007; Lachenicht and Aswegen, 1999). The strain-softening model was combined to the Drucker-Prager and Mohr-Coulomb models to characterize the behaviour of the strata in the surface zone and those in the main and intermediate zones, respectively.

Datasets from a bespoke closuremeter underground monitoring were gathered and patterns of convergence of mine workings are used in the numerical analysis of stress and displacement distribution, and resulting ground subsidence.

1.3 Research Aim and Objectives

The aim of this research is to investigate the reliability of comparatively simple cross-section models of mine working convergence to real world settings. The research has been conducted through three main objectives, using the Boulby Mine area as a study site:

- The first main objective is to undertake short term measurements of the temporal patterns of mine working convergence in order to:
  - (a) examine spatial effects on patterns of convergence;
  - (b) examine the effects of excavation geometry or type (i.e. stub, roadway) on the patterns of convergence; and
  - (c) investigate the effects of age (i.e. date of mining) of monitoring sites on the patterns of convergence.
- The second main objective is to use the Fast Lagrangian Analysis of Continua (FLAC 2D) code to analyze numerically the patterns of stress and displacement distribution in a real world system, and further to:
  - (a) investigate the effects of lithological heterogeneity on the patterns of stress and displacement distribution;
  - (b) investigate the effects of geological structures on the patterns of stress and displacement distribution.
- The third main objective is to compare the patterns of levelling subsidence measured on the surface with the patterns of predicted subsidence using the simplistic and more realistic finite difference models.

1.4 Structure of the thesis

The thesis is structured in nine chapters. The first three form the literature review while the bulk of the work is given in the remainder chapters. A general introduction to the

research is given in chapter 1 whilst chapter 2 summarizes the existing literature on ground surface deformation, mine roof closure and ground subsidence monitoring techniques and modelling methods, especially the FLAC 2D code based on the Finite Difference Method.

Chapter 3 describes the area of study and reviews the mechanics of salt and potash rocks. The geotechnical characteristics of materials, the mining activity and mechanics of mine roof at the Boulby Mine are discussed. The laboratory behaviour of salt and potash rocks, and some models and failure criteria of materials are also discussed. This chapter also reviews the Drucker-Prager, Mohr-Coulomb and strain-softening plasticity models of rock masses used in the current study to characterize the behaviour of the overburden strata at Boulby. The creep of salt and potash and estimated *in-situ* stresses are also reviewed. The chapter ends with the discussion of roof monitoring technique used at Boulby mine and the results.

Chapter 4 describes the approach used to monitor short-term mine workings convergence at Boulby Mine. It includes the design and field test of the closuremeter used to monitor the mine workings closure.

Chapter 5 describes the procedure of short-term monitoring of closure and analyzes the monitoring results. The criteria of selection of sites, sites characteristics and instrument layout are described. This chapter has also attempted to characterize the actual behaviour of the mine workings at Boulby and determine the influential factors on the basis of the data collected at four monitoring sites.

Chapter 6 describes the FLAC 2D modelling approach used to numerically analyze the patterns of stress and strain distribution on the basis of measured mine workings convergence in order to better understand the mechanics of rock deformation and also determine controlling factors of patterns of stress and strain distribution during deep mining at Boulby. The chapter also examines the sensitivity of the models and the effect of water on distribution and magnitude of stress and displacement, and ground subsidence.

Chapter 7 presents the modelling results. The analysis results demonstrate the dependency of the patterns of stress and displacement distribution upon the lithological heterogeneity. In contrast, a fault has limited effect on patterns of stress and displacement distribution. They also demonstrate that patterns of ground subsidence are a function of both the lithology and fault, including the nature of the fault.

As far as strata parameters variation (i.e. stiffness and strength) is concerned, the analysis has shown evidence of sensitivity on displacement within the structure and a limited sensitivity on the maximum stress. Pore pressure affects both patterns and magnitudes of ground subsidence. The analysis also shows that patterns of subsidence have limited sensitivity to the variation of the material parameters.

Chapter 8 is a discussion on some variables which affect the patterns of stress and displacement distribution during deep mining at Boulby within the objectives of the thesis.

As for the patterns of stress and displacement distribution, the analysis of results indicates that the magnitudes of maximum stress and total vertical displacement are also a function of the lithological heterogeneity and geological fault. The analysis shows the linkage between the zone of disturbance at the surface and the increase of heterogeneity of the overburden strata. The comparison of FLAC predicted with levelling measured subsidence shows discrepancies in the patterns of subsidence and predicted subsidence underestimated measured subsidence.

Chapter 9 presents the conclusions drawn from the findings; the limitations of modelling approach and concludes with some recommendations for further study. It gives the contribution of the research to the understanding of the mechanics of rock deformation and stress-displacement state transmission during underground mining.

Chapter 2
Ground surface deformation

2.1 Introduction

Ground deformation due to underground mining (i.e. mining or tunnelling) is of concern for they may strike with or without warning.

Some of the fundamental concepts and relevant features of ground movements related to underground activities, in particular to active potash mining at Boulby are herewith presented. Driving factors of mine workings closure and ground subsidence, monitoring techniques and modelling methods used to study these phenomena are examined. The understanding of these concepts is essential for the comprehension of the stress-strain related geomechanics and accordingly for the modelling of the process of ground subsidence.

This chapter has seven sections. Section 2.1 describes the ground subsidence hazard and its occurrence. Section 2.2 gives some key parameters which drive the ground subsidence. In section 2.3 the response of rock mass to underground mining activity is examined. It describes the state of stress within the pre-excavated rock mass, the deformation mechanics of mine roof, and examines the concepts of brittle and ductile deformation of rocks. In section 2.4 some monitoring methods of roof closure are described with an emphasis on the method used at Boulby mine. Section 2.5 is devoted to the ground subsidence monitoring techniques, describing the levelling monitoring technique used at Boulby mine. Section 2.6 gives an overview of the different methods used for modelling ground subsidence (either surface or subsurface mining). Section 2.7 gives an overview of the Finite Difference Method and the FLAC 2D code in support to the methodology used in this research to examine the patterns of stress and strain distribution in a real world system, including the effects of heterogeneous lithological properties and geological structures at Boulby Mine.

The term subsidence is generally applied to the Earth's surface and refers to a given point sinking to a lower level. Therefore, subsidence could be defined as the lowering of ground surface by mass movement (Holzer, 1984). This failure of ground surface is characterized by nearly vertical deformation or downward sinking of earth materials.

Ground subsidence is a time-dependent process of ground deformation. The formation of trough on the surface results from the readjustment of the overlying strata above the mine. The trough develops from the immediate roof (i.e. the first layer of roof) and propagates laterally and vertically upward towards the surface (Jarosz *et al*., 1990).

Subsidence hazard, particularly underground mining-related subsidence may result in damage to surface structures (e.g. building, bridges, houses, roads and so forth); disrupt subsurface facilities such as sewerage, water, gas and electricity supply, and in the modification of groundwater regime. Depending on its geographical location ground subsidence may occur at any scale between local scale (i.e. collapse of mine shaft) affecting few people and houses, and continental scale (i.e. plate tectonic movement), affecting whole continents (Kemeling, 2006). Critically, subsidence studied in this research is not deemed a hazard due to the depth of the workings, the lack of surface differential subsidence and the slow rates of deformation.

The deformation of ground surface during trough formation occurs in both vertical and horizontal directions. The magnitude of the vertical component is generally greater than the magnitude of the horizontal movements (Gray and Bruhn, 1984). Damage to surface features is a function of the position of the structures along the trough and also on the maximum subsidence developed. Surface structures are mostly affected by the horizontal movements and the strains (or displacements) which result from the ground deformation.

The trough of subsidence does not form during one period of ground deformation. The formation may take place during the mining activity and long after the mining terminated and is a function of several parameters including the type and the extent of mining, the lithology and mechanical characteristics of the overburden and the floor, the depth of seam and so forth (Holzer, 1984).

Land subsidence may be triggered either by natural causes or human activities (Mousavi *et al*., 2001). On a very local scale subsidence results from the collapse of the ground into underground cavities which generally originate from the dissolution of soluble rocks. The dissolution of limestone beneath the surface by groundwater results in the occurrence of Karst topography of closed depressions at the surface. The thawing of frozen ground (i.e. melting permafrost), compaction of recently deposited sediment, and the shrinking of expansive soils will also result in ground subsidence.

Human-induced subsidence is generally associated with underground mining for mineral resources extraction (Gledan, 2004) and withdrawal of fluids (i.e. oil, gas and water) from the subsurface reservoirs (Mousavi *et al*., 2001). The extraction of mineral removes natural support from the overlying strata (Kratzsch, 1983). The rocks above the mine workings gradually bend under the influence of gravity. The deformation of the overlying strata progressively propagates upward towards the surface to form the trough during the mining or long after mining terminated (Kemeling, 2006; Ge *et al*., 2003). The propagation of the deformation takes place at the same time as the underground excavation is closed up. The extent of deformation propagation through the overlying strata is dependent of the deformational behaviour of the layers. In room-and-pillar mining, such that at Boulby mine the closure of the mine roof is caused by the yielding with time of pillars left behind to support the overlying strata. The final shape of subsidence at the surface occurs long after the supporting pillars have been fully compressed (Kratzsch, 1983).

The lowering of the surface related to the withdrawal of fluid results from the deformation of clay or sand layers by compression and the compaction of the sedimentary grains of the fluid reservoir (Chang and Wang, 2006). Indeed, the withdrawal of large volumes of fluids leads to the reduction in fluid pressure. The stresses on the rock matrix are increased and the bulk volume of the reservoir is reduced. The reservoir loses its supporting capacity of the earth stresses. Displacements (in 3-D) are induced within the reservoir and deformation may propagate vertically and laterally upward towards the surface. The decline of groundwater level is correlated to the occurrence of subsidence at the surface (Djaja *et al*., 2004). In

geothermal reservoirs the deformation of the reservoir may be due to the combined effects of the mechanical and the thermal processes (Narasimhan and Goyal, 1984).

Based on the size of the area affected at the surface, ground subsidence can be grouped into two categories:

1. Chimney also referred to as pit, sinkhole or pothole subsidence. It is associated with the collapse of mine roof constituted of materials such as shale rocks or mudstone within a small area. It is characterized by an abrupt sinking of the ground surface and results in a circular steep-sided depression. This form of subsidence is not studied herein.

2. Sag or trough subsidence. This latter is associated with pillars punching in deeper mines. It is of circular or semi-elliptical shaped form and is characterized by a gentle and gradual setting or depression of ground over a broad area. This is the type of subsidence which occurs at Boulby Mine and of interest in this study.

2.2 Ground subsidence controls

The mechanical behaviour of overlying strata is controlled by several factors (Kratzsch, 1983) whose combined effects account for the trough and magnitude of the subsidence observed at the surface. For underground mining, in addition to mining method, eight controlling factors are given in Table 2.1 (Gledan, 2004; Holzer, 1984):

Table 2.1 Controlling factors of subsidence trough

Factor	Effects on ground subsidence trough
	The width of the extracted area (i.e. width of opening) is a key factor in the occurrence and magnitude of subsidence on surface. Ground subsidence occurs when a critical width of

Width of the excavation	extraction is exceeded (Holzer, 1984). Subcritical width: For an excavation width less than the critical value, mine roof bridges over the excavated area inducing a sinusoidal trough at the surface. The trough is not fully developed and at the center, the subsidence is less than the maximum value. Critical width: As the width of the excavation increases, the subsidence at the center of trough becomes deeper and reaches its critical subsidence (i.e. maximum value). Supercritical width: Beyond the critical width, maximum vertical subsidence remains constant with the increase of width. Subsidence trough extends horizontally, resulting in a flat-bottomed trough shape. Vertical movement of the flat portion equals the maximum value of subsidence (Gray and Bruhn, 1984; Holzer, 1984; Kratzsch, 1983).
Depth of the excavation	For an extraction of constant area (i.e. width), depth increase induces a wider trough of subsidence with a less maximum subsidence. Trough flattening at increasing depths of mine workings reduces the tilt, curvature, displacement and linear change (i.e. tensile and compressive strain). Depth increase results in the increase of proportion of firm rock in the overlying strata. As a consequence, the arm of angle of limit becomes steeper in the lowest and flatter in the uppermost zones of the overlying strata (Kratzsch, 1983).
Width/depth ratio	It expresses the ratio of mined area width and the seam depth beneath the surface. Maximum subsidence occurs at a

	surface particular point when a minimum (or critical) value of ratio is exceeded in the two dimensions plan of the extracted area. The size of extraction area increases with seam depth increase (Gray and Bruhn, 1984).
Height of the excavated area	The excavation height controls the redistribution of stresses which affect the ground surface and induce subsidence. Maximum subsidence of roof beds increases with increasing excavation height (i.e. seam thickness). It may amount 30% or 40% of excavation height (Kratzsch, 1983).
Angle of draw	It is the inclination angle of the straight line joining the edge of the extraction area and the trough rib on the surface (Kratzsch, 1983). It is measured from the vertical line in UK and USA, and from the horizontal in other European countries. The angle of draw is always positive since the surface area affected is generally larger than the area of the seam extracted. It is a function of the characteristics of the overburden. Thick deposits of unconsolidated materials increase the angle of draw whereas thick and competent rock strata decrease the angle of draw. The angle of draw widens and flattens with increasing height above the mining horizon (Gray and Bruhn, 1984; Kratzsch, 1983).
Closure of the excavation	Closure or roof-to-floor convergence is a controlling factor of subsidence in that, the closure is itself driven by factors which govern the occurrence of subsidence on the surface. These include depth of excavation, width of excavation and size of mine workings, characteristics of overlying strata (i.e. bending resistance), seam thickness (i.e. excavation height) (Kratzsch,

	1983).
Geological structure of the overburden	Geological structure increases or decreases the angle of draw hence, the subsidence trough depending on its location within the area undergoing subsidence and also the geometrical relationship between the geological structure and mine workings (The Geological Society, 2008).
Mechanical characteristics of the overlying rocks	Variations of subsidence trough shape are a function of rock mass composition and deformation. Overlying layers respond in a different manner to mining, thus affect the development of subsidence (Kratzsch, 1983). Hard rock layers with effective self-support capability delay subsidence occurrence at the surface; weak rock layers however, are likely to deform under lower stresses (Brady and Brown, 2006; Kemeling, 2006). They may flow into the opening under high pressure and temperature or through fractures and cracks in the overburden (Dyne, 1998). Where the floor is constituted of relatively weak rocks (e.g. Shale, Sandstone), the floor may heave due to yielding of floor material under pressure or shear stress acting on the wall side beneath the excavation (Brady and Brown, 2006). As a consequence, the bearing capacity of the floor is altered. Both types of rocks may widen or reduce the angle of limit of subsidence trough depending on the path of fracture propagation, and the strength and degree of fragmentation of the overlying strata. Fracture (e.g. plastic shear strain) propagates laterally upwards to the surface along the path of least resistance such

	as discontinuities.

2.3 Rock mass response to mining

Rock masses in deep mining environment are anisotropic media in a well-distributed elastic stress state (Brady and Brown, 2006). Understanding the concepts of stress and strain is essential to the comprehension of response of rock mass to mining activity.

Prior to mining, orebody rock exerts forces to support the surrounding rock mass (Jumikis, 1983). Mining the seam eliminates supporting forces and creates equivalent but opposite forces which act at the surfaces of the excavated area toward the opening. The immediate roof (i.e. first layers of the roof) detaches from the host upper strata and deflects into the excavation. High stresses and strains are induced in yield and abutment pillars, and strain energy in zones of high stress concentration increases due to insufficient orebody rock left in place (Brady and Brown, 2006).

2.3.1 Stress state in sound rock

Stress in virgin undisturbed rock originates from the weight of the overburden rock (also known as roof pressure), gravitational and tectonic forces (Islam, 2009; Brady and Brown, 2006). Geological features (e.g. fractures, joints, folds) considerably affect the virgin stress within rock (Jumikis, 1983) and its magnitude increases with increasing depth below the surface.

The stress-strain regime has control on stability of excavations and its evaluation provides indicators of instability of excavations in mining activity (Baryakh and Samodelkina, 2005). At any point of an undisturbed, homogeneous and isotropic rock mass, the stress state is shown in Figure 2.1.

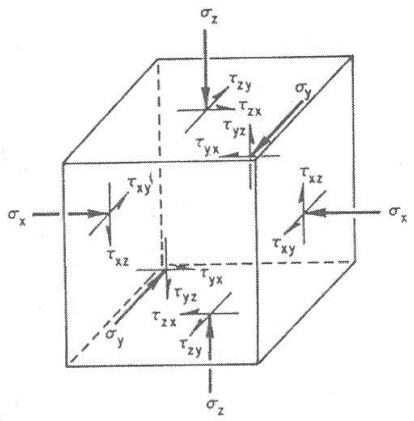

Figure 2.1 Components of stress in a sound, homogeneous and isotropic rock (Jumikis, 1983)

Distribution of stress gradients in a rock mass in static equilibrium is depicted in Figure 2.2. The stress due to surface forces (i.e. force acting on the surface of a body – e.g. normal and shear forces) and body forces (i.e. force acting throughout the volume of a body – e.g. gravity) is expressed by the equations below (Brady and Brown, 2006).

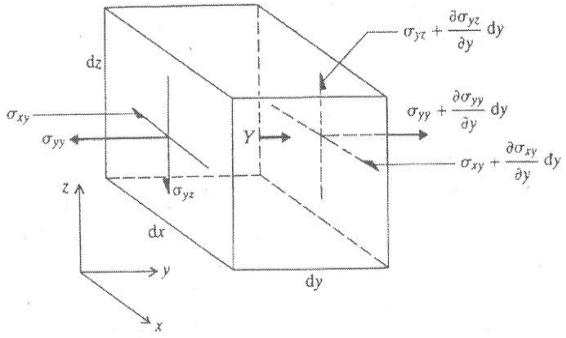

Figure 2.2 Diagram of free-body for the development of the differential equations of equilibrium (Brady and Brown, 2006)

$$\frac{\partial \sigma_{xx}}{\partial x} + \frac{\partial \sigma_{xy}}{\partial y} + \frac{\partial \sigma_{zx}}{\partial z} + X = 0 \qquad (2.1a)$$

$$\frac{\partial \sigma_{xy}}{\partial x} + \frac{\partial \sigma_{yy}}{\partial y} + \frac{\partial \sigma_{yz}}{\partial z} + Y = 0 \qquad (2.1b)$$

$$\frac{\partial \sigma_{zx}}{\partial x} + \frac{\partial \sigma_{yz}}{\partial y} + \frac{\partial \sigma_{zz}}{\partial z} + Z = 0 \qquad (2.1c)$$

where X, Y, Z are magnitudes of components of forces per unit volume in positive x, y, z co-ordinate directions; $\partial\sigma_{xx}/\partial x$, $\partial\sigma_{xy}/\partial y$, etc. are stress gradients of stress distribution in the rock mass.

For a rock mass with similar density overlying strata, the *in-situ* vertical stress exerted by the superimposed rock weight at any subsurface point is given by (Jumikis, 1983):

$$\sigma_{zz} = \gamma * z \qquad (2.2)$$

where:

σ_{zz}=vertical stress at a point, [Pa]
γ=unit weight of rock
z= the depth below ground surface, [m]
$\gamma = \rho_x g$
ρ=density of rock, [kg/m^3]
g=gravity, [m/s^2]

The horizontal *in-situ* stress is estimated from the vertical stress on the basis of elasticity theory. Elasticity theory assumes homogeneous, isotropic and linear-elastic rocks fully restrained in lateral direction. This implies that the rock is not subjected to residual stresses or tectonic stresses associated with folding, faulting and shrinkage on a large scale in the earth's crust (Hebblewhite, 1977; Patchet, 1970).

Therefore, for a cubic rock mass element surrounded by a mass of rock at a similar pressure to itself, the tendency to expand laterally is inhibited, i.e. no lateral strain will occur. Consequently, a lateral restraining pressure (i.e. horizontal *in-situ* stress) must be built up and is given by (Brady and Brown, 2006; Jumikis, 1983):

$$\sigma_{xx} = \sigma_{yy} = \left(\frac{\upsilon}{1-\upsilon}\right) * \sigma_{zz} \qquad (2.3)$$

where,

$\sigma_{XX} = \sigma_{YY}$ = horizontal normal stress components, [Pa]
σ_{zz} = vertical stress at a point, [Pa]
v = Poisson's ratio for the rock mass

From equation 2.3, the lateral pressure at any subsurface point is v/(1-v) times the vertical pressure at that point. For most of rocks, values of Poisson's ratio lie

between 0.2 and 0.3; hence the ratio of horizontal stress to vertical stress should be in the range 0.25 to 0.50.

2.3.2 Mechanical behaviour of mine roof in a stratified rock

Stratified rock masses are generally non-isotropic media as a result of the persistent bedding (Brady and Brown, 2006). The mechanical behaviour of mine roof above underground mining rooms is governed by the behaviour of the immediate roof. In a stratified rock mass, this roof is considered as a series of beams of equal width spanning the excavation and abutted by pillars at their edges, and detached layers are subject to their own weight (Alejano *et al*., 2008). Roof beam behaviour is similar to the voussoir arch of timber layers sequence in structures of masonry. Compressive force acting along the voussoir arch withstands the overlying materials weight by transmitting it to the abutments.

Prior to mining, rock mass is subjected to both vertical and horizontal stresses at the mine horizon. The former (Equation 2.2) results from the weight of the overlying rock (i.e. gravity load) whereas the latter (Equation 2.3) from the reaction of rock mass to the vertical stress (Brady and Brown, 2006). The removal of seam body prevents stresses from propagating through the opening; consequently the vertical stress is transferred to the adjacent rock of the opening sides. As a result, the immediate roof only carries its own weight and portion of weight of the material below the pressure arch.

In room-and-pillar mining, the overburden load is initially carried by pillars. As the load exceeds the strength of pillars, they yield (i.e. deform plastically) and the stress is transferred to the ribwalls of excavation and eventually to barrier pillars. A pressure arch is then formed in the rock above the excavation (Brady and Brown, 2006). The increase of excavation dimensions increases the height of pressure arch and accordingly, the increase of stress on pillars. The presence of weak strata – e.g. shale and sandstone layers in the overburden may allow pressure arch to intercept the weaker beds. However, given that weak layers are unable to sustain pressure, this pressure arch breaks down. The full load of the overburden is then carried by the pillar, which with

time yields leading to mine roof closure. Roof deformation propagates upwards towards the surface and induces subsidence trough (Brady and Brown, 2006; Kratzsch, 1983).

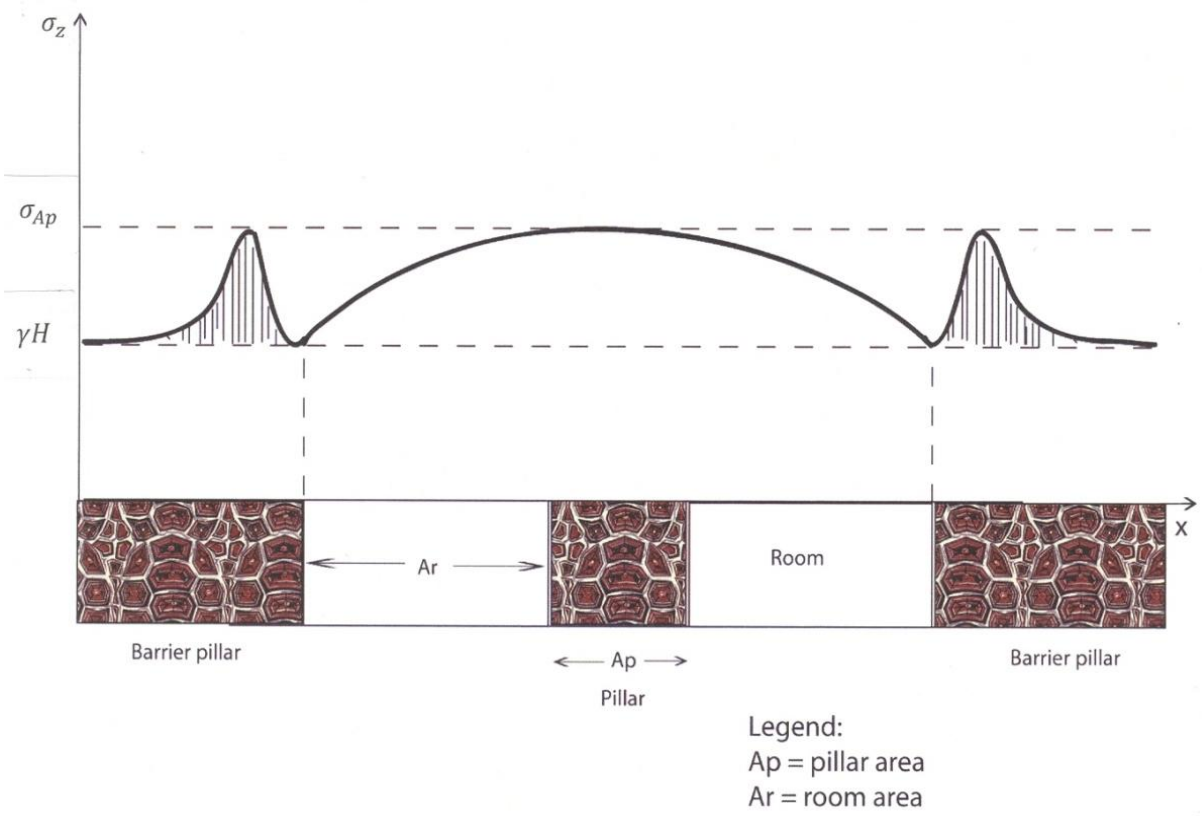

Figure 2.3 Distribution of overburden pressure in chamber working underground mining (after Kratzsch, 1983).

Vertical pressure σ_z on the pillar is distributed in a bell-shaped pattern exceeding the specific surface load, γH at its central point (Kratzsch, 1983):

$$\sigma_{Ap} = \frac{A_p + A_r}{A_p} \gamma H \qquad (2.4)$$

where A_p and A_r are pillar and room area, respectively.

On the basis of voussoir beam model, some principles of deformational behaviour of rock material over the excavation have been formulated, including (Brady and Brown, 2006):

(1) Roof bed behaviour is a function of horizontal stresses induced by the deflection of roof under gravity loading (i.e. the voussoir beam against the confinement of the abutting rock);

(2) A voussoir beam behaves elastically (i.e. the lateral stresses – vertical deflection relation is linear and reversible) over the range of its satisfactory performance;

(3) Shear failure at the abutments will occur for voussoir beams with low span/thickness ratio;

(4) Failure of roof with low rock material strength or moderate span/thickness ratio will occur by crushing or spalling of central or abutment voussoirs; and

(5) A roof with high span/thickness ratio will fail by beam buckling with less spalling of central or abutment voussoirs.

2.3.2.1 Factors influencing roof failure

Several factors influence mine roof failure and the amount of closure. Ground conditions (i.e. material strength and quality) of immediate roof; *in-situ* stress and geological conditions of the overburden are predominant factors which control mine roof stability and failure (Duzgun, 2005). Others factors influencing roof failure include mining method and mine layout (i.e. roadway spanning, pillar sizes and distribution) (Mark *et al*., 2007). The first three factors are described in Table 2.2 below.

Table 2.2 Controlling factors of mine roof failure

Factor	Effects on mine roof
Ground conditions (i.e. material quality, material strength) of immediate roof	Rock mass strength controls failure of roof. It is dependent of intrinsic texture or mineralogical properties inherent to the rock. Failure of roof also originates from horizontal stress and involves flexure or buckling (Phillipson, 2008).

Geological conditions of the overburden (i.e. layers types and thicknesses, faults, fractures, folds)	Pre-existing geologic discontinuities affect the strength of rock mass and act as planes of weakness (Phillipson, 2008; Brady and Brown, 2006). Weak rock layers (e.g. shale, sandstone, salt and potash) will flow into the opening under high pressure and temperature or through fractures and cracks in the overburden (Brady and Brown, 2006). Interbedded weak strata separate parallel to bedding planes at contact zones as a result of overlying strata pressure and their own weight. Interbedded structures, with weak strata, are susceptible to horizontal stresses; and the presence of thin bedding and weak strata in the immediate roof exacerbates failure of roof.
Pre and post-excavation conditions at the excavation boundary and in the interior of the rock mass	Mine roofs fail in response to excess *in-situ* horizontal stress and involve slabbing. High *in-situ* horizontal stress induces plastic flow or heave of mine workings floor. Horizontal stress also induces compressional roof failure. Relatively weak roof and thinly bedded roof in the overburden are more susceptible to stress-induced damage. Low horizontal stress induces either sliding of delaminated roof along vertical joints or buckling over the span. In soft roof, high stress causes large plastic deformation and mine roof failure (Alejano *et al*., 2008; Shen *et al*., 2008; Mark *et al*., 2007).

2.3.3 Brittle and ductile deformation of rocks

Rock masses deformational behaviour is generally classified in two main regimes: brittle and ductile regimes. Both regimes depend on pressure and temperature conditions. Brittle failure is the process of fracture of rock material without any appreciable permanent deformation (Raynaud *et al*., 2008) and generally occurs at relatively low confining stresses. It is associated with the strain-softening or strain-weakening

behaviour of material (Figure 2. 4a) (Brady and Brown, 2006) and is a characteristic of bonded and cohesive materials. Material is initially loaded and undergoes a short elastic strain phase. Increasing load results in the break of weakest or intensely stressed bonds leading to the loss of material strength (Birtel and Stockhert, 2007).

Brittle deformation of salt is similar to that of most of rocks; and failure of salt is sensitive to pressure and a function of plastic strain. The temperature controls the strain rate and increases with the increase of temperature (Fossum and Fredrich, 2002).

Ductile behaviour is the deformation process which follows the permanent deformation of the rock mass; a characteristic of loose geomaterials with little or no intraparticle bonding. Materials deformation results in intraparticle restructuring at constant porosity.

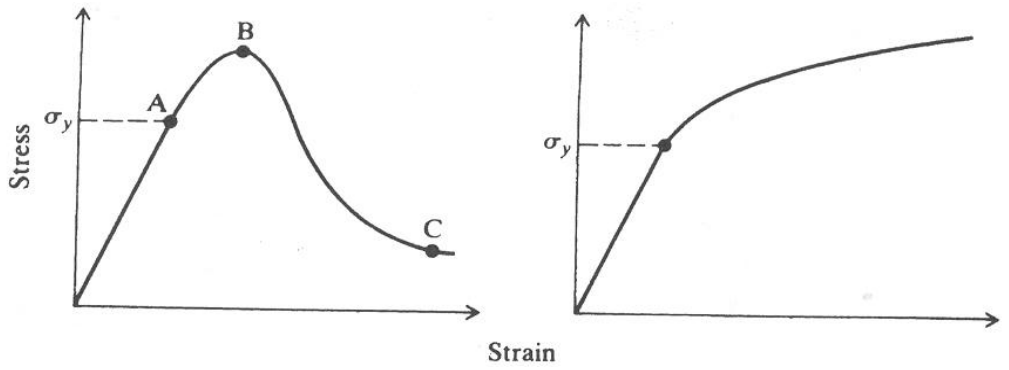

(a) (b)

Figure 2.4 Stress-strain curves, (a) strain-softening; (b) strain-hardening (Brady and Brown, 2006)

where σ_y is the yield stress (i.e. the stress at which irreversible or permanent deformation first appears), A = Limit of elasticity and corresponds to the onset of the yielding of material, B = the peak strength and corresponds to the maximum stress the rock can sustain, C = the minimum or residual strength and corresponds to the load-carrying capacity or strength the rock may still have after the peak strength has been exhausted.

Rock deformation occurs as the material sustains additional permanent deformation without failure (i.e. loss the load-bearing capacity) at constant stress and may be associated with strain-hardening of the rock masses (Figure 2.3b) (Birtel and Stockhert, 2007; Brady and Brown, 2006). Deformation of rock mass occurs at high effective stresses or pressures and/or high temperatures. Strains do not localize or coalesce to form a shear band along which material failure will occur.

2.4 Mine roof closure monitoring

Roof stability is a long-standing issue and mine roof closure has long been of concern in active underground mines. Generally, failure of rock mass is preceded by a precursory manifestation of behaviour of the rock (Szwedzicki, 2003). Several techniques are used to monitor the precursory behaviour of rock mass, and geomechanical data can be used for assessing roof behaviour (Schleinig and Lukas, 2007).

Deformation or displacement, stress and acoustic emissions are measured over a relatively short periods and data are used to analyze rock mass behaviour (Bigby, 2004; Jarosz *et al*., 2002). A range of methods are used to monitor the stability and deformation of mine roof thus, failure of the whole structure. Some key techniques are described in the following sections.

2.4.1 Acoustic Emission/Micro-seismic Emission and stress-strain distribution

Change in *in-situ* stress of rock mass brought by excavation is detrimental to the stability of openings. Stress and strain redistribution leads to failure and collapse of rock mass underground excavations (Szwedzicki, 2003). Several studies have been conducted over the subject in various aspects of mining activities for mineral resources (Aguado and Gonzalex, 2009; Islam *et al*., 2009; Mark *et al*., 2007); tunnelling and research laboratories (Cantieni and Anagnostou, 2009; Henk, 2006; Hao and Azzam, 2005; Kontogianni and Stiros, 2002), energy storage caverns & power stations (Martin and Christiansson, 2009; Alkan *et al.,* 2007; Klayvimut *et al*., 2007); repositories for radioactive waste (Martin and Christiansson, 2009; Alkan *et al.,* 2007; Klayvimut *et al*., 2007).

Rock mass failure is generally accompanied by acoustic emission/microseismic (AE/MS) signals propagating through rock mass. Such signals are reliable tool for predicting failure of mine roof (Wang and Ge, 2008; Szwedzick, 2003). The analysis of monitored signal intensities enables determination of location, extent and magnitude of damage, and progression of failure in rock mass consequently, the assessment of instability of underground structures (e.g. mines, tunnels) (Meglis *et al*., 2004).

Numerical analysis provides means of understanding the behaviour of rock masses under stress, the mechanisms of stress-strain state transmission within the rock and failure of rock mass (Mitra, 2006; Hart, 2003). We hereby provide four previous studies relevant to our research for three reasons: (a) the similarity of objectives with the present research; (b) the numerical code used, and (c) the models used to represent the behaviour of strata.

Cai *et al*., (2001) developed a damage-driven numerical model for rock mass behaviour on the basis of monitored microseismic events using a micro-mechanics-based constitutive model to account for rock mass softening a result of fracture. The model inputs are: intact rock Young's modulus and Poisson's ratio, and the microseismic monitoring information (e.g. location and source size of each event). Developed model was implemented into the FLAC 2D code. Models were validated against extensometer-based data from the Atomic Energy of Canada Limited (AECL's) Mine-by Experiment at the Underground Research Laboratory (URL) tunnel. Predicted results showed good agreement with radial deformation measurements.

Cai *et al*., (2007) studied the mechanism of crack formation as a result of stress and strain distribution during the excavation of the Kannagawa powerhouse in Japan. The finite difference code, FLAC 2D and distinct element Particle Flow Code (PFC 2D) were coupled to simulate and capture acoustic events during cavern excavation. Rock material was treated as strain-softening material. Areas of rock mass under stress or failing, and patterns of stress and strain distribution were determined. Acoustic events models were in good agreement with field measurements.

Despite the FLAC/PFC approach gave insight into patterns of crack formation and distribution of stress and strain AE/MS techniques have some advantages and drawbacks. The advantages include real-time observation of damage process during the entire load history without any disturbance to structures, and that measurement can be carried out remotely. The disadvantages include, quantitative measures such as AE counts and centre frequencies for the assessment of damage are limited, and the techniques are sensitive to noise. Consequently, monitoring data may significantly be impaired.

Mark *et al*., (2007) analyzed ground behaviour, stress redistribution and reinforcement at a longwall tailgate at the Emerald coal mine in Southwestern Pennsylvania. FLAC 2D code was used and material was treated as Mohr-Coulomb material exhibiting strain-softening post-failure behaviour. The strain-softening was simulated by incorporating a plane of weakness in the model. Analysis results showed failure of immediate roof occurs along slip plane and bedding, inducing a partly distressed (i.e. softened) zone in the roof. The results also indicated occurrence of stresses redistribution above the immediate roof before significant deformation occurred as a result of bedding shear. Induced shear bedding in the immediate roof redirected stress pathway despite the relatively slow deformation of roadway. Horizontal stresses increased as a function of site geometry, and deformation and failure of mine roof reoriented stresses in the vicinity of the entry. Modelling results showed good agreement with results of roadway behaviour monitoring.

Of particular interest herein is the dependency of stress and deformation particularly on the discontinuity and behaviour of immediate roof. Another significant finding is the dependency of magnitude of deformation on the monitoring point at the site.

Islam *et al*., (2009) numerically evaluated stress redistribution caused by the extraction of coal and its effect on the overlying strata, aquifer system and land at Barapukuria mine in Bangladesh. Finite element method (FEM) and Mohr-Coulomb failure criterion were applied to determine patterns of tectonic stress distribution at the basin whereas the boundary element method (BEM) was used to determine patterns of stress distributions induced by coal extraction. Modelling results showed tensional

failure concentration within the coal sequences and around faulted zones. Rock failure results from the presence of low strength zones and discontinuities (e.g. faults, fractures and joints) interconnecting the zones. Whilst shear stress bands are higher along the faulted zone, they gradually decrease away from the fault. The result also reveals that huge amount excavation of coal results in large scale deformations and upwards bending shear stress contours. Furthermore, mining-induced stress results in the development of upwards propagating fractured zones in overlying strata. The results show shear stresses in the mine roof than at the rib sides (i.e. sidewall of excavation). The study demonstrates fracture development and propagation as a function of strength of strata. Coal extraction significantly alters stress redistribution around opening and induces deformation along faults and fissures. Stress redistribution leads to strata subsidence. Groundwater flow through existing and induced discontinuities results in underlying aquifers discharge and therefore, in development of ground subsidence on the surface in close vicinity of the mine.

The above studies obviously demonstrate the effectiveness of numerical methods in analyzing stress and strain distribution in rock mass as a result of underground mining. They reveal the effects of rock strength and faulting on stress redistribution, and also concentration of stress along fault and near the rib sides of openings.

Although some of the referred studies by Islam *et al*., and Mark *et al*., gave insight into controlling factors of stress and strain distribution, most of them failed to focus either on factors which highly influence the stress and strain distribution in rock mass surrounding the excavation or on the nature of this influence. As a consequence, limited information is known on the mechanism of stress and strain redistribution and resulting failure of rock mass above underground excavation. Most importantly, stress provides boundary condition of forces therefore; changes in stress regime detrimentally affect the stability of the excavation and also the mine surrounding environment. Additionally, rock mass response to mining activity and accordingly, stress and strain redistribution are dependent of the rheology of individual strata that form the structure. Furthermore, geological discontinuities also control the stress and strain redistribution

as they affect the stiffness and strength of strata. Therefore, a better understanding of deformation and failure mechanism of rock mass would be achieved through the analysis of controlling factors including lithological heterogeneity and geological features.

2.4.2 Extensometers

Underground excavation deterioration results from changes in geometrical configuration, boundary conditions and loading environment. However, in most cases geotechnical and environmental parameters used in excavations design are rather accurate owing to limitations in the techniques applied for obtaining such parameters. As a result, unsafe design and long-term performance of the excavations is likely to be affected (Bhalla *et al*., 2005). In order to ensure excavations long-term performance, continuous monitoring is required for evaluating strata deformation and damage (e.g. roof closure, roof-to-floor convergence, wall deflections) occurrence (Singh, 2002). This also assists in mitigating potential hazards.

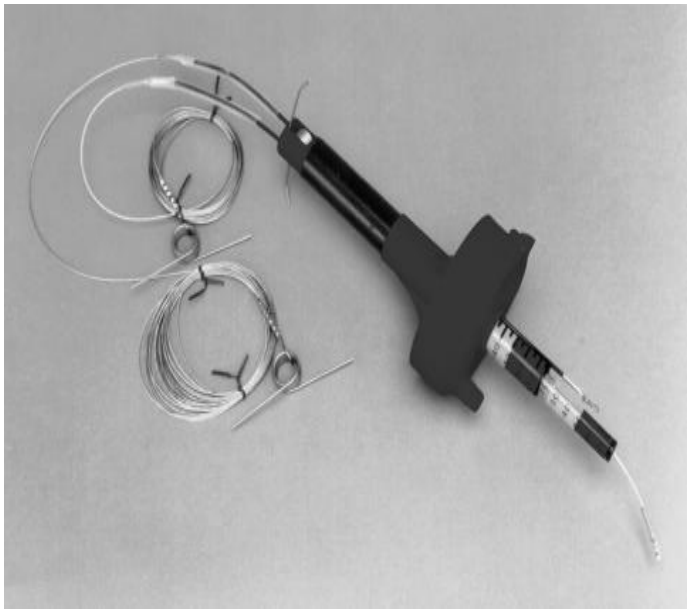

Plate 2.1 Dual height telltale extensometer (Bigby *et al*., 2004)

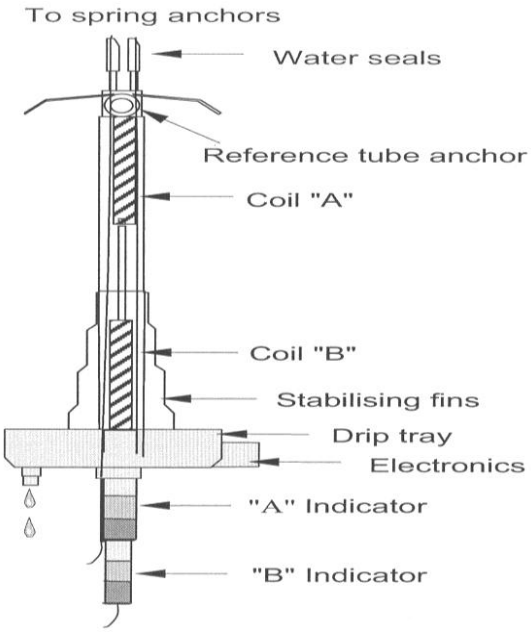

Figure 2.5 Section of a dual height telltale extensometer (Bigby *et al*., 2004)

Extensometers are widely used for recording relative displacement as precursor to rock mass failure and testing the rigidity of materials (e.g. metals, plastics and composites). Underground mining, the instruments are used to monitor roof deformation and provide insight into roof behaviour (Estershuizen *et al*., 2007), and also to monitor mine workings convergence. The instruments are of different types: (a) tape extensometer, (b) borehole extensometer and (c) dual-height telltale extensometer. Tape extensometer measures the relative displacement between two points in terms of convergence while borehole extensometer measures the relative displacement between several points. This latter provides displacement distribution in large rock volumes and is mostly used as the basis of safety monitoring systems. They are effective in identifying and measuring changes or movement in roof of excavations. However, given that the recording process is manual in both techniques, measurements accuracy may be affected (Bhalla *et al*., 2005).

Dual-height telltales are the simplest and widely used borehole extensometers. They were developed and patented by British Coal in 1992 as a safety device for coal mine tunnels, and monitor differential movements. When rockbolted underground mine, the instruments give visual indication of roof movement at the monitoring point and provide immediate information on mine roof conditions (Bigby, 2004). Dual-height telltales allow determination of magnitude, position and rate of movement of rock mass surrounding excavation. They also provide valuable clues to the appropriate support for the remediation of instability (Iannacchione *et al*., 2005; Bigby *et al*., 2003). The operating principles, advantages and disadvantages of dual-telltale extensometers are given in Table 2.3. A picture and section of the instruments are given on Plate 2.1 and in Figure 2.5 above.

Table 2.3 Operating principles, advantages and disadvantages of dual-telltale extensometers (Bigby *et al*., 2004)

Operating principles	Advantages	Disadvantages
The two freely suspended concentric cylinders are anchored into the borehole such the upper “AA” cylinder	- Low cost and simple to install	- Can be trapped into the hole owing to shear,

visible length indicates movement of roof within the rockbolted height while that of lower “BB” cylinder indicates movement of roof above the rockbolted height. To achieve this, the “AA” cylinder should be anchored below the rockbolts top and the “BB” cylinder at about twice the rockbolted height. Reading is by noting either the color of visible upper band (green, yellow or red each 25 mm wide) or marks on the scale.	- Can be connected up to 100 units along a single roadway at 20 m intervals and remotely read	consequently prevented from movement - Cannot be run in a borehole with minimum shear.

2.5 Ground subsidence monitoring techniques

Surveying is the science of measuring relative positions of natural and artificial (i.e. man-made) features on the earth’s surface and the geographical (i.e. mapping) or numerical representation of this information (Bannister and Baker, 1994).

Generally, ground deformation monitoring techniques may be grouped into two categories: ground-based or terrestrial techniques and geospatial-based or remote sensing/aerial monitoring techniques. Some techniques used for monitoring ground subsidence at Boulby are described in sections that follow.

2.5.1 Terrestrial monitoring techniques

Ground-based geodetic techniques are based on repeated measurements of distances and angles between surveying devices. Their use requires accessibility to the area of

interest and clear lines of sight. These techniques include levelling, theodolite and traverse, triangulation, trilateration and terrestrial photogrammetric surveying (Bannister and Baker, 1994).

2.5.1.1 Levelling surveying

Levelling is a discipline encompassing all methods of gathering and processing information about the physical earth and its environment. The technique compares heights of points on the surface of earth relative to one point or plane (i.e. datum) (Bannister and Baker, 1994).

Basic levelling equipments are: the optical level and the gradual staff (Levelling Staff). The former gives horizontal line whereas the latter gives vertical heights. A third equipment, a chain and tape or tacheometer, may be required for locating levelled points relative to each other on a map, plan or section. Levelling long distances is made by applying trigonometrique technique, and using a theodolite and a target. At least two people, one observer on the instrument and one staff-man are required. To speed up measurement, a third person is needed for locating and cleaning change-points and benchmark.

Although levelling survey is not affected by rain and light breeze, bright and windy conditions affect levelling accuracy (CPL, Survey Dept., 2002). Hilly and mountainous environments with inaccessible topography also affect temporal and spatial accuracy of levelling. At a regional scale (i.e. large scale), levelling surveys are less accurate (Allan Fulton, 2006).

2.5.2 Geospatial-based monitoring techniques

Geospatial monitoring is the application of geospatial tools such as geographic information systems (GIS), global positioning system (GPS) and remote sensing data devices (e.g. InSAR) for gathering, analysing and reporting information related to features on the Earth's surface (Ward and Johnson, 2007).

The Global Positioning System (GPS) and other advanced geodetic surveying techniques (e.g. D-InSAR, InSAR) have been used to monitor ground subsidence associated with the extraction of potash (Chrzanowski *et al*., 1997) and withdrawal of water (Stramando *et al*., 2008; Chang and Wang, 2006; Chatterjee *et al*., 2006).

Introduced in the late 1980's, the system is a satellite-based navigation system (Hurn, 1993). GPS enables tracking and computing geographic positions. It provides spatio-temporal patterns of ground subsidence over the undermined area for mineral extraction (Akcin *et al*., 2006; Hu *et al*., 2005; Gledan, 2004) and water withdrawal (Meckel, 2008; Sneed *et al*., 2001) with an accuracy of few and several centimetres in the horizontal and vertical directions, respectively.

The Interferometry Synthetic Aperture Radar (InSAR) and more advanced Differential Interferometry Synthetic Aperture Radar (D-InSAR) exploit SAR image archives to provide high spatial coverage of the area under consideration. These techniques are widely used to determine ground subsidence in urban, rural temperate and arid areas (Herrera *et al*., 2007; Kemeling, 2006).

2.6 Ground subsidence prediction methods

The knowledge and understanding of the real world is often represented in the form of models. Assumptions and simplification about the reality are made to explain the complexity of the world. The essential part of structure (i.e. real world) is then represented in the form of models (Stockburger, 1996) to help investigate some key aspects of systems or structures.

Different methods are used for understanding and predicting ground subsidence (Kratzsch, 1983) and methods can be classified into two groups: empirical methods, and deterministic and numerical methods (Aston *et al*., 1987).

2.6.1 Empirical methods

Empirical methods are the earliest methods for predicting ground subsidence associated with mining activity. Subsidence empirical study started in 1825 in Belgium and was intended to investigate surface damage associated with shallow coal mining activities in city of Liege (Kemeling, 2006).

The methods assume that amount of subsidence is a function of seam thickness, dip of beds, quantity of stowing material and age of workings (Kratzsch, 1983). They are based on a combination of experience and the analysis of data gathered from study of existence subsidence for predicting future subsidence (Hood *et al*., 1983). The fact that the methods use existing surface movement data to predict further subsidence effects makes them suitable only for predicting subsidence in areas where initial data are available (Cui *et al*., 2000).

The techniques are basically of three methods: the data or NCB graphical method, the profile function method, and the influence function method (Karmis and Agioutantis, 1999; Aston *et al*., 1987).

The graphical National Coal Board (NCB) approach is a data method widely used in the United Kingdom for predicting subsidence above coal mines (Hood *et al*., 1983; NCB, 1966). It is based on two specific underground mining conditions: the length of panel should be 1.4 times the depth of excavation and the panels should be rectangular (Kratzsch, 1983; NCB, 1966).The spatial extent of the affected area is estimated using two profiles of subsidence, the longitudinal and transverse subsidence profiles. The maximum subsidence factor (S/m) (with m extracted seam thickness and S the maximum subsidence in any profile), and the horizontal distance between extraction centre and disturbed area limit are computed from the width to depth (w/h) ratio of individual panels (NCB, 1966).

The profile function method is a curve fitting technique. The method uses the actual field data-based function for predicting subsidence profiles over future areas of mining once the mathematical profile function is deduced. Given a critical mining area, the mathematical function commonly used to predict ground subsidence is of the form (Aston *et al*., 1987):

$$S(x) = Sf(B,x,c) \quad (2.5)$$

where s(x) is the subsidence at point x, S the subsidence at panel centre, B the control parameter for the range of function, x the horizontal distance from the panel centre, and c a constant.

The influence function method is based on the hypothesis that effects of mining on subsidence of a given point at the surface may be superposed (Kratzsch, 1983). The principal concept of the method is that the extraction area is composed of infinite number of infinitesimal elements and the displacement of any given point at the surface is described by the influence function. Therefore, subsidence of a point at the surface is obtained by integrating the influences of all the infinitesimal elements of the excavation area (Hood *et al*., 1983; Kratzsch, 1983).

Generally, these data-based methods require measurable and well defined input parameters. However, in many processes of deformation, such parameters are difficult to determine given the complexity of natural systems, stress conditions and temperatures, groundwater conditions and the nonlinear rheology of rock mass at the site (Kemeling, 2006).

Although empirical methods adequately estimate ground subsidence over mining activities, the universality of methods may be limited owing to the conditions on which the methods are based but also the types of mining situations they apply to. Additionally, because the methods are primarily based on past experience, they are conservative for area that had no surface movement surveying conducted across them despite the fact that they produce good surface settlement predictions.

2.6.2 Analytical methods

Analytical methods are purely mathematical and consist of set of governing differential equations of the process under investigation – e.g. ground subsidence. They require simplifications and model construction given the complexity of field situations to be simulated. Assumptions or simplifications are rather restrictive and analytical solutions generally require that the medium be homogeneous and isotropic (Wang and Anderson,

1982). In modelling mining-related subsidence, strata behave according to constitutive equations of continuum mechanics (Aston *et al*., 1987).

2.6.3 Statistical methods

Physical interpretation of deformations of rock mass induced by stress redistribution can be carried out statistically. In modelling deformations related to mining, statistical approach analyzes the correlation between causative factors (i.e. stress) and observed deformations (or strains) (Szostak-Chrzanowski *et al*., 2005).

2.6.4 Deterministic and numerical methods

Deformational behaviour of systems is generally described by a set of governing differential equations. Numerical methods are computer techniques used to solve such differential equations (Itasca, 2005) as opposed to analytical methods. The techniques are based on the knowledge of the properties of overlying strata, constitutive laws (i.e. stress-strain law) and on making simplifying assumptions to simulate complex field problems and model the behaviour of material (Itasca, 2005; Szostak-Chrzanowski *et al*., 2005).

Numerical and deterministic models are excellent approaches to quantitatively analyze ground subsidence and strata mechanics problems associated with underground activities. The models may be arranged into two main groups: the group of Finite Element Methods (FEM) and Finite Difference Methods (FDM), and the group of Discrete Element Methods (DEM), Boundary Element Methods (BEM), and Universal Distinct Element Codes (UDEC) (Brady and Brown, 2006; Jing and Hudson, 2002). The former group of methods is appropriate for modelling the behaviour of continuum systems whereas the latter group is more appropriate for modelling discontinuous rock masses behaviour (Alejano *et al*., 2008; Hao and Azzam, 2005; Hart, 2003). FEM is ideal for inhomogeneous and nonlinear materials (i.e. the Young's modulus is not constant over a range of strains). Whereas, FDM is based on the Fast Lagrangian Analysis of Continua (FLAC 2D/3D) code and accommodates with large-strain and nonlinear problems (i.e. the output is not proportional to the input or which do not satisfy

the superposition principle) associated with the development of subsidence. It is an explicit (i.e. no matrices are formed), dynamic approach and successfully used for analyzing instable systems (Hart, 2003).

In analyzing material behaviour, finite difference method replaces every derivative in the governing equations (i.e. differential equations) by an algebraic expression written in terms of field variables (e.g. stress or displacement) at neighboring grid points. For the finite element method however, field variables vary throughout the elements in a prescribed manner controlled by specific functions and parameters (Itasca, 2005). In modelling process, both methods consider the rock mass as a continuous medium therefore; can be represented by a continuum constitutive model. Because the complexity of Boulby structure and with the assumption that the system is continuum, the FLAC 2D code of the Finite Difference Method will be used in this research for modelling rock mass response to mining.

2.7 The FLAC 2D modelling subsidence

Numerical methods are powerful tools in modelling ground deformation related to underground excavations or withdrawal of fluids. In order to elucidate the effectiveness of FLAC 2D in modelling ground subsidence associated with underground mining activity, some cases of study will be described. These cases of study were chosen given their similarity in the seam with the potash seam at the Boulby Mine and in some cases, the model used to characterize be behaviour of overlying strata. Other cases of study are summarized in Table 2.4.

Alejano *et al*., (1999) investigated coal mining ground subsidence in Spain amid concerns about empirical techniques used for predicting subsidence. No correlation was found over steep coal seams despite estimated subsidence over flat seams agreed with observations. To address the issues and predict subsidence for both flat-lying and inclined coal seams, the FLAC 2D code and elasto-plastic model for the material behaviour were combined; and an actual material behaviour-based technique was developed.

The approach successfully simulates flat and gently inclined coal seams (i.e. seam dipping from 0 to 45^{o}) ground subsidence and numerical results were in good agreement with empirical observations, and validated against the Central England coal basins. In contrast, when the approach was applied to steeply inclined and sub-vertical seams (i.e. seams dipping from 45^{o} to 90^{o}), troughs of subsidence with two maxima covering large areas were obtained. This explained the discrepancy between empirical (i.e. observed) and predicted patterns of subsidence over coal mines in Spain.

Tan and Ranjith (2003) analyzed steel pipe effect on ground surface settlement and deformation at a tunnel face in cohesive clay soil. The FLAC 2D code and Mohr-Coulomb criterion were combined, and ground movement was assumed to originate from stress release around tunnel cavity. Steel pipe reduced tunnel deformation and induced 40-50% of ground subsidence on the surface. However, because the face deformation significantly contributes to tunnel closure and in order to take account of longitudinal pipe effect, either 3D or axisymmetric analysis is recommended for the improvement of results.

Karakus and Fowell (2005) investigated ground movement and stress redistribution above and around a tunnel in Austrian. The FDM and FEM codes and Mohr-Coulomb plasticity, Modified Cam-clay plasticity and Drucker-Prager plasticity models were applied to the materials. Subsidence and stress redistribution models were validated against data from the Heathrow Trial Tunnel excavation. FDM analysis predicted much closer surface settlement for the sidewall excavation than FEM predictions. Analysis results indicated horizontal stresses decrease from the geostatic to a low stress level owing to the dependency of stresses to the excavation process.

Predicted horizontal movements disagreed with subsurface settlement despite both agreed with inclinometer and magnetic measurements of tunnel enlargement because of the anisotropic behaviour of London clay due to elasticity modulus variation with depth. To improve both FDM and FEM predictions, such anisotropic behaviour should be considered.

Fuenkajorn and Archeeploba (2009) developed predicting analytical method of location, depth and size of caverns created at salt and overlying layers interface of the

stratified Maha Sarakham structure, northeast of Thailand. Statistical, numerical analyses and empirical formulae were combined and applied to the overburden elasto-plastic behaviour. Data from ground survey over the subsiding areas were statistically analyzed. Components and profile of ground subsidence were calibrated against the predicted subsidence with both FLAC 2D and UDEC codes.

The former code correlated subsidence components with cavern size and depth, and overlying strata properties (i.e. stiffnesses and strengths). Predicted subsidence overestimated calculated subsidence probably because the hyperbolic function used in subsidence calculation did not consider overlying strata stiffnesses. Whereas, the latter code revealed uncertainties of ground movement and sinkhole development owing to the complexity of post-failure deformation and joint movements in the overburden under super-critical condition as the analytical method is inappropriate for modelling ground subsidence under such condition.

Table 2.4 Summary of cases of study of FLAC 2D-based ground subsidence

References	Location	Results
Shahriar *et al*., 2009	Parvadeh coalfield, Eastern part of Iran	FLAC 3D predicted subsidence profiles were compared to measured profile and profile functions. FDM underestimated maximum subsidence (i.e. S_{max}) by 30 % than measured and profile subsidence. This is because FDM neglected residual subsidence while profile function predicted final subsidence trough. Additionally, FDM predicted uplift over the panels' rise side at the surface and confirmed by visual observations. Measured profile method was more devoted to modelling downwards ground movement. Depth increase shifted the position of maximum subsidence in shallow coal seams towards panel rise side.

Wang *et al*., 2008	Beijing, China	FDM was used to determine ground subsidence law and profile during construction of the Beijing fifth line metro. Simulation results showed increase of surface settlement ahead of the main face. This necessitates close attention to upper structure change during the construction of the tunnel and reinforcement measurement should be taken.
Zangerl *et al*., 2008	Gotthard highway tunnel, Central Switzerland	High magnitude of levelling-based subsidence above Gotthard tunnel was of concern. Unexpected magnitude of ground settlement is generally associated with large-scale consolidation as a result of groundwater drainage and pore-pressure changes around the tunnel. FDM and FEM combined results showed that observed subsidence was a consequence of fracture deformation and poro-elastic consolidation of the intact matrix.
Shen *et al*., 2006	Shanghai, China	The FDM and FEM were combined for estimating land subsidence associated with groundwater withdrawal. FDM enabled spatial discretization and FEM temporal discretization of governing equation of groundwater seepage. The results showed good agreement with those from Terzaghi's one-dimensional consolidation theory and oedometer test.
Coulthard *et al*., 1988	Coalfields, New South Wales, Australia	FLAC 2D and UDEC were used to model underground mining induced subsidence. The results showed that small spans of excavation roof deform essentially as elastic beams, with possible separation and slip along bedding plane fractures. Large spans of excavation result into collapse of immediate roof

		leading to upper strata deformation increase. Maximum subsidence is a function of excavation thickness.

The above studies clearly show the efficiency of numerical methods in modelling ground subsidence known all parameters involved in ground subsidence occurrence. Though the studies produced valuable results, none of them focused on the mechanism of underground excavations related ground subsidence. As a consequence, no or less attention was given to the effects of factors such as lithology, faulting considered to significantly control the occurrence of subsidence and profiles of trough on the ground surface. Ground subsidence occurrence should be considered as a cause and effect process (Szostak-Chrzanowski *et al*., 2003). In this regard, both causative factors and resulting effects have to be considered in the modelling process. Causative factors include the mechanical behaviour of the overlying formation, the layout of the mine workings, including size and depth of excavation, and so forth.

Additionally, Akcin *et al*., (2006) showed that ground subsidence is a result of the collapse of strata from the mining production plane to the surface owing to orebody extraction-induced stress and strain redistribution. This may be assessed in terms of roof-to-floor convergence and stress-strain state propagation upwards the surface. Furthermore, Matsuki *et al*., (2009) and Henk, (2006) demonstrated the influence of geological features (e.g. fault, joint and fold) on occurrence of subsidence and patterns of stress and strain distribution within undermined rock. Consequently, such controlling factors should be considered in simulating ground subsidence process. Therefore, in modelling patterns of stress and deformation distribution, and resulting ground subsidence associated with underground mining, particular attention should be given to such controlling factors.

2.8 Summary

Mining activity, either surface or underground involves stress-strain state redistribution as a result of excavation of orebody and generally results in mass movement on the surface. This chapter has examined some fundamental concepts and relevant features to the understanding of geomechanics processes, and resulting ground subsidence associated with underground mining. It also provides an overview of previous studies on the subject and the use of our methodology. Among relevant investigated concepts is the stress state redistribution. Some monitoring techniques of mine roof closure, roof-to-floor convergence and ground subsidence have been reviewed.

The chapter has also examined key factors of mine roof closure and ground subsidence, and modelling methods. An emphasis has been given to finite difference method (FDM) based on the Fast Lagrangian Analysis of Continua (FLAC 2D) code used in this research for simulating mining potash and modelling mine workings convergence on the basis of measured convergence patterns.

Chapter 3
The area of study:
Boulby mine

3.1 Introduction

The Boulby mine is operated by Cleveland Potash Ltd, producing potash and salt minerals.

The North-Eastern England potash seam was discovered in 1939 by D'Arcy Petroleum Company from a borehole drilled for oil and gas. Because of the seam depth and the lack of technology for deep-mining, the extraction of potash was limited despite the drilling exploration conducted between 1948 and 1952 revealed the richness of the deposit (David, 1996; Cook, 1974).

The availability of deep-mining technology enabled the Imperial Chemical Industries (ICI) to begin mining in 1968 with the sinking of two main shafts. Each shaft is 1,100 metres deep and 5.5 metres in diameter and both shafts pass through the Bunter Sandstone aquifer (Hebblewhite, 1977). The excavation of potash started in 1973 after the completion of the shafts. The surface installation consists of a site of 32.4 hectares with the shaft entrances, an ore treatment plant and a rail loading facility (Kemeling, 2006; David, 1996).

The Boulby potash mine is currently one of the deepest active mines in Western Europe. The mine is located in the sensitive coastline area of the North Yorkshire Moors National Park in the East coast of Northern England (Figure 3.1). The area lies at the boundary of a number of authorities and two regions, Yorkshire and the Humber and the North East (Highley *et al*., 2006). Mining activities at Boulby extend over approximately 300 km^2, measuring 20 kilometres North-South and 15 kilometres in East-West direction. The main shaft location is at approximately $54^o51'$ North and $1^o15'$ West in geodetic coordinates, or N51819W47610 in OSGB coordinates (Kemeling, 2006).

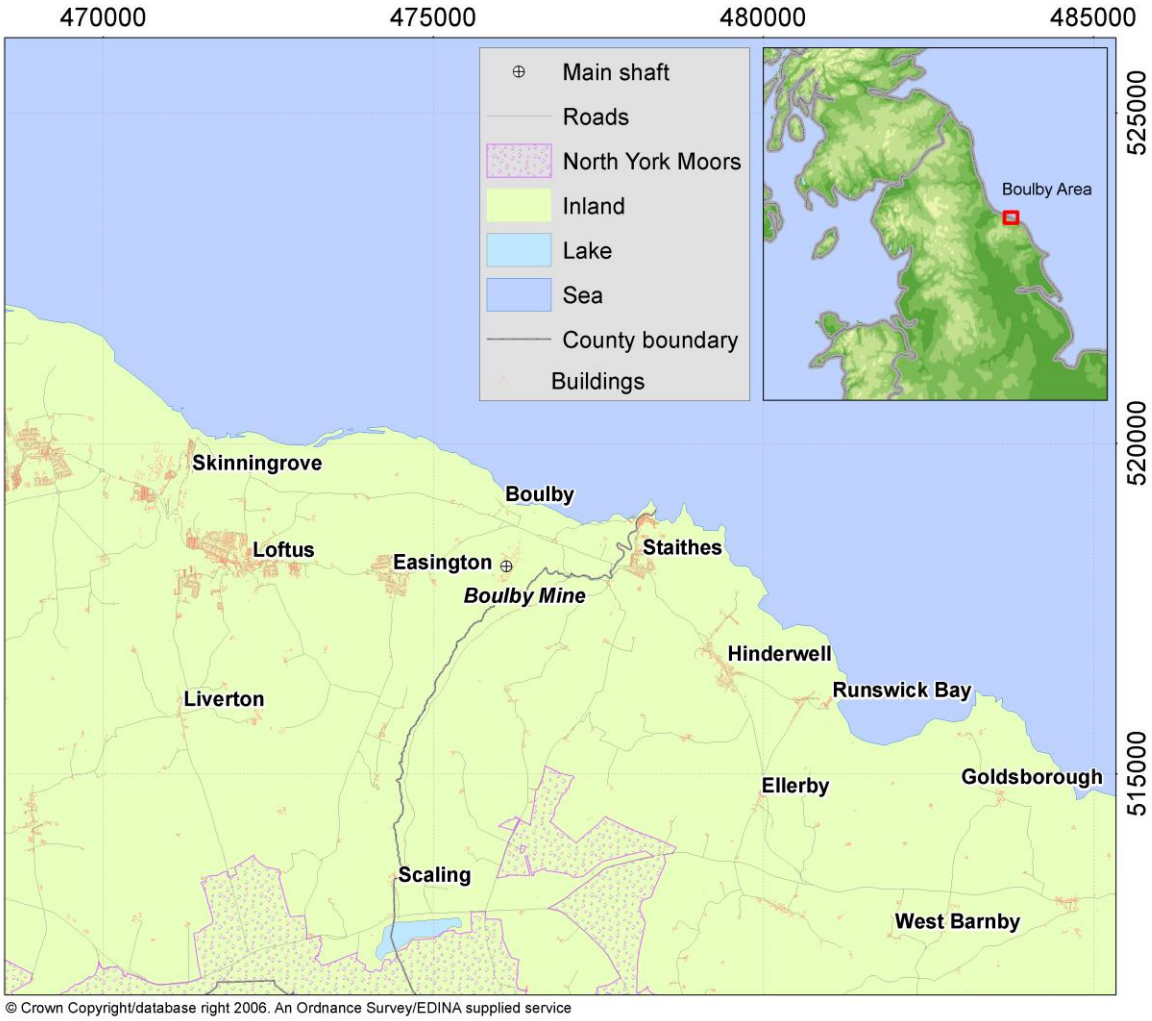

Figure 3.1 Study Location map of the Boulby Mine, N. Yorkshire (from: Kemeling, 2006)

The mining of potash and salt takes place from Permian aged rocks zone at depth around 1,100 meters. The potash seam ranges between 1,100 meters below sea-level in the North, increasing to between 1,200 and 1,500 meters below the land surface in the South with a seam ranging in thickness from 0-20 m with 7 m of average. The difference in depth is due to the fact that the potash seam dips at a shallow angle of 5^0 from North-West to South-East (Kemeling, 2006; Hebblewhite, 1977; Cook, 1974).

3.2 The nature and origin of potash deposits

Evaporite deposits precipitate as a result of the evaporation of sea water. The Yorkshire evaporites were deposited during the Permian age in the Zechstein Sea formation and

formed by crystallization from the saturated brine solution (Hebblewhite, 1977). All the evaporites have commercial value. Gypsum is used for manufacturing plaster, plasterboard and tiles for building purposes. Rocksalt is for domestic use and roads de-icing during winter, and is also used for the production of caustic soda in industries. Potash is primarily used as a fertilizer and also in industries.

The commonly occurring evaporites are the least soluble calcium sulphates ($CaCO_3$) or limestone-dolomite ($MgCO_3$), gypsum ($CaSO_4$-$2H_2O$), anhydrite ($CaSO_4$), rock salt or halite (NaCl), and the most soluble potassium and magnesium salts. The latter primarily consist of soluble potassium chloride or sylvite (KCl) and is the most valued for its potassium (K) and higher K_2O equivalent

For comparison reasons, the most common potassium minerals and deposits are expressed in terms of the oxide equivalent, K_2O equiv. (Table 3.1) (Hebblewhite, 1977; Cook, 1974; Patchet, 1970).

Table 3.1 Common potash minerals (from Hebblewhite, 1977; Cook, 1974 & Patchet, 1970)

Mineral name	Composition	Equivalent K_2O content (%)
Sylvite	KCl	63.1
Carnallite	$KCl.MgCl_2.6H_2O$	17.0
Kainite	$KCl.MgSO_4.3H_2O$	18.9
Polyhalite	$K_2SO_4.MgSO_4.2CaSO_4.2H_2O$	15.5
Langbeinite	$K_2SO_4.MgSO_4$	22.6

The mined sylvinite mineral at Boulby mine is a mixture of sylvite (KCl) and halite (salt, NaCl) in varying proportions. The potash salts occur at two beds: the most extensive Boulby potash bed and the higher Sneaton potash bed. In both beds, sylvite is the main potassium mineral though potash in the form of Carnallite ($KCl.MgCl_2.6H_2O$) and polyhalite ($K_2SO_4.MgSO_4.2CaSO_4.2H_2O$) also occurs.

3.3 The Boulby area

3.3.1 Geological and tectonic evolution of Boulby area

The Boulby area is part of the approximately horizontally bedded Cleveland Basin sedimentary deposits. It initially formed part of the Upper Permian Zechstein Sea which covered the majority of the lands of the current Europe (Kemeling, 2006). It is during this period the evaporite formations were deposited (Hebblewhite, 1977). Boulby area is situated within the depressive Cleveland basin formed as a result of differential subsidence from the end of Triassic (Rhaetian) period, followed by periodical massive sedimentation, erosion and uplift (Rawson and Wright, 2000; Rayner and Hemingway, 1974).

Tectonically, the area is nowadays naturally stable despite experiencing continuous marine erosion. This relative stability has been however disturbed over the past three centuries by the impact of anthropogenic processes such as mining-induced subsidence (Rawson and Wright, 2000). The evolutive geological and tectonics processes of Boulby occurred over four main periods: the Carboniferous (363-290 Ma), Permian (290-245 Ma), Triassic (245-208 Ma) and Jurassic (208-146 Ma) periods.

The Carboniferous strata underlay most part of the Northeast of England (Johnson, 2001). The Lower Carboniferous basement of the Cleveland area formed between 363 and 320 Ma (Anderson and Owen, 1980). The upland of East of England in the commencement of the Carboniferous period may have originated from the Caledones orogeny which formed the Pennines. The Carboniferous period was followed by a long and alternating period of eustatic transgression and regression (i.e. change of sea level due either to climate change or tectonic plates' movement).

Favourable equato-tropical climate conditions as England and Wales gradually lowered led to the expansion of the present landmass in the present British Isles (Kemeling, 2006; Simms *et al*., 2004). The buried Upper Carboniferous tropical forests produced the coal beds formerly mined in the Midlands and Northern England. Because of the depth of occurrence coal mining in Boulby area is not economic so far. The Permian period is significantly important in the North-East of England because of the

outcrop of minerals – e.g. potassium chloride (Johnson, 2001). Huge earth deformation commenced during the transition to this period (Anderson and Owen, 1980).

The evaporites at Boulby area were formed during three cycles in the Lower Permian period and were set down during the Upper Permian period (Kemeling, 2006; Talbot *et al*., 1982). The flat topography of the Boulby area may have caused a rapid but smooth incursion of the Upper Permian Zechstein Sea into the Cleveland Basin resulting in the valued evaporites observed at the present time in the area. Evaporites experienced cycles of subsidence whose evidence may be found in the Permian layers. Folds induced plastic deformation and flow of materials while gravitational forces induced uplift and interaction of evaporite layers with the Triassic Sherwood Sandstone (Kemeling, 2006; Rayner and Hemingway, 1974). Potash rock at Boulby mine is extracted from the sub-horizontal zone of chloride minerals of the third Zechstein Cycle (EZ3) (Talbot *et al*., 1982).

According to Rayner and Hemingway (1974), the Yorkshire Triassic is not well known because of the glacial deposits that masked large section of the outcrop. However, it is believed that the deposits result from the continuous sedimentation which occurred between the Permian and Triassic periods. The Triassic is a period of deposition of significant quantity of sandstones and mudstones (e.g. Mercia Mudstone-Upper Triassic) under shallow marine environments (Johnson, 2001). Permian layers are overlain by fossiliferious Triassic sandstone and layers of marl. Mercia Mudstone is made of laminated red-brown dolomitic mudstone or silty mudstone. Gypsum beds, anhydrite and halite are also found within the Mercia mudstone segment. The end of the Triassic period occurred with the deposition of a thin grey material layer in the Rhaetian Era (219-213 Ma) (Kemeling, 2006).

The Jurassic depositional sequence in the Cleveland basin was essentially formed in marine environments. The stratigraphic sequence in the basin was set down in marginal marine to non-marine environments (Hesselbo, 2008). Osborne and Bowden (2002, in Kemeling, 2006:74) showed that Cleveland basin transformation from shallow sea into coastal delta begun during the Jurassic period from 213 Ma during the uplift of the extensive granite Market Weighton Block to the Cleveland basin south. The

Lias layer deposited during the Lower Jurassic (208-178 Ma) currently forms the flat wavecut platforms of the coastline. The Middle Lias (e.g. the Cleveland Ironstone) was formed during the Upper Pliensbachian-Domerian period (Kemeling, 2006; Lim, 2006).

Other periods of the geological and tectonic transformations of the Cleveland basin are the Cretaceous, Tertiary and Quaternary periods.

Massive extinction of species occurred at the end and beginning of the Cretaceous and Tertiary periods, respectively between 144-2 Ma. The Yorkshire Cretaceous system is divided into two main groups: the Lower Cretaceous clays with no topographical expression and the Upper Cretaceous Chalk which forms the principal topographic feature of some coastal scenery (Rayner and Hemingway, 1974). The terrestrial Cleveland basin occurred at the end of the Jurassic era which marked the end of deposition. The increase of sea-level resulted in the deposition chalk period. Traces of Cretaceous rock at Boulby area extinguished as a result of erosions in 70 Ma.BP (Rawson and Wright, 2000).

The Quaternary period covers the last two million years (i.e. 2-0 Ma) of the earth history and can be divided up into two parts: the Pleistocene and the Holocene. The former is during which cold and glacial episodes alternated with temperate and interglacial episodes while the latter is the elapsed time since the end of the last glaciation (Rayner and Hemingway, 1974).

It is during the Quaternary period that the whole area of North Yorkshire was buried in ice between 478,000 and 473,000 years ago. Massive erosion occurred and shaped the present day landscape beneath ice-sheets and glaciers (North Yorkshire Geodiversity Partnership, 2006). The contemporaneous Boulby area is the result of three periods of ice sheet movement and sea level change in the last 2 million years (Shennan, 1988 in Kemeling, 2006:75).

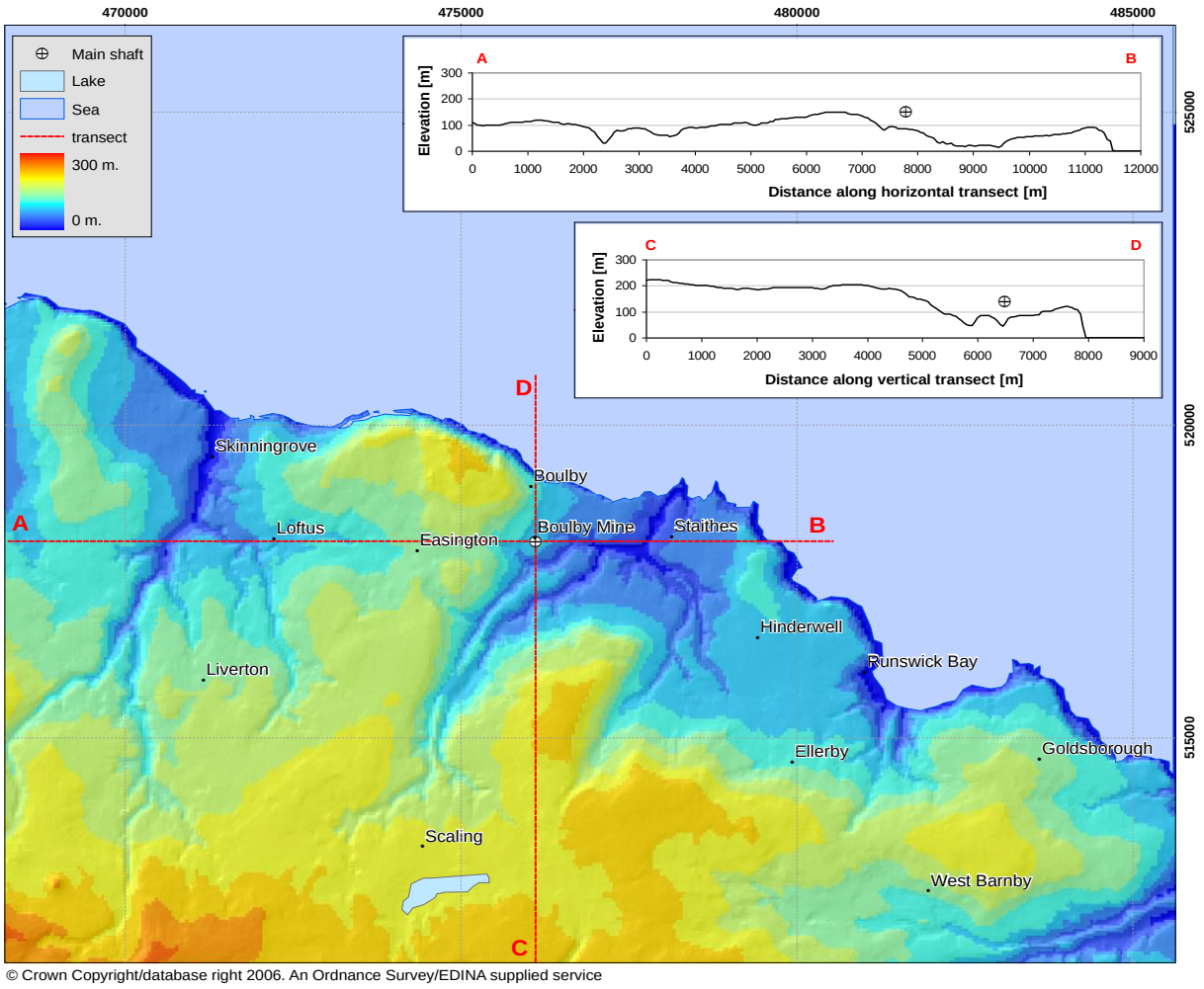

Figure 3.2 Digital elevation model (DEM), based on the Ordnance Survey Profile dataset (from: Kemeling, 2006)

Kemeling (2006:75, quoting Horton, 1979) emphasized that ice sheet from the North covered the Boulby area and units of glacial diamicton (i.e. poorly-sorted sediment containing a wide range of particles sizes) with minimum thickness of 30 m deposited across the area. The last glaciation, known as Devensian, caused the extension of ice along the present North Yorkshire coast impounding a number of valleys and resulted in flooding. With the retreat of ice sheets, gravel-sandy glacial diamicton deposited and covered the cliffs at Boulby; resulting in steeper parts in the South East and cliffs along the coast observed in the topography of the Boulby area. The present marine erosion originates from the sea level which raised around 9000 BP, but also the deforestation which probably commenced at the same period.

Successive transformations occurrence across the Boulby area resulted in a down sloping general trend of the area from the South-West to the North-East which follows three catchments formed in valleys draining into Skinningrove Beck, Staithes Beck and Runswick Bay (Figure 3.2). These valleys constitute the lowest parts of the Boulby area with irregular steeper coastline made of unstable dark Liassic shale and sandstone and small valleys (Kemeling, 2006; Lim, 2006).

3.3.2 The geological sequence of Boulby

Earlier drilled boreholes (1938-1939) showed significant potash thickness and the presence of brine. Strata overlying the potash at Boulby mine are mixture of marine sediments and evaporites, and most of strata are relatively thick (Cook, 1974). This stratigraphy is considered continuous across the whole Cleveland Potash Ltd concession area, and strata are flat and fairly regular (i.e. in composition) though beds thicknesses may vary within the area (Talbot *et al*., 1982; Hebblewhite, 1977). Consequently, strata sequence and description are based on borehole S20 drilled over the area (Kemeling, 2006; Hebblewhite, 1977) and also from 4-inch diameter cores from North Yorkshire (Patchet, 1970). The borehole locations (ordered on the basis of distance from the borehole S04 in North-West to South-East direction) and boundaries depth between layers (from boreholes data) are shown in Figure 3.3.

Generally, the geological sequence at Boulby may be classified into two groups of strata: the upper strata and the near-seam strata groups. The units present in each group are discussed in the following sections.

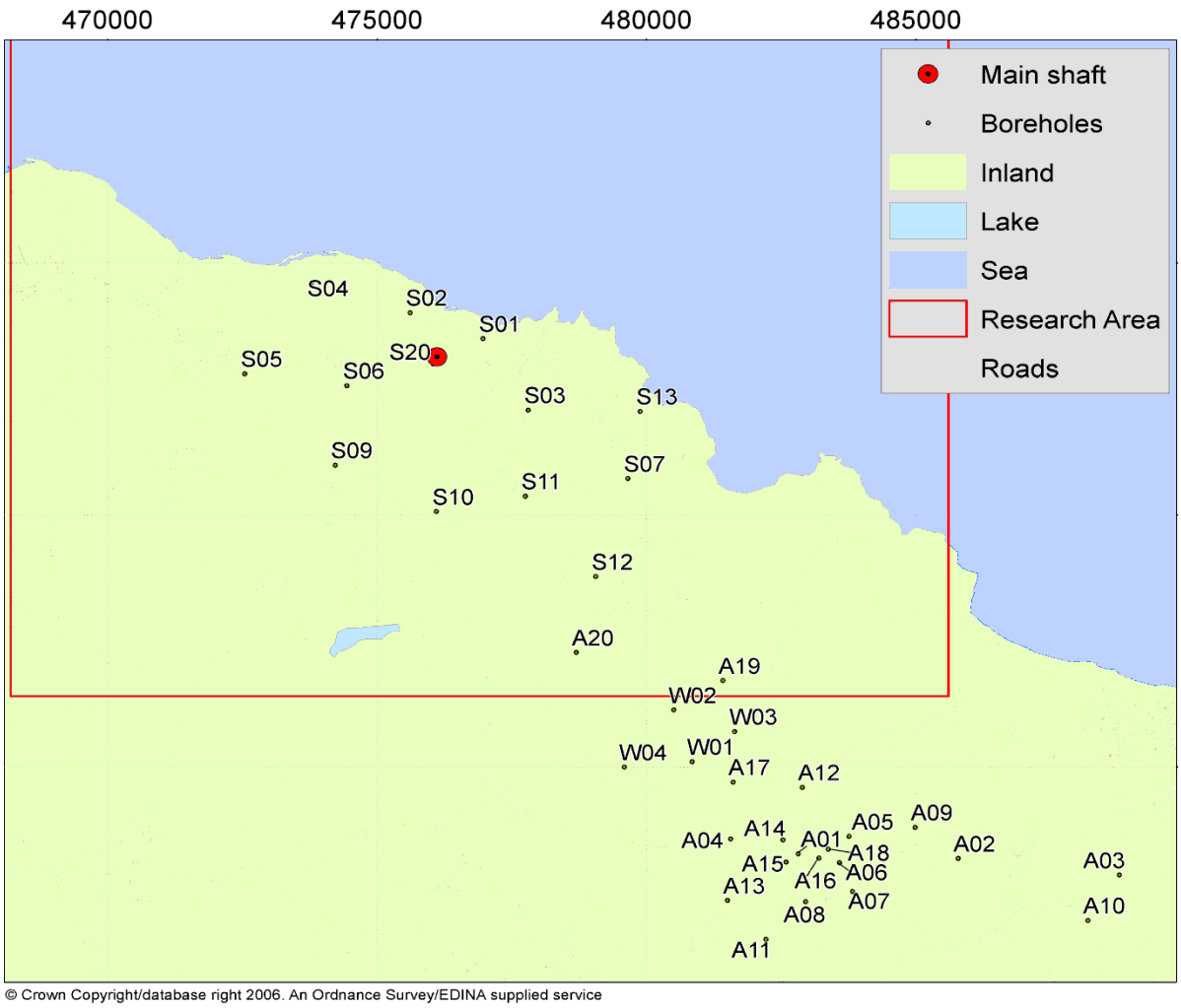

Figure 3.3 Borehole locations (37) in relation to the Boulby area (red square) (from: Kemeling, 2006)

3.3.2.1 The upper strata

Boulby area is mostly moorland used primarily for farming and sheep raising. The surface is covered with soil, glacial drift, and clays deposits underlain by the Estuarine Sandstone of Jurassic age composed of moderately permeable water-bearing massive sandstones. This sequence of rocks forms the reservoir of wells water and springs in the area. Below the Estuarine sandstone is found the Lias also of Jurassic age which could be divided into three parts: the Upper, Middle and Lower. The average thickness of Lias amounts 366 meters. The Lower Lias is the major bed and constitutes the three

quarters of the Lias rocks, and is made of shales and mudstones. The Middle Lias is composed of ironstone seams of 0-3 meters in the centre portion which were extensively mined in the late 1950's. The Upper Lias is the minor part of the series and is composed of shales with sandstone and clay bands (Cook, 1974; Patchet, 1970).

The Rheatic rock lies below the Lias and is the principal bed of Triassic age. This thinner stratum is laminated and averages about 15 meters thick. It consists mainly of shales and sandstones, and partings containing carbonaceous material.

The Rheatic bed is successively overlain by the Mercia Mudstone, the Mercia Salt and the Sherwood Sandstone. This series of strata constitutes the major Triassic Period in the area. The Mercia Mudstone is mostly gypsiferous. It is about 259 meters thick and contains bands of anhydrite, marls and sometimes sandstone layers. Structurally, the Mercia Mudstone is regular in composition and is impermeable. The Mercia Salt is an average of 9-30 meters thick though it does not occur over the entire mining area and also in the shaft area. It is often made of shale.

The Sherwood Sandstone is the only single stratum within the upper strata averaging about 305 meters thick. It is entirely constituted of massive red sandstones. Apart from the near-surface Estuarine Sandstones, the Sherwood sandstone is the only water-bearing stratum within the Boulby area. Drilled boreholes indicated water at high pressures despite small flows. However, higher flows noticed in some boreholes resulted from faulting in close proximity to the boreholes (Cook, 1974). Overall, water in the Sherwood sandstone is semi-saturated brine at high hydrostatic pressures. Because of the low permeability of the stratum, flow of the brine to the Upper Sherwood Mudstone is reduced. The exact position of the contact with the Upper Permian Marl at the base is difficult to be determined (Hebblewhite, 1977; Patchet, 1970).

The Sherwood sandstone overlies the Permian age strata from which potash is mined. They are mainly composed of the Upper Permian Marl and Zechstein Evaporites beds. The former is similar in appearance to the Mercia Marl averaging about 120 meters of thickness. It is red and primarily contains marls with siltstones and occasionally shale occurring in its centre. This impermeable bed forms the barrier

between the water-bearing Sherwood sandstone and the underlying evaporite rocks preventing flow of water downward to the mine workings (Patchet, 1970). The Zechstein Evaporites has the Upper Evaporite Group which consists of the Upper Halite and Upper Anhydrite. The Upper halite is made of massive rock salt of about 46 meters of thickness. The halite is coarse-grained varying in colour from orange to brown (Cook, 1974; Buzdar, 1968).

Generally, rocks in this zone possess elastic characteristics therefore, are likely to deform accordingly (Patchet, 1970). The general geological succession of the upper strata is given in Figure 3.4.

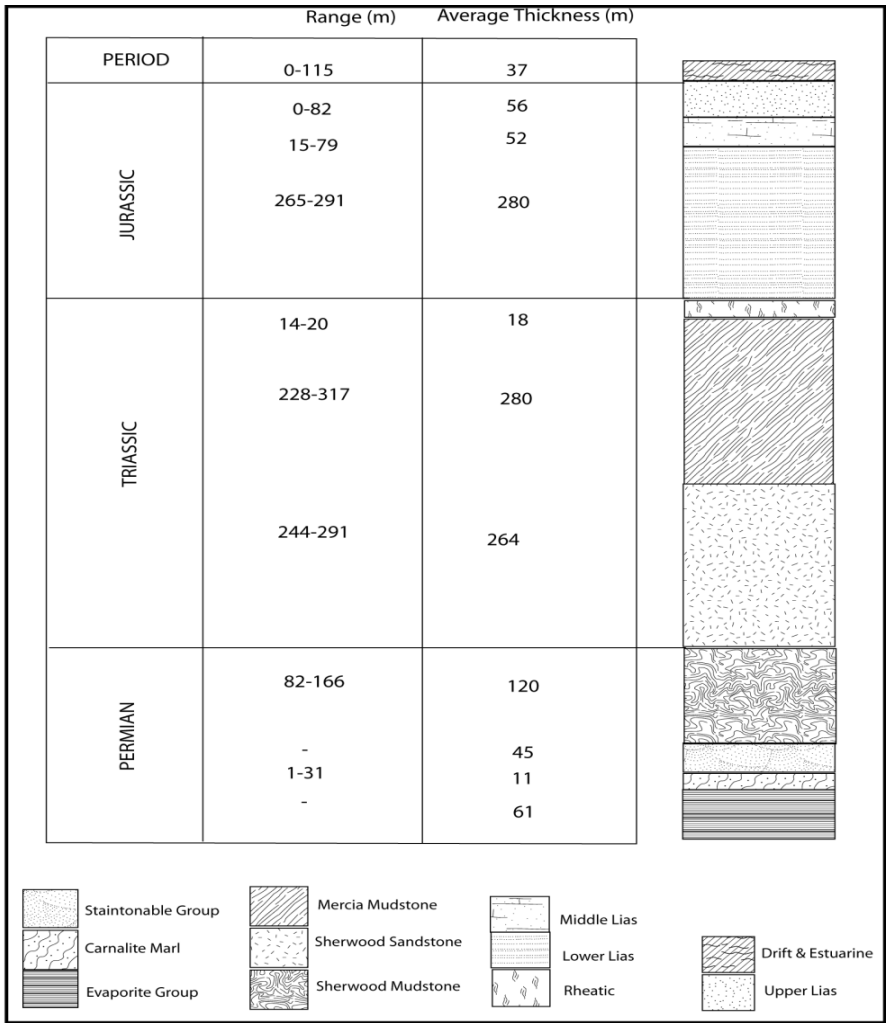

Figure 3.4 Schematic cross-section of the upper strata geological succession

3.3.2.2 The near-seam strata

The near-seam strata are composed of the Upper Anhydrite, Carnallite marl, Halite parting, Middle potash and Middle halite beds. The Upper Anhydrite is about 8 meters thick varying locally and gradually. It is the strongest rock in the North Yorkshire and formed of three zones with varying thicknesses (Patchet, 1970). The thickest and moderate grain size zone on the top contains primarily of pseudomorphs and veins halite. The middle and bottom zones are fine-grained and contain halite and silt, respectively. The bottom zone is moderately impermeable and together with the Upper Sherwood Mudstone forms the major barrier to the influx of water through the evaporite strata into the mine workings (Caughill and Beddoes, 1996; Hebblewhite, 1977). Generally, Anhydrite behaves elastically though this behaviour may be altered by the type and amount of impurities present in the rock (Patchet, 1970).

The Carnallite marl is composed of mudstones and marls with low cohesion. This bed is the weakest of strata in compression and tensile because of the presence of halite and potash veins within it which affect its strength (Patchet, 1970).

The Halite parting is a fairly uniform thin bed with an average of 2 meters thick. The upper and lower delineations are often variable, and the lower demarcation is difficult to determine. Lithologically, the Halite parting may be absent within the near-seam sequence.

The Middle potash is the only potash stratum in the Boulby area with an average of about 7 meters thickness. The Middle (or Boulby) potash bed is fairly uniform and changes within it occur gradually. It varies in colour from an iron-staining related deep rich red to greyish and colorless. The rest of the Boulby potash bed is mainly made of halite and anhydrite with clay. Borehole measurements at the level of Boulby potash gave temperatures of rock between 35 to 45^{o}C.

Below the potash seam is the Middle halite with massive halite bed of 45 meters average thickness. More competent and homogeneous, this bed contains in its top 1 to 3 m portion of argillaceous materials. The Middle halite is generally coarse-grained and grey to clear in colour despite the finer-grained orange halite locally bands (Cook, 1974;

Buzdar, 1968). Underlying this bed are successively the Middle anhydrite and Upper magnesian limestone rocks averaging 10 and 30 m thick, respectively (CPL, 2008; Cook, 1974). The geological succession near-seam is shown in Figure 3.5.

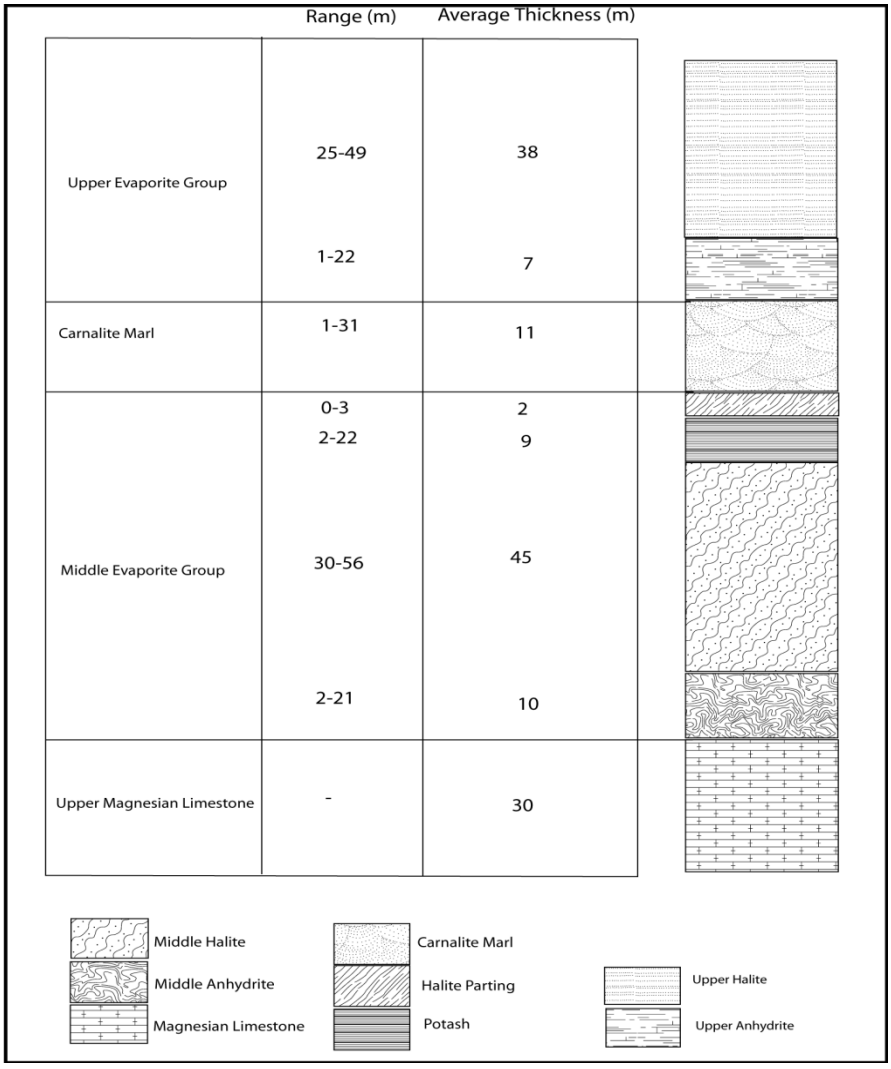

Figure 3.5 Schematic cross-section of the near-seam geological succession

Despite slight strata thickness variations observed across Boulby area, the geological succession is continuous. Strata are flat and the geological structure is fairly regular throughout the mining area (Kemeling, 2006; Talbot *et al*., 1982; Hebblewhite, 1977; Cook, 1974; Patchet, 1970).

3.3.3 Geological structures at Boulby

Fissures exist in Boulby area despite the apparent regular geological sequence of the mining area. At Boulby, faulting occurs on the surface near the south-eastern boundary of the mining area. However, the occurring faults may not continu down to the evaporite deposits though small throws are found within the Middle potash.

Cook (1974) and Patchet (1970) showed that rocks sequence throughout the North Yorkshire dips eastward. Most of the upper post-Permian beds fairly dip at about angle between 2^{o}-3^{o}, and occasionally reaching 5^{o}. However, the near-seam evaporites across the area dip between 3^{o} and 5^{o}. They also indicated that the boundary between the Boulby potash and Middle halite forms a zone of weakness with less resistance to shear.

Hebblewhite (1977) pointed out fractures filled with water from the Sherwood sandstone bed and localized within the Upper Permian marl up to 75 m above the potash were found during the sinking of the shaft.

3.3.4 Geological and structural setting of the Cleveland basin

The geological and structural setting of the Cleveland basin is depicted in Figure 3.6.

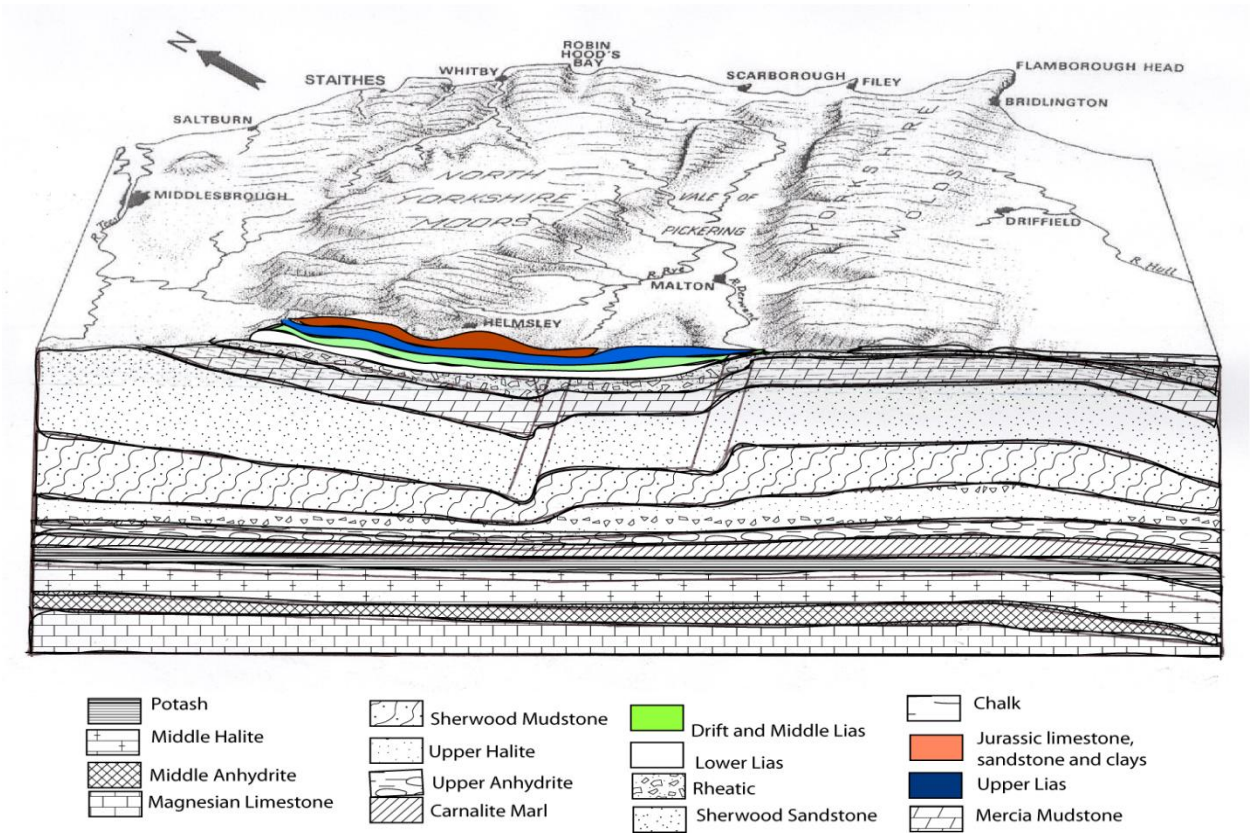

Figure 3.6 The geological and structural setting of the Cleveland basin. The geology dips north-south resulting in the exposure of older sediments northwards. The near-seam evaporites fairly dip eastward. Faulting which occurs on the surface does not cross Sherwood mudstone (Adapted from Lim 2006; Kent, 1980).

3.4 Geotechnical properties of strata

3.4.1Laboratory tests

The geology of the North Yorkshire has been intensively studied for many years and the mechanics of rocks at Boulby area has long been investigated from the initial exploration stages up to present time. The Department of Mining Engineering at the University of Newcastle upon Tyne carried out fundamental research on the mechanical and rheological properties of strata from rock cores obtained from exploration boreholes (Cook, 1974). The results of research were applied to the design of the mine excavations and shafts. Intensives laboratory modelling and *in-situ* measurements were

also carried out to monitor ground conditions in the mine in order to provide realistic estimates of parameters for the design of mine (Hebblewhite, 1977).

Hebblewhite (1977) investigated the design of potash underground mine in order to obtain maximum and efficient extraction ratio, long-term stable and safe workings conditions and no damaging subsidence on the surface. He combined theoretical, laboratory and *in-situ* analyses for determining design criteria for an optimum mining layout to satisfy the aforementioned requirements.

Additionally, data from underground measurements of stress, time-dependent deformations around mine roadways and strain distributions within pillars were gathered. These data were associated with subsidence monitoring data and laboratory based-rheological properties of overlying strata for numerical modelling the mining layouts. Based on the gravitational force-related method, Hebblewhite determined values of -27.4 MN/m^2 and -9.1 MN/m^2 of virgin vertical and horizontal stresses, respectively at 1097 m seam depth for a given Poison's ratio value of 0.25.

Cook (1974) carried out triaxial creep laboratory tests on the rheological properties of evaporite strata to analyze the stability of shaft excavations through the Upper evaporite strata. After modelling the excavation of the shaft in halite, Cook instrumented shaft No. 2 during its sinking. The study showed that 0.46 m between rock and concrete shaft enables lining through Upper halite for the time-dependent closure of the excavation. Rock mechanics sites were installed in the mine workings, and roadway closures and strata deformations were monitored for the first time.

Patchet (1970) examined the mechanical properties and strengths of the entire geological succession at Boulby. A series of laboratory tests, including tensile, uniaxial and triaxial compression, and compression uniaxial creep tests were carried out on roof, floor and near-seam materials. Tensile tests showed that the Carnallite marl is very weak in tension, whereas the near-seam beds have a fairly uniform strength. The Boulby potash is also weaker in tension than both Halite partings and Middle halite. The Sherwood sandstone and Upper Anhydrite however, are very competent in tension and twice stronger than the near-seam beds.

Uniaxial compression results also indicated the weak nature of Carnallite marl. However, the Middle potash was stronger than the Halite partings and Middle halite in contrast to its tensile behaviour. Additionally, the tests showed that the Sherwood sandstone and Upper Anhydrite are very strong in compression. This latter bed behaves elastically though impurities may alter this behavior.

Carnallite Marl is competent (i.e. having higher mechanical strength) under triaxial conditions despite being a weak bed. Its strength increases and stringers and veins have insignificant effects on the ultimate strength of the rock. The strength of the near-seam materials, including the Boulby potash and Upper Anhydrite substantially increases under triaxial conditions. The creep tests showed visco-elastic behaviour of the Middle potash.

Buzdar (1968) carried out initial laboratory investigations on the mechanical properties of sedimentary rocks with reference to potash. The work was intended to provide the tensile and compression strengths of materials required for the development of the mine. Buzdar determined the mechanical properties of rocks for the development of the Potash mine on the North Yorkshire Coast. This experience was then utilized for planning extensive investigations and therefore, development of the mine at Boulby.

Laboratory investigations on core samples from boreholes 1067 meters deep from Newton Mulgrave and Staithes included tensile, uniaxial compressive and triaxial compressive tests. Roof materials comprised carnallite marl, halite partings and layer of mixed sylvinite above the potash seam, and floor materials primarily consisted of pure halite. The tests results are provided in Table 3.2.

Overall, triaxial compression tests showed that ductility and strength of Carnallite marl and Halite increase with increases in confining pressures (Buzdar, 1968). The Carnallite marl is weaker than the halite partings and pure halite in the roof and on the floor, respectively.

Table 3.2 Materials parameters from tensile and triaxial tests

		Triaxial tests		Tensile tests	
		Elastic modulus (GPa)		Strength (MPa)	
		At Newton Mulgrave	At Staithes	At Newton Mulgrave	At Staithes
Carnalite marl		4 - 5	2.9	1.4 - 1.7	0.9 - 1.6
Halite	Roof	5	-	1.0 - 1.1	-
	Floor	9	-		

3.4.2 Similar lithologies

Evaporite deposits generally occur at depth and are liable to deformation as a result of gravitational forces. Although evaporite deposits occur within relatively similar formations, deposits at Boulby could be unique owing to the great depth at which they occur. Such transformations have influenced the geological sequence of deposits and overburden across the area (Buzdar, 1970). Herewith some analogues of potash mining with close similarity to the Boulby geology.

Potash deposits have been mined since 1959 at Saskatchewan in Canada at depth between 1,100 m and 1,450 m. These are flat-lying interbedded deposits within the upper Patience Lake Member of the Prairie Evaporite Formation of about 200 m thick (Halabura and Hardy, 2007; Boys, 1990; Annan *et al*., 1988).

Three intervals make the Central Saskatchewan stratigraphy: (a) the upper sequence extending from the surface to about 175 to 200 m deep and consists of glacial tills, gravels, and clays; and forms the fresh water aquifers; (b) the medial sequence which extends from the base of the glacial sediments to a depth of about 800 m made of Jurassic to Cretaceous shale, siltstones, and sandstones and forms the brackish reservoir water; (c) the lower sequence extending from the Paleozoic/Mesozoic Unconformity to below 1,900 meters and consists of Cambrian to Upper Devonian carbonates, evaporites and basal shales and sandstones. The strata above the Central Saskatchewan form the Phanerozoic sequence underlay the Precambrian sequence of gneisses and granites with the Upper Devonian rocks below the Precambrian rocks.

The Prairie Evaporite Formation is made of: (a) the Patience Lake Member, also known as the upper potash-bearing beds, primarily made of sylvinite and halite rocks, and locally with Carnallite marl and Anhydrite minerals. The evaporites are overlain by bedded halite capped by the dolomitic mudstones of the Second Red Beds of the Dawson Bay Formation within the Manitoba Group; (b) the salt and potash of the lower members of the Prairie Evaporite Formation, and the carbonates of the Winnipegosis Formation (Boys, 1990). Mining activity at Saskatchewan results in creep (i.e. slow plastic deformation) of the evaporite rocks as a result of stress redistribution and in development of stress-relief cracks particularly within the weak clayey zones (Annan *et al*., 1988).

Rock salt is also mined at Winsford mine, the oldest mine in Britain at shallow depth between 130 m and 220 m below surface. The rock salt lies in the Permo-Triassic formation within the Cheshire basin of the North-West England. It is interbedded with bands of marl within the Northwich Halite Formation and has 30 m of thickness consisting of 95% of sodium chloride (Swift and Reddich, 2005).

The geological sequence of the Winsford area is essentially composed of Triassic formations. The top of the Winsford area is covered by glacial drift and sand or clay of Quaternary age. This formation is underlain by an unconformity of disintegrated red and grey marls resulting from the weathering and solution of the glacial drift and sand or clay on the top. Below this formation is found the Wych Mudstone Formation, the upper part of the former Middle Mercia mudstone. The Wych Mudstone Formation is overlain by the Byley Mudstone Formation which represents the Middle Mercia mudstone, the Northwich Halite Formation formerly known as the Lower Mercia Saliferous Beds and the Bollin Mudstone Formation formerly known as Lower Mercia mudstone.

3.4.3 Geotechnical parameters of strata

The geotechnical parameters of strata at Boulby mine are primarily the deformability and strength properties, and tensile strength of the formations; as listed in Tables 3.3 and 3.4, respectively.

Table 3.3 Geotechnical parameters of geological units at Boulby mine (from CPL, 2008; Liang *et al*., 2007; Foley, 2006; Swift and Reddish, 2005; Caughill and Beddoes, 1996; Bell, 1994; Jeremic, 1994; Coulthard and Bell, 1993; Hebblewhite, 1977; Cook, 1974; Patchet, 1970)

STRATA	GEOTECHNICAL PARAMETERS			
	Deformability Parameters		Strength Parameters	
	Young's modulus (GN/m^2)	Poisson's ratio	Cohesion (MN/m^2)	Friction (degrees)
Drift & Middle Lias	26.6	0.37	0.02	25
Lower Lias	16.8	0.20	0.02	33
Rheatic	13.0	0.05	-	-
Mercia Mudstone	34.05	0.08	6.0	41
Sherwood Sandstone	20.8	0.10	11	45
Sherwood Mudstone	20.3	0.07	26	47
Upper Halite	1.90	0.24	16	35
Upper Anhydrite	19.09	0.22	17	37
Carnallite Marl	5.03	0.35	3.0	35
Boulby Potash	7.23	0.27	10.0	36
Middle Halite	23.7	0.28	10.0	40
Middle Anhydrite	30.6	0.32	26.3	41
Upper Magnesian Limestone	27.0	0.27	6.72	42

Table 3.4 Geotechnical parameters of geological units at Boulby mine (from CPL, 2008; Liang *et al*., 2007; Foley, 2006; Swift and Reddish, 2005; Caughill and Beddoes, 1996; Bell, 1994; Jeremic, 1994; Coulthard and Bell, 1993; Hebblewhite, 1977; Cook, 1974; Patchet, 1970)

STRATA	Thickness (m)	GEOTECHNICAL PARAMETERS		
		Density x10^3 (Kg/m^3)	Tensile strength (MN/m^2)	U.C.S. (MN/m^2)
Drift & Middle Lias	110	2.5	3.9	44.7
Lower Lias	295	2.6	3.88	77.57
Rheatic	18	2.5	4.24	51.59
Mercia Mudstone	266	2.7	2.76	113.0
Sherwood Sandstone	335	2.5	5.20	59.86
Sherwood Mudstone	120	2.3	6.86	85.74
Upper Halite	38	2.2	1.59	30.99
Upper Anhydrite	7	2.8	6.07	49.78
Carnallite Marl	11	2.3	1.24	14.66
Boulby Potash	9	2.1	1.79	29.03
Middle Halite	45	2.2	1.63	26.77
Middle Anhydrite	10	2.79	8.2	91.7
Upper Magnesian Limestone	30	2.8	1.58	54.6

Tables 3.3 and 3.4 summarize the mechanical and rheological properties of strata at Boulby mine and similar lithologies gathered from literature review on various laboratory tests. Although the data are from technical literature figures in Table 3.3 show low values of Poison's ratio of strata in the intermediate and main zones. Such unusually low values suggest that the materials in these zones are subject to a lower horizontal stress component (i.e. lateral restraining pressure) though sporadic

observations indicate a higher horizontal stress component in the non-creeping strata above upper halite is expected from the regional stress field of Britain and Europe (Lachenicht and Aswegen, 1999). High horizontal stress may originate from tectonic forces due probably to faulting and folding (Hebblewhite, 1977). As a consequence, the materials will expand laterally when compressed as the compressed molecular bonds within the material lattice accommodate the stress. This may result in the development of ground subsidence more laterally than vertically hence, lowering the magnitude of maximum subsidence on the top of excavation.

3.5 Mining activity at Boulby

Extraction methods for underground mining mostly depend on the subsurface conditions (e.g. virgin vertical and horizontal stresses) and the sensitivity of the surface to disturbances associated with the underground activity (Brady and Brown, 2006).

3.5.1 Room-and-pillar mining

Room-and-pillar mining is a stress-relief method initially developed for extracting as much coal as possible while providing roof control by means of pillars (Holzer, 1984). The method is effectively used at Boulby for mining potash deposits by leaving parts of the unmined deposit to support the overlying strata (Brady and Brown, 2006; Hartman and Mutmansky, 2000).

Two parallel arterial roadways of 8 metres wide and 4 metres high are excavated into the underlying stronger rock salt (i.e. with respect to potash) and serve as principal access to the current mining areas, and also enable exploration and development of new areas for potash production. From these two roadways, four parallel chambers 8 meters wide and 3.40 meters high are then driven into the overlying weaker potash deposits, separated by 2.5 to 4 meters wide pillars (Kemeling, 2006; CPL, 2004). The mining patterns at Boulby mine are symmetrically positioned.

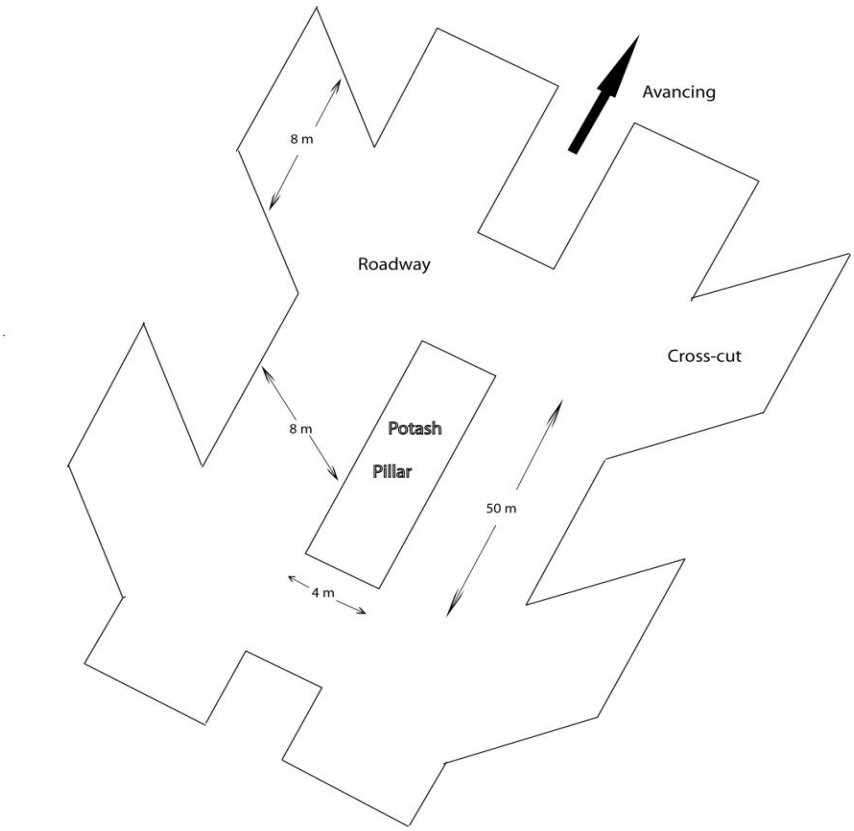

Figure 3.7 Two roadways in room-and-pillar mining for the production of potash

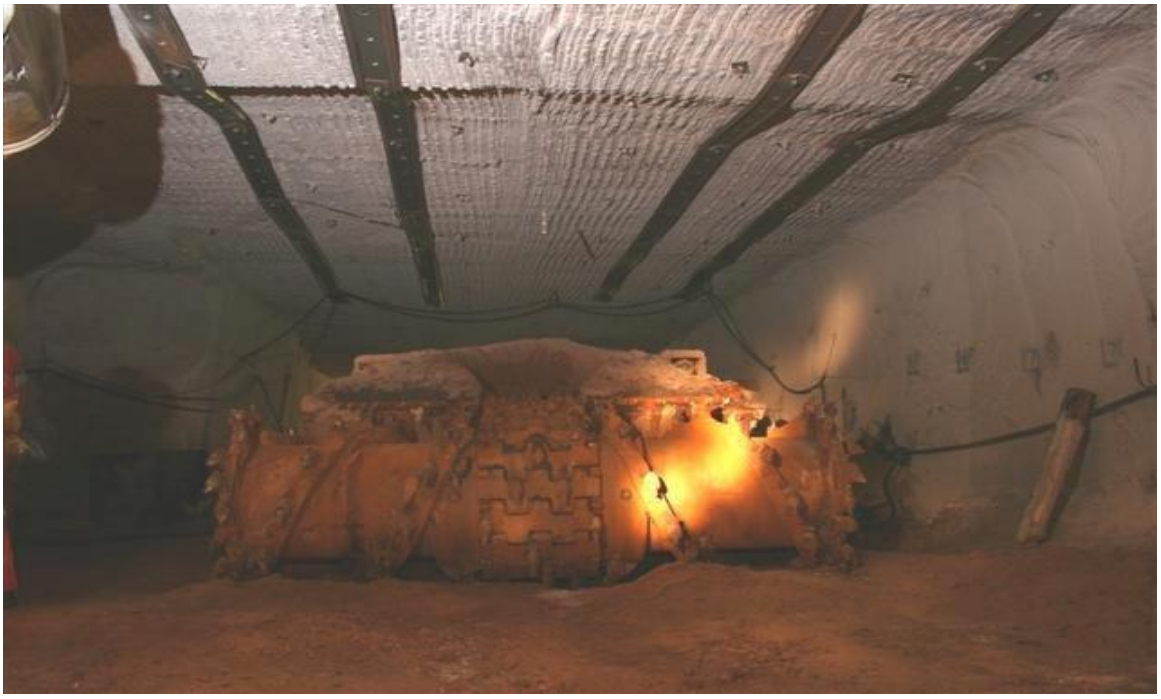

Plate 3.1 A continuous miner at a working salt face at Boubly mine (source Boulby, 2009)

Because of the greater stresses below 1,200 m depth, the conventional continuous miners were converted to remote-controlled operation. Two-road with stubs (or cross-cuts) (Figure 3.7) rather than four-road technique is used and more mining per shift is achieved. The extracted potash is partially crushed underground and conveyed to the surface where it is processed. A tailings pipe 1770 meters of length is used for the offshore disposal of the waste into the North Sea.

3.6 Deformation and failure of rocks

"The behaviour of macroscopic systems is generally described by non-linear laws. The non-linear laws may explain irreversible phenomena like instabilities, dualism, unevolving societies, cycles of growth and decay of societies. The linear laws are only linear approximations of the non-linear laws at a point in time and space"

Ilya Prigogine, Nobel Laureate (Singh and Goel, 1999, p. 136).

Deformation of soils and rocks is generally caused by the externally applied loads on *in-situ* rock or by tectonic forces (i.e. compressive and/or shear forces). Stress in rock generates strain and displacement and may result in folding, faulting (i.e. shear) and flow of the solid (Lee, 2005). Several factors including rock defects (e.g. joints, bedding), mechanical properties of the rock, direction and magnitude of acting loads, fissures and/or cracks brought about by the excavation, seismic effects and the virgin stress state of the rock mass significantly affect the deformability and strength of the rocks (Jumikis, 1983).

Most of soils and rocks undergo continuous slow deformation when stressed. This permanent deformation of rocks also referred to as creep is a time-dependent movement (i.e. plastic displacement) and a complex response of strain to stress of rock under a sustained load. The concept of creep was introduced by Terzaghi (1950) and has been associated with the occurrence of landslides. The strain increases during the course of time under constant stress and its amount is a function of the stress level such at high stress creep accelerates leading to the failure of the rock mass (Jumikis, 1983).

3.6.1 Suitable models and failure criteria of rock mass

Determination of rock failure conditions is essential to the development of underground excavations. Fracture of rock is the common mechanism of rock failure at high pressures and temperatures at depths as the strength of the rock is exceeded. A number of models and criteria have been developed to characterize and predict rock mass behaviour as a function of applied stress. Three of them are discussed in sections that follow.

3.6.1.1 Mohr-Coulomb plasticity model (1773)

The Mohr-Coulomb plasticity model is one of the models widely used to represent shear failure in soils and rocks (Itasca, 2005). Plasticity of materials occurs when the shear stress is beyond the limit shear strength of the materials (Boidy, 2002; Jumikis, 1983). Basically, the concept of this model is that, failure of material in shear is primarily a function of major and minor principal stresses, and can be expressed by a shear yield function (Bizjak *et al*., 2009; Itasca, 2005)

$$f^s = \sigma_1 - \sigma_3 N_\phi + 2c\sqrt{N_\phi} \quad (3.1a)$$

$$N_\phi = \frac{1+\sin\phi}{1-\sin\phi} \quad (3.1b)$$

where ϕ is the angle of friction, c the cohesion and σ_1 and σ_3 are the principal stresses.

In the principal stress space, failure of material desplays an irregular hexagonal pyramid (Figure 3.8) with one of the plans described the equation 3.2 (Itasca, 2005; Boidy, 2002):

$$\sigma_1 - \frac{1+\sin\phi}{1-\sin\phi}\sigma_3 - \frac{2c\cos\phi}{1-\sin\phi} = 0 \quad (3.2)$$

For a purely cohesive material (i.e. ϕ = 0) equation 3.2 degenerates to the Tresca's criterion.

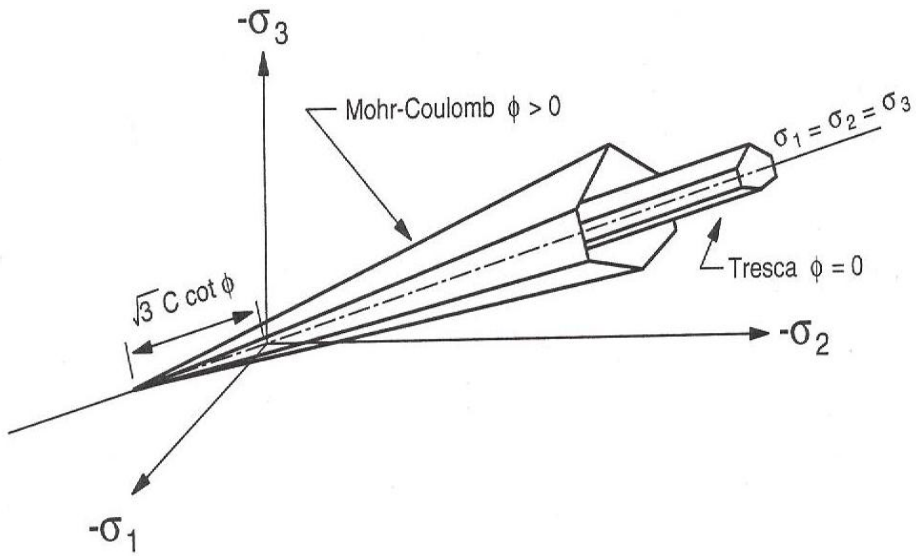

Figure 3.8 Mohr-Coulomb and Tresca yield surfaces in principal stresses space (from: Itasca, 2005)

Mohr-Coulomb model has been used by Karakul *et al*. (2010) to characterize the behaviour of Sandstone and Limestone layers during the analysis of material strength anisotropy associated with discontinuity orientation. Results showed good agreement between observed and predicted values. Bizjak *et al*., (2009) applied this shear failure criterion to the behaviour of Marl, Sandstone and Limestone layers to model numerically the Slano Blato landslide above the Lokavec village, Slovenia. Simulating the stability of cavern, Foley (2006) treated the Limestone layer to behave according to Mohr-Coulomb law. Ghafoori *et al*. (2006) modelled Marl and Limestone strata as elasto-perfectly plastic materials which obey the Mohr-Coulomb failure criterion to characterize numerically the performance of the Kallat tunnel in Iran. Most importantly, Swift and Reddish (2005) demonstrated that the strata from the Mercia mudstone to the base of Sherwood mudstone above the evaporite rocks at Boulby mine are non-creeping strata. Therefore, they treated the strata as Mohr-Coulomb materials when modelling the stability of the Winsford salt mine in Cheshire.

3.6.1.2 Drucker-Prager plasticity model (1952)

Drucker-Prager plasticity model has been developed to simulate the behaviour of granular and polymeric materials with low or without friction such as soft clays, sand and gravel (Boidy, 2002; Hofer and Kamlah, 2005; Itasca, 2005). The model involves the von Mises's criterion and the yield function is analytically expressed as:

$$F(\sigma_{ij}) = \tau + \zeta_{\phi}\,\sigma - k_{\emptyset} = 0 \qquad (3.3)$$

where ζ_{ϕ} and k_{ϕ} are the constant characteristics of the material, and τ is the equivalent deviator (i.e. shear stress) and σ is the mean stress expressed as:

$$\sigma = \frac{1}{3}(\sigma_1 + \sigma_2 + \sigma_3) = \frac{1}{3}tr(\sigma) = \frac{1}{3}\sum_{i=1}^{3}\sigma_{ii} \qquad (3.4)$$

where σ_1, σ_2, σ_3 are principal stresses. The conical failure envelope in principal stress space is shown in Figure 3.9 (Itasca, 2005).

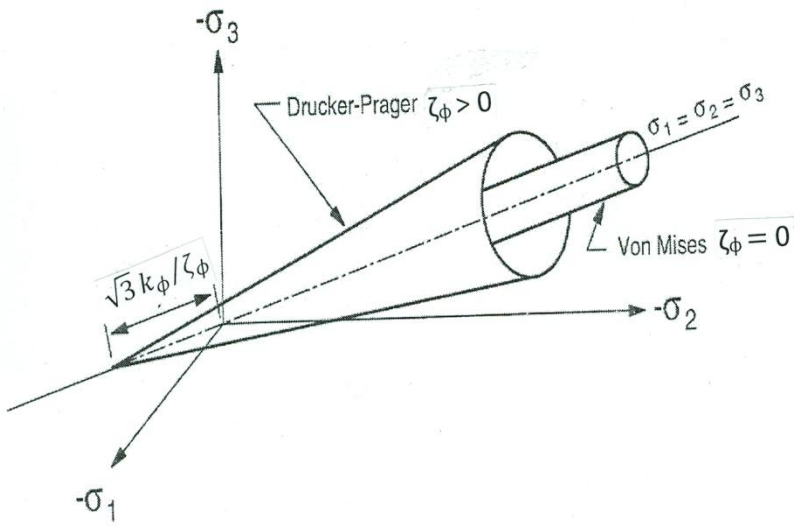

Figure 3.9 Drucker-Prager and von Mises yield surfaces in principal stress space (from: Itasca, 2005)

Parameters ζ_{ϕ} and k_{ϕ} are estimated from cohesion and friction angle values. They are defined according whether the failure envelope circumscribes or inscribes the Mohr-Coulomb envelope.

The Drucker-Prager failure envelope circumscribes when

$$\zeta_\phi = \frac{6}{\sqrt{3}(3-\sin\phi)}\sin\phi \quad \text{and} \quad k_\phi = \frac{6}{\sqrt{3}(3-\sin\phi)}c\cos\phi \quad (3.5)$$

whereas it inscribes when

$$\zeta_\phi = \frac{6}{\sqrt{3}(3+\sin\phi)}\sin\phi \quad \text{and} \quad k_\phi = \frac{6}{\sqrt{3}(3+\sin\phi)}c\cos\phi \quad (3.6)$$

The tensile strength of the material for the Drucker-Prager model is defined as the maximum value of the mean normal stress for the material under consideration. It is estimated as follows:

$$\sigma_{max}^{t} = \frac{k_\emptyset}{\zeta_\phi} \quad (3.7)$$

The model has been successfully used in engineering and mining to represent the behaviour of rocks. Yu *et al*. (2010) applied the Drucker-Prager approach to estimate numerically and experimentally the behaviour of confined concrete. Yu *et al*. modified the approach by incorporating a yield criterion which includes the third deviatoric stress invariant, a hardening/softening rule as a function of confining pressure and a flow rule which depends on both confining pressure and rate of confinement increment. Comparisons of FEM predicted with available tests results proved the capability of the modified model in providing close predictions of confined concrete behaviour. Despite some limitations the modified model enables damage concrete simulation in terms of strain softening and the degradation of elastic constants.

Crosta *et al*. (2009) numericall simulated the landslide mass movement based on properties and topographies of rocks and debris entrainment and deposition during avalanches. The investigation intended to model both erosion and deposition, but also their interaction with obstacles of different characteristics. Investigated structure chiefly consisted of loose material made of rock, soil materials with talus deposits and glacial till. Because of its nonlinear path-dependent, failure of materials was modelled as Mohr-Coulomb and Drucker-Prager elasto-plastic models. The analysis results showed the

dependency of failure of rocks and debris avalanches upon both mechanical and hydraulic properties of the materials.

Hofer and Kamlah (2005) applied the Drucker-Prager approach to the behaviour of pebble beds. The analysis intended to understand the interaction of solid breeder and beryllium pebble beds with the surrounding material on the basis of experimental study. Both breeder and beryllium pebble beds display nonlinear stress-strain relationship depending upon the level of applied stress. They were treated as elastic and plastic materials, respectively which undergo creep deformation, and models were calibrated against oedometric test fitting curves. If both experimental and numerical analysis provided good correlation however, parametric studies showed disagreement between experimental and modelling results. As a consequence, hardening law was modified for the improvement of the creep behaviour of the model.

Cela (1998) numerically analyzed the behaviour of reinforced concrete structures under dynamic loads. Material parameters were determined experimentally on the basis of stress-strain relationships. In the analysis, steel was treated as elasto-perfectly plastic material whereas the concrete behaved as a softening elastoplastic material which exhibits dilatancy. Applying the approach to real cases of study - e.g. impact on a cooling tower and gas explosion in reactor containment - the method produced plausible results. Models were validated against experimental and literature data.

3.6.1.3 Strain-softening Mohr-Coulomb model

Strain-softening Mohr-Coulomb model has been developed to represent nonlinear softening material behaviour as a result of degradation in shear strength of rock mass when loaded. Rock mass undergoes both brittle softening (due to a reduction in cohesion) and gradual softening (due to a reduction in friction angle) (Itasca, 2005).

Strain-softening also termed as strength-weakening behaviour is based on the incremental theory of plasticity such the flow rule indicates the evolution of plastic strain rates and specifies the direction of plastic strain increment. The material behaviour is

characterized by a failure criterion *f* and a plastic potential *g.* Both functions depend not only on the stress tensor, but also on the plastic or softening parameter. Consequently, the behaviour of the material is a function of plastic strain.

Given a softening parameter ζ, the failure criterion is defined as (Alejano *et al*., 2009):

$$f(\sigma_r, \sigma_\theta, \zeta) = 0 \tag{3.8}$$

The materials behaviour is represented by a gradual transition from a peak failure criterion to a residual failure criterion governed by the softening parameter ζ. Such a transition is defined as follows:

$$\begin{cases} \zeta = 0 \ \text{elastic regime} \\ 0 < \zeta < \zeta^* \ \text{softening regime} \\ \zeta > \zeta^* \ \text{residual state} \end{cases} \tag{3.9}$$

where ζ* is the value of the softening parameter controlling the transition between the softening and residual stages, σ_r and σ_θ are normal and shear stress respectively.

Erickson *et al*. (2004) developed a plasticity constitutive rule for strain-softening materials composed of a yield function and a plastic flow rule. The former governs the onset of the plastic behaviour whilst the latter governs the plastic flow, and are expressed in Equations 3.10 and 3.11, respectively:

$$f = \tau + \sigma \sin \emptyset - \mathrm{C} \cos \emptyset \tag{3.10}$$

$$g = \tau + \sigma \sin \psi - C \cos \psi \tag{3.11}$$

where τ is the maximum shear stress, σ the mean stress, ϕ the internal friction angle, ψ the dilation angle and C the cohesion.

Generally, values of dilation angles are less than friction angles and range between 10^o and 20^o (Itasca, 2005). When friction and dilation angles are different, the plastic rule is nonassociated that is, the yield function is not associated with the plastic flow rule. Progressive failure of materials occurs as a result of strength reduction with increasing materials strain. Whilst cohesion, friction, dilation and tensile strength are

kept constant in Mohr-Coulomb model, in the strain-softening model these parameters will soften (i.e. decrease) after the onset of the plastic yield as a function of increasing plastic shear strain. Accordingly cohesion, friction and dilation are defined as piecewise-linear laws of a softening parameter which measures the plastic shear strain and/or plastic tensile strain, respectively.

Figure 3.10 portrays the curves indicating the softening upon yielding and attaining residual strength, the variations of cohesion and friction angle as a function of the plastic portion of the total strain. The stress-strain curve shows that beyond the yield point, the total strain is a sum of elastic and plastic parts.

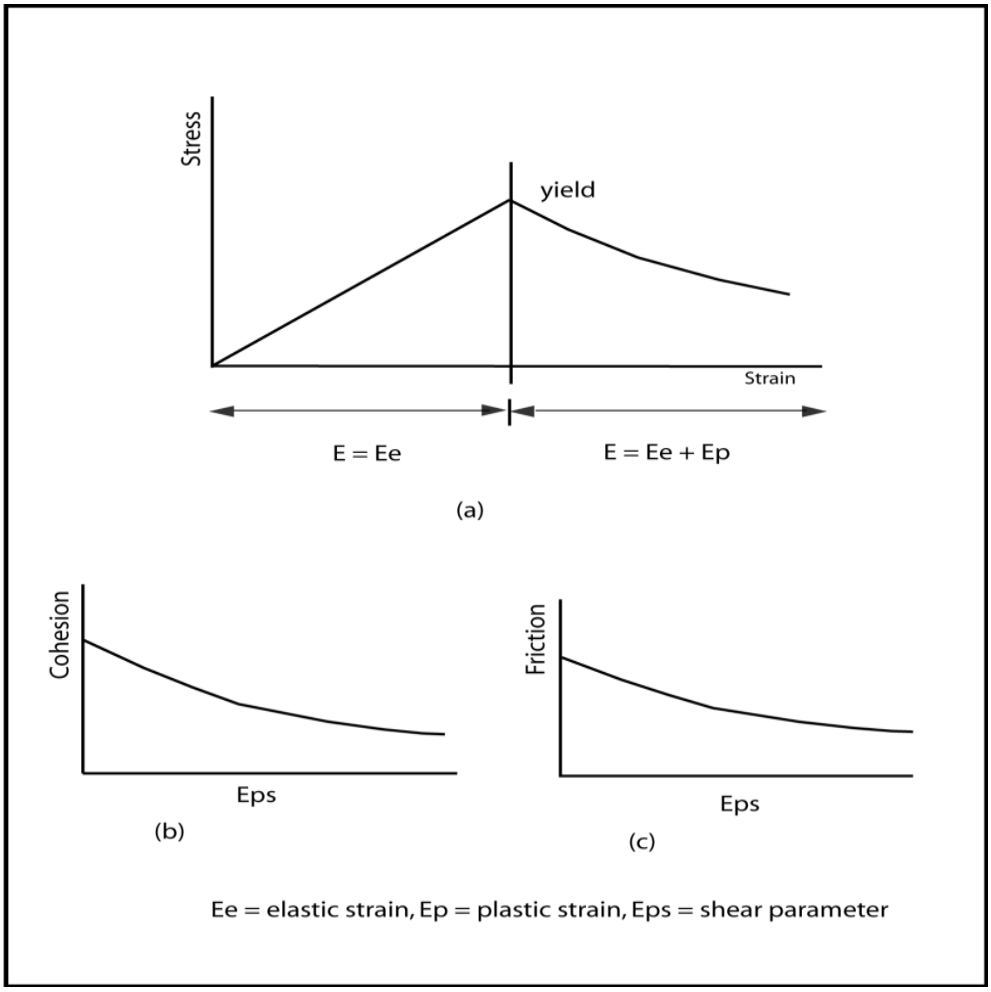

Figure 3.10 Softening related stress-strain curve (a), variation of cohesion (b) and friction angle (c) with plastic strain.

Strain-softening approach has been widely used to investigate materials exhibiting softening or hardening behaviour. Xie *et al*. (2009) investigated into the patterns of stress distribution in rock surrounding caving faces in coal mining. The nonlinear behaviour of coal rock was modelled as a strain-softening material. Laboratory mechanical and strength parameters of materials were reduced by factors to account for the sclale effects and the presence of both discontinuities and heterogeneities in the rock mass. The results showed occurrence of stress shell in the rock surrounding the caving face acting as voussoir and supporting the structure by transferring overlying strata loads to the wallsides.

Kumar *et al*. (2008) applied the FLAC 2D code to analyze the behaviour of a tunnel excavated in sandstone medium. The material was treated as strain softening and Mohr-Coulomb plastic material. The analysis showed that tunnel softening significantly depends on the mechanics of materials and the strain softening model induces predominant effect around and near tunnel boundary as a result of low confinement adjacent to the boundary tunnel.

Lloyd *et al*. (1997) numerically analyzed surface and subsurface subsidence associated with longwall coal mining in the United Kingdom. The non-linear material behaviour was characterized by the strain-softening model and the FLAC 2D code was used. Analysis results established the relationship between RMR and depth for pre and post failure stiffness despite the sensitivity of the approach to the extraction thickness and panel width variation for the propagation zone of influence above the panel. Good results were achieved between patterns of stress around panels and displacement distribution at the surface.

Most importantly, Caughill and Beddoes (1996) successfully analyzed the behaviour of panels as a function of behaviour of carnalite marl layer using the FLAC 2D code. Creep power law and strain-softening model were used to characterize the behaviour of carnalite marl. The results revealed that in the range of 1050 to 1100 m depth, predicted closure rates with strain-softening in carnalite marl were in good agreement with the measured closure rates than those with creep model whereas, in the range of 1200 to 1250 m depth, both predicted and measured closure rates were

similar for both creep and strain-softening model of carnalite marl. This finding is of relevance to the current research.

3.6.1.4 Comparison of Mohr-Coulomb, Drucker-Prager and Strain-softening Mohr-Coulomb models

Mohr-Coulomb, Drucker-Prager and Strain-softening models have numerous applications in rock mechanics and several fields of engineering particularly in underground mining (Section 3.6.1). Among them, the Mohr-Coulomb model is the commonly used to represent shear failure of geomaterials. The differences between the models, their inherent advantages and disadvantages with reference to Boulby structure are summarized in Tables 3.5 and 3.6, respectively.

Table 3.5 Comparison of Drucker-Prager, Mohr-Coulomb and Strain-softening models (After: Itasca, 2005)

Model	Description and Representative Material	Applications
Drucker-Prager plasticity	Simple failure criterion with the shear yield stress as a function of isotropic stress Not suitable for representing failure of geological materials Application limited to materials with low friction and to some extent with low cohesion (e.g. soft clays). Degenerates to the von Mises model	Commonly used for comparison of FLAC to other numerical programs (e.g. implicit finite-element) having not Mohr-Coulomb model
Mohr-Coulomb plasticity	Applicable to materials that yield under shear loading Yield stress is only a function of major and minor principal stresses; the intermediate principal stress has no effect on the yield stress Does not allow direct calculation of plastic strain Parameters for cohesion and friction angle	Generally applicable for most engineering studies in rocks and mining activity.

	readily available than other geo-material properties Tensile failure criterion identical to that in Strain-softening model Applicable to loose and cemented granular materials (e.g. soils, rock, concrete) Degenerates to the Tresca model	
Strain-Softening Mohr-Coulomb	A variation of the Mohr-Coulomb model Appropriate for materials showing degradation or decrease in shear strength when the load (i.e. shear stress) exceeds the failure shear strength limit. Allows direct plastic strain computation Tensile failure criterion identical to that in Mohr-Coulomb model Produces results similar to those for Mohr-Coulomb as high values are assigned to the additional material parameters (e.g. shear and bulk moduli) Applicable to granular materials that exhibit nonlinear softening	Studies in post-failure (e.g. progressive collapse, yielding pillar, caving, backfilling)

Table 3.6 Models advantages and disadvantages with reference to Boulby structure

Model	Materials	Advantages	Disadvantages
Drucker-Prager	Lias Rheatic	Prevent complete failure of materials accordingly, low defomartion is induced on the surface The model is appropriate to represent the behaviour of these rocks These materials, particularly Rheatic have	Materials will fail in shear only if induced stresses are isotropic Difficult to determine the nature of induced stresses given the behaviour (i.e. nature) of the underlying strata and the presence of

		low friction and cohesion hence, are expected to deform under gravity.	water within sandstone.
Mohr-Coulomb	Mercia mudstone S. sandstone S. mudstone Anhydrite	Common model for characterizing shear failure of geomaterials With consideration of the nature and texture (i.e. consistency) of these materials, the model suits well for characterizing the mechanics particularly of the first three materials. Materials fail in shear as a result of mining-induced stress Although impurities present in the rock may alter its behaviour, Anhydrite behaves elastically Patchet (1970) despite being evaporitic thus, may creep.	Anhydrite is an evaporitic rock and creeps under shear stress. It is a strong and dense rock. Its location in close proximity to the excavation may constitute a barrier to the upwards transmission of mining-induced stress. Redistribution of stress and resulting displacement are affected. As a consequence, patterns, magnitudes of stress and displacement, and subsidence may not reflect the actual patterns if creep or strain-softening model was used.
Strain-softening	Carnalite marl Potash Halite	Appropriate for modelling nonlinear post-failure process (e.g. yielding pillar) due to the decrease of shear strength of material. Yielding pillar may be considered as a relatively rapid movement as opposed to creep Thus, the model suits to model the short term	Lack of information on the level of stress to cause deformation of evaporite rocks given their creeping nature. Its use may negatively impact on the stress and displacement redistribution consequently, the structure behaviour driven by the mechanics

		behaviour – before complete failure of the strata. May adequately represent the behaviour of evaporitic rocks since the material strengths decrease as a result of overburden pressure and loading time scale (Kwon and Wilson, 1999).	of strata on the roof and floor will be affected. Again, patterns, magnitude of stress and displacement, and subsidence may not represent the actual patterns if creep model was used.

The application of the three models is limited to the materials they best represent the behaviour. The Drucker-Prager model suitable to low friction materials will adequately model the behaviour of cohesionless soft strata above the Mercia mudstone despite Lias friction is rather high. The failure envelope of the materials circumscribes the Mohr-Coulomb envelope.

Mohr-Coulomb plasticity model successfully portrays the behaviour of loose and cemented granular materials including Sandstone and Mudstone as well. At Boulby mine, the model can simulate the elasto-plastic behaviour of strata in the middle part of structure from the Mercia mudstone down to the base of Anhydrite as a result of mining-induced shear stress. However, given the nature of Anhydrite the model may not well describe the long-term (creep) behaviour of this material as the material could behave in elastic manner (Patchet, 1970). Material creep causes the migration and relaxation of stress concentrations away from around the excavation.

Although intended to analyze nonlinear post-failure processes, the strain-softening model may not provide the time-dependent behaviour of the evaporitic rocks. However, because evaporitic rocks underground mine fail as a result of pillars support extraction and also of strength decrease due to the overburden pressure and loading time scale, the model can be well used to model the short-term behaviour of potash, carnalite and halite rocks at Boulby mine.

3.6.2 Mechanics of roof at Boulby mine

Mining activity at Boulby mine disturbs the equilibrium of stress state of rock mass surrounding the excavation. Mine roof deforms under the weight of the overlying strata which through time close the excavation (Kemeling, 2006) (Plate 3.2).

Mine roof deformation at Boulby is controlled by the rheological behaviour of the overlying strata mainly the salt and potash rocks. The removal of potash induces convergence of mine workings. As a result, the overlying Carnalite marl flows into the opening in attempt to achieve a new equilibrium state of stress. The Anhydrite and Halite strata bend owing to the shear stress developed within and the lack of support. Shear stress concentrates at the base of the Halite layer and initiates volumetric strain which propagates laterally and upwards towards the Mudstone layer (Lachenicht and Aswegen, 1999).

Plate 3.2 Closure in the underground working of Boulby mine in 2007. The roof has closed from over 3 m to less than 1.5 m in the foreground and almost completely in the background.

Deformation propagation is a function of the mechanical properties (i.e. elastic and strength properties) of the strata, shear stress, geological structures (e.g. fault, fold or slip plane) and amount and rate of excavation closure (Caldwell, 2006; Kratzsch, 1983). Pore pressure at the mudstone/sandstone interface may exacerbate the deformation by reducing the normal stresses acting against the volumetric propagation.

The Triassic Sherwood sandstone of Northeast England forms an aquifer containing highly saline water. According to Lachenicht and Aswegen (1999), the gradient pressure within the Sherwood Sandstone aquifer at Boulby is linear and is of 1 MPa every 96 m. This gradient pressure is connected to sea level and thus, the water (i.e. the brine) within this layer is at pressure equals the gradient times the depth below sea level. Because of fractures within the semi-permeable Sherwood mudstone (i.e. Upper Permian Marl), the gradient pressure may extend through the Sherwood mudstone to the top of the Upper halite.

3.6.2.1 Creep of salt and potash

"No material is perfect. All materials contain in some proportion the characteristics of elasticity, plasticity and flow" (Jumikis, 1983, p.180).

Salt and sylvinite rocks creep is primarily a result of the time-dependent of the properties of the rocks. In underground excavations, the properties of the rocks are controlled by several factors including stress (i.e. pressure) magnitude, conditions and time scale of loading, temperature (Kwon and Wilson, 1999).

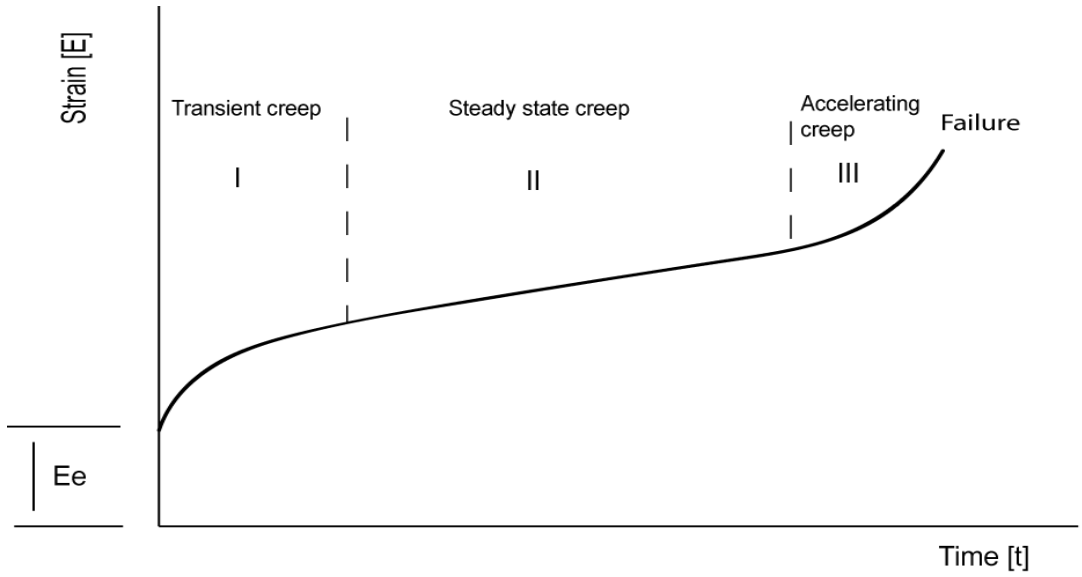

Figure 3.11 Model of the creep deformation in function of time, with Ee = elastic strain

Creep of evaporite rocks is similar to that of most of soil or rock materials and generally consists of four stages (Figure 3.11): instantaneous and recoverable elastic deformation, a transient or primary creep stage, a steady or secondary creep stage, and an unstable tertiary or accelerating creep stage (Amitrano and Helmstetter, 2006; Jeremic, 1994).

The application of a constant stress on the materials induces an instantaneous deformation or elastic strain. In underground mining activity, this phase takes place once the material is excavated. The instantaneous phase is followed by a primary or transient creep characterized by an exponential decrease of strain rate. The transient creep is followed by a secondary or steady-stage creep characterized by a quasi-constant slope or strain rate. With time, deformation of material evolves to the tertiary or accelerated phase of creep. The tertiary phase of creep is the phase of strain increase at increasing rate. During this phase, microcracks within the deforming material interact and eventually coalesce as the material is subjected to high pressure. The material is weakened, fractured and then fails (Miura *et al*., 2003).

Although the mechanics of roof at Boulby mine is controlled by the creep behaviour of evaporite rocks however, creep will not be used in this study. This is because the current study is primarily interested in the behaviour of the overlying strata

which most control the distribution of stress and displacement and which may not exhibit creep behaviour over short-period of time. Instead, models described in section 3.6.1 will be used to analyze the response of the overlying strata to mining potash through the analysis of stress and displacement distribution, and resulting ground subsidence. Most importantly, the strain-softening model will be used as an approximation to the creep behaviour of Potash, Carnalite and Halite rocks.

3.6.3 Estimated *in-situ* stresses

Determination of stress state in a rock mass is fundamental prior to development of any mining activity and numerically simulating of excavation process. *In-situ* stress state knowledge enables prediction of stresses around opening and assessment of excavation deformation. Methods for measuring stress are based on stress-relief techniques and studies of deformation in the rock between a stressed and unstressed state; the latter state is carried out by overcoring.

Generally, numerous methods used to estimate the *in-situ* state of stress assume that no geological anomalies or tectonic forces are present in the rock mass under consideration. On the basis of such assumption, the virgin stress directions will be vertical and horizontal, and the virgin vertical stress increases at the rate of - 22.6 kN/m^2 per metre of depth increase. Therefore, at Boulby the virgin vertical stress at depth of about 1,200 m would be - 27 MN/m^2.

The above assumption holds for structures with materials of same density. When materials of different densities are present within structures such as that of Boulby mine, the vertical *in-situ* stress is estimated by considering the loading due to the weight of the overburden, and is computed from the equation (Hebblewhite, 1977):

$$\sigma_V = -\rho * g * \left(\sum_{i=1}^{n} (\gamma_i * h_i) \right) \qquad (3.12)$$

where ρ is the density of water, g is the gravitational constant, γ_i is the specific gravity of each stratum and h_i is the thickness of the overlying strata.

The horizontal component of *in-situ* stress is estimated from equation (2.3) on the basis of elasticity theory. *In-situ* tests indicated Poisson's ratio values higher than 0.5 and occasionally greater than 1.0 (Patchet, 1970). This suggests that stresses at depth in sedimentary deposits are lithostatic, implying that both horizontal and vertical stresses are equal. A Poisson's ratio greater than 1.0 implies a horizontal stress component greater than the vertical component; consequently strain is unlikely to occur within stretched materials. Such geomaterials behaviour may be unusual for that most of geomaterials increase their volume slightly when stretched and have Poisson's ratios around 0.3 with a maximum of 0.5 for rubber whose volume does not change (Wakai and Nikolic, 2011; Miao *et al*., 2010). Critically, Poison's ratios values greater than 1.0 may not exist at Boulby mine given that most of the strata, particularly those used in this research have Poison's ratios less than 0.4 (Table 3.3) despite high tectonic forces and residual stresses may induce high values of horizontal stress.

Indeed, measurements of horizontal stress show that the theory of elasticity is not generally a valid basis for predicting horizontal stresses for it does not explain values of horizontal stresses greater than the vertical stresses. Such high values of horizontal stresses would originate from tectonic forces or residual stresses (Hebblewhite, 1977).

Tectonic stresses result from geological changes such as faulting and folding, and locking in the stresses owing to lateral constraint which prevents rock from releasing them. Residual stresses may be thermal stresses due to change in the material volume as a result for instance of water absorption-induced swelling. Lateral constraint permanently locks tectonic and residual stresses into rock until occurrence of free boundary allowing them to be released. Residual stresses mostly exist in horizontal plane because of constraint at the boundary of this plane whereas vertical stress is relieved by the free, surface boundary.

The Cleveland area is subject to uplift as a result of Pennines general uplift. However, the uplift movement may have not brought about tectonic stress at depth because of its localisation at the area and also faults do not extend down to the evaporite deposits despite the presence of minor faults within the deposits (Patchet,

1970). Evaporite rocks at Boulby mine are in lithostatic stress state whereas, rocks from the Sherwood mudstone horizon to the surface may be at high horizontal stress in Northwest-southeast (NW-SE) direction (Lachenicht and Aswegen, 1999). Because of the creeping nature of evaporites, the rocks in-*situ* stress state, through geological time, will equal the lithostatic state regardless the tectonic environment. However, this observation does not agree with the field stress measurements conducted in the mine (Hebblewhite, 1977).

In fact, overcoring measurements showed vertically and horizontally orientated stress distribution in the vicinity of potash seam with uniformely distributed stress in the horizontal plane (Hebblewhite, 1977). Measurement indicated values of -30.1 MN/m^2 and -15.4 MN/m^2 for virgin major vertical and minor horizontal principal stress, respectively at 1,100 m depth. Because of weak shales and time-dependent deformation of evaporite rocks, ratios of virgin stresses are higher than those predicted by equation 2.3. According to Equation 2.3, the vertical stress and horizontal stress are in elastic equilibrium. That is, for a given value of Poisson's ratio the virgin horizontal stress would be one third of the vertical stress. Additionally, variations and distortion of potash seam along its upper boundary prevent time-dependent distribution of stress resulting in a value of 0.51 of horizontal to vertical stress ratio at this depth.

Consequently, using values of specific gravities and thicknesses of strata above the seam listed in Table 3.3 Equation 3.1 would produce values of -30.1 MPa and -15.3 MPa for vertical and horizontal virgin stress, respectively at the seam horizon at Boulby. This ratio of horizontal to vertical stress will be used in the present study for the estimation of horizontal stress of evaporite rocks for modelling the patterns of stress and strain distribution at Boulby mine.

3.7 Ground subsidence monitoring at Boulby mine

Ground movement (i.e. subsidence) at Boulby mine is continuously monitored to determine the impact on the environment caused by the mining activity. Different techniques are used including levelling and geospatial techniques.

3.7.1 Levelling technique

Levelling surveys have been undertaken annually since 1976 over the mine area of approximately 216 km^2 to monitor ground movement. A Sokkia SDL1 Digital Level and invar staff with an accuracy of 0.001 millimetres are used to record the coordinates of bench mark associated with the date of monitoring. Ground deformation is obtained by differencing the elevation (i.e. vertical measurement) between two successive measurements (equation 3.13). The rate of deformation is the elevation difference between two dates with the time being taken as the midpoint of the two dates (equation 3.14) and ranges between 0 and 50 $mm.a^{-1}$ (Kemeling, 2006).

$$(elevation2 - elevation1) * 1000 = S[mm] \quad (3.13)$$

$$\frac{elevation2-elevation1}{day2-day1} * 1000 * 365 = S[mm \cdot a^{-1}] \quad (3.14)$$

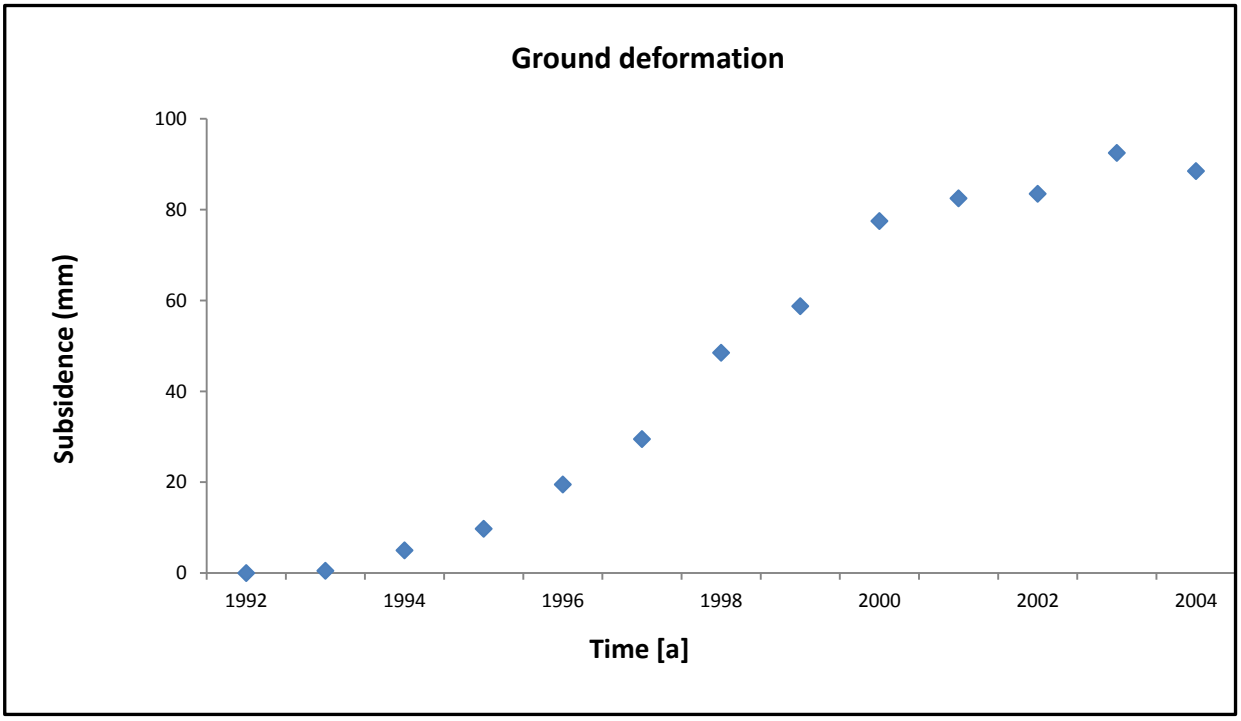

Figure 3.12 Subsidence at a monitoring point at Boulby mine from 1992 to 2004 using levelling technique (After Kemeling, 2006).

Figure 3.12 portrays pattern of ground deformation at monitoring station 193 in Staithes from annual levelling surveys data over the mine area for a period of twelve years between 1992 and 2004.

The graph shows smooth ground subsidence at the monitoring point over the entire period of measurement. The plot indicates a period of quasi-null subsidence over the two first years of surveying followed by increasing rate of subsidence over the next seven years, i.e. between 1994 and 2001. This increasing subsidence rate period is followed by a decreasing rate movement over the remaining period of measurement. The change in the rate of subsidence may be attributed to the behaviour of overlying strata and also to the time scale factor.

3.7.2 Geospatial monitoring techniques

At the Boulby mine, geospatial models of ground subsidence taking place over the mine area started in 1998. The first geospatial model of ground subsidence associated with the mining activity was obtained by combining the geographic information system (GIS) and levelling monitoring data.

The empirical model for estimating ground subsidence is given by the equation (Kemeling, 2006):

$$Y = -753.63 * ln(X) - 677.33 \quad (3.15)$$

where Y is the distance from the central entrance shaft of the mine in metres and x is the ground surface deformation rate in millimeter per year (mm.a^{-1}).

The rate of ground deformation is given by the equation:

$$X = e^{-\frac{Y+677.33}{753.63}} \quad (3.16)$$

Recently, Kemeling (2006) developed a cone model in order to improve understanding of patterns of subsidence associated with the mining activity. The model combined InSAR (Interferometric Synthetic Aperture Radar) deformation, levelling survey and excavation datasets. A data-driven model was developed based upon the mineral extraction patterns and the surface subsidence data. The mineral extraction pattern inputs included the mined area, horizontal distance between panel and survey point, panels distribution within the influence zone and the time after panel extraction. The model established the relationship between the input variables and the ground surface deformation. To visualize ground surface behaviour in response to mining, a map was generated by interpolation. Multiple regression analysis permitted prediction of ground deformation rates. The model enabled the linkage between deformation of stations on the surface and patterns of subsurface extraction.

3.8 Summary

Selection of research area was motivated considering mining related convergence suitable for short-term monitoring. At Boulby mine, mine workings performance can be assessed using specially designed closuremeter. Boulby mine geological setting is well understood and the mechanical properties of the overlying strata are well known through laboratory tests and similar lithologies. Mine workings convergence and ground subsidence that take place at the mine have been monitored and their patterns have been recognised.

Mining potash at Boulby is undertaken by leaving parts of the unmined deposit to support the overlying strata. The roof gradually subsides while the floor heaves and the mine workings close with time leading to the occurrence of subsidence trough on the surface. Levelling surveys showed that ground deformation over the mine area occurs smoothly over the entire period of measurement. The maximum rate and magnitude of ground deformation since the start of the mining activities in 1973 are 50 $mm.a^{-1}$ and about 70 mm, respectively.

The overlying strata below the Sherwood mudstone deform in plastic (i.e. nonlinear) manner and the strata from the base of this formation will likely exhibit elasto-plastic behaviour when stressed. This information is of relevance in modelling convergence of excavation. In accurately monitoring short-term convergence, controlling factors of mine workings mechanics may be determined. With a well-known lithology, patterns of stress and displacement distribution may be modelled and driving factors determined, based on measured convergence patterns.

Chapter 4
Monitoring of convergence

4.1 Introduction

The mechanics of underground excavations roof is complex because of the controlling factors whose individual influence may not be determined a priori. Mine workings behaviour monitoring, particularly in underground active potash mining, is fundamental for the safety of workers, subsurface and surface structures. Results analysis and interpretation enable to characterize workings deformation patterns in response to mining activity. This may help understand both short-term and long-term deformational behaviour of workings and therefore contribute to the long-term stability of the workings. The measured deformation patterns may also be used to numerically model the opening closure and the behaviour of strata above the excavation. Results from numerical modelling are used in predicting future closures and the overlying strata behaviour (Schleinig and Lukas, 2007).

One of the key objectives of this research has been to monitor short-term temporal patterns of workings convergence at Boulby mine. To achieve this objective, a special closuremeter has been designed to measure the short-term behaviour of the mine workings in terms of floor-to-roof closure. The wire extensometer technique used at Boulby measures net change of the excavation height as a result of roof sagging (or roof closure) and floor rising (or floor heave). The bespoke closuremeter measures the reduction of the vertical dimension of the excavation in order to produce the cumulative movement of the mine workings.

This chapter describes the main components of the closuremeter and field test results to evaluate the functioning of the specially designed underground monitoring instrument.

4.2 Design of closuremeters

Monitoring changes in the behaviour of workings underground mines require high resolution instruments and several techniques are used. A closuremeter was specially designed to monitor the roof and floor closure to allow determination of the vertical displacement of the excavation at the monitored points underground the active Boulby potash mine.

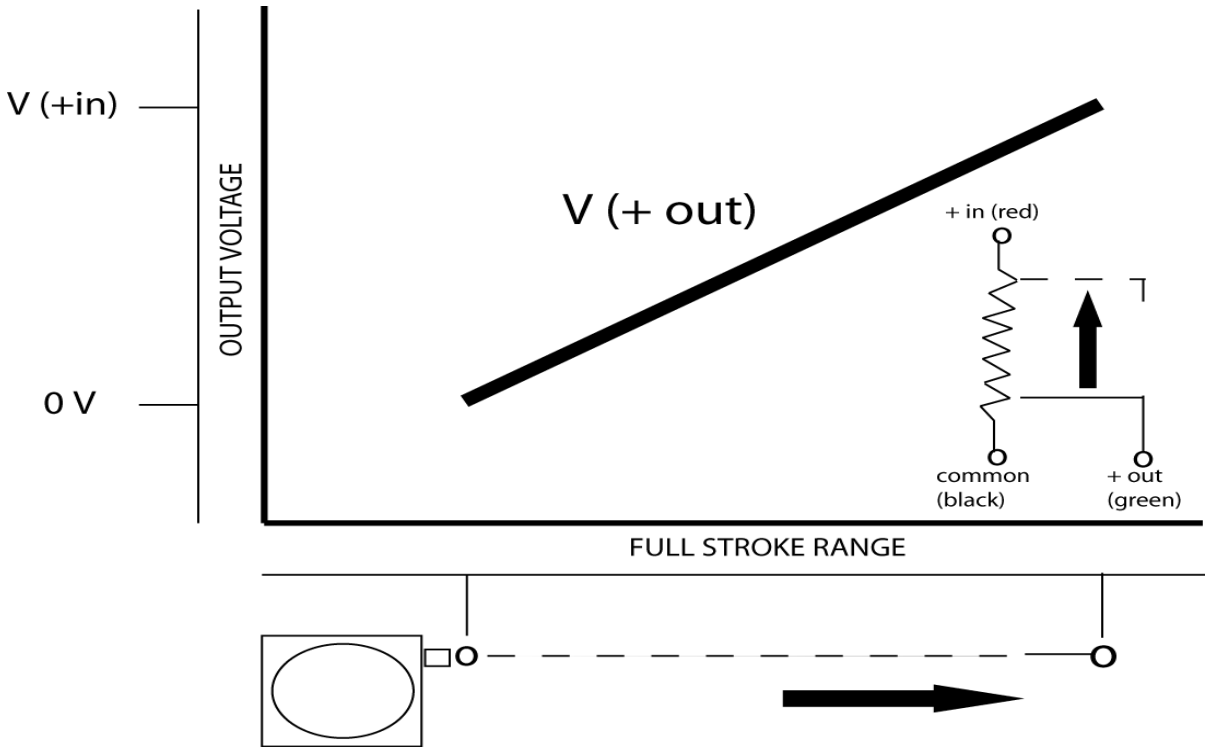

Figure 4.1 Signal output of the potentiometer of the bespoke closuremeter (after Celesco, Compact String Pot).

The main components of the monitoring instrument are: one position transducer, two pulleys, and one logger device. The position transducer is a potentiometer that produces an electrical signal proportional to the linear extension of a wire (Figure 4.1). Position transducers are generally of stroke ranges (i.e. length of extending cable) between 0-1.255 m for the voltage output signals.

Given the height of the excavation at Boulby mine, four meters of nylon fishing wire were added to the 1.255 m of transducer extending-cable using two frictionless pulleys

to bridge the gap between the roof and floor of the excavation. The modified position transducer was placed inside a PVC pipe of 1.50 m in length and fixed at the two ends to the covers of the pipe (Plate 4.4).

4.2.1 Closuremeter components

4.2.1.1 Position transducer

Position transducers are water resistant SP2 Strings Pot made and commercialized by Celesco (Plate 4.1). They consist of a flexible cable, a spring-loaded spool and a conductive plastic potentiometer for detecting and measuring linear position of a given point. The instruments can be used in tight spaces and high cycle applications, and enable measurement of cable misalignment (Celsco, 2008).

Plate 4.1 SP2 String Pot spring-loaded potentiometer (Celesco, 2008)

The potentiometer delivers a voltage output signal proportional to the travel of the spring-loaded cable with a precision of 10 K-ohm. Mine workings convergence at the monitored point pulls the transducer spring-loaded cable and generates impulse (i.e. stroke). The generated impulse is transmitted to the data logger through cable and recorded as voltage. This action is repeated at sampling time interval sets depending on

the purpose of the monitoring process. In the present study, a time interval of five minutes was set to allow capture of small changes which occur in the mine workings. The characteristics of the position transducer are given in Table 4.1 below.

Table 4.1 Linear cable-extension position transducer specifications (Celesco Transducer Products, Inc. Version: 4.2, 2008)

SPECIFICATIONS	**TRANSDUCER**	**MODEL: Celesco SP2-50**
SPECIFICATIONS		**VALUES**
GENERAL		
Dimensions		260mmx460mmx880mm
Weight		3 oz. (86.25 gms) (without mounting bracket)
Full stroke range		50 inches (1,255 mm)
Output signal		Voltage divider (potentiometer)
Accuracy (% off.s.)		0.25 %
Repeatability		± 0.05% full stroke
Resolution		Essentially infinite
Measuring cable		0.019-in. dia. Nylon-coasted stainless steel
Cable tension (±25 %)		7 oz.
Max. cable acceleration		30 G
Sensor		Plastic-hybrid precision potentiometer
Potentiometer cycle life		250K cycles
Enclosure material		Polycarbonate
Mounting bracket material		Stainless steel
ELECTRICAL		
Input resistance		10K ohms, ± 10%
Power rating, Watts		0 at 250^{o} C
Recommended maximum input voltage		30 V (AC/DC)
Output signal change over full stroke		94% ± 4%
ENVIRONMENTAL		
Operating temperature		-18^{o} C to +70^{o} C
Vibration		Up to 10 G's to 2000 Hz maximum

4.2.1.2 Data logger

The data logger is a battery-powered electronic device that records data over time with a built-in sensor. The HOBO U12 logger used in this research has four external channels which allow four instruments to be connected (Plate 4.2). Generally, the logger records two types of data: samples and events. Samples are measurements recorded

by the sensor at each logging interval for instance, every minute voltage measurement. Events on the other hand, are independent occurrences generated by a logger activity. Examples include asynchronous events recorded when the logger battery is low, the data file end at the stop of the logger (MAN-U12-006, 2005).

The HOBO U12 may also be used to monitor temperature, relative humidity (RH), light intensity, CO_2, AC current, 4-20 mA, and 2.5 V DC (i.e. voltage).

In this research, the Hobo logger is used to monitor the voltage transmitted by the position transducer (Section 4.2.1). The logger enables scaling of recorded data (voltages) to millimetres in order to deliver the output in millimetres. The characteristics of the HOBO U12 4-External channels are given in Table 4.2 below.

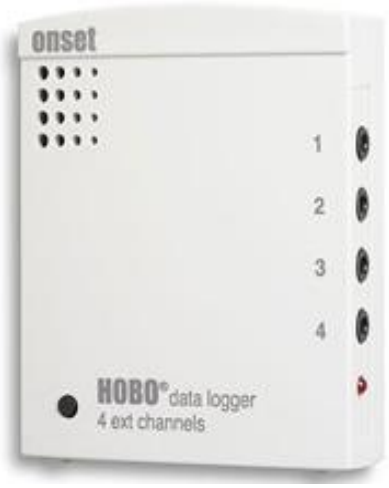

Plate 4.2 Onset HOBO data logger 4 ext channels (Onset Computer Corporation, 2005)

The HOBO U12 logger is of 12-bit (i.e. binary digit) resolution implying that it is capable of recording changes in magnitudes of workings convergence more precisely (i.e. with high resolution). Compared to for instance an 8 bit resolution HOBO logger, a 12-bit logger provides high quality of short-term mine workings movement underground excavations than the 8-bit one. This is of relevance in underground mining where monitoring short-term workings behaviour requires high resolution monitoring instruments.

Table 4.2 Logger data device specifications (Onset Computer Corporation, 2005)

SPECIFICATIONS	**LOGGER DATA DEVICE**	**Model: HOBO U 12**
Dimensions	58x74x22 mm	
Weight	Approx. 46 gms	
Measurement range	± 2mV ± 2.5% of absolute reading	
Resolution	0.6 mV	
Time accuracy	± 1 minute per month at 25^{o} C	
Operating temperature range	Logging: -20^{o} to 70^{o} C	
Relative humidity measurement range	0 to 95% RH, non-condensing	
Battery life	1 year typical use	
Measurements	43,000 12-bit	
Complete download	In 30 seconds	
Output	Voltage/Millimeter (possibility of scaling)	
Memory	64K bytes (43,000 12-bit measurements)	

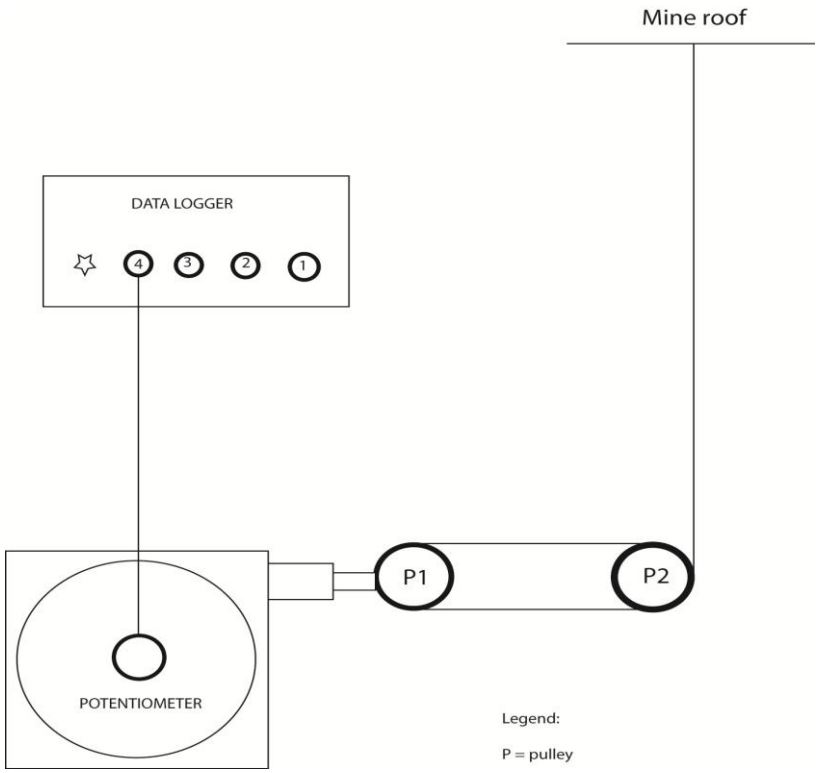

Figure 4.2 Sketch of closuremeter showing the connections between potentiometer, data logger and mine roof per means of pulleys

For the bespoke closuremeter to be effective in monitoring the actual behaviour of mine workings, care should be taken when connecting the two main components (i.e.

position transducer or potentiometer and data logger) of instrument. The assembled bespoke closuremeter is shown in Figure 4.2 and on Plate 4.3.

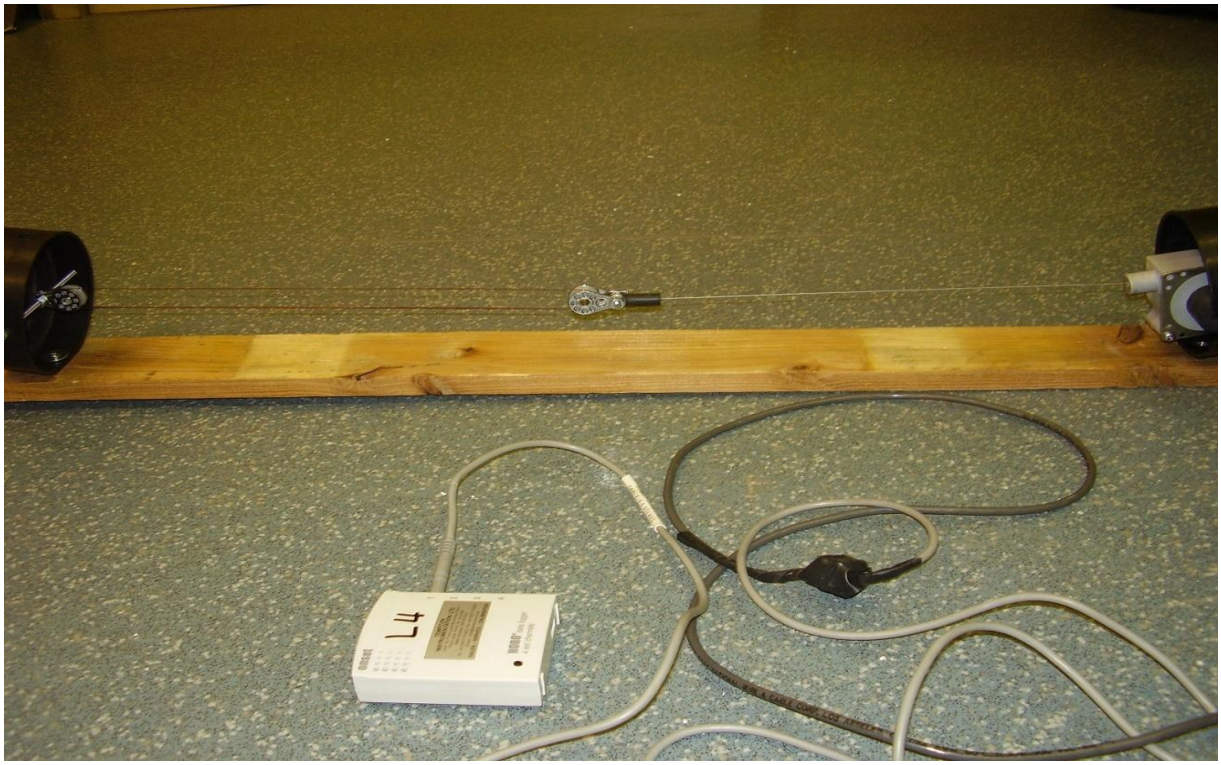

Plate 4.3 Bespoke closuremeter connections within the pipe and the data logger (here it is mounted on piece of wood)

4.2.2 Setting maximum limits of closuremeter

Prior to the installation underground mine, a setting of the closuremeters maximum limits is undertaken as follows: first: the instrument cable (i.e. spring-loaded and added wire) is pulled out to its maximum and released. A voltage value corresponding to the length of the cable is read. The process is repeated at least twice till a steady voltage value is displayed and then recorded. This value serves as the minimal value of convergence the instruments will record at the site (i.e. corresponds to small movement of the mine workings). Second: the cable is fully pulled out repeatly and the associated steady value in volts is recorded. This value serves as the maximum value of convergence to be recorded at the monitoring site (i.e. corresponding to a complete

convergence of workings). The setting limits data of the three instruments are given in Table 4.3 below.

Table 4.3 Closuremeters setting maximum limits and mine workings height (i.e. initial value)

	Closuremeter 1	Closuremeter 2	Closuremeter 3
Min. Value	0.69 V = 0	0.86 V = 0	0.75 V = 0
Max. value	2.29 V = 4.35 m	2.31 V = 4.53 m	2.33 V = 4.67 m
Mine workings height	2.75 m	2.75 m	2.63 m

4.2.3 Closuremeter field test

Three instruments (closuremeter 1, closuremeter 2, and closuremeter 3) were installed in the mine (Plate 4.4) to test their functioning and assess their effectiveness in monitoring short-term workings convergence over the period of measurement.

Plate 4.4 Closuremeters installed at stub of an ongoing mined panel

Two closuremeters are connected to data logger (DL1) and one closuremeter is connected to data logger (DL2). The monitoring site is a stub in close proximity to a workings access roadway. Data were collected over a period of forty one days from 20th April 2007 to 30th June 2007 and are processed in terms of cumulative convergence over time. The results are discussed in section 4.2.3.1.

4.2.3.1 Closuremeter precision

The quality of the output of a monitoring process is an issue and may be characterized in terms of errors that affect the measurements. Several means are used to quantify the goodness of the outputs, among which is the short-term variability or instrument precision.

Generally, monitoring instruments precision is controlled by the standard deviations from repeated measurements. Monitoring instrument repeatability (i.e. precision) is determined knowing the actual (i.e. true) value of the measured variable. However, for cases with unknown true value, such a technique is practically difficult because of the large amount of data. Therefore, different approach should be adopted to determine the precision of the monitoring instrument from the collected dataset. In the present research, the smoothing technique is adopted.

Data collected at a monitoring point over the measurement period are smoothed and the precision of each instrument is equal to the change in the magnitude of displacement (i.e. workings convergence) between successive ranges of smoothed data within a column.

The analysis of dataset of convergence from the three instruments gave values of 1.63 mm, 1.78 mm and 1.87 mm of precision for closuremeter D2_1, closuremeter D1_1 and closuremeter D1_2, respectively. The discrepancy in the magnitudes of individual closuremeter precision translates the dependency of the instrument precision on the resolution of the data logger used as component of the bespoke closuremeter despite the influence of position of the monitoring point.

From the three values, the bespoke closuremeter precision (i.e. mean value) is 1.76 mm with a standard deviation of 0.099 mm. With such a precision of order of millimeters, the bespoke closuremeter is capable of monitoring small changes of order of millimeters expected to occur in deep underground mining.

4.2.3.2 Analysis of results and discussion

In order to access the functioning of the bespoke closuremeters, the monitoring data were analyzed in terms of cumulative displacement and presented in graphical form as convergence-time curves at each monitoring point over the entire period of measurement.

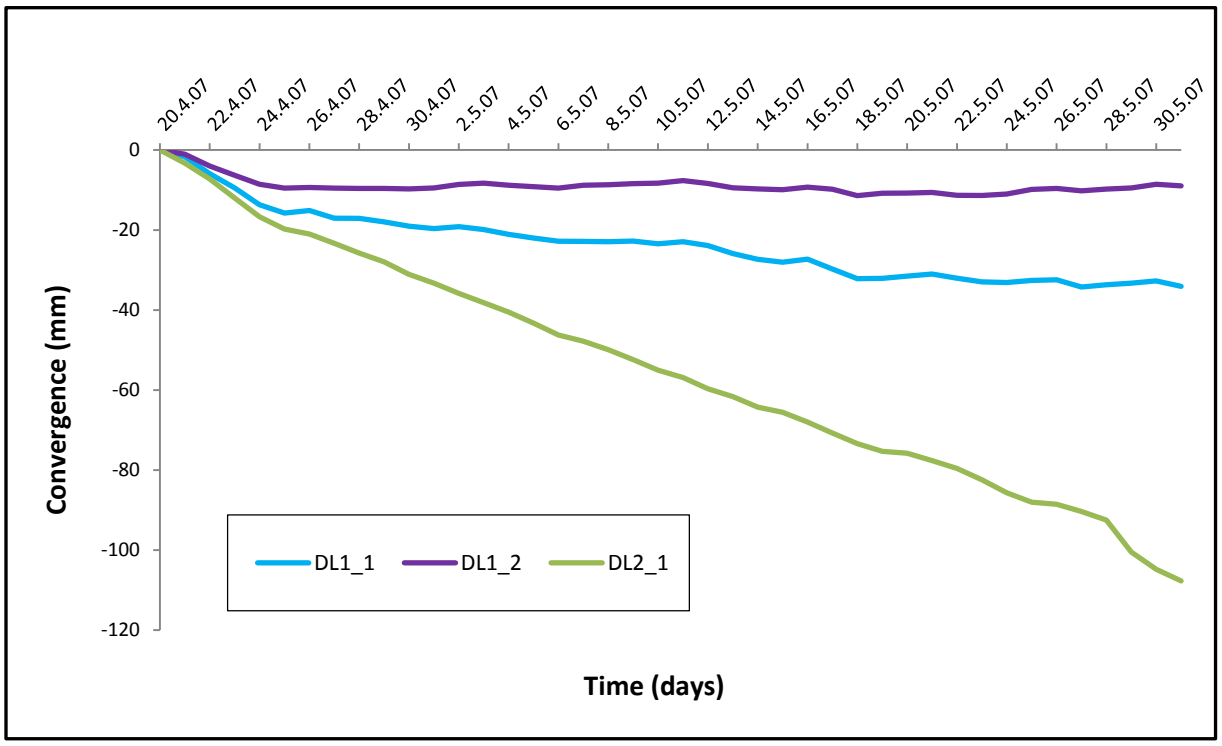

Figure 4.3 Convergence recorded by the three closuremeters at the monitoring site between 20th April and end of May, 2007

Figure 4.3 shows quite similar patterns of movement at the three monitoring points, but occurring at different rates. The plot indicates two trends of movement: an initial movement with high rate occurred over the first five days after the commencement

of monitoring followed by a gradual and linear movement which occurred over the entire remaining period of measurement between 26th April and 30th May 2007. The early rapid movement should be attributed to the fact that the site was newly excavated and its instrumentation took place few days after excavation. Because of the close proximity of the three monitoring instruments, the discrepancy observed in the rate of convergence might be due to the position of the instruments at the site.

An alternative explanation is, with the assumption that the materials in the immediate roof, floor and in the overburden are similar and the excavations geometry and sizes are comparable, high rates convergence are expected to occur along the main axis of excavation whereas low rates movement would occur at the rib (i.e. sidewall) of excavation. At stub, high rate movement occurrence is expected far away from the rib and low rate movement will occur in close proximity to the wall (Brady and Brown, 2006; Hartman and Mutmansky, 2002). In room-and-pillar mining in a stratified rock, roof strata over the excavation will detach more from their host by relaxation at the center of the excavation than at the pillar (Alejano *et al*., 2008). As a consequence, high rates of roof movement are expected to be recorded at the center of the excavation.

At the monitoring site, closuremeter DL2_1 was installed far away from the rib and in close proximity to the workings access main roadway, whereas closuremeters DL1_1 and DL1_2 were installed relatively more close to the rib.

After a relatively rapid and high rate initial movement over the five first days of measurement, the rate of movement at DL1_1 and DL1_2 significantly decreased to a relatively low value with a quasi-null rate of movement at DL1_2. Meanwhile, the rate of movement at DL2_1 was higher despite the slight decrease on 24th April, 2007, as observed after five days of monitoring. The initial first five day movement is probably due to the relaxation of the stressed potash rock in the roof due to the removal of the support. This process generally results in the detachment and falling of the rock as slab.

The decrease of movement rate resulted in gradual and linear movement at the three points over the remaining period of measurement. At DL2_1, mine workings closed up at rate of about three and twenty-three times the rate of movement at DL1_2

and DL1_1, respectively. At DL1_2, convergence of workings occurred at rate of about six times the rate at DL1_1.

From the patterns of convergence, but also the convergence rate ratios between DL2_1 and DL1_1 on one hand and between DL1_2 and DL1_1 on the other hand, it is obvious that the workings at DL1_1 was rather stable after the initial rapid movement on 24th April, 2007 owing to the position of this point relative to the rib of the stub.

4.3 Summary

Closuremeter has been specially designed to monitor mine workings deformation behaviour in terms of roof-to-floor convergence. The short-term mine workings movement datasets allowed the assessment of the functioning of the closuremeters. The analysis of data clearly indicates gradual downward movement of mine workings at the monitoring site despite the discrepancy in the rate of movement at the three points as a result of the instruments position at the site relative to the rib of the excavation and also the fact that the site was newly excavated and instrumented few days after excavation.

The rate of workings movement is higher at the point in close proximity to the roadway, while low rate of movement is recorded at points in the vicinity of the rib of the stub. In terms of precision, the specially designed closuremeter is capable of recording small changes in mine workings deformation of about 1.76 millimeters with a standard deviation of 0.099 mm depending on the position of the monitoring point at the site.

As such, this is a sustainable device to monitor mine workings convergence in similar mining areas to the Boulby mine. Data from the bespoke closuremeter used to monitor the mine workings convergence at Boulby are discussed in Chapter 5.

Chapter 5
Mine instrumentation and short-term convergence monitoring

5.1 Introduction

The relevant information on mine instability at Boulby has been outlined from a theoretical point of view and on basis of data from various laboratory and field works detailed in the previous chapters. However, the most important source of information is the mine itself.

Monitoring is fundamental to the stability of underground mine workings, particularly during the life of the mines. Thus, a properly designed monitoring survey enables accurate assessment of any effect on mines stability.

One of the objectives of this research is to characterize the actual behaviour of mine working on the basis of short-term convergence dataset. Hence, particular attention has been given to the installation, monitoring and interpretation of results from the monitoring sites throughout the course of the investigation. This chapter describes the actual short-term monitoring process of workings convergence at Boulby mine and evaluates data from sixteen bespoke closuremeters installed at four sites. The information collected is essential for the determination of controlling factors of the mechanics of excavation underground mines. This information is also fundamental for the numerical analysis of stress-displacement distribution and resulting subsidence associated with the mining activity.

5.2 Mine workings instrumentation

5.2.1 Selection of monitoring sites

Instrumentation and monitoring underground mines provide information on changes occurring within the immediate roof (i.e. first layers of roof) and floor for the stability of the workings. In line with the objectives of the study four key criteria guided the selection of the sites:

(1) The location of the sites in the North or South of the mine;

(2) The age of the sites (i.e. date of excavation);

(3) The location of the sites near an active main or new face; and

(4) The conditions or geometry of the sites (i.e. roadway or stub).

The main drive was to secure the determination of variables which may affect the patterns of mine workings convergence at Boulby mine. The results of the investigation will be used to understand the mechanics of underground excavations as a function of some variables such as the location, geometry and age of the sites.

Mine workings mechanics is affected negatively by the age of the sites because most of controlling factors have pronounced influence on the workings behaviour at the early stage after excavation. The geometry and size of excavation are also significant controlling factors of mechanics of mine workings (Wang *et al*., 2000).

Given that mining of potash at Boulby is still active, the selection of sites for data collection was also guided by the environmental conditions and regulations for safety. Four locations of sites were selected and are shown in Figure 5.1.

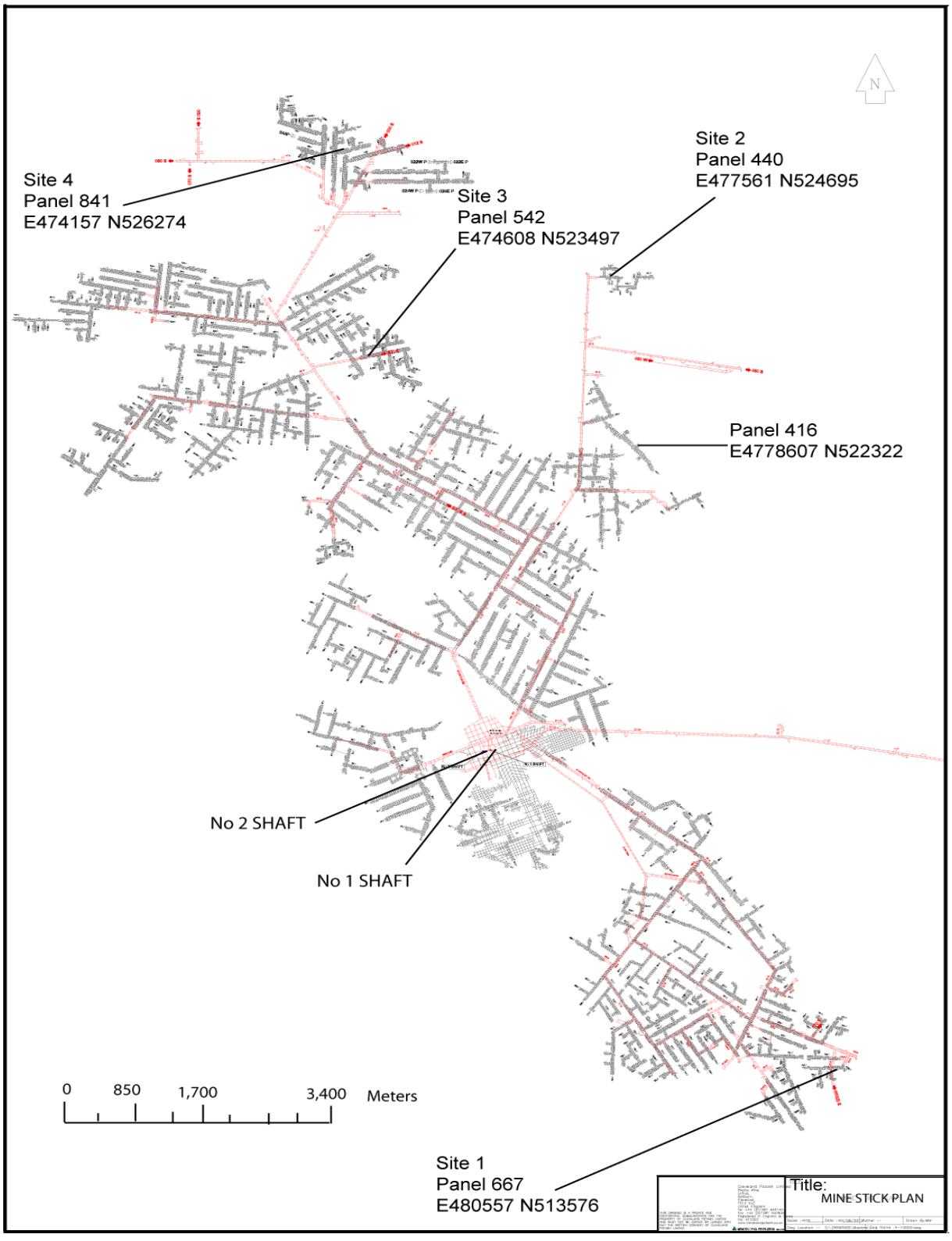

Figure 5.1 Underground mine layout and instrumented site locations (source: Boulby Mine); where red colour indicates salt roads and black colour indicates potash panels

5.2.2 Closuremeters layout

Monitoring instruments for area of concern should be placed where high expected behaviour (i.e. convergence of mine workings) is likely to occur. In room-and-pillar mining, high magnitudes of convergence are expected to occur along roadways (i.e. rooms) and cross-cuts axes, whereas low magnitudes of convergence are expected at stubs (Caughill and Beddoes, 1996).

The monitoring network consisted of four sites: one located in the South (i.e. site 1) and three in the North of the mine (i.e. sites 2 - 4) and they are of two types, either roadway or single/multiple stubs (see Figure 5.2. for layout). At each of the sites, four instruments were installed accordingly: for sites of roadway type (sites 1 and 2), the instruments were installed along the roadway and cross-cuts axes; at a single stub (site 3) the instruments were installed close to one another, while in a series of stubs (site 4) they were placed at each stub (Figure 5.2, plates 5.1 and 2; and plate 5.3).

At site 1, installed closuremeters observed greater closure within panel 667 (Figure 5.1) in the hotter South of the Boulby mine than the North as a result of gradient of both overburden pressure and temperature (Section 3.1). Borehole temperature measurements indicate rock temperatures ranging from 25^{o}C to 30^{o}C in salt panel (in the North) and from 40^{o}C to 45^{o}C in potash panel (in the South) and rock temperature is 40^{o}C and 45^{o}C for 1050 to 1100 m depth and 1200 to 1250 m depth, respectively (Caughill and Beddoes, 1996). This increase in pressure and temperature affects the mechanical properties of evaporites (i.e. potash, salt and carnalite marl) and exacerbates the deformation behaviour of the rocks.

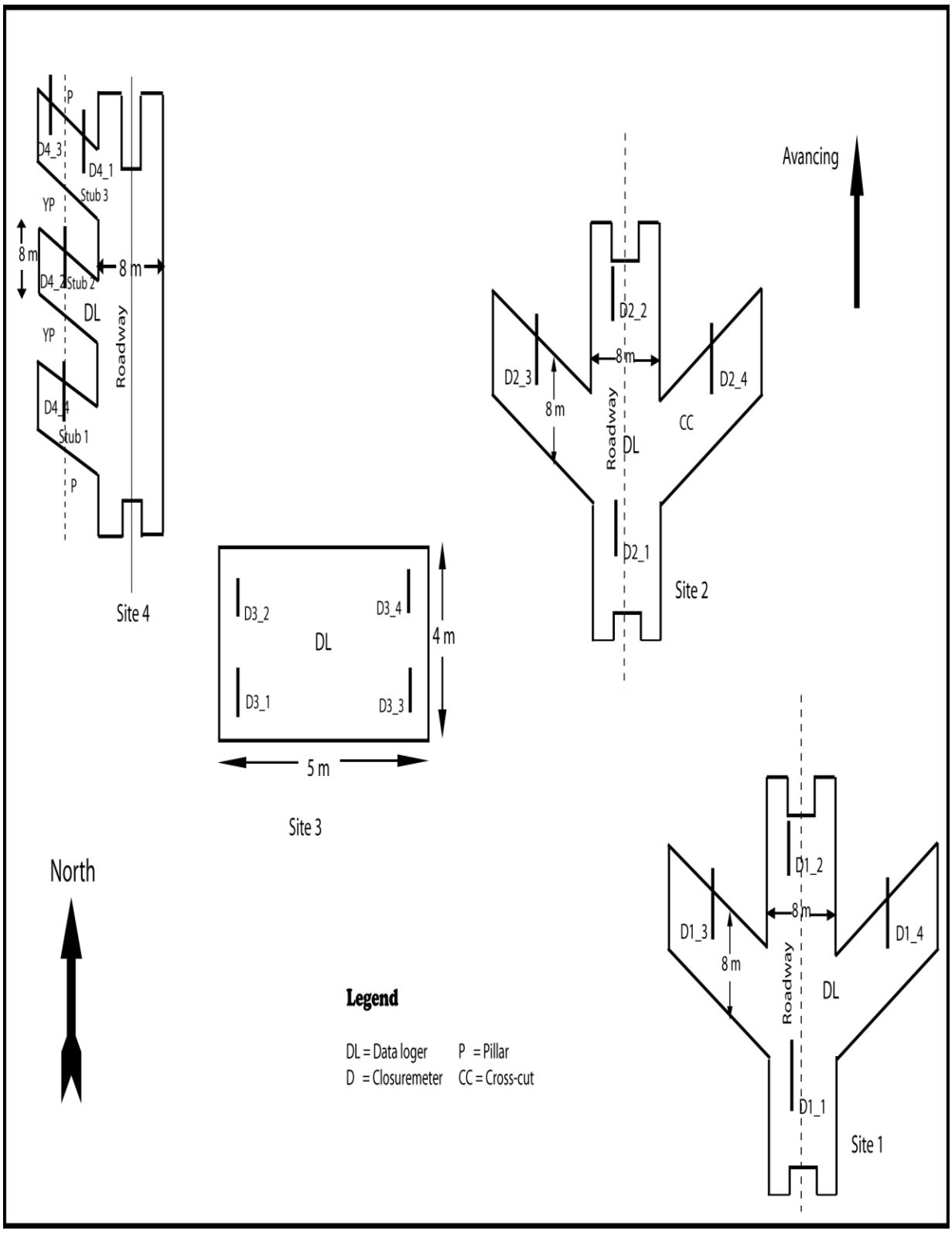

Figure 5.2 Instrumentation of mine workings and sites' plan showing geometry of sites and location of closuremeters with reference to Figure 5.1

Plate 5.1 Closuremeter installed along roadway at site 1 in the South

Site 2 is the oldest among the monitored sites undergoing smaller closure. It is an abandoned area within panel 440 and may have experienced later stage of closure. Because of high temperature owing to lack of ventilation, this site was abandoned few months after the monitoring process has begun. Like site 1, site 2 is of type of roadway with two closuremeters installed along roadway axis and the two along cross-cuts axis.

Plate 5.2 Closuremeter installed at cross-cut at site 2 in the North

Site 3 is of stub type within the abandoned panel 540/542 in close proximity to a roadway for workings access. Because of the reduction of height of the roadway as a result of roof sagging preventing access to the workings, the roadway floor was milled on 29th March 2007. The process consisted in the removal of floor layer in order to increase the height of excavation at the determined location. The closuremeters arrangement is shown on Plate 5.3.

Plate 5.3 Closuremeters installed in parallel at stub at site 3 in the North

Site 4 is within panel 841 in close proximity to a new face and consists of three stubs separated one from another by a yield pillar of about 2 meters wide. Four instruments were installed at the site: two at the third stub and the other two at the first and second stub, respectively (Figure 5.2). The characteristics of the four sites are given in Table 5.1.

Table 5.1 Sites characteristics

Site 1	**Panel number: 667**		**Location zone: South**	
Dates of excavation				
Starting: 05/12/2007	Stopping: 12/2007		Milling: None	
Date of instrumentation: 28/02/08				
	Clm1	Clm2	Clm3	Clm4
Initial excavation height at the monitored point (m)	3.53	3.14	2.88	3.04
Distance of Clm to data logger (m)	12	6	4	3.80
Site 2	**Panel number: 440**		**Location zone: North**	
Dates of excavation				
Starting: 06/06/2005	Stopping: 06/2006		Milling: None	
Date of instrumentation: 28/02/08				
	Clm1	Clm2	Clm3	Clm4
Initial excavation height at the monitored point (m)	3.01	2.92	3.06	2.86
Distance of Clm to data logger (m)	15	14	10	5

Site 3	**Panel number: 540/542**			**Location zone: North**	
Dates of excavation					
Starting: 11/12/2007	Stopping: 12/2007			Milling of floor: 29/03/2008	
Date of instrumentation: 28/02/2008					
			Clm1	Clm2	Clm3	Clm4
Initial excavation height at the monitored point (m)			3.542	3.662	3.422	3.342
Distance of Clm to data logger (m)						
Site 4	**Panel number: 841**			**Location zone: North**	
Dates of excavation					
Starting			Stopping: 14/12/2007	Milling: None	
Stub1 42/43 29/11/07	Stub2 44/45 07/12/07	Stub3 45/46 13/12/07			
Date of instrumentation: 28/02/2008					
			Clm1	Clm2	Clm3	Clm4
Initial excavation height at the monitored site (m)			3.205	3.465	3.506	3.876
Distance of Clm to data logger (m)						
Legend: Clm = closuremeter						

5.2.3 Geological setting of sites

Borehole exploration and seismic surveys carried out across Boulby area indicate sequence of strata made of both marine clastic sediments and evaporites overlying potash in the mining area. Although the results revealed a regular succession over both onshore and offshore mining area, the stratigraphy at the monitoring sites is different owing to the irregularities of geology particularly in the near-seam potash (Hebblewhite, 1977).

At Boulby mine the roof around the seam is a mixture of potash, halite, shale and sylvinite, halite parting, shale with marl, and carnalite marl with varying thicknesses throughout the mine workings (Figure 5.3). Such geological variations result in different rates of roof-to-floor convergence of workings (Hebblewhite, 1977). Table 5.2 summarizes the variation of rates of roof-to-floor closure at some monitoring sites in potash with a mixture of potash, halite and shale in the roof.

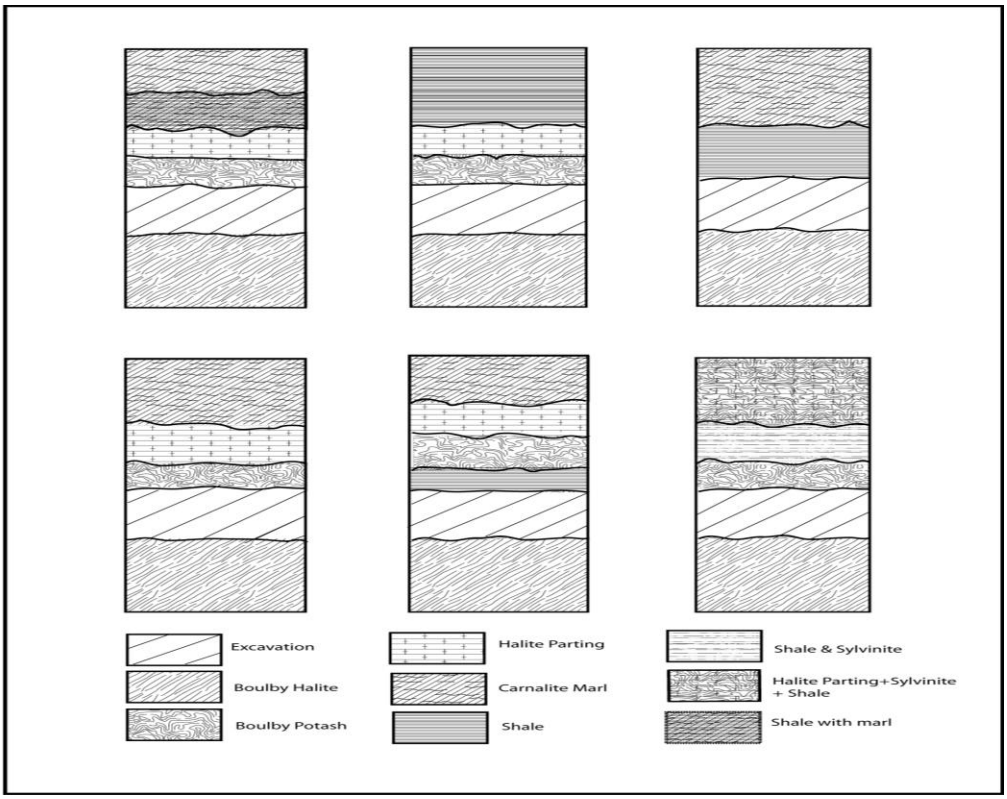

Figure 5.3 Geological setting near-seam indicating variation in thickness and layers in the immediate roof (Adapted from Hebblewhite, 1977); Not to scale - Schematic only

Table 5.2 Summary of rates of closure (mm/day) of mine workings at monitoring sites at Boulby mine (Adapted from Hebblewhite, 1977)

Site	Station	10 days	25 days	50 days	100 days	200 days
NU02	C1		2.00	0.94	0.37	0.26
NU04	C3		2.11	0.96	0.71	0.44
NU05	C7	6.01	-	1.19	0.94	0.69
NU06	C11		2.57	1.49	0.84	0.38
NU07	C14		2.00	1.47	1.14	0.57
NU08	C17		3.17	1.95	1.29	1.00
NU10	C21		0.88	0.92	0.39	0.21
NU11	C23		2.25	-	-	1.10
NU12	C25				1.44	0.43
NU13	C30				0.67	0.57
NU14	C26				1.10	1.00
NU15	C29					0.57
NU16	C32				0.43	0.57
1P1	BH3	3.00	1.25	0.71	0.28	0.36

1P1	BH6	3.00	1.71	0.86		
1P1	BH7	4.00	1.57	-	0.50	0.38
1P1	BH8	0.30	0.57	-	0.31	0.31
1P2	BH11	8.00	2.56	1.57	1.71	
1P2	2P	5.80	-	-	1.43	
1P2	2Q			1.81	1.18	
1P7	A C2			2.75	1.86	
1P8	A C2		4.88	2.56		
1P8	A C2		2.50	0.75	0.43	
1P9	B C2	5.80	3.30	1.43	0.86	
1P9	C C2	3.67	1.57	0.86	0.50	
SD1	C2			9.33	5.33	
SD2	C2			7.28	4.43	
SD3	C2		1.25	2.50	0.61	0.43
SD4	C2		1.25	0.62		
SD6	C2				1.52	
SD7	C2			1.75	1.75	
H4	C5	1.50	0.20	0.21		
H5	C5	0.75	1.00	0.29		
EP1	C2		4.25	3.14		
EP7	C2	6.00	5.33	7.20		
2P1	C2	8.00	3.67	1.80		
2P2	C2		5.33	1.80		

Table 5.2 shows convergence rate variation as a function of monitoring sites and most importantly as a function of stations at the sites. This latter variation is probably a result of the geological variations near the seam at the monitoring sites. The table aslo shows high excavation convergence rates occur in the South (SD: South Development) than in the other parts of the mine, particularly after 50 days of measurement and the decrease of rates of convergence over time. Geological variations constitute interface between layers and form locus of beds separation. Consequently, control the behaviour of the excavations regardless of the geometry and age of the openings. High roof

deformation occurs at the interface between the halite parting and potash as a result of beds separation. Roof with a mixture of potash, halite and halite parting shows stability of roadway at the sites. The presence of shale in the roof results in the instability of roadways. Generally, competent potash and halite beams of at least 2 m to 3 m thick in the roof below the weak shales and marl provide long term stability of the roof.

In general, closure of roof of workings at Boulby is driven by the geological variations in the near-seam roof throughout the mine though geometry and age significantly control the behaviour of mine roof. These geological variations might also have influenced the patterns of convergence displayed by the workings behaviour at the four sites.

5.3 Assessing floor heave

Rearrangement of geostatic stresses results in the narrowing of the height of excavated areas in underground mining. This relative movement referred to as convergence generally comprises both roof sag and floor heave (Kratzsch, 1983).

Given that a detailed FLAC analysis is presented in Chapter 6, a brief description of the analysis process is introduced herein. The modelling process may be described as follows: (1) applying vertical stress (i.e. stress exerted by the overburden) on each layer, (2) excavating two rooms in potash, (3) running the model, (4) monitoring movement at two opposite points on the middle of excavation – i.e. one on the roof and another on the floor, and (5) plotting on a single graph roof closure, floor heave and convergence (i.e. sum of roof closure and floor heave) to visualize the contribution of floor heave to workings convergence. The vertical stresses are estimated using equation 3.1 and horizontal stresses are obtained using the ratio value of 0.51 (Section 3.6.1).

Because convergence of workings is mostly controlled by the behaviour of the immediate roof (Kratzsch, 1983), the FLAC model used in this process includes all strata of the near-seam to 85 m above mine level. In the process, the potash excavation was assumed to take place at 1,200 m of depth. The general geological sequence and mechanical properties of the strata are given in Table 5.3. Anhydrite layer was modelled

as Mohr-Coulomb material while the other strata were treated as strain-softening materials.

Table 5.3 Geotechnical properties of near-seam strata used for modelling (from McLellan *et al*., 2008; Shin et al., 2008; Liang *et al*., 2007; Foley, 2006; Swift and Reddish, 2005; Caughill and Beddoes, 1996; Bell, 1994; Jeremic, 1994; Coulthard and Bell, 1993; Sepehr, K., and Stimpson, B., 1988; Hebblewhite, 1977; Cook, 1974; Patchet, 1970)

STRATA	Thickness (m)	Geotechnical Parameters						Tensile Strength (MPa)
		Deformability		Strength				
		Bulk Modulus (GPa)	Shear Modulus (GPa)	Cohesion (MPa)		Friction (degrees)		
				Peak	Residual	Peak	Residual	
Upper halite	38	12.25	9.19	16.0	9.4	35	10	1.59
Anhydrite	7	14.43	10.83	17.0		43		6.08
Carnalite marl	11	3.9	2.93	3.0	1.0	35	18	1.24
Potash	9	28.73	8.18	10.0	6.0	36	33	1.79
Halite	45	17.93	9.25	10.0	9.4	40	10	1.63

A series of simple models were run using three sets of material parameters one with laboratory data and the two others obtained by reducing laboratory data (Table 5.2) by a factor of 2 and 3, respectively to account for scale effects and also the presence of discontinuities and heterogeneity within the rock masses. Because the modelling analysis is primarily intended to assess floor heave, in other words whether or not the bespoke closuremeter was monitoring relative movement of the excavation, closure models validation is not considered here. For this, excavation closure is modelled only on basis of laboratory data and not observed data. Validation of closure models against observed closure is considered in Chapters 6 and 7 devoted to modelling approach and results analysis, respectively.

The modelling results have been presented in graphical form as roof closure, convergence versus floor heave-timestep curves for comparative analysis. Taking

advantage of symmetry of domain geometry, only deformation at one excavation is presented below. The FLAC code used for modelling floor heave is given in Appendix A.

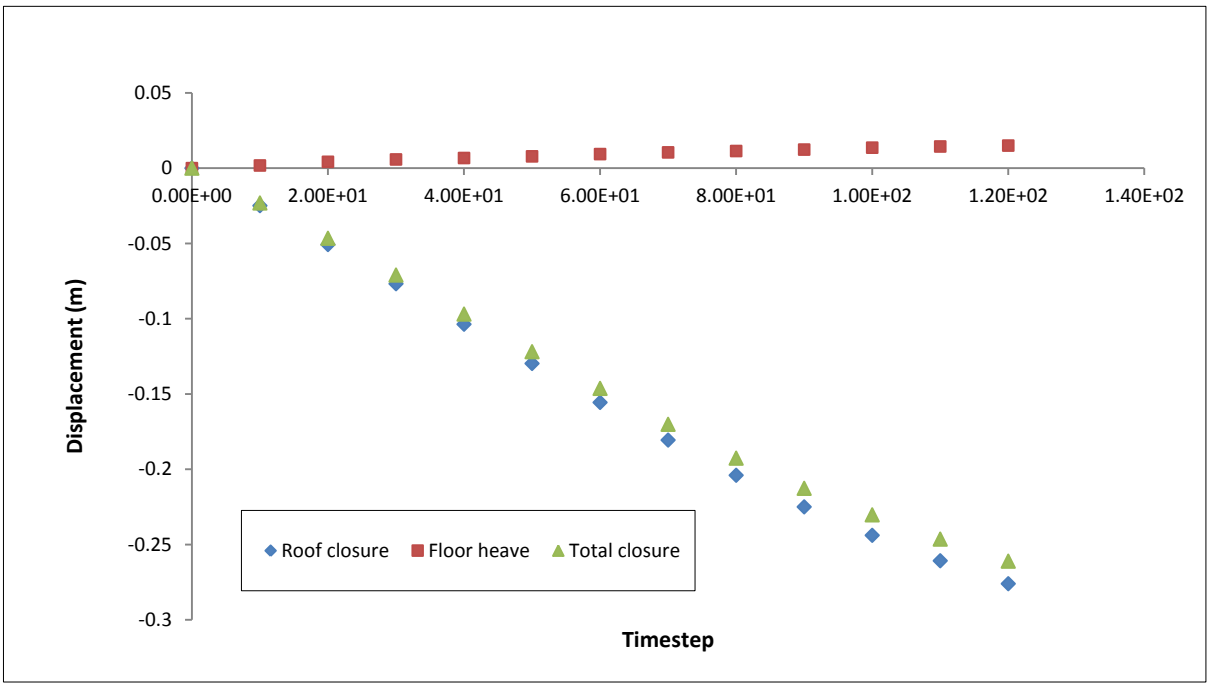

Figures 5.4 Modelled roof closure, floor heave and total closure using laboratory data

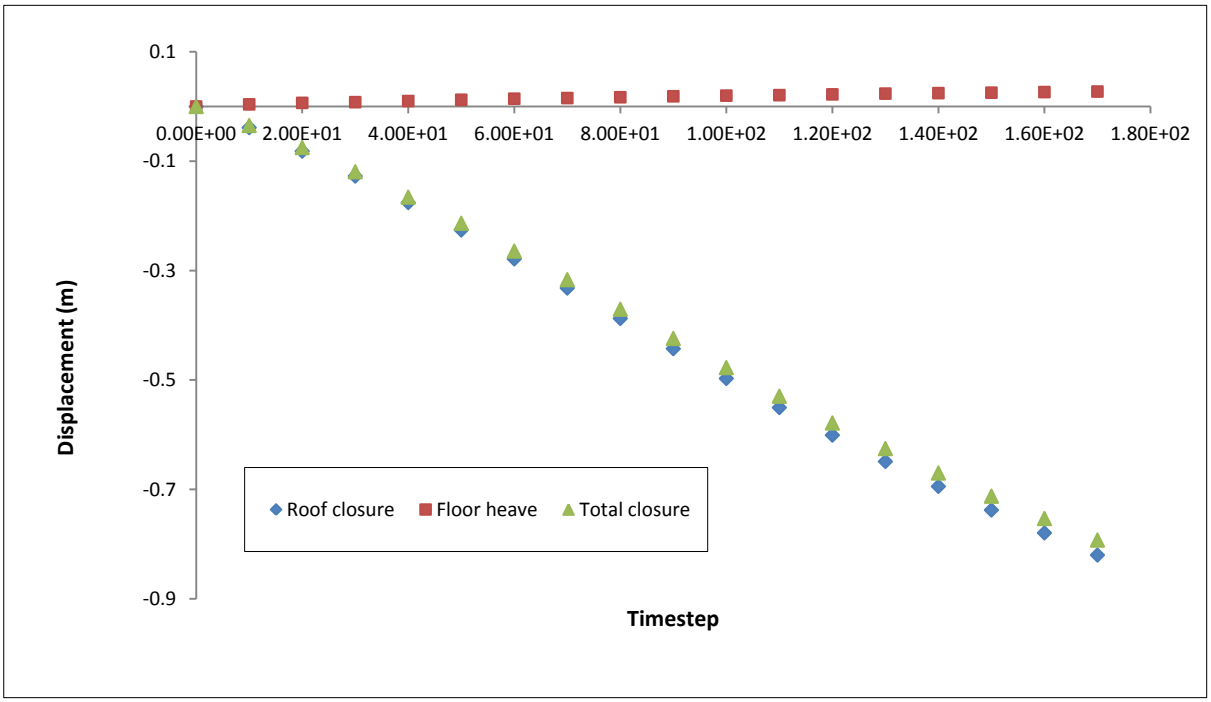

Figure 5.5 Modelled roof closure, floor heave and total closure by reducing laboratory data by a factor of 2

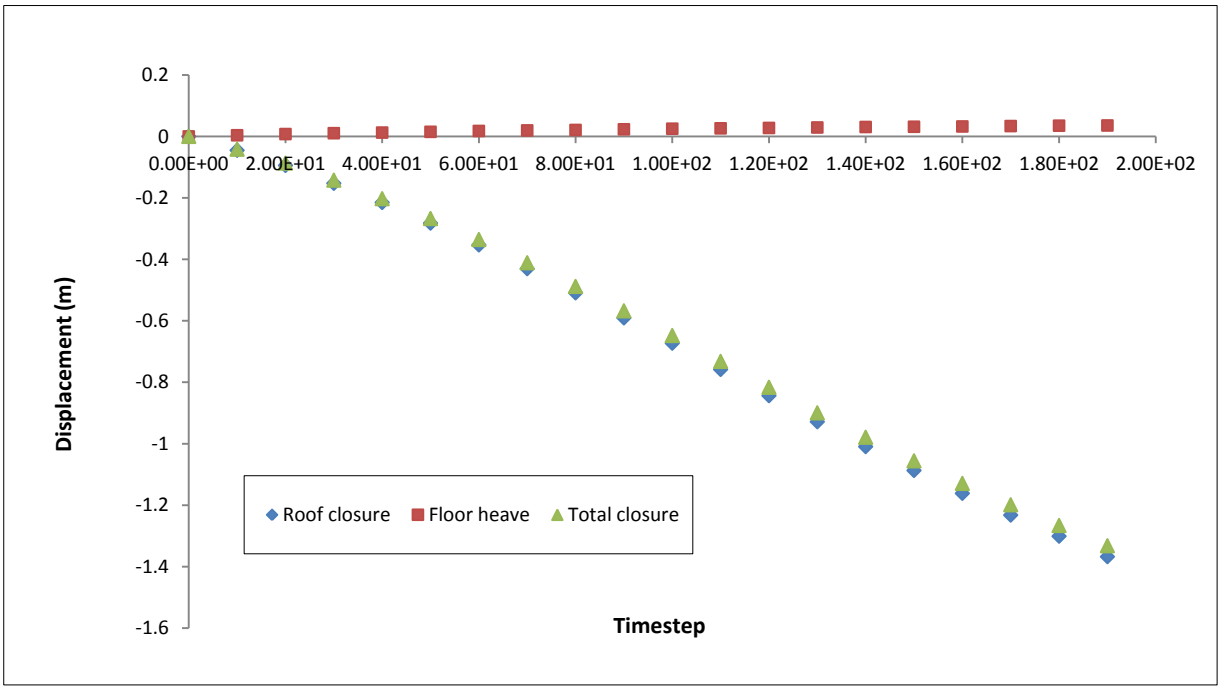

Figures 5.6 Modelled roof closure, floor heave and total closure by reducing laboratory data by a factor of 3

Figures 5.4-6 portray that mining potash at Boulby results in both roof closure and floor heave. Although the rheology of Halite rock dictates the floor deformation, high horizontal stresses on both sides of the openings also control the floor behaviour. In addition, punching of pillars owing to the weight of the overlying strata may also contribute to the deformation of the floor. Magnitudes of both roof closure and floor heave are sensitive to the strata mechanical properties variation. Floor heave contribution to the excavation convergence decreases with the decrease of stiffness and strength of strata as a result of roof failure increase.

Table 5.4 FLAC predicted roof closure, floor heave, and percentage of floor heave

Model	Max. roof closure (m)	Max. floor heave (m)	Max. convergence (m)	Floor heave (%)
Lab data	0.28	0.02	0.26	8
Factor 2	0.82	0.03	0.79	4
Factor 3	1.37	0.04	1.33	3

Figures in Table 5.4 show that, floor heave contributes to the roof-to-floor convergence of opening despite at low magnitude. Therefore, the actual short-term underground monitoring should be understood to measure roof-to-floor convergence of excavations at the sites.

5.4 The actual short-term monitoring of convergence

The mechanics of underground deep excavations is complex and its time-dependent (i.e. long-term) behaviour is analyzed by continuously monitoring changes in the height of workings over a long period of time.

However, in underground active mining and particularly in active potash mining, long-term monitoring of workings may be limited to short-term monitoring owing to problems associated with the ongoing mining activities. Even so, with a well designed monitoring technique continuous short-term monitoring data of workings is capable of providing high quality information on the mechanics of workings and therefore understanding the nature of behaviour of openings in deep active mines.

5.4.1 Data collection frequency

Data sampling frequency was determined with consideration of the deformational behaviour time-scale of both roof and floor strata within the mine. In underground mining, the characterization of short-term deformation patterns of mine working requires sampling openings behaviour at high frequencies. For this reason, a sampling frequency of five minutes has been chosen to capture the short-term behaviour of workings at Boulby potash mine.

5.4.2 Data processing and results

5.4.2.1 Determination of time interval data processing

Monitoring results may be difficult to interpret owing to not only the great amount of data but also the fluctuations in the data associated with the instrument. Generally, different techniques are used to reduce or eliminate such fluctuations and provide a better idea of the overall pattern of mine workings deformation. However, such processing techniques may result in the loss of valuable information or impair the actual behaviour of the deforming structure. Therefore, it is good practice that care be taken when carrying out processing of monitoring data.

In this study, a smoothing technique has been used to eliminate fluctuations in data and effects related to the stability of data logger at the onset of the measurement. The technique consisted in simultaneously removing fluctuations in the closuremeters readings at the monitoring site until steady readings are obtained at the four instruments.

However, given the large amount of data, pattern of the function or curve that captures the mechanical behaviour of mine working may be affected by the time interval over which data are processed. Therefore, in order to determine the interval of time which allows capturing the short-term pattern of the actual behaviour of workings, data were successively processed using smoothing 5 minutes, 30 minutes, hour, 6 hours, 12 hours and 24 hours time intervals. The convergence-time curves were plotted for comparative analysis to determine the appropriate time interval of data processing (Figures 5.7-30). Values of mean and standard deviation of convergence were also determined (Table 5.5).

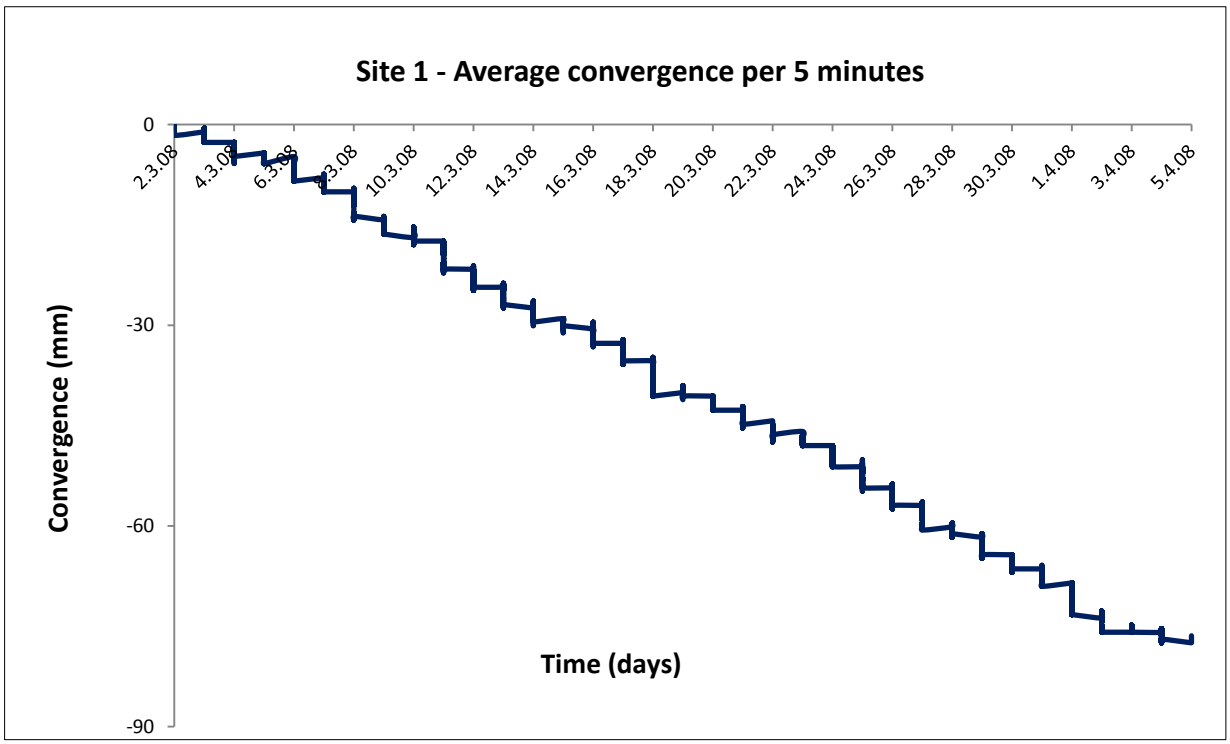

Figure 5.7 Average convergence per smoothing 5 minutes at site 1 between beginning of March and April 2008

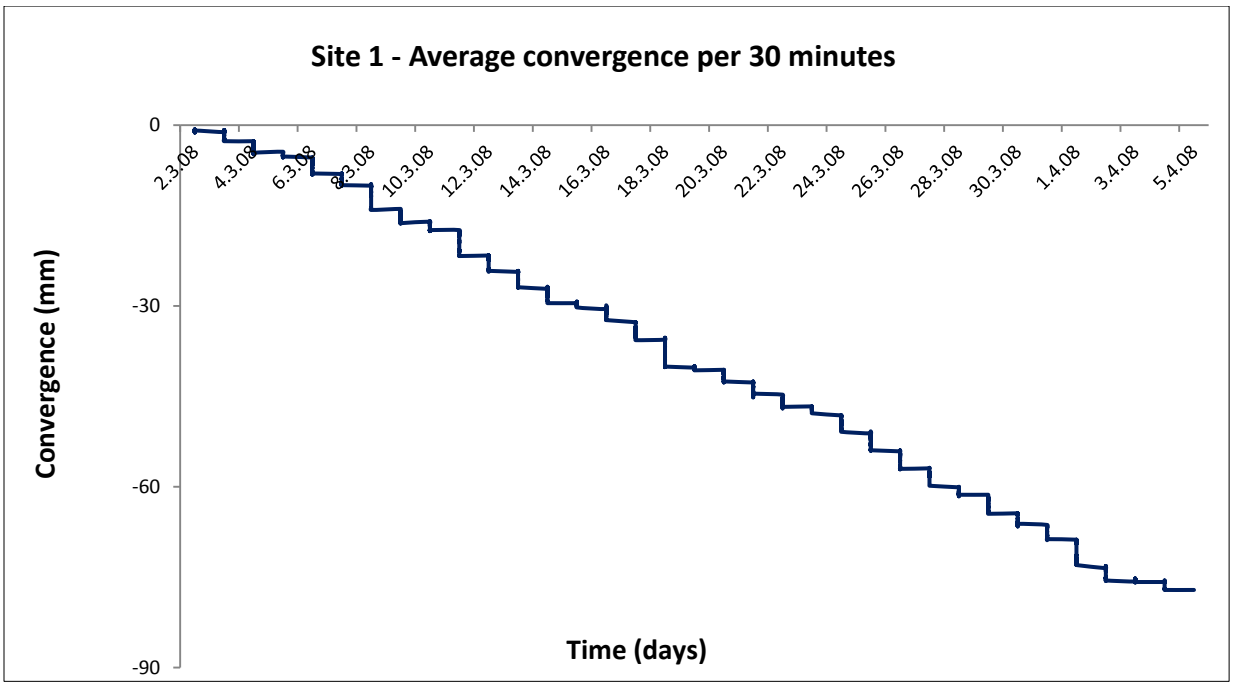

Figure 5.8 Average convergence per smoothing 30 minutes at site 1 between beginning of March and April 2008

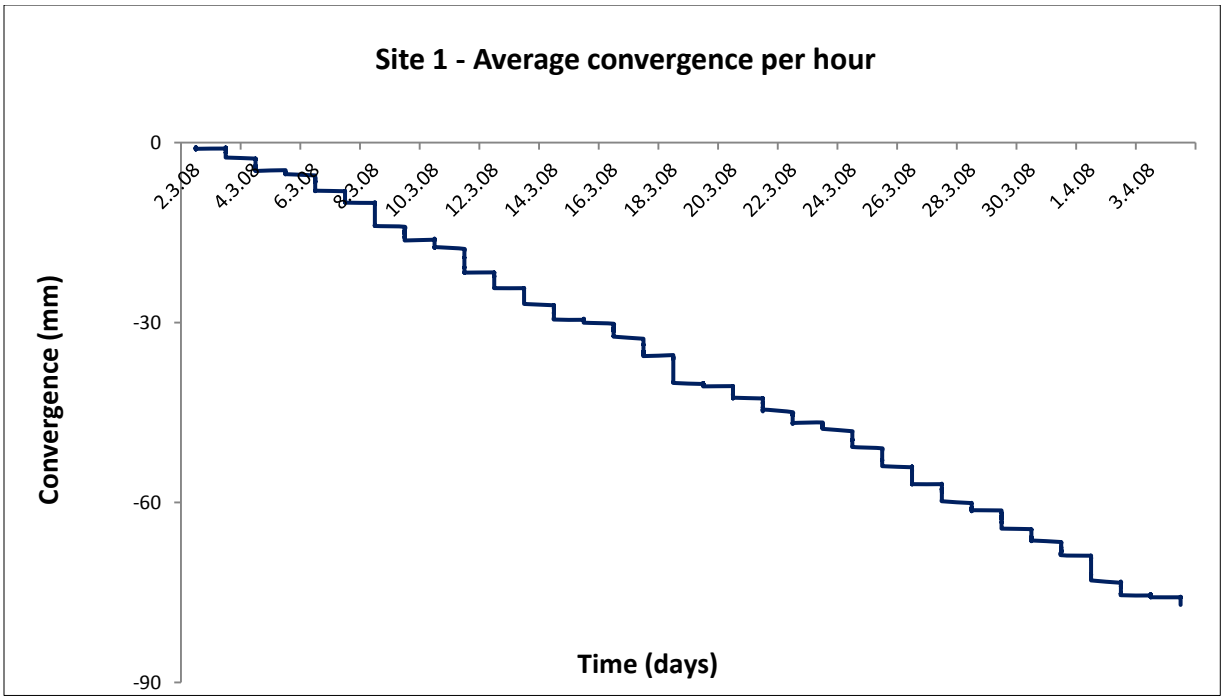

Figure 5.9 Average convergence per smoothing an hour at site 1 between beginning of March and April 2008

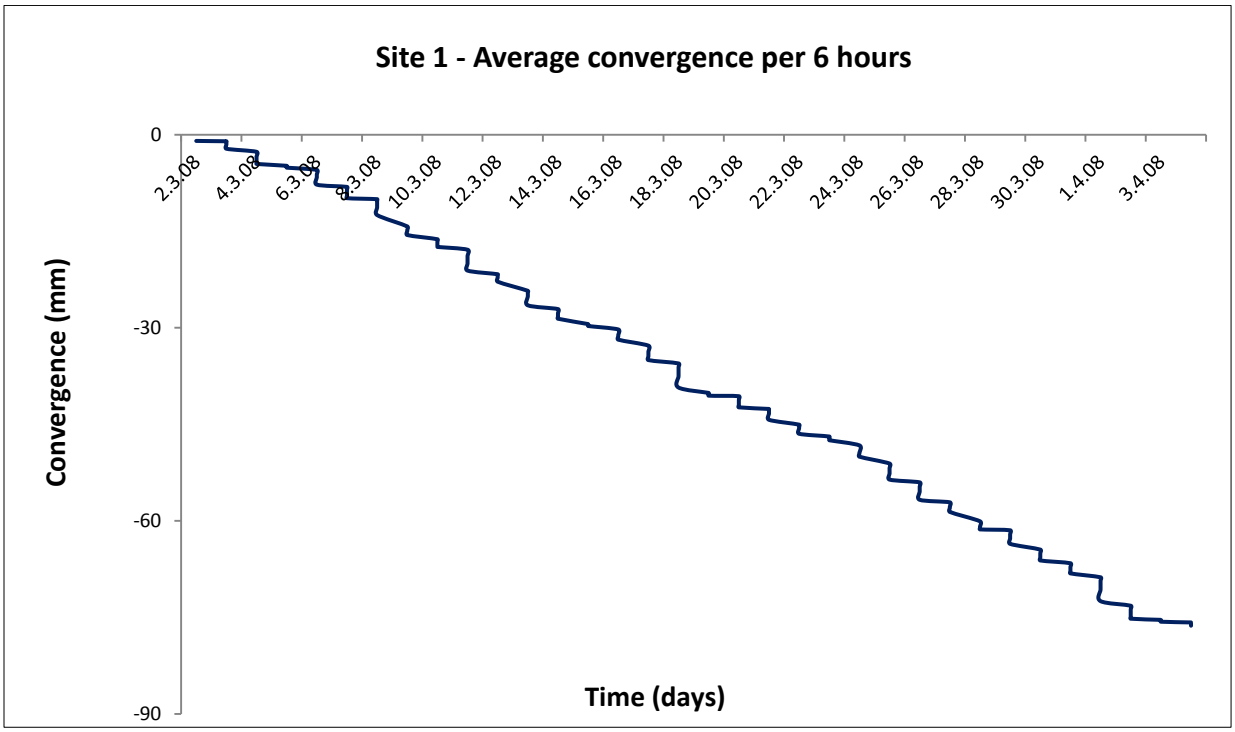

Figure 5.10 Average convergence per smoothing 6 hours at site 1 between beginning of March and April 2008

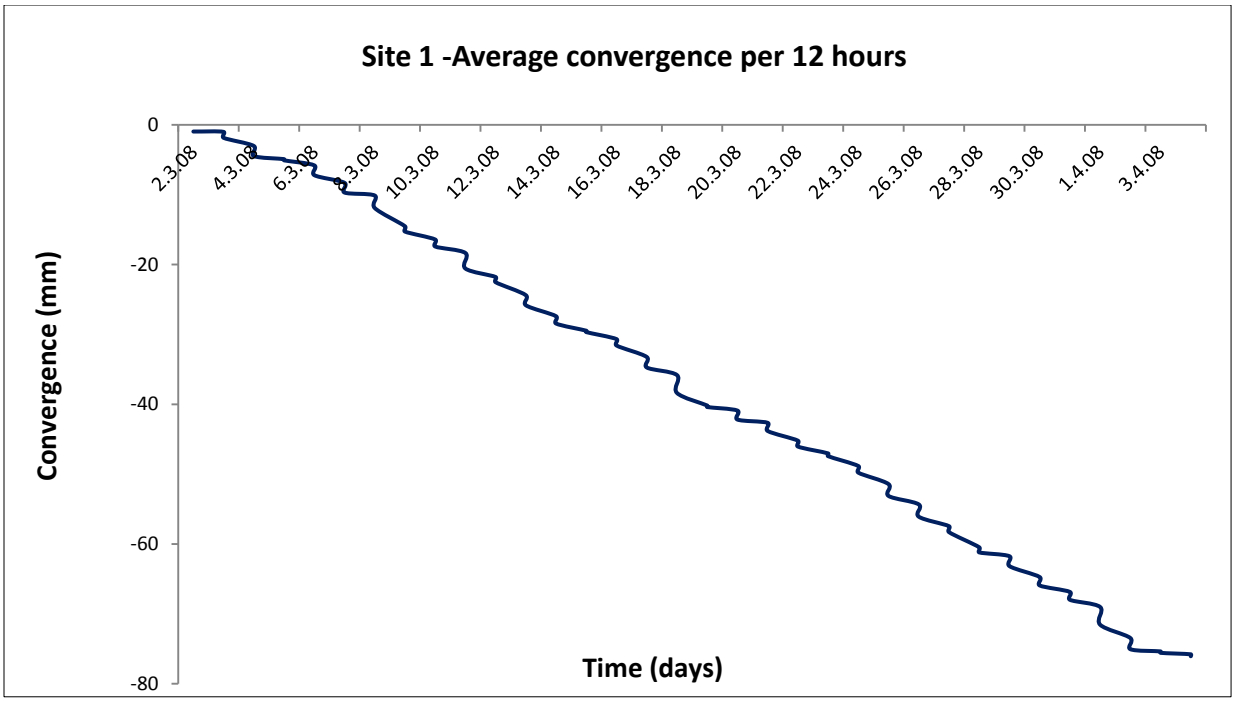

Figure 5.11 Average convergence per smoothing 12 hours at site 1 between beginning of March and April 2008

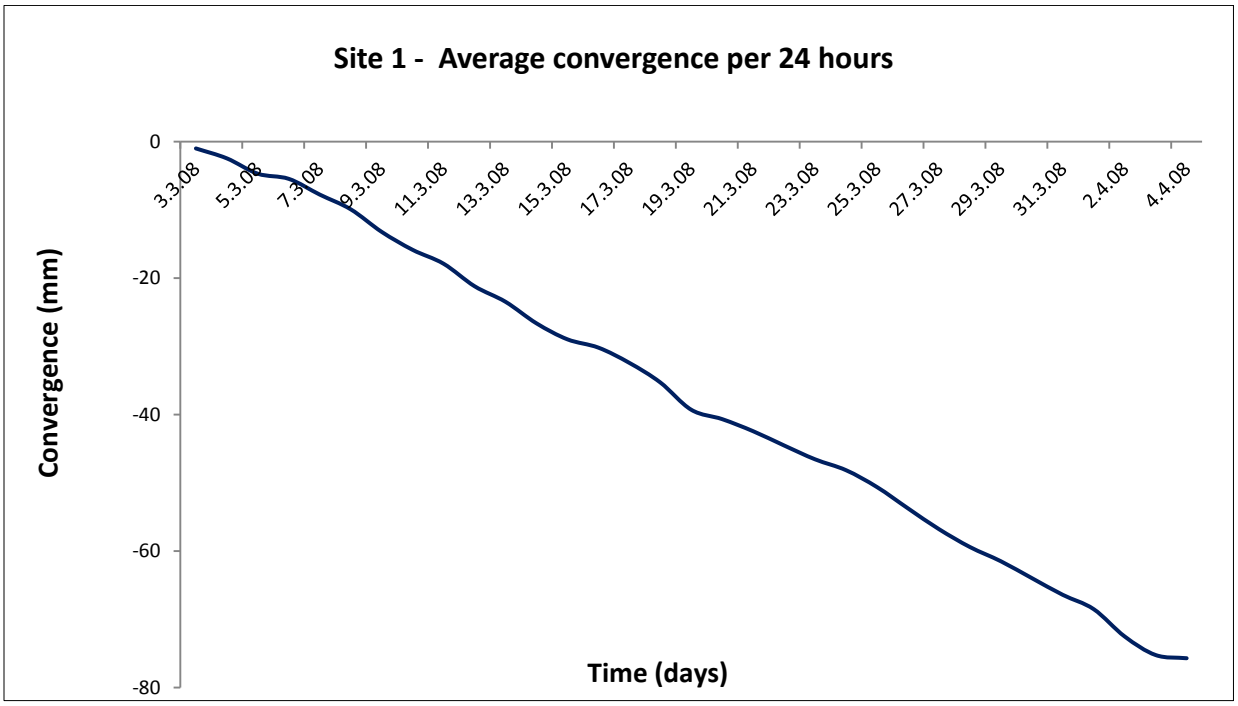

Figure 5.12 Average convergence per smoothing 24 hours at site 1 between beginning of March and April 2008

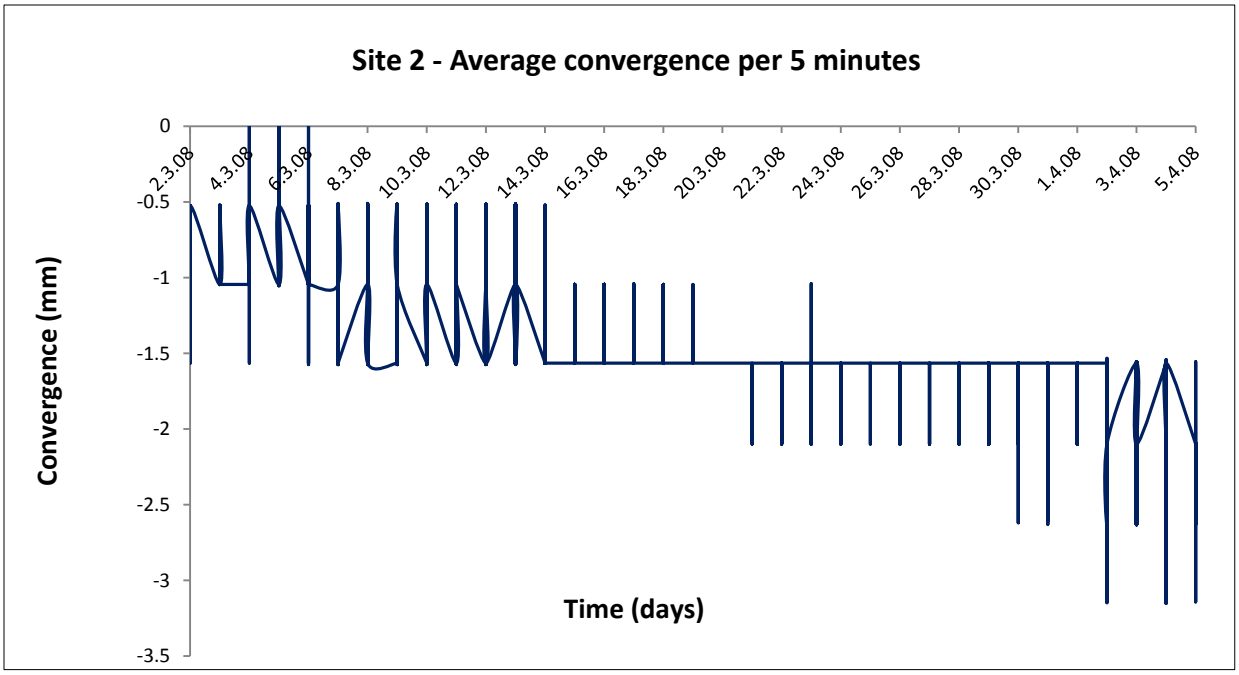

Figure 5.13 Average convergence per smoothing 5 minutes at site 2 between beginning of March and April 2008

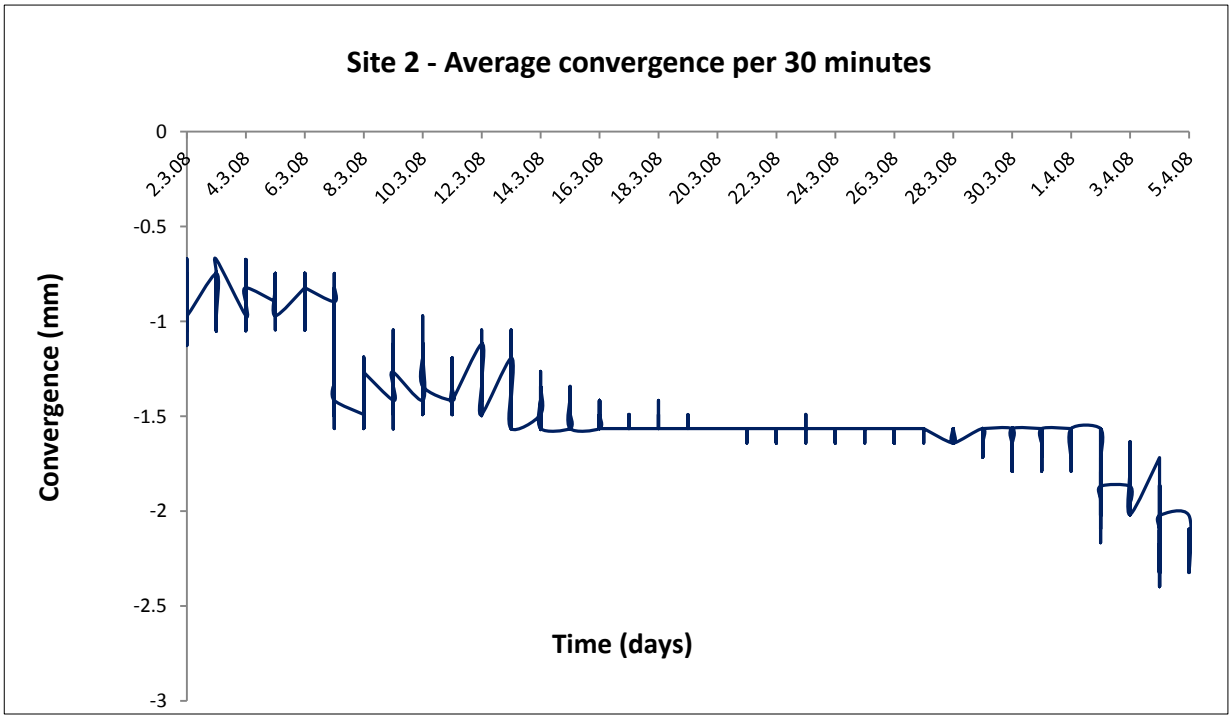

Figure 5.14 Average convergence per smoothing 30 minutes at site 2 between beginning of March and April 2008

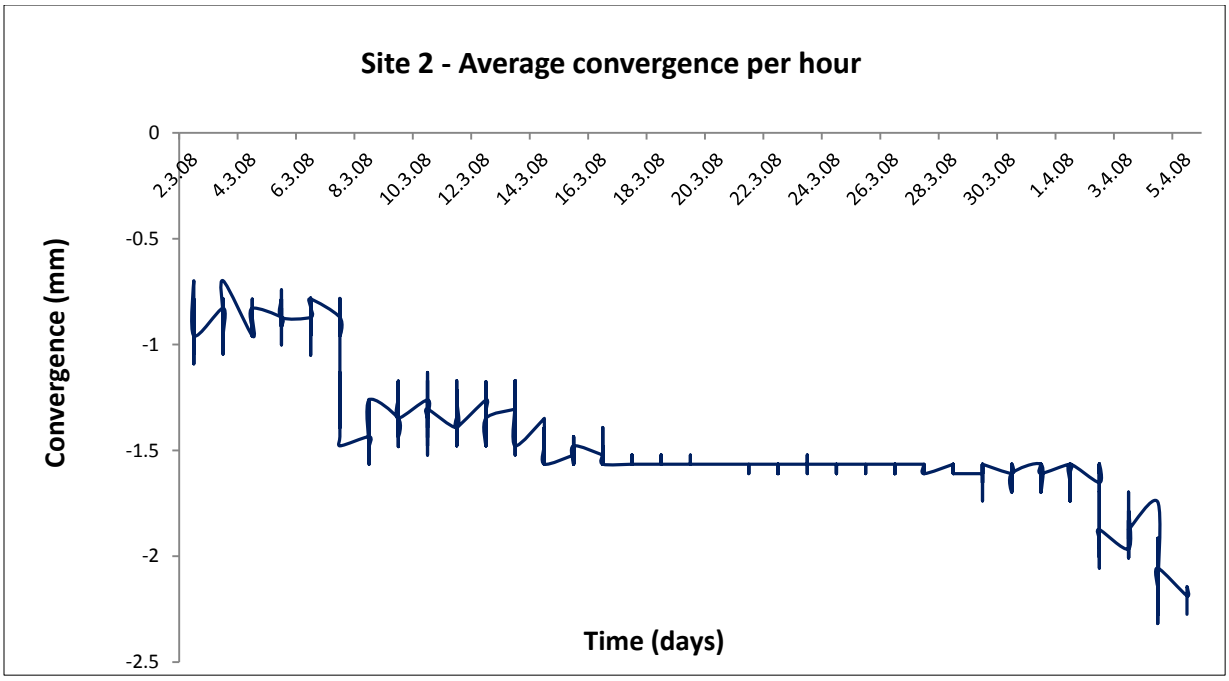

Figure 5.15 Average convergence per smoothing an hour at site 2 between beginning of March and April 2008

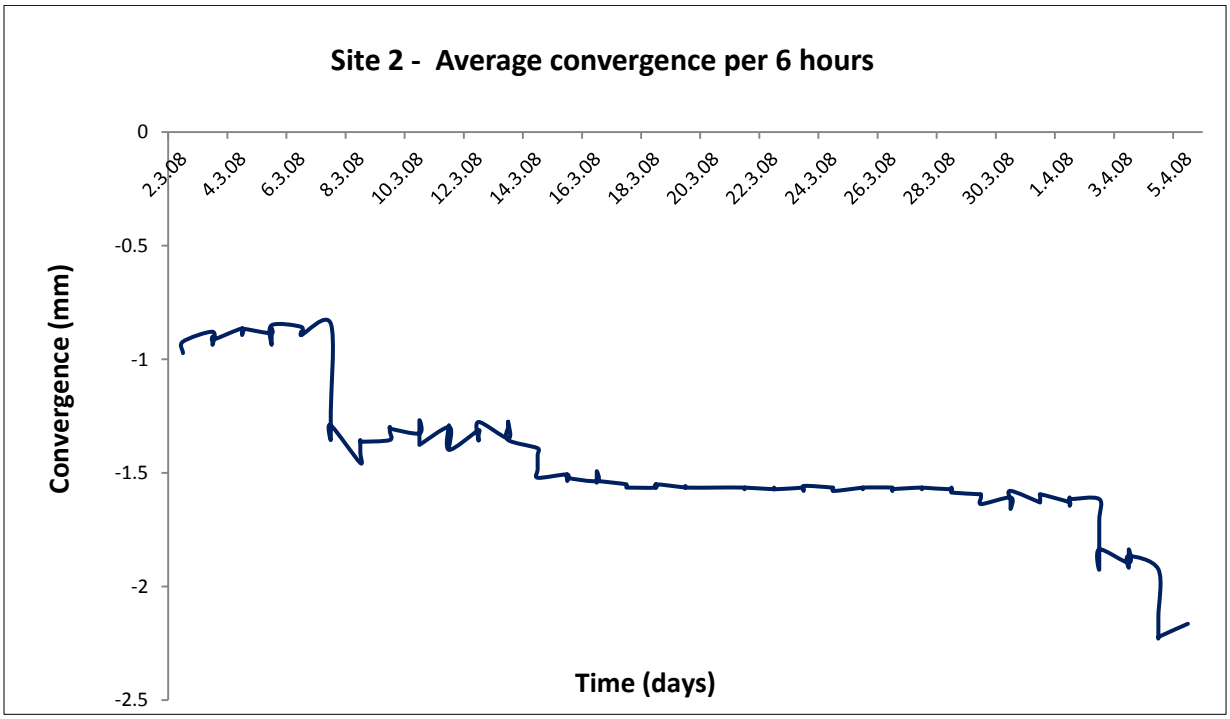

Figure 5.16 Average convergence per smoothing 6 hours at site 2 between beginning of March and April 2008

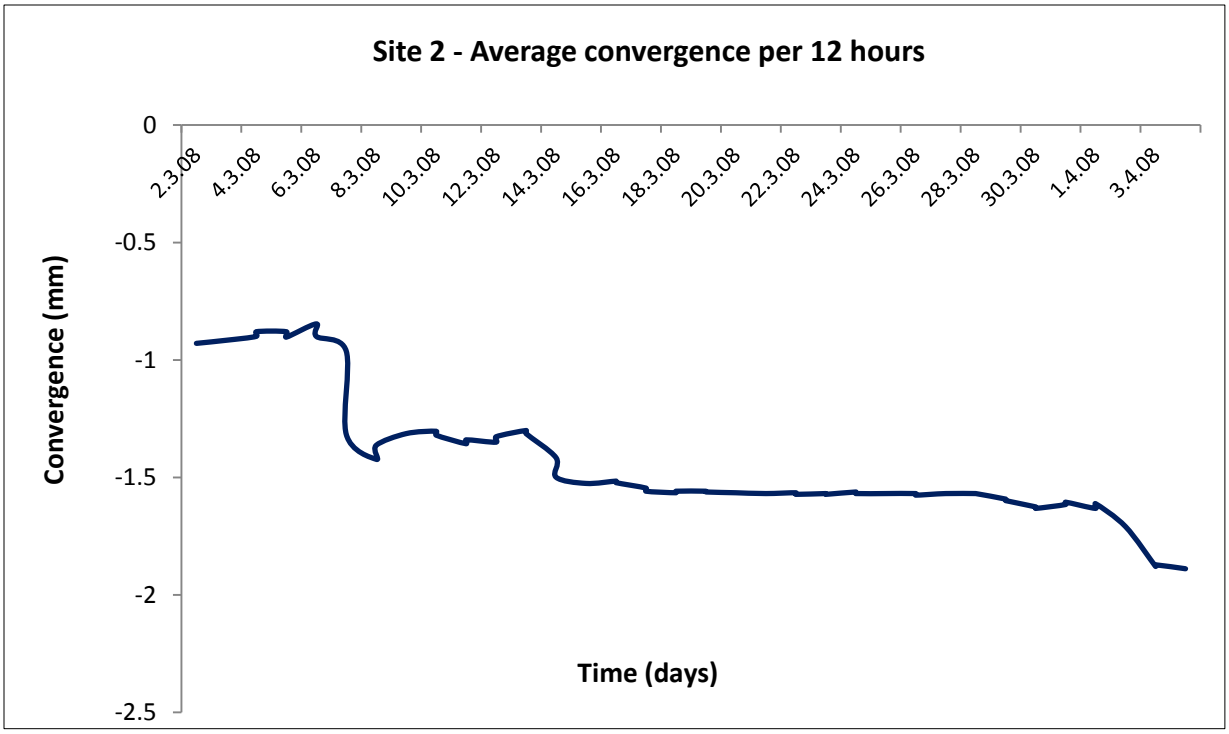

Figure 5.17 Average convergence per smoothing 12 hours at site 2 between beginning of March and April 2008

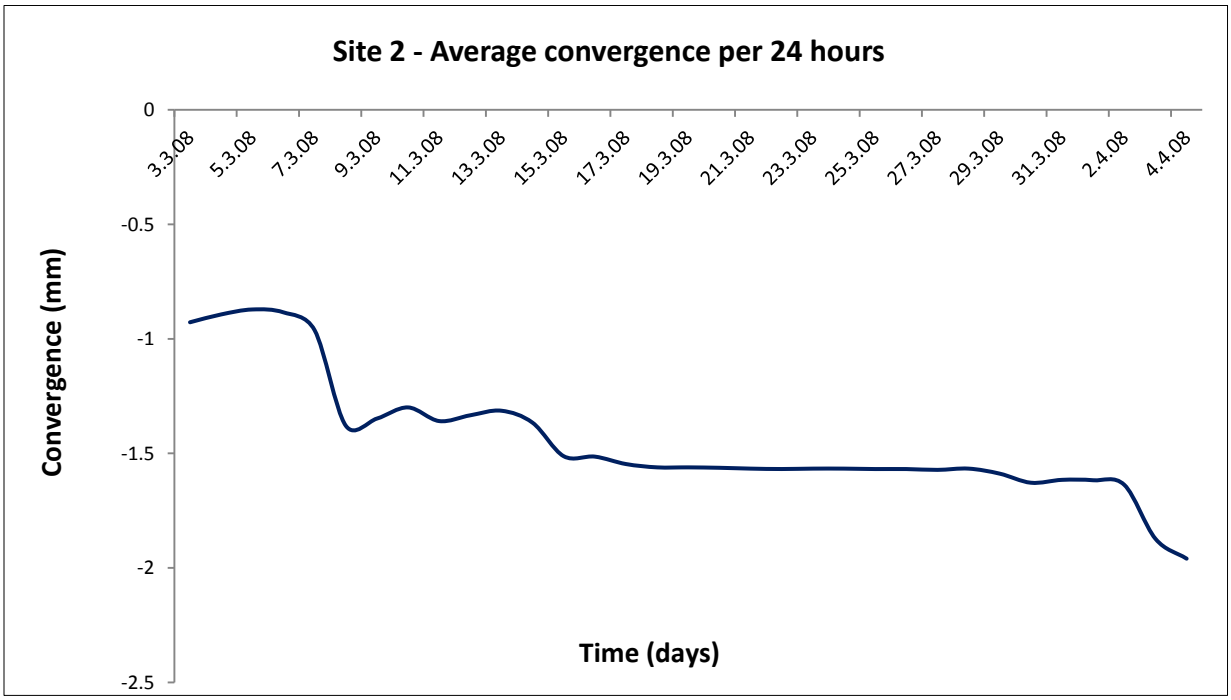

Figure 5.18 Average convergence per smoothing 24 hours at site 2 between beginning of March and April 2008

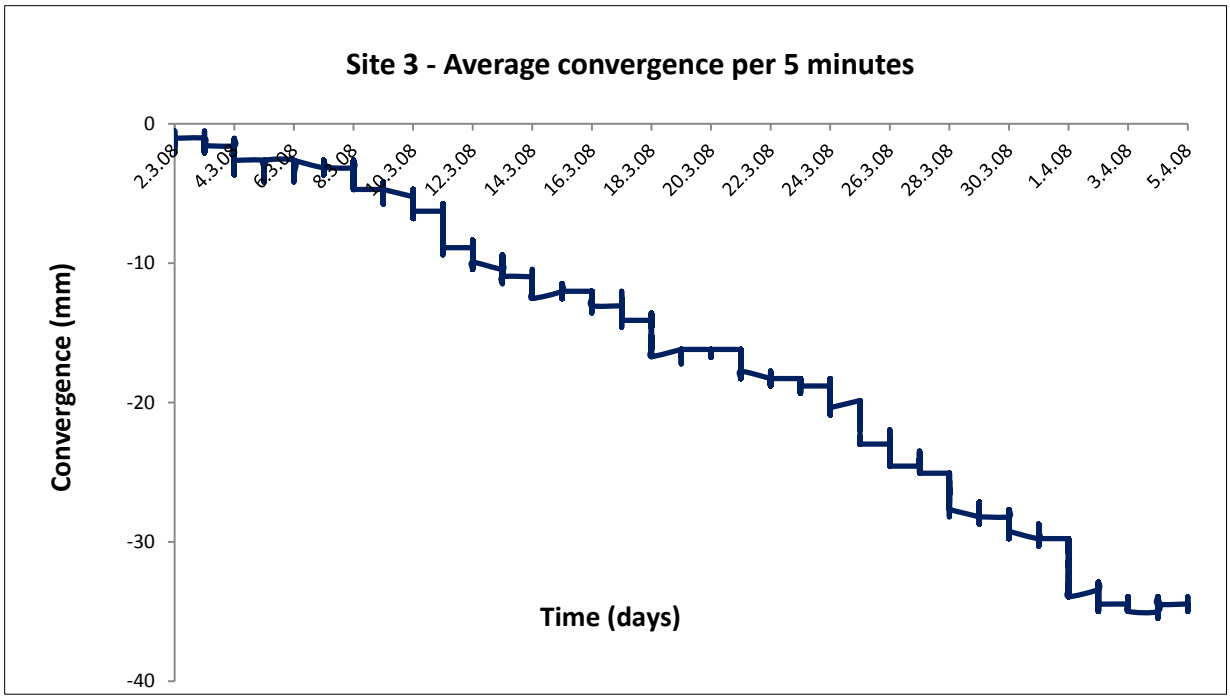

Figure 5.19 Average convergence per smoothing 5 minutes at site 3 between beginning of March and April 2008

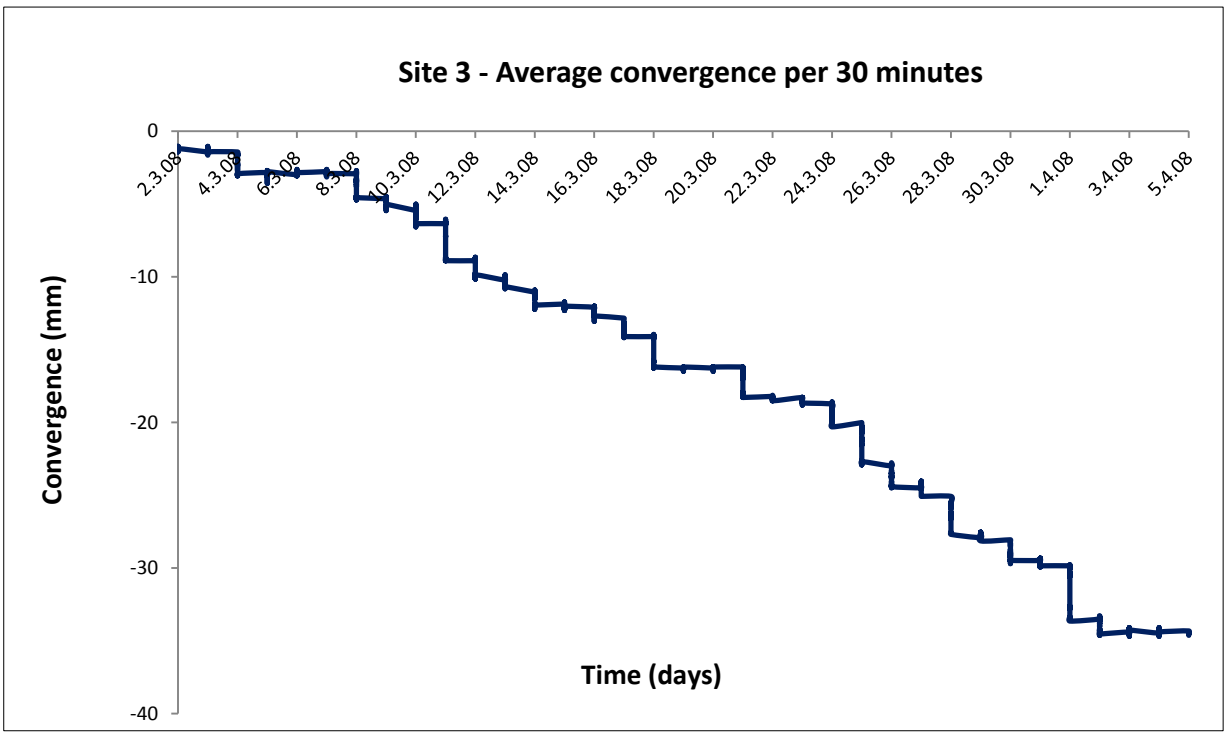

Figure 5.20 Average convergence per smoothing 30 minutes at site 3 between beginning of March and April 2008

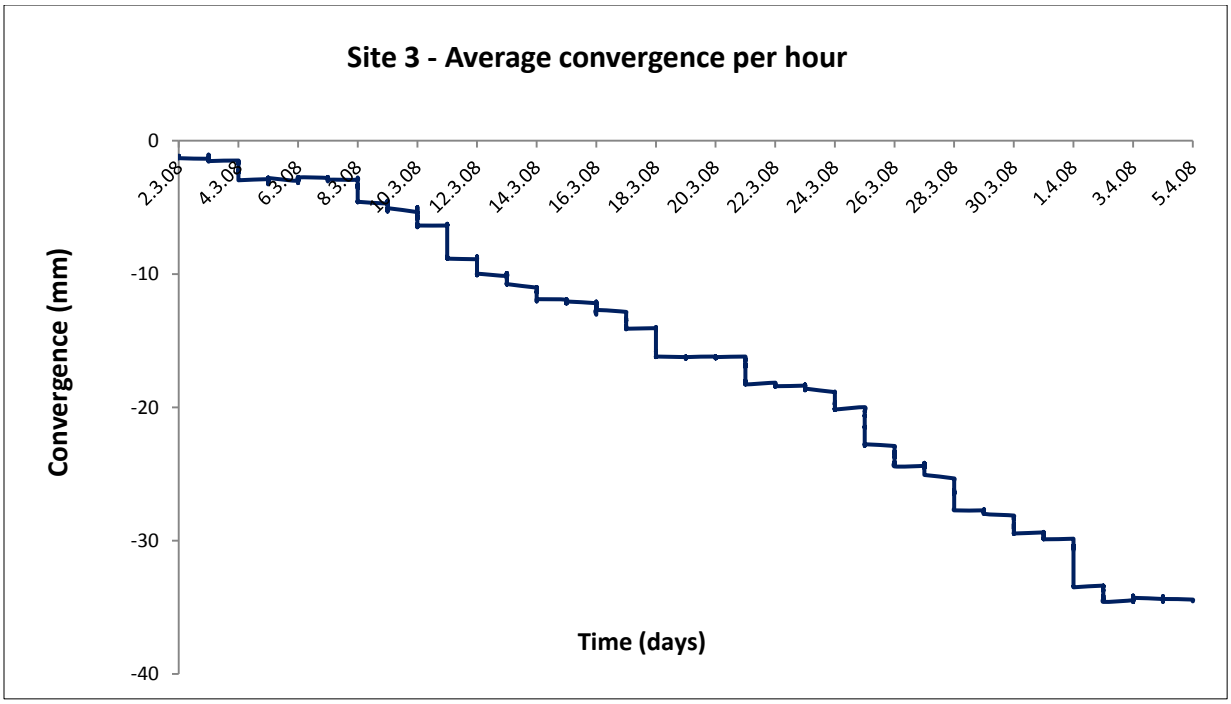

Figure 5.21 Average convergence per smoothing an hour at site 3 between beginning of March and April 2008

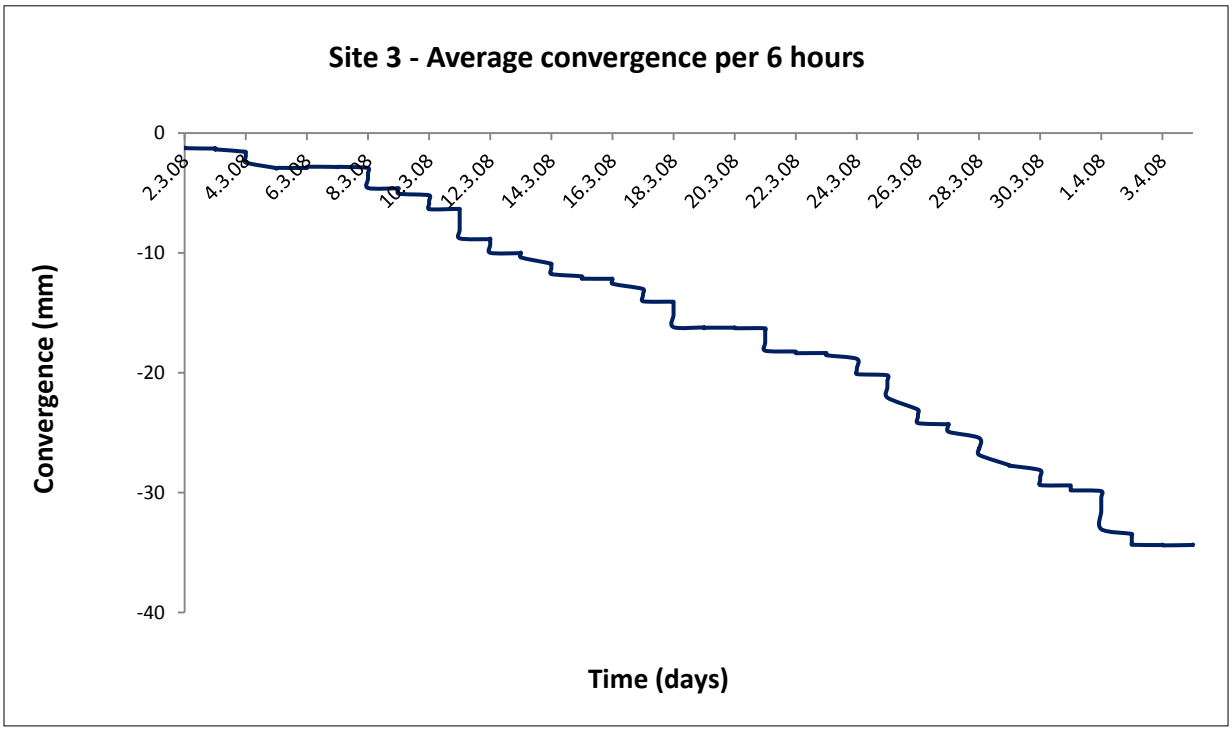

Figure 5.22 Average convergence per smoothing 6 hours at site 3 between beginning of March and April 2008

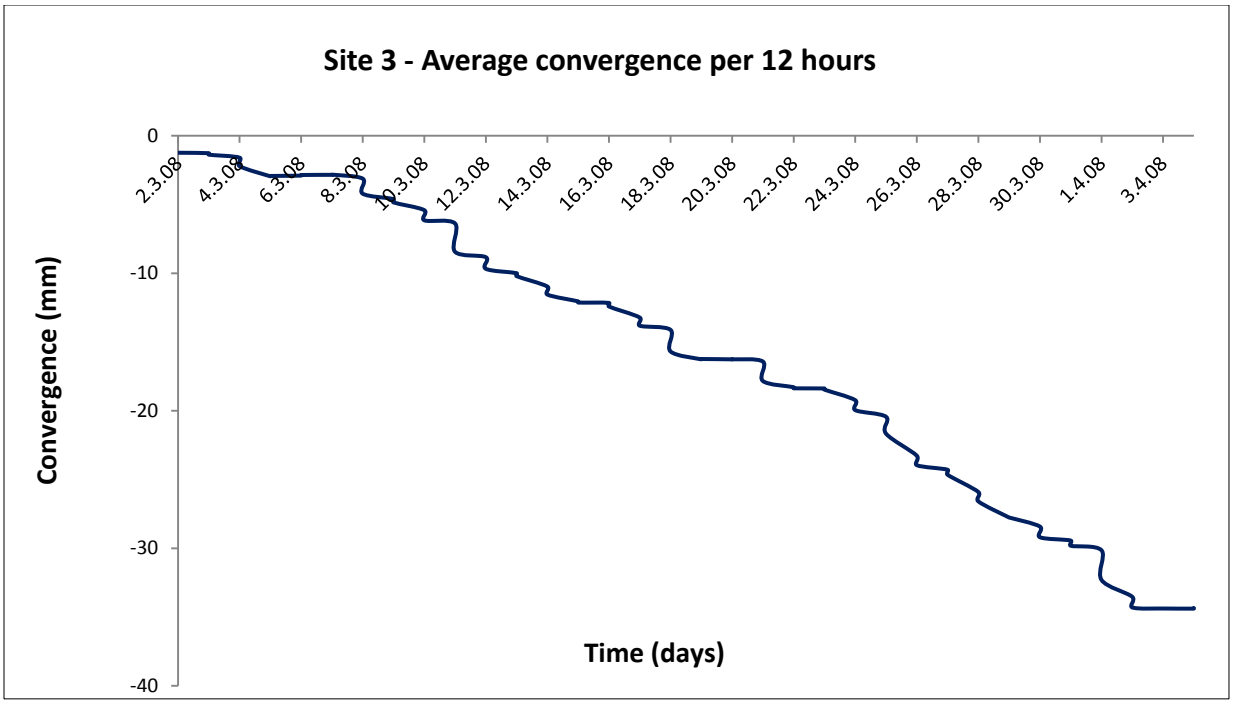

Figure 5.23 Average convergence per smoothing 12 hours at site 3 between beginning of March and April 2008

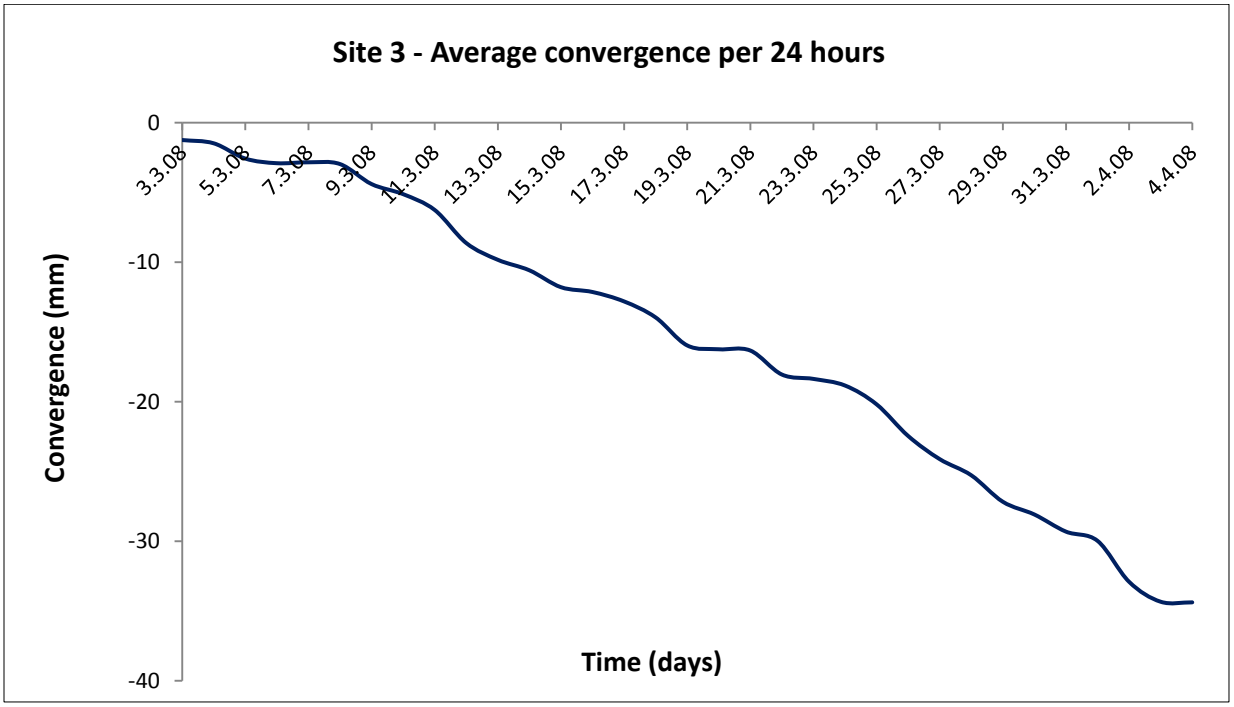

Figure 5.24 Average convergence per smoothing 24 hours at site 3 between beginning of March and April 2008

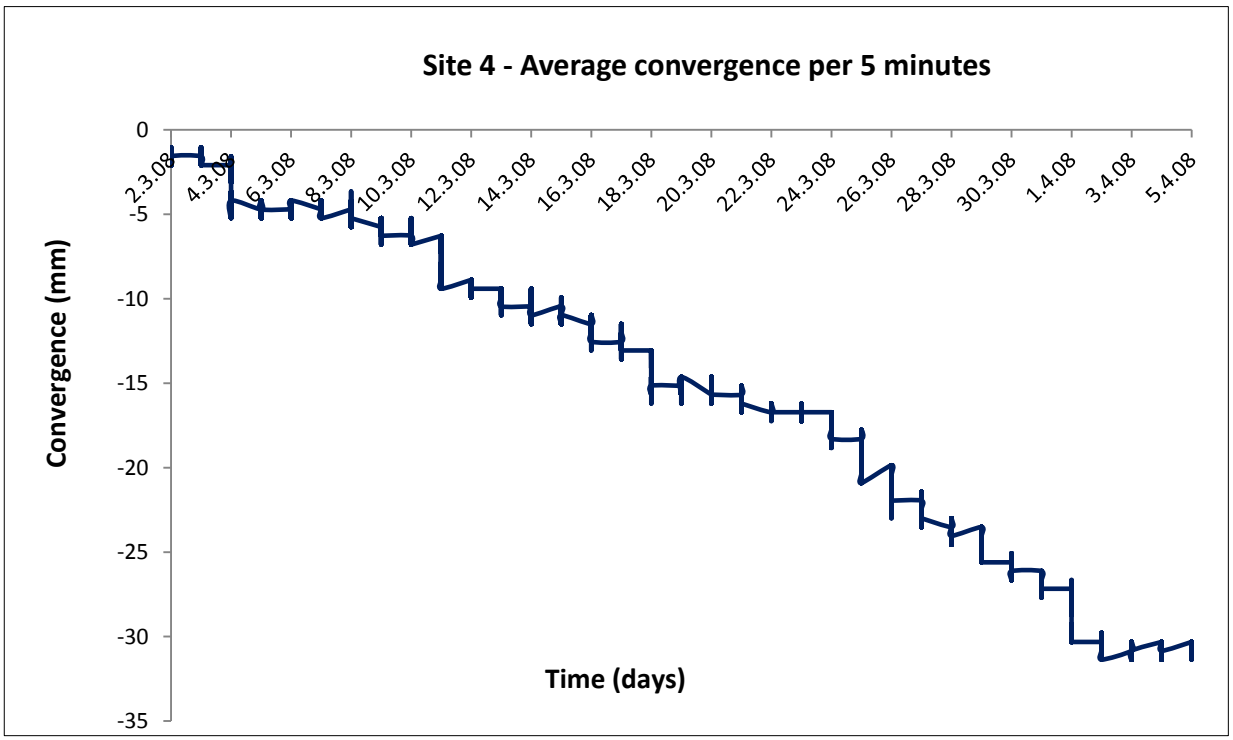

Figure 5.25 Averagec convergence per moothing 5 minutes at site 4 between beginning of March and April 2008

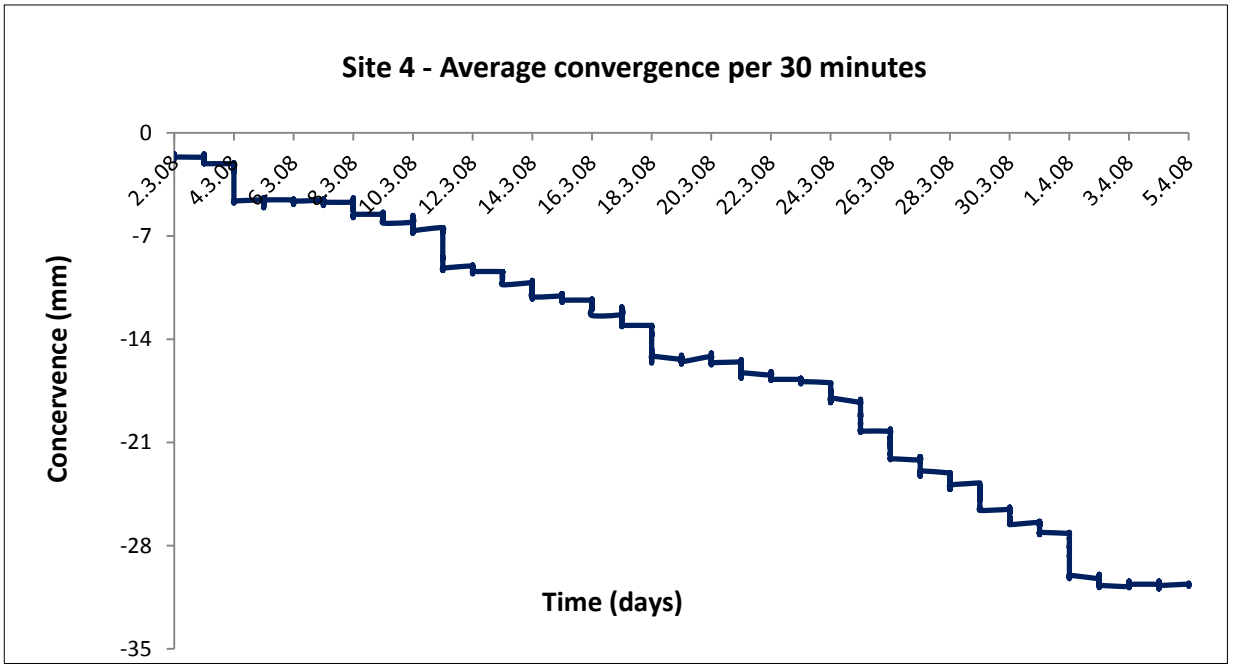

Figure 5.26 Average convergence per smoothing 30 minutes at site 4 between beginning of March and April 2008

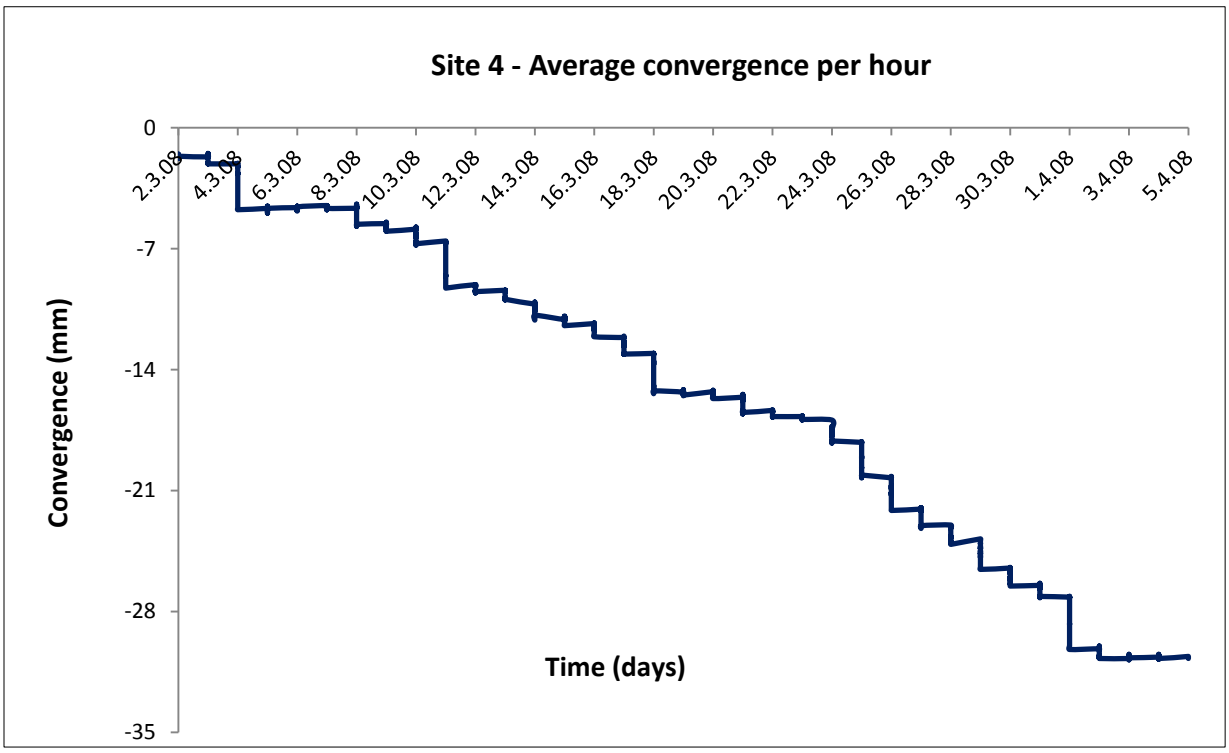

Figure 5.27 Average convergence per smoothing an hour at site 4 between beginning of March and April 2008

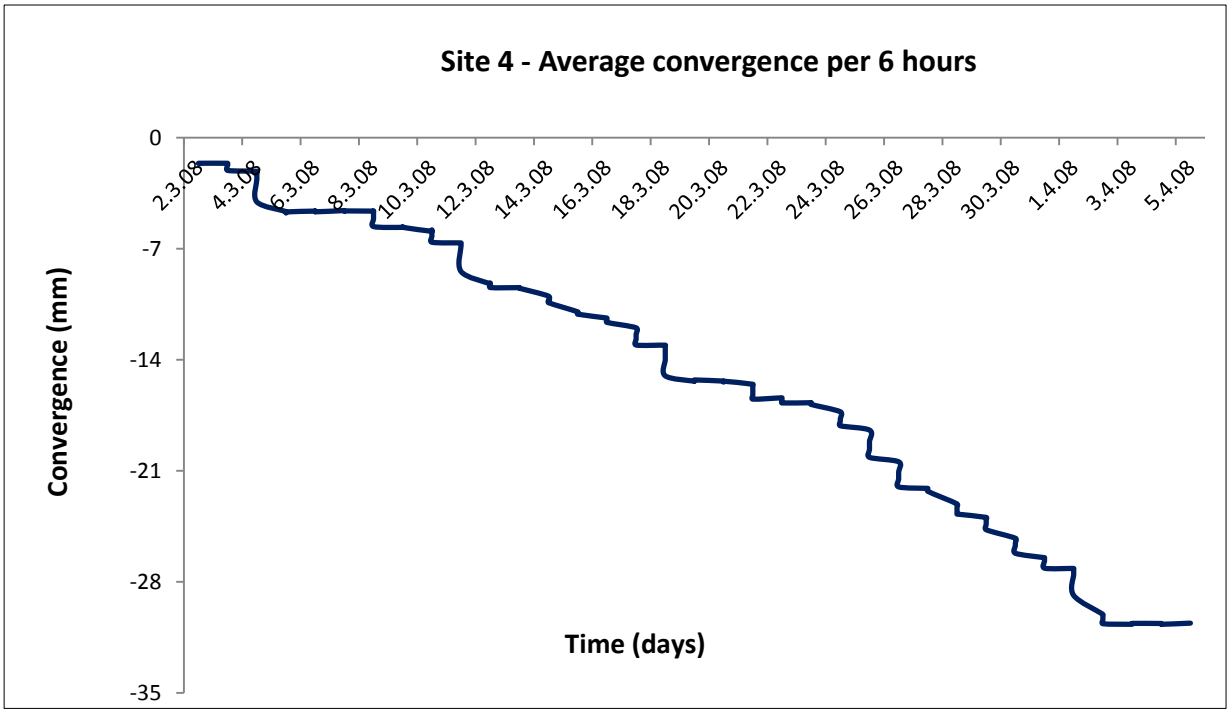

Figure 5.28 Average convergence per smoothing 6 hours at site 4 between beginning of March and April 2008

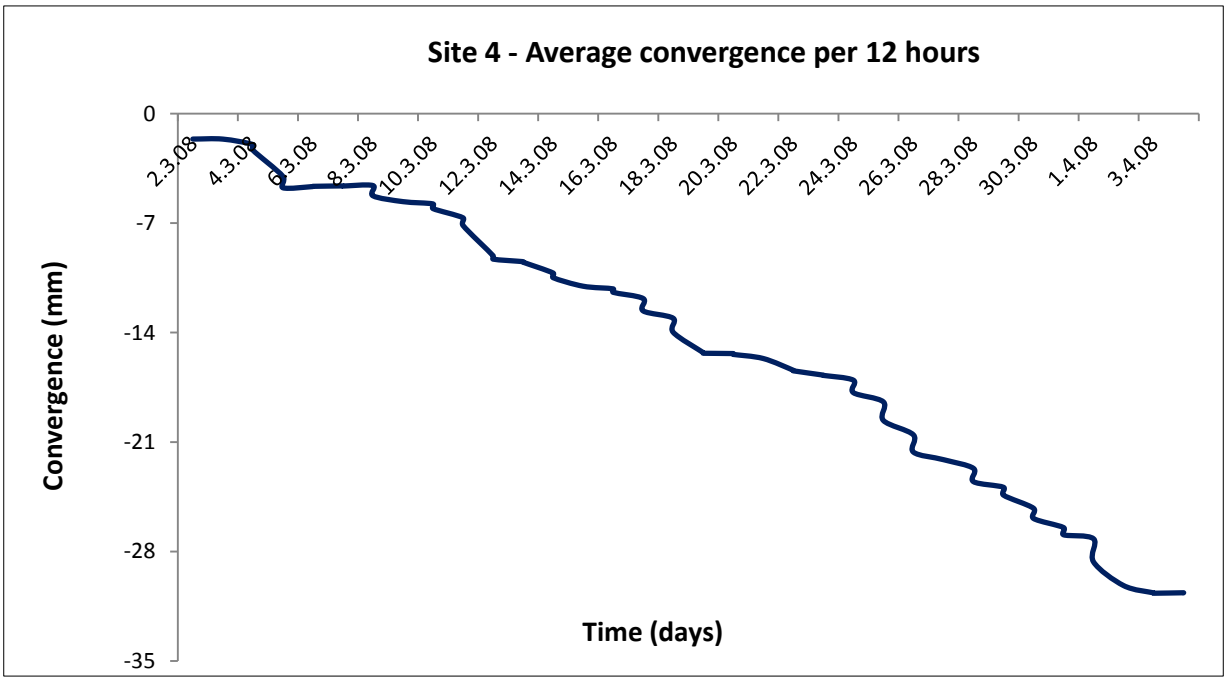

Figure 5.29 Average convergence per smoothing 12 hours at site 4 between beginning of March and April 2008

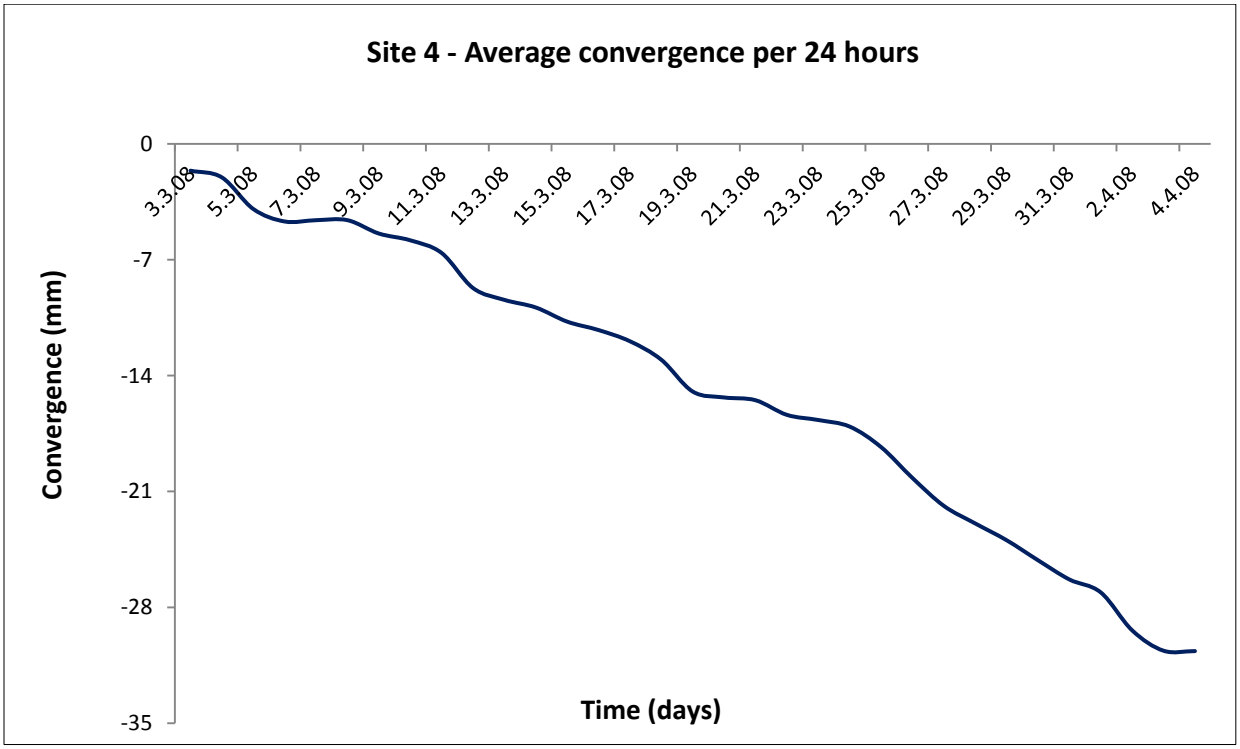

Figure 5.30 Average convergence per smoothing 24 hours at site 4 between beginning of March and April 2008

Table 5.5 Mean and standard deviation of average convergence at monitoring sites per processing time interval between beginning of March and April 2008

Time interval	**Average convergence**	
	Mean (mm)	**STDEV**
	Site 1	
5 minutes	-38.33	23.34
30 minutes	-38.33	23.26
1 hour	-33.31	23.25
6 hours	-38.21	23.24
12 hours	-38.21	23.24
24 hours	-37.64	23.21
	Site 2	
5 minutes	-1.46	0.32
30 minutes	-1.46	0.30
1 hour	-1.46	0.29
6 hours	-1.46	0.28
12 hours	-1.46	0.28
24 hours	-1.44	0.27
	Site 3	
5 minutes	-16.18	10.51
30 minutes	-16.17	10.49
1 hour	-16.17	10.48
6 hours	-16.08	10.48
12 hours	-16.08	10.47
24 hours	-15.81	10.41
	Site 4	
5 minutes	-15.10	8.91
30 minutes	-15.10	8.91
1 hour	-15.09	8.90
6 hours	-14.10	8.87
12 hours	-14.10	8.87
24 hours	-14.75	8.82

Data processing results clearly show the quality "smoother**"** of convergence patterns of workings regardless of the geometry of the sites. The quality smoother increases with the increase of processing time interval as a result of increase of data quantity. Between smoothing 5 minutes and 12 hours convergence occurs in a stepped manner probably due to the precision of the monitoring instrument which itself depends on both the resolution of the data logger and the sampling frequency. For instance, considering sampling at site 1, the closuremeter measured movement of approximately

2.08 mm of magnitude. This implies that movement no more than 2.08 mm of magnitude will be recorded at this closuremeter every 5 minutes despite the high 12 bit resolution of the data logger. The lack of synchronization (i.e. same time of occurrence) between the sampling frequency (i.e. working movement) and the data logger resolution (i.e. emitted impulses) results in a few and more discrete amount of readings. Therefore a stepped movement of workings is displayed when the readings are processed using smoothing 5 minutes.

With the increase of smoothing interval (e.g. 24 hours) the amount of readings is increased and data are more clustered despite the lack of synchronization. This explains the highly smoothed curve exhibited by the patterns of convergence at all the monitoring sites.

The analysis of convergence patterns associated with twenty-four hours of time interval shows different trends of mine workings behaviour at the sites. Mine workings behaviour is linear at sites 1 and 2 though the rate of movement at site 2 is lower than at site 1, whereas the behaviour of workings at sites 3 and 4 is nonlinear with increasing rate. The discrepancy in the behaviour of workings might be primarily related to the position of the sites. Sites 1 and 2 are located out of disturbance (e.g. proximity of roadway, adjacent excavation). In contrast, sites 3 and 4 were in close proximity to a workings access roadway and a main active face, respectively which might have influenced the workings behaviour.

Magnitudes of standard deviation (Table 5.3) show the decrease of error (i.e. standard deviation) on convergence with the increase of data processing time interval. Therefore, 24 hours of time interval is selected for data processing, based on both the quality (i.e. degree of smoothing) of convergence and magnitudes of standard deviation.

5.4.2.2 Data processing and results analysis

One of the major problems often experienced when carrying out measurements of workings deformation in an active mine is the ongoing activity and the behaviour of

workers. Consequently, few monitoring sites may be lost within time. Owing to its close proximity to a main face (i.e. ongoing mining activity) site 4 was lost one month after the commencement of measurements. Site 1 was also lost after two months of measurements owing to vandalism despite a warning sign against vandalism in visible at location.

Another major problem which may impair the monitoring process in deep mining is the high temperatures. The lack of ventilation resulted in the abandonment of site 2 two months after the beginning of measurements. Although the aforementioned unpleasant incidents considerably affected the monitoring process and consequently limited data collection, effort has been made in processing and analysing the available dataset to get greater insight into the mechanical behaviour of mine workings. Dataset collected at the four sites were further analyzed in terms of convergence patterns as a function of associated variables.

For determining the influence of the position of monitored points at the site, patterns of convergence recorded over one month at the four closuremeters were plotted together. The influence of geometry, location and age of sites was evaluated in terms of average convergence at the monitored sites.

(a) Patterns of convergence

Mine working movement at sites 1 and 2 was recorded over two periods of one month each between beginning of March and June 2008. Site 3 was where workings deformation was recorded over a relatively long period of time. Working movement including, the effect of floor milling was recorded over five periods of one month each between beginning of March and end of December 2008. At site 4, movement of mine working has only been recorded between beginning of March and April 2008. The findings are discussed below.

i. <u>Site 1</u>

Figure portrays occurrence of two types of movement at the monitored points in spite of the gradual and linear closure of workings. Whilst relatively high magnitude

movement at different rates occurs over the first period of measurement between beginning of March and April 2008 (Figure 5.31), movement of low magnitude of closure occurs over the second period of measurement between end of April and beginning of June 2008 at the monitored points (Figure 5.32).

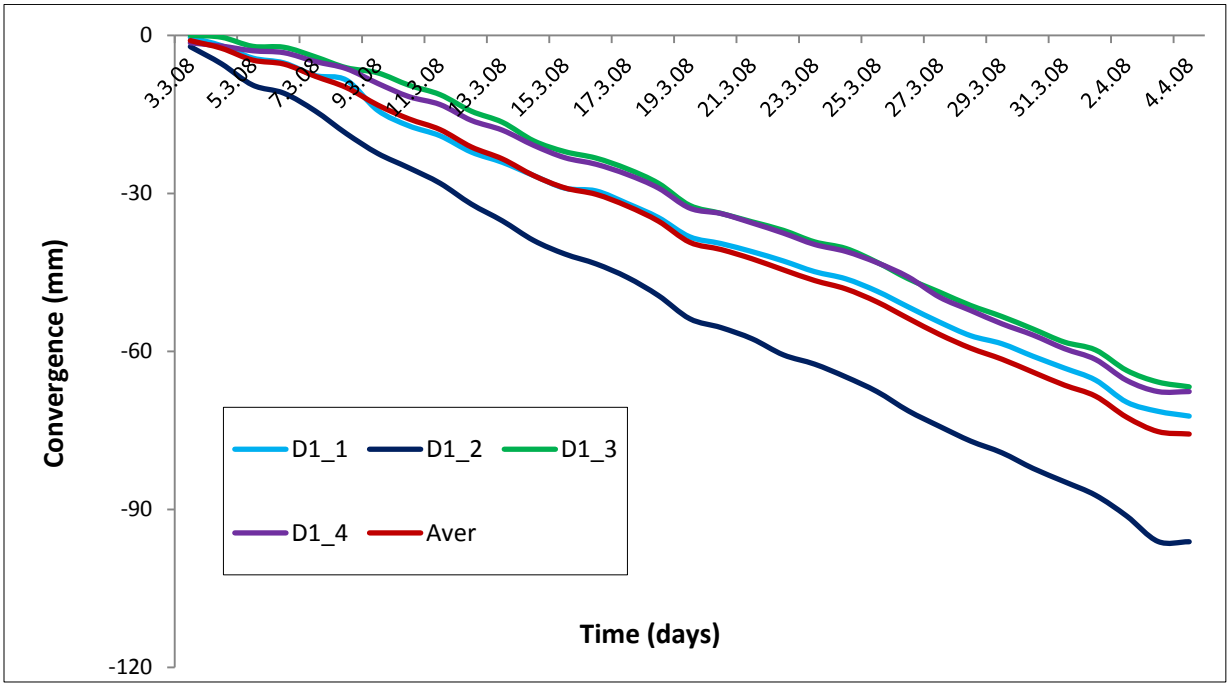

Figure 5.31 Convergence at site 1 between beginning of March and April 2008

Over the first period of measurement, the rate of convergence varies from one instrument to another. High magnitude of working convergence is recorded along the roadway (i.e. along D1_1 and D1_2 axis) than along the stub axis (i.e. along D1_3 and D1_4 axis) (Figure 5.31). Over the second period of measurement however, magnitude of convergence is lower.

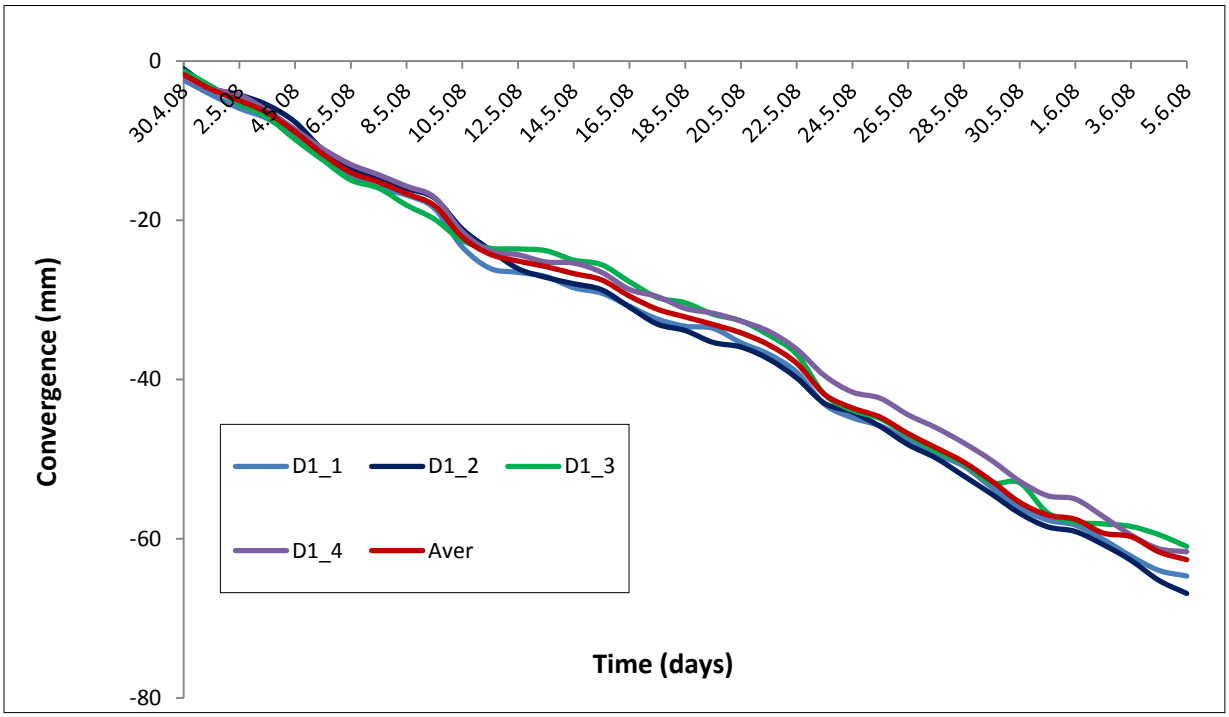

Figure 5.32 Convergence at site 1 between end of April and beginning of June 2008

Unlike the movement over the first period of measurement, mine workings movement over this period (Figure 5.32) occurs at comparable rate at the four closuremeters though the rate of movement along the roadway is relatively higher than along the stub axis.

Although high magnitude of closure is expected to occur along the roadway than at stub (Brady and Brown, 2006; Caughill and Beddoes, 1996), the discrepancy in the magnitude and rate of convergence over the two periods of measurement is probably due to localized movement of roof material at the monitored point. Indeed, rock mass gradually looses as a result of overburden stress, detaches from its host layer and falls as slab under gravity. Such localized event might have occurred in proximity of closuremeter D1_2 by the start of site instrumentation and increased the magnitude and rate of movement of working at that point (Figure 5.31). However, at closuremeter D1_1, convergence rate is relatively lower than at D1_2 but higher than that at D1_3 and D1_4 probably owing to its position along the roadway axis. At the two latter closuremeters, mine working gradually and linearly closes up at similar rate over the entire period of measurement.

After the episodic and localized event, with time the rate of closure at D1_2 gradually decreases to the rates of closure at D1_1, D1_3 and D1_4 (Figure 5.32). The decrease of rate continues over the entire second period of measurement over which patterns of convergence displayed similar trends.

At the end of the monitoring process, mine working closed up about 138.9 mm, such that 75.9 mm and 63 mm over the first and second period of measurement, respectively. Over the two periods of measurement, rapid movement occurs linearly along the roadway axis.

ii. <u>Site 2</u>

The abandoned roadway site 2 being the oldest of the monitored sites might experience later stages of convergence during the monitoring periods. Over the first monitoring period between the beginning of March and April 2008, no significant movement was recorded despite the slight movement recorded at some closuremeters. Patterns of convergence indicate irregular movement of working during the first fifteen days (i.e. up to 19th March 2008) after the instrumentation at the site; probably due to the fact that magnitude of movement is lower than the resolution of the monitoring instrument.

An alternative explanation of the irregular patterns of convergence could be the high temperature at the site as a result of lack of ventilation. Temperatures which range at the seam potash horizon from 40^{o}C to 45^{o}C might have temporarily affected the functioning of the closuremeters. Consequently, relatively long time might have been required for the closuremeters to stabilize before recording changes in working behaviour. A regular but scarcely perceptible movement started by 21st March 2008 along the roadway particularly at D2_1. At cross-cuts, no change was recorded in the behaviour of mine workings.

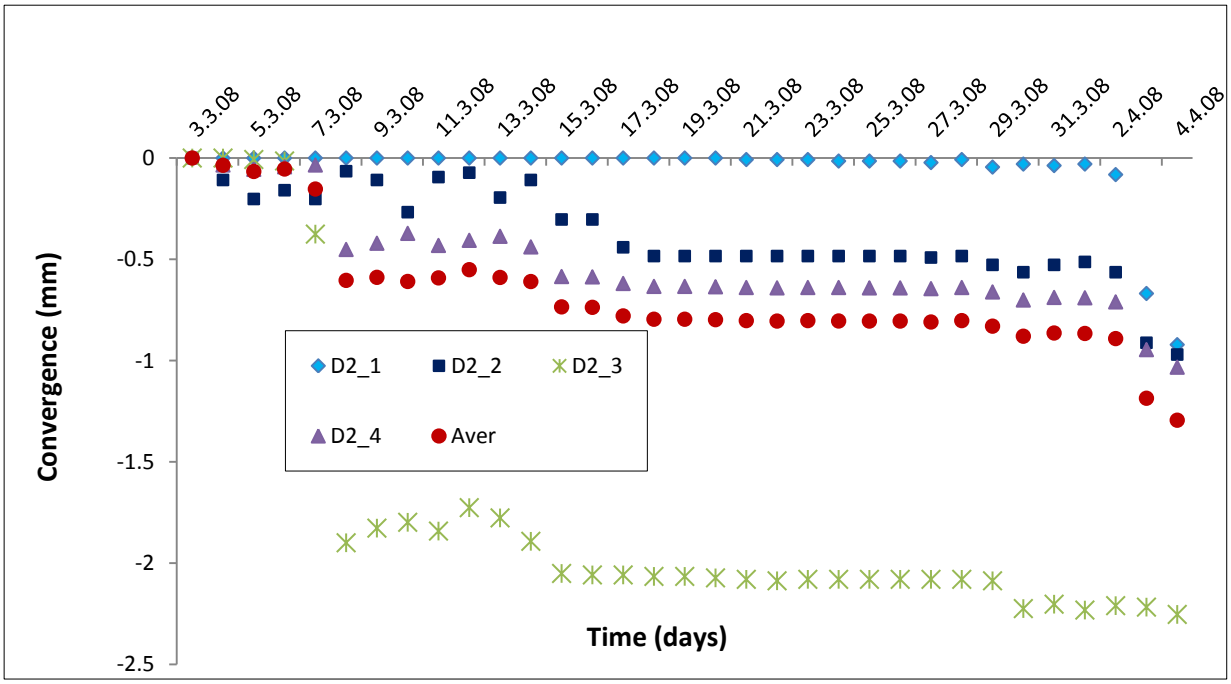

Figure 5.33 Convergence at site 2 between beginning of March and April 2008

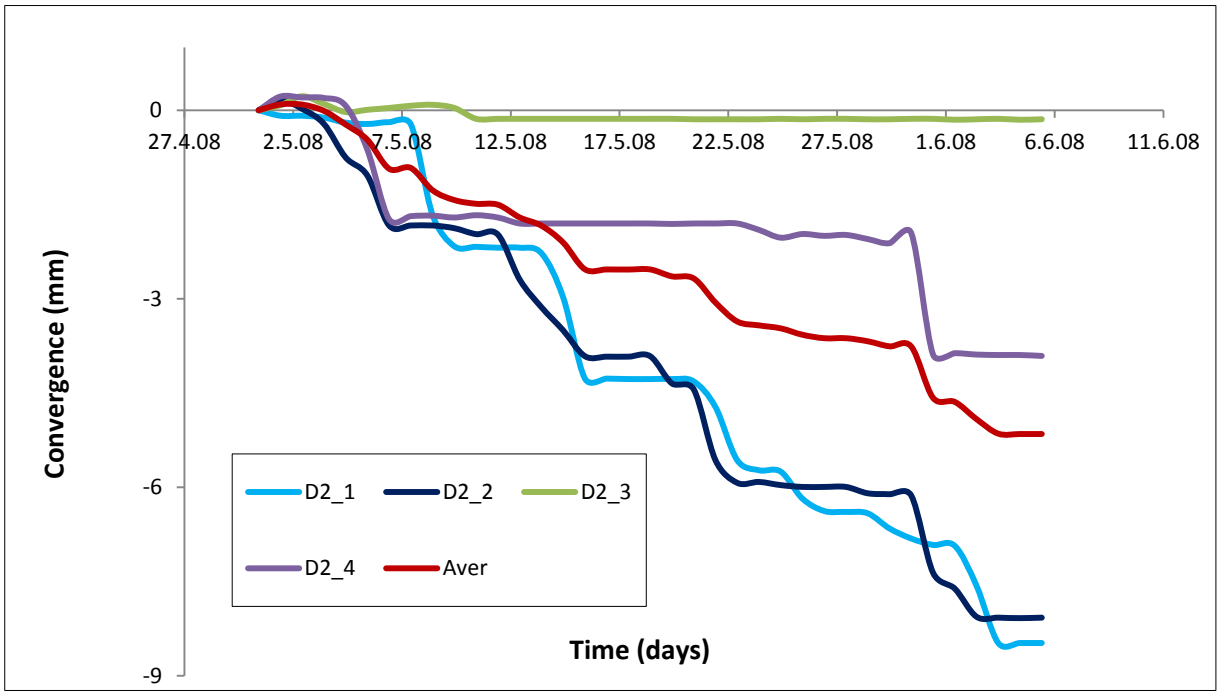

Figure 5.34 Convergence at site 2 between end of April and beginning of June 2008

At the beginning of the second period (Figure 5.34), the slight movement initiated by the middle of the first period gradually and linearly increases over the entire period of

measurement. Although high magnitude and rate of convergence are recorded along the roadway, no significant movement occurs along the cross-cuts axis. By the end of monitoring, the magnitude of convergence along roadway is about two times that along the cross-cuts axis. As at the first site, working movement at site 2 is dependent on the position of the monitored point though the movement did not exhibit linear patterns than at site 1, probably due to the age of the site. At the end of measurement mine workings closed up to about 5.2 mm.

iii. <u>Site 3</u>

Site 3 is adjacent to a workings access main roadway. Between the beginning of March and April 2008, movement at the four instruments is nonlinear exhibiting smoothed patterns of convergence although not highly pronounced. Magnitude of movement differs from one monitored point to another despite the close proximity of the instruments. High magnitude movement is recorded at D3_4 than at the three other closuremeters (Figure 5.35) where movement of comparable magnitude is recorded. Closuremeters D3_3 and D3_4 were in close proximity to the roadway, whereas closuremeters D3_1 and D3_2 were close to the sidewall of the stub (Plate 5.3).

A major change occurs at the four instruments between the end of April and the beginning of June 2008, resulting in well-defined linear patterns of movement. Another major change in the working behaviour is the shift of occurrence location of highest magnitude of movement at D3_3 (Figure 5.36) instead at D3_4 as observed over the first period of monitoring (Figure 5.35).

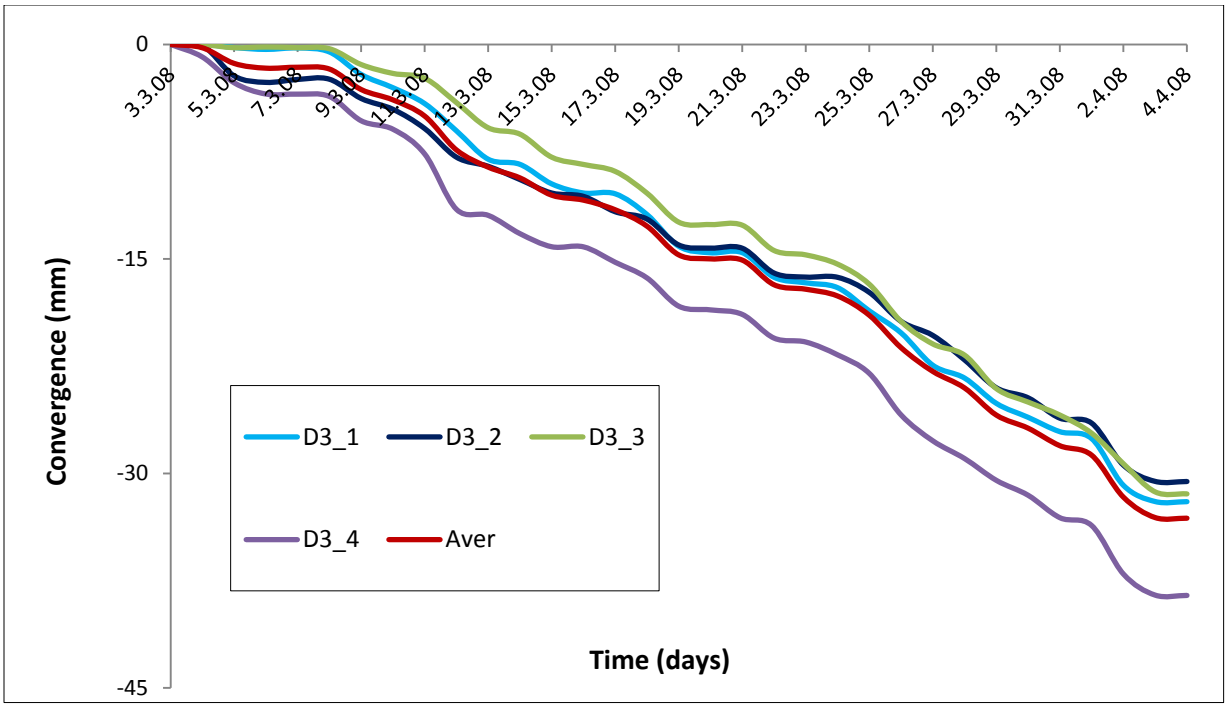

Figure 5.35 Convergence rate at site 3 between beginning of March and April 2008

Because mine working behaviour over April 2008 is not recorded, it is difficult to determine the main cause of the shift in location for highest magnitude. However, since there was no adjacent excavation, this shift probably translates the onset of the effect of roadway milling which took place one month after the instrumentation of the site. Roadway milling induced changes in the trend of working deformation and decreases the magnitude and rate of convergence at the four instruments (Figure 5.36). Mine working closed up about 33.12 mm and 32.31 mm at the end of the first and second periods of monitoring measurement, respectively.

From the end of June 2008 roadway milling related effect strongly controlled the working behaviour over the entire remaining period of measurement between the ends of August and December 2008. Floor layer removal disturbs the initial equilibrium leading to stresses and load resisting forces rearrangement. The structure fails as the material strength is exceeded. Then, stresses and load resisting forces can no longer readjust to form a stable structure. The milling effect is significantly observed between the end of August and September 2008 (Figure 5.37).

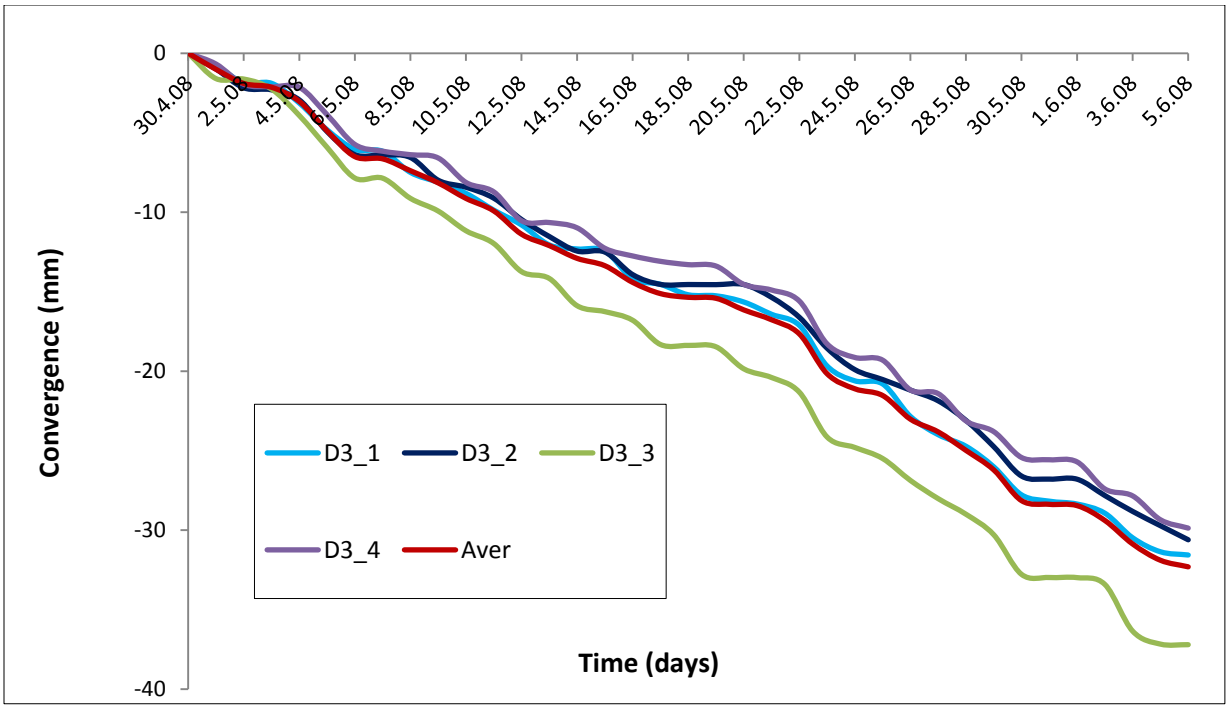

Figure 5.36 Convergence at site 3 between end of April and beginning of June 2008

A noticeable change in the patterns of deformation is observed on 25th August 2008 which gradually shaped patterns of movement and induced smoothed convergence patterns at decreasing rate (Figure 5.37). Roadway milling might have probably resulted in significant floor heave due to stresses acting laterally and beneath the floor, and led to change in the trend of deformation patterns. High magnitude of convergence is recorded at D3_3 and D3_4 in close proximity to the roadway than at D3_1 and D1_2 close to the wall of the stub (Plate 5.3). The rate of convergence at the four instruments gradually decreases over this monitoring period. Unlike the patterns of convergence over the first and second periods of measurement, convergence patterns display a smoothed and curved trend. At the end of measurement, mine workings closed up to about 13.24 mm.

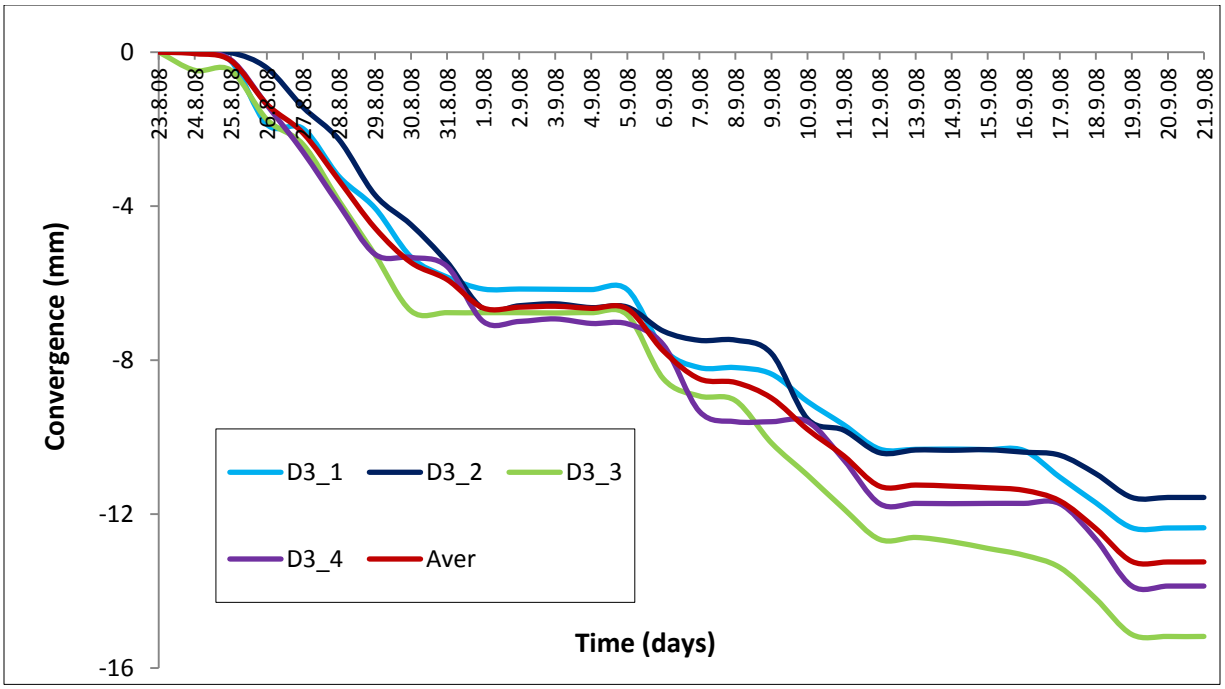

Figure 5.37 Effect of floor milling on convergence at site 3 between 23rd August and 20th September 2008

An ultimate change in the trend of deformation occurred by the end of October and exacerbated over November 2008. This period is characterized by: (i) the disruption of the direction of working deformation, probably in an attempt to resume its normal linear behaviour, (ii) the shift of location of deformation highest magnitude and (iii) the decrease of magnitudes of convergence.

Relatively high magnitude convergence is recorded at D3_3 and D3_1, whereas similar movement of lower magnitude is recorded at D3_2 and D3-4 (Figure 5.38). Again, patterns of convergence exhibit smooth trend of deformation at increasing rate though not clearly defined. The overall rate of convergence at the four instruments decreases and mine workings closes up at about 9.49 mm at the end of the monitoring.

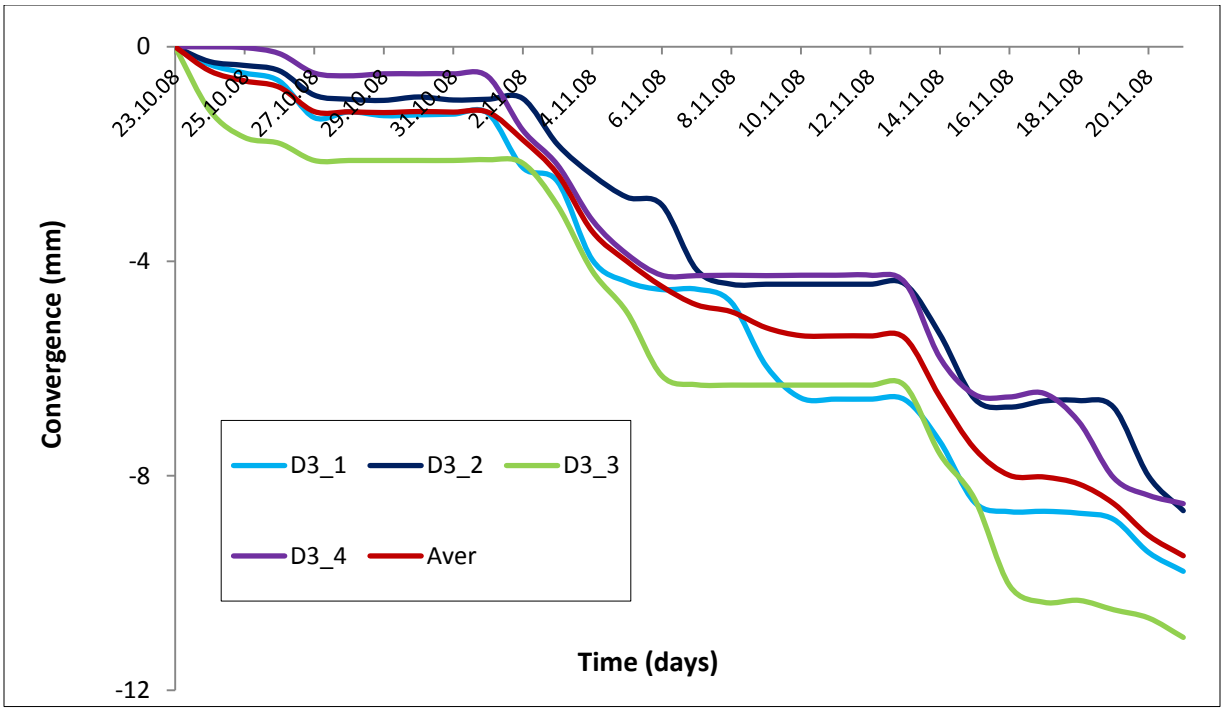

Figure 5.38 Effect of floor milling on convergence at site 3 between 23rd October and 20th November 2008

Workings deformation trend which started during the previous periods continued over the last period of monitoring between the end of November and December 2008 (Figure 5.39). Commencing by the end of October 2008, patterns of convergence finally recovered their relatively linear trend as during the first period of measurement, probably due to the termination of the floor heave effect. Although smoothed, patterns of convergence with increasing rate are well-defined and magnitudes of convergence slightly increased. Magnitudes and rates of convergence at D3_1, D3_2 and D3_3 are higher than at D3_4 though located in close proximity to the roadway.

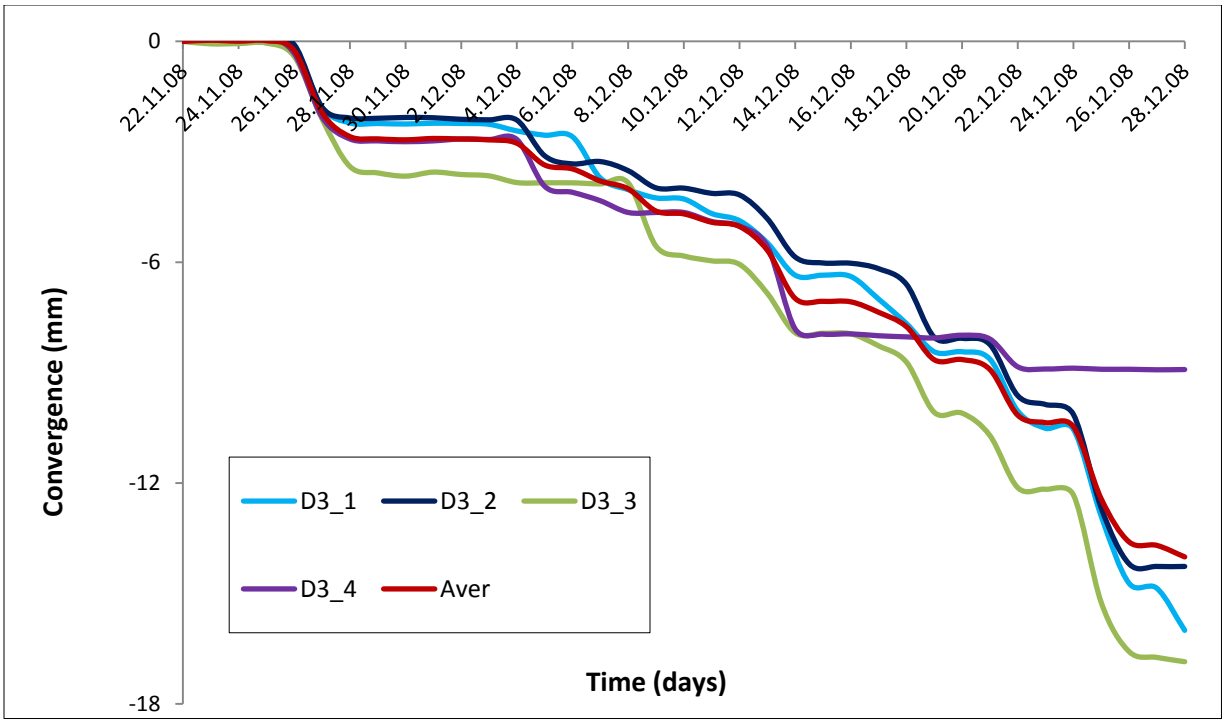

Figure 5.39 Effect of floor milling on convergence at site 3 between 22nd November and end of December 2008

Generally, the analysis of convergence patterns before roadway milling shows dependency of mine working behaviour on the position of monitored point. Rapid and smooth movement occur at point in close proximity to the roadway. Roadway milling affected the dependency of patterns, magnitudes and rate of convergence on the position of monitored points at the site over the second and third periods of measurement. It changed movement trend, patterns and magnitudes of convergence at the monitored points.

iv. Site 4

Site 4 was close to a main face and consisted of three stubs. The instruments were arranged such that D4_1 and D4_3 were positioned at the third stub, and D4_4 and D4_2 were at the first and second stub, respectively (Figure 5.2). Owing to the ongoing mining activity in the vicinity, this site was only monitored between the beginning of March and April 2008.

Patterns of convergence (Figure 5.40) indicate discrepancy in the magnitude of convergence recorded by the four instruments. The position of the monitored points at the stub and most importantly relative to the pillar significantly controlled the magnitude of convergence. Closuremeters D4_1 and D4_3 were in close proximity to the roadway and pillar, respectively; whereas closuremeters D4_2 and D4_4 were on the middle of stub at relatively equal distance to the roadway axis (Figure 5.2).

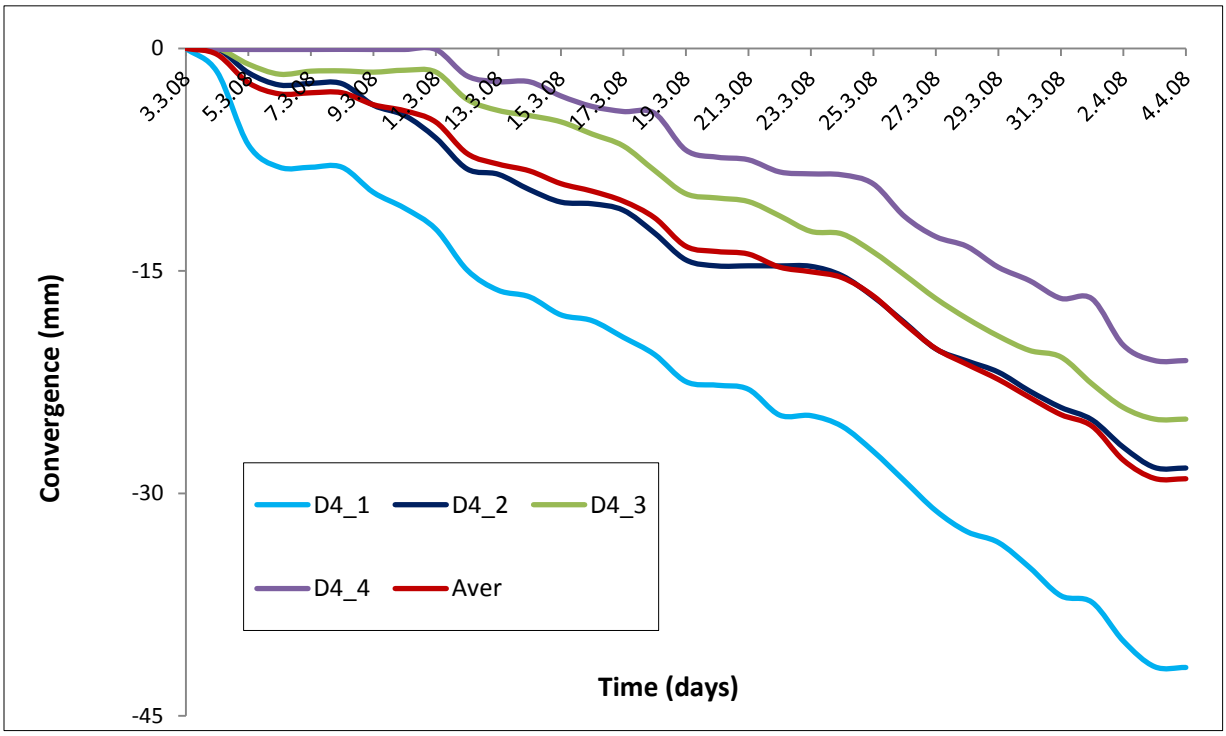

Figure 5.40 Convergence at site 4 between beginning of March and April 2008

Unlike at site 3, mine workings convergence at site 4 occurs at different rate at the four instruments, mostly controlled by the pillar. Given the size and geometry of the stub, roof materials might have bridged over the pillar developing a compressive arch acting along the roof. This compressive arch withstood and transmitted the weight of the overlying materials to the pillar.

The analysis of patterns of convergence in Figure 5.40 also shows variation of convergence magnitude from one instrument to another. Although D4_1 and D4_3 are located at the same stub, the magnitude of convergence recorded at D4_1 is higher than at D4_3. This is because D4_1 is close to the roadway, thus has least support than

D4_3 with extra support provided by the edges of stub. The relatively high magnitude and rate of convergence measured at D4_2 might be attributed to the location of the instrument between two yield pillars. Although stub 1 was first excavated, it took longer to reach equilibrium owing to its close proximity to the pillar. Consequently, lower magnitude of convergence is recorded at D4_4.

In conclusion, mine workings movement at this site is strongly dependent on the position of the monitored point. For the points between pillars, patterns and magnitude of convergence are controlled by the pillars. A roof-to-floor convergence of about 29 mm is recorded at the end of the measurement.

(b) Dependency of convergence

The mechanics of mine workings is complex because of controlling variables involved; thus their effects may not be determined a priori. To deepen understanding and characterize the mechanics of openings in underground mining, it is essential to examine some of relevant controlling variables which include, age, location and geometry of sites.

i. Relationship with the age of sites

Generally, convergence rate decreases with the age of the excavations. Given the limited data due to unpleasant incidents (Section 5.4.2.2), three criteria are set on the datasets used for analyzing the effect of sites age on the working convergence: the datasets must (1) be of same depth (i.e. site depth), (2) have same amount of data and (3) be of same monitoring period. An additional and fourth criterion is for the datasets to be of different age, implying for them to be of different sites. This latter permits comparative analysis of sites age effect on the working behaviour within the monitoring network.

Two datasets were gathered from three sites only, owing to the loss of site 4 after one moth of measurement. The first consists of data for sites 2, 3 and 4 between

beginning of March and April 2008. The second dataset is for sites 2 and 3 between end of April and beginning of May 2008. These three sites are situated in the northern part of the mine where mining activity is suposed to take place at about 1,100 meters below the sea level (Section 3.1; Figure 5.1).

Patterns (Figure 5.41) and rates (Figure 5.42) of convergence indicate discrepancy in the behaviour of mine working at the three sites.

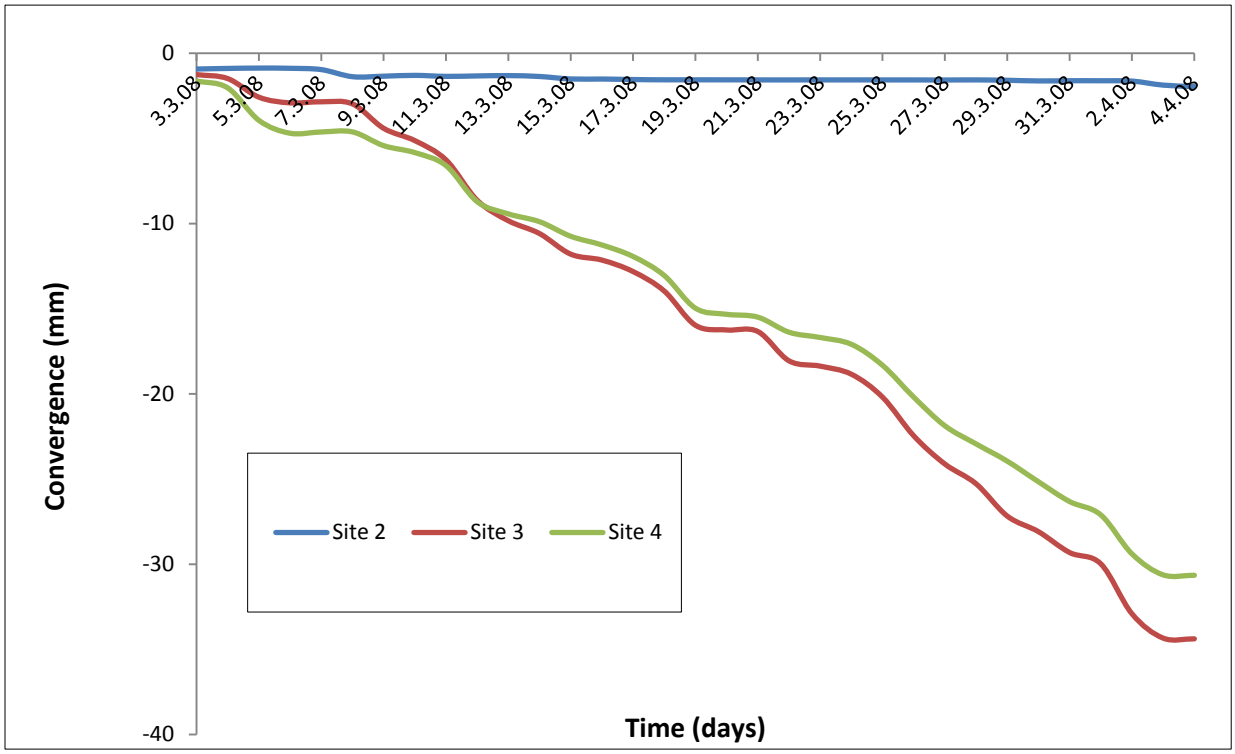

Figure 5.41 Effect of age on convergence at sites 2, 3 and 4 between beginning of March and April 2008

Figure 5.41 shows insignificant movement at site 2, whereas gradual and linear movement is recorded at sites 3 and 4 over this monitoring period. The age effect is also seen in the amount of convergence recorded at the sites after one month measurement. Mine workings closed up over about 1.96 mm, 34.38 mm and 30.64 mm at site 2, site 3 and site 4; respectively. Additionally, the age effect is also evidenced by the average rate of convergence at the three sites (Figure 5.42).

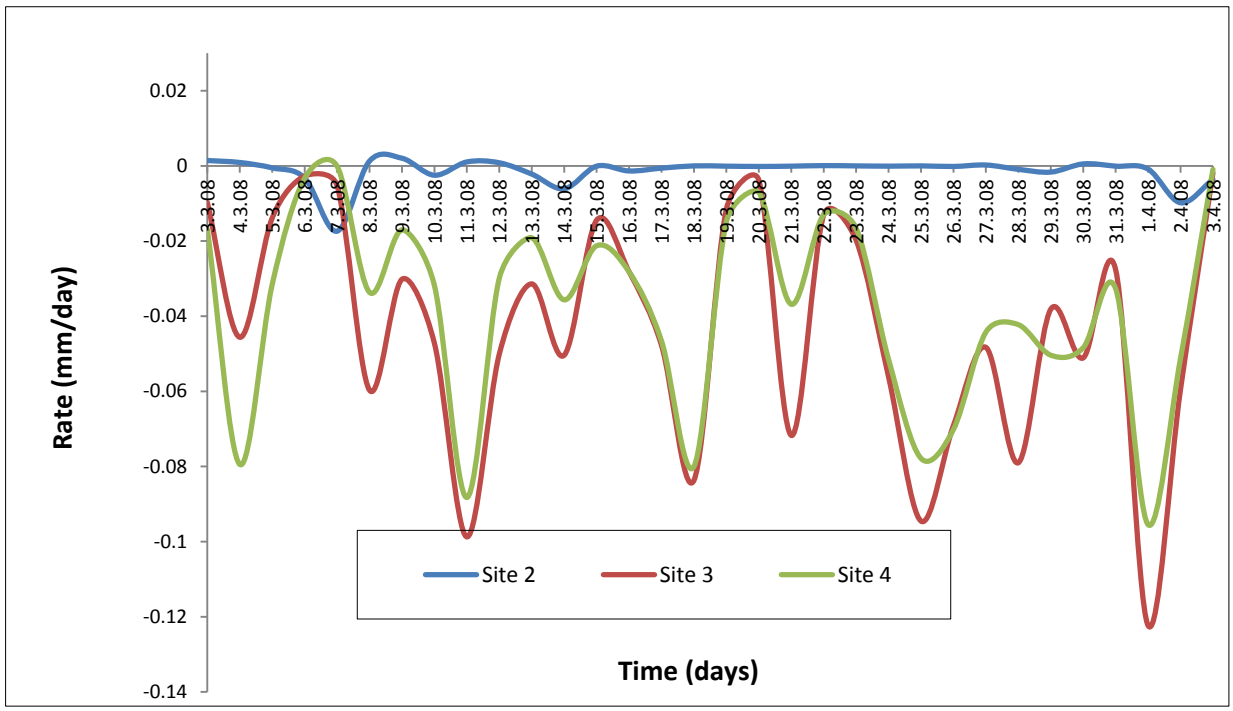

Figure 5.42 Effect of age of sites on convergence rate at sites 2, 3 and 4 between beginning of March and April 2008

As for the magnitudes of convergence, mine workings close up at similar rate at sites 3 and 4 than at site 2 where the rate of deformation is quasi-null. The slight discrepancy in the average rate at sites 3 and 4 might be attributed to the geometry of the site. Although being of stub type, site 4 is a series of three successive stubs separated by pillars which might decrease the rate of convergence, whereas site 3 consists of one stub (Figure 5.2). This effect is also proven by the slopes of convergence patterns at the sites (Figure 5.41).

The average convergence of workings at sites 2 and 3 over the second period of measurement is depicted in Figure 5.43. The difference in magnitudes of convergence at the two sites obviously indicates the effect of age on the behaviour of mine working. At the end of the monitoring, workings closed up over 6.28 mm and 32.93 mm at sites 2 and 3, respectively. Workings at site 2 close up relatively higher over the second period than over the first period of measurement. In contrast, mine workinsg at site 3 close up lesser than over the first period.

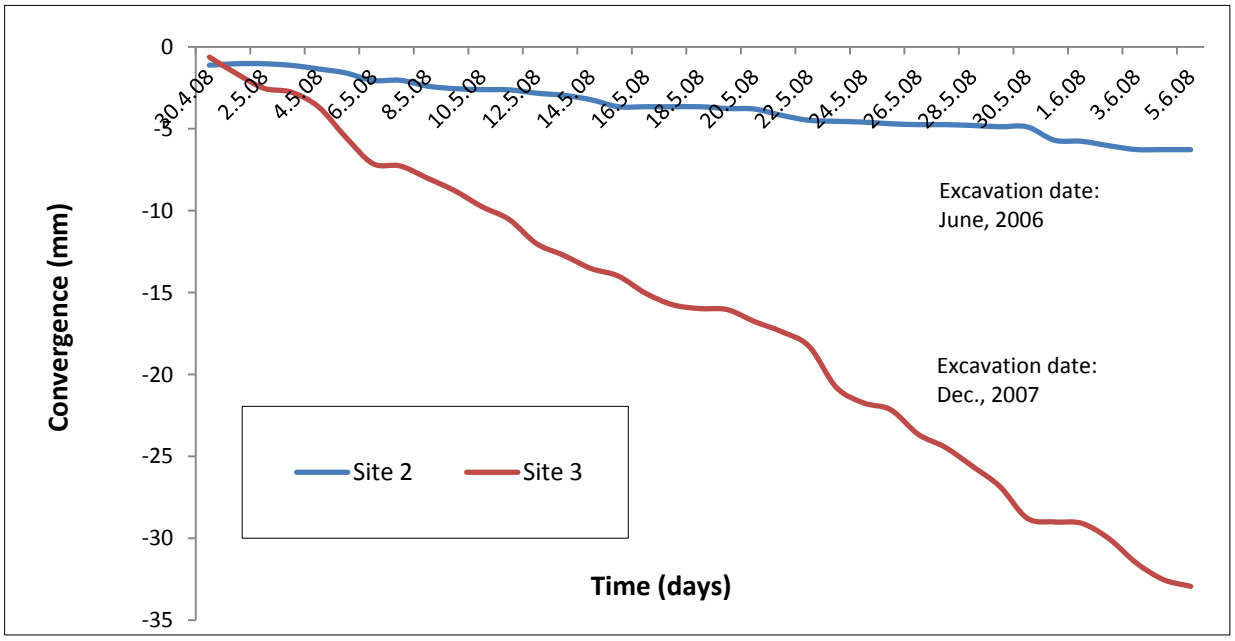

Figure 5.43 Effect of age of sites on convergence at sites 2 and 3 between end of April and beginning of June 2008

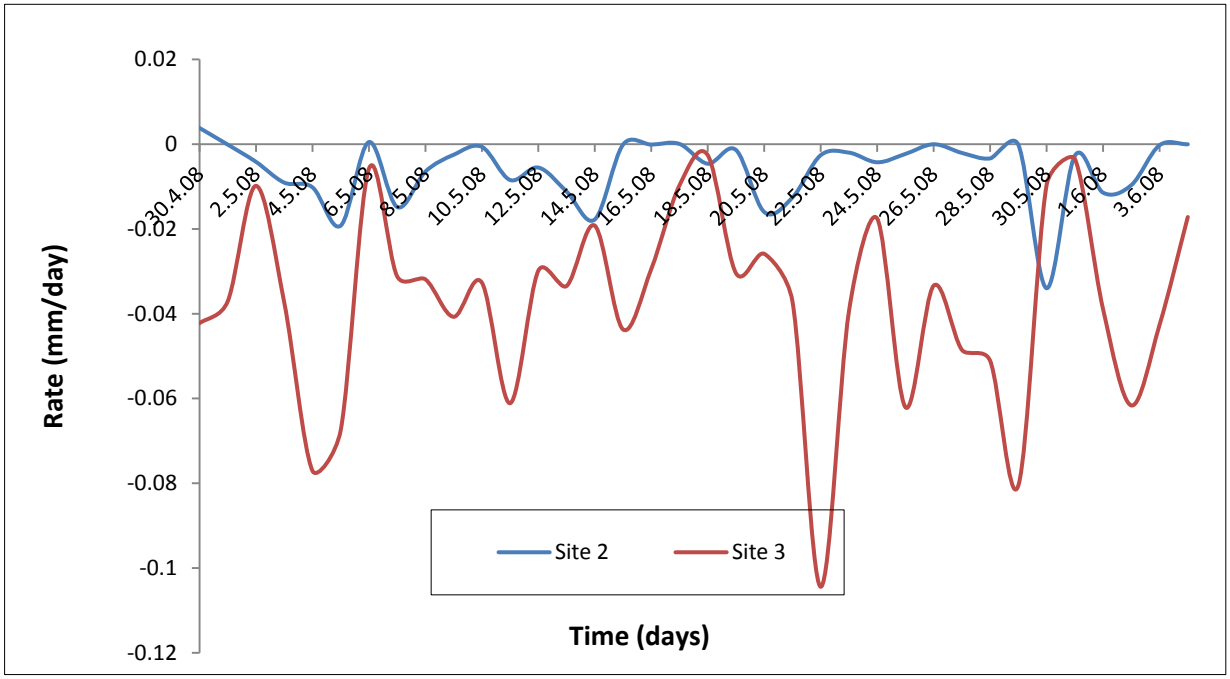

Figure 5.44 Effect of age of sites on convergence rate at sites 2 and 3 between end of April and beginning of June 2008

Patterns of convergence rate (Figure 5.44) also portray the effect of age on the behaviour of workings at both sites. The plot shows different trends of rate at the two

sites over this period of measurement. At site 2, the rate of convergence increases over the second period, whereas it decreases at site 3. If the decrease of convergence rate at site 3 could be attributed to both the time interval between the two periods of measurement and roadway milling process, the unexpected increased rate of convergence at site 2 might be due to the environmental site conditions which temporarily impeded the functioning of the bespoke closuremeter (Sections 5.2.2 and 5.4.2).

It appears from the above analysis that the age of the sites controls the magnitudes and rate of convergence of excavation underground mines. The discrepancy on the excavation behaviour observed at the sites over the two periods of measurement is attributed to the behaviour of both roof and floor, particularly in the near-seam at the three sites. At the oldest site 2, the overlying near-seam layers might be in their later stages of deformation. In contrast, at the newly mined sites 3 and 4, these layers are still deforming under gravity and the weight of the overburden. In addition, the geological near-seam sequence at the sites might have also influenced the behaviour of the excavation. Although geological structures at the three sites are similar, the near-seam sequence may vary from site to site (Section 5.3) (Hebblewhite, 1977)

Other factors which might have influenced the behaviour of excavation include the proximity of the sites to mining activity (e.g. floor milling at site 3 and main face at site 4) and the geometry of the sites. Generally, convergence of excavation at the sites occurs gradually and linearly over the two periods of measurement despite the discrepancy in the behaviour of excavation and rapid movement which manifests at new sites and at those in close proximity to ongoing mining activity.

ii. Relationship with geometry and location of sites

Sites geometry and location have controlling effect on the behaviour of underground excavation. Ideally, a qualitative analysis of the effect of geometry of sites on the excavation behaviour would be better undertaken with sites of different geometry but

with same age and same location. Meanwhile, the effect of sites location would be qualitatively analyzed with sites of same age and geometry but with different locations. Due to limited data, available dataset of movement at sites 1, 3 and 4 are used to examine effects of both geometry and location of sites. Selected sites are of different locations (i.e. North or South) and different geometry (i.e. roadway or stub) and grouped in two datasets. For each dataset (i.e. period of measurement), patterns and rate of convergence at the monitored sites are examined. The effect of both geometry and location of sites on the behaviour of working is also investigated by analyzing the convergence of workings over day.

The first dataset consists of deformation at site 1 (in the South) and sites 3 and 4 both (in the North) and covers the period between beginning of March and April 2008. Patterns and rate of convergence and daily workings behaviour for each period of measurement are shown in Figures 5.45 and 5.46, and Figures 5.47-49, respectively.

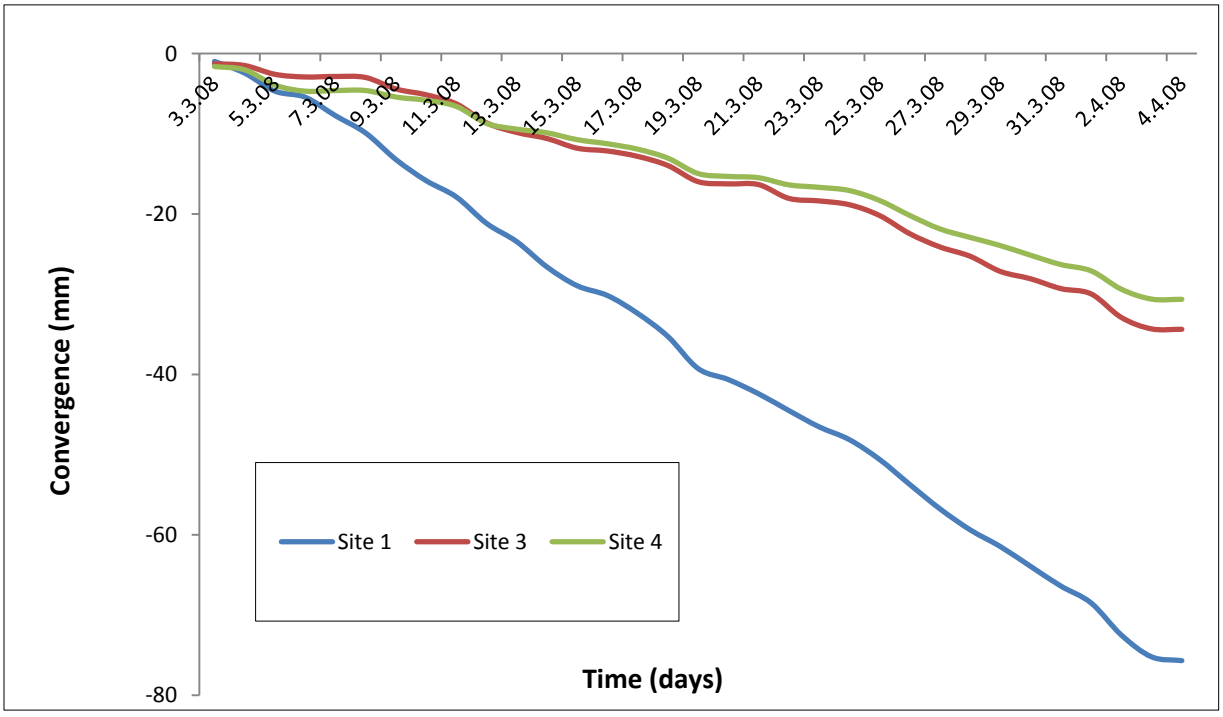

Figure 5.45 Effect of geometry (i.e. stub, roadway) and location zone (i.e. North, South) of sites on convergence at sites 1, 3 and 4 between beginning of March and April 2008

Figure 5.45 portrays the influence of geometry and location of the sites upon the behaviour of workings. The plot indicates higher magnitude of convergence in the South than in the North. In the South, underground excavation closed up over 75.69 mm at site 1, and over 34.38 mm and 30.64 mm in the North at site 3 and site 4, respectively. The difference in magnitude of convergence is due to the difference in depth at which mining activity takes place as the seam potash dips approximately 5 degrees in South-East direction (Section 3.1). An additional explanation is the temperature gradient (Section 5.2.2). Both depth increase and high temperature result in flow of salt, potash and carnalite marl rocks into excavations. Consequently, higher magnitudes of convergence are observed in the South than in the North. This phenomenon has also been reported at Boulby.

The effect of geometry and location of sites is also translated by the rates of convergence. Although convergence of opening at the three sites occurs gradually and linearly however, deformation of opening occurs at different rates (Figure 5.46).

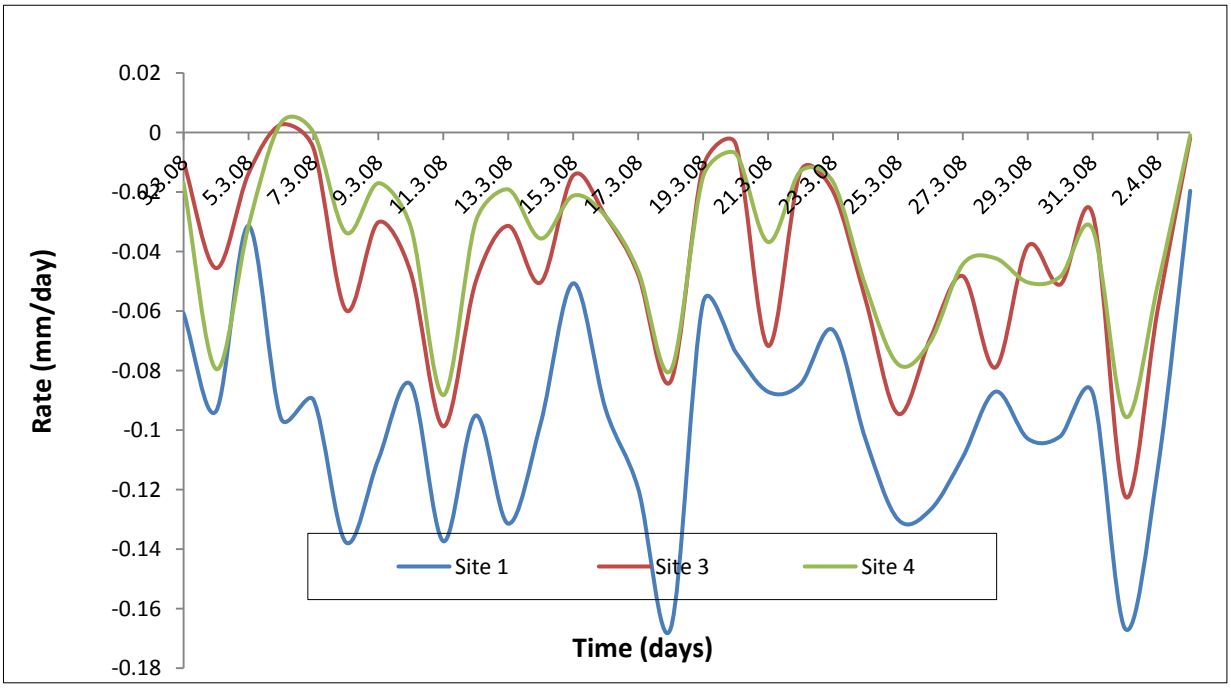

Figure 5.46 Effect of geometry (i.e. stub, roadway) and location zone (i.e. North, South) of sites on convergence rate at sites 1, 3 and 4 between beginning of March and April 2008

Deformation rate is higher at site 1 in the South than at sites 3 and 4 both in the North where the excavation deforms at relatively similar rates. It is also shown by the slopes of patterns of convergence. The slope of convergence at site 1 is twice and about three times that at sites 3 and 4, respectively.

The effect of both sites geometry and location upon patterns of convergence is further analyzed through the daily movement of mine workings by averaging the data collected at each site on an hourly basis and expressed in terms of height of excavation (Figures 5.47-49).

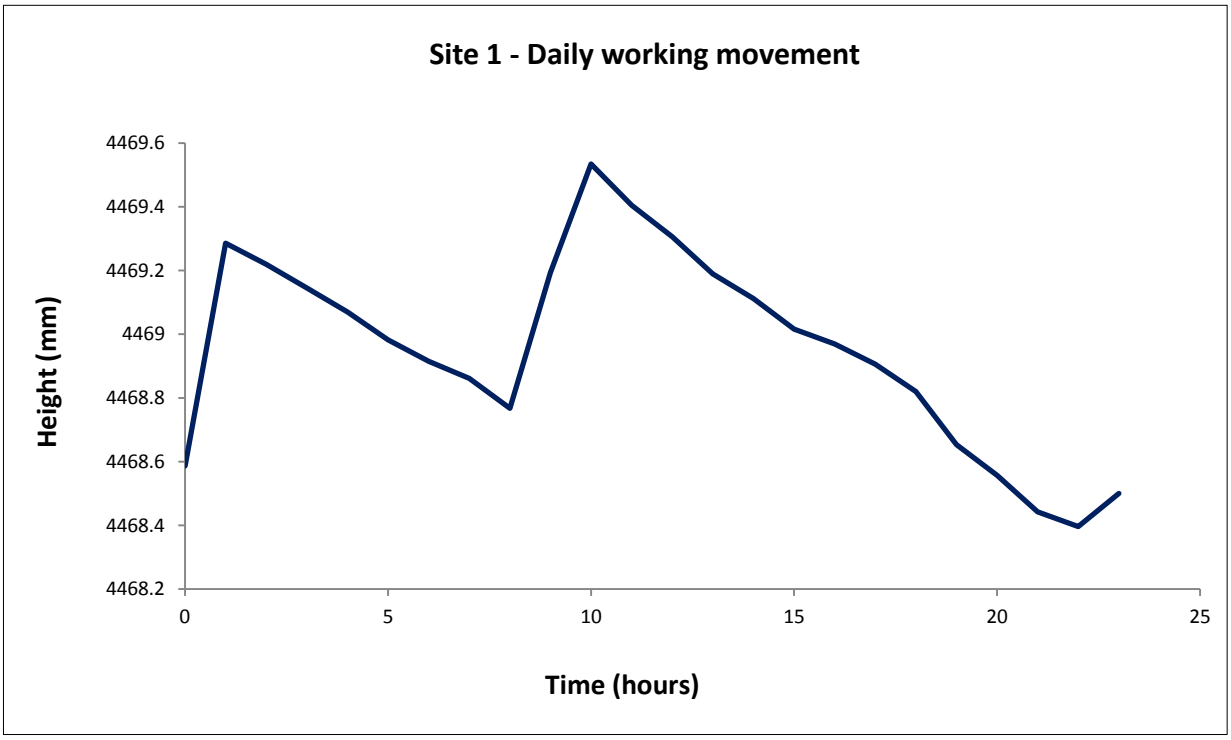

Figure 5.47 Mine workings movement over day at site 1 between beginning of March and April 2008

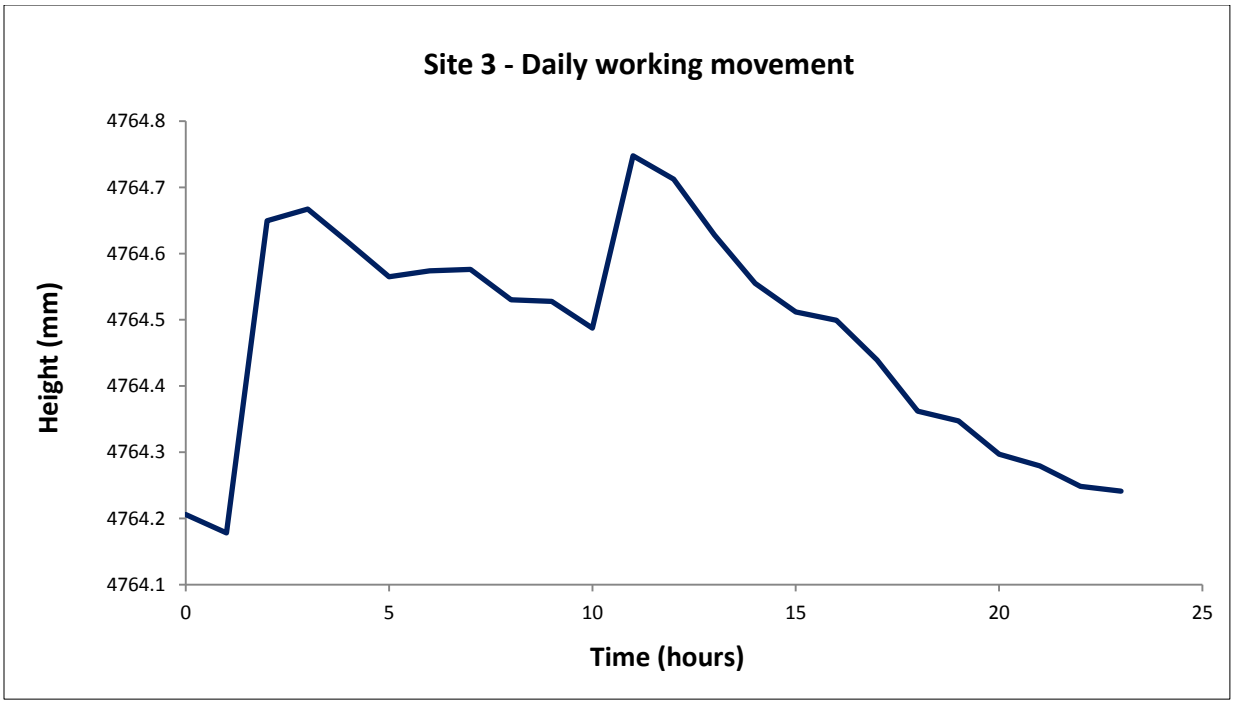

Figure 5.48 Mine workings movement over day at site 3 between end of February and beginning of April 2008

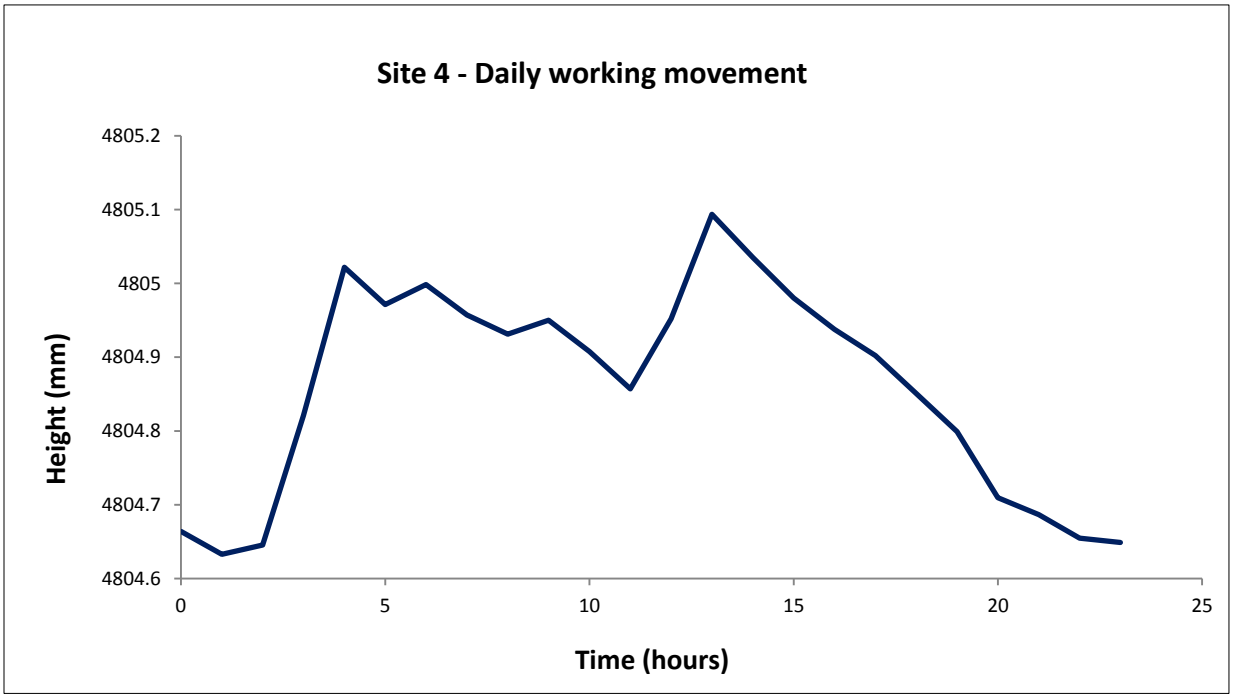

Figure 5.49 Mine workings movement over day at site 4 between end of February and beginning of April 2008

Figures 5.47-49 show similar patterns of workings behaviour over one day. Although the similarity of daily patterns, movement of workings fluctuates over day and magnitude of movement varies from one site to another. The fluctuating behaviour of workings is associated with the dependency of deformation on the mechanics of potash itself as a function of several factors mainly the temperature (Kwon and Wilson, 1999).

At site 1, the peak of movement occurs at about 9:00 am (Figure 5.47), whereas at sites 3 and 4 the movement peak occurs at about 11:00 am (Figure 5.48) and 14:00 pm (Figure 5.49), respectively. The difference in the time of peak occurrence at sites 3 and 4 might be due to the geometry of the site (Section b.i). The discrepancy in the time of peak occurrence at the three sites is a result of both the ventilation cycle of the mine and the time-dependent properties of evaporite rocks. Switching off the ventilation system overnight for maintenance purpose increases temperature within mine culminating around 2:00 am and 3:00 am in the South and North of the mine, respectively. The sharply increase of temperature induces micro-movement (i.e. deformation) of working immediate roof and floor mainly made of potash and salt rocks. When the ventilation system is turned on around 4:00 am, fresh air circulates within the mine. Consequently, the temperature sharply decreases resulting in the decrease of working movement (i.e. salt and potash deformation) till around 9:00 am before the ventilation system is turned off again for maintenance. The temperature rises again, inducing high mine workings movement around noon. The decline in the patterns of movement after noon results from the natural cooling (i.e. moment of day of decrease of temperature) of the mine although the cooling air from the ventilation system also plays significant role in the decrease of temperature.

An alternative explanation to the discrepancy in the time occurrence of peak of movement in the South and North is the pressure due to the weight of the overburden. With seam potash dipping at an angle of 5 degrees in South-East direction (Section 3.1), the overburden exerts a pressure of about 27 MPa at 1,200 m depth and 25 MPa at 1,100 m depth in the South and North, respectively assuming a vertical stress increase rate of -22.6 KN/m^2 per metre (Section 3.6.3).

The second dataset analyzed consists of movement at sites 1 and 3 between end of April and beginning of June 2008. Movement of workings manifests more rapidly at site 1 than at site 3 as indicated by both convergence and rate of convergence patterns (Figures 5.50-51). At the end of this period, movement magnitude of 62.64 mm and 32.93 mm are recorded at site 1 and site 3, respectively.

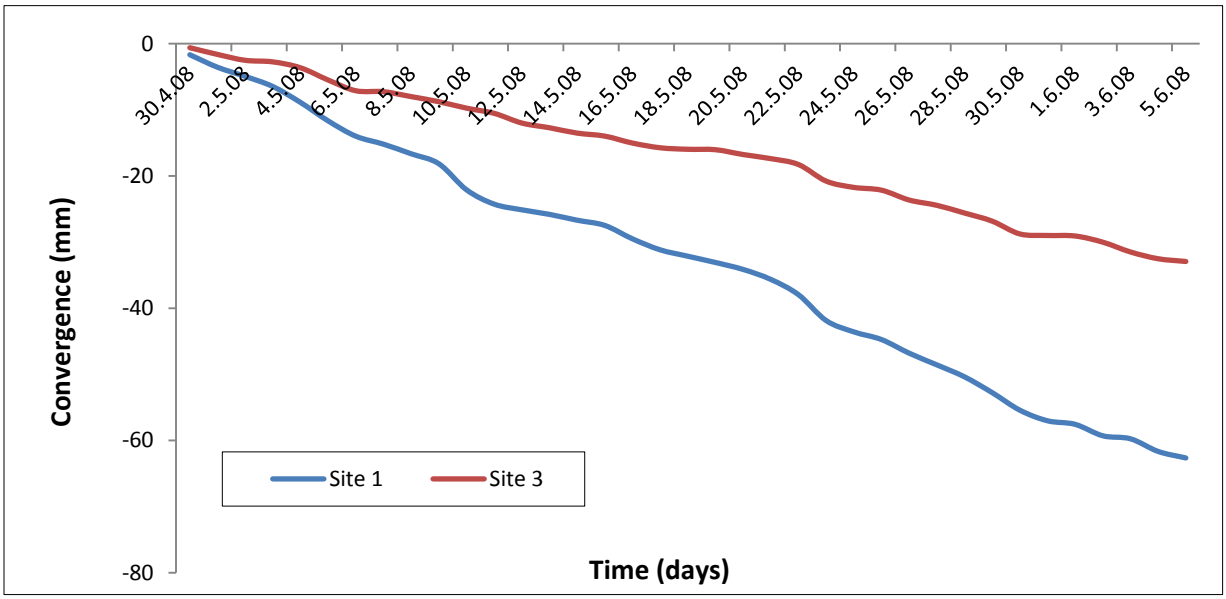

Figure 5.50 Effect of geometry (i.e. stub, roadway) and location zone (i.e. North, South) of sites on convergence at sites 1 and 3 between end of April and beginning of June 2008

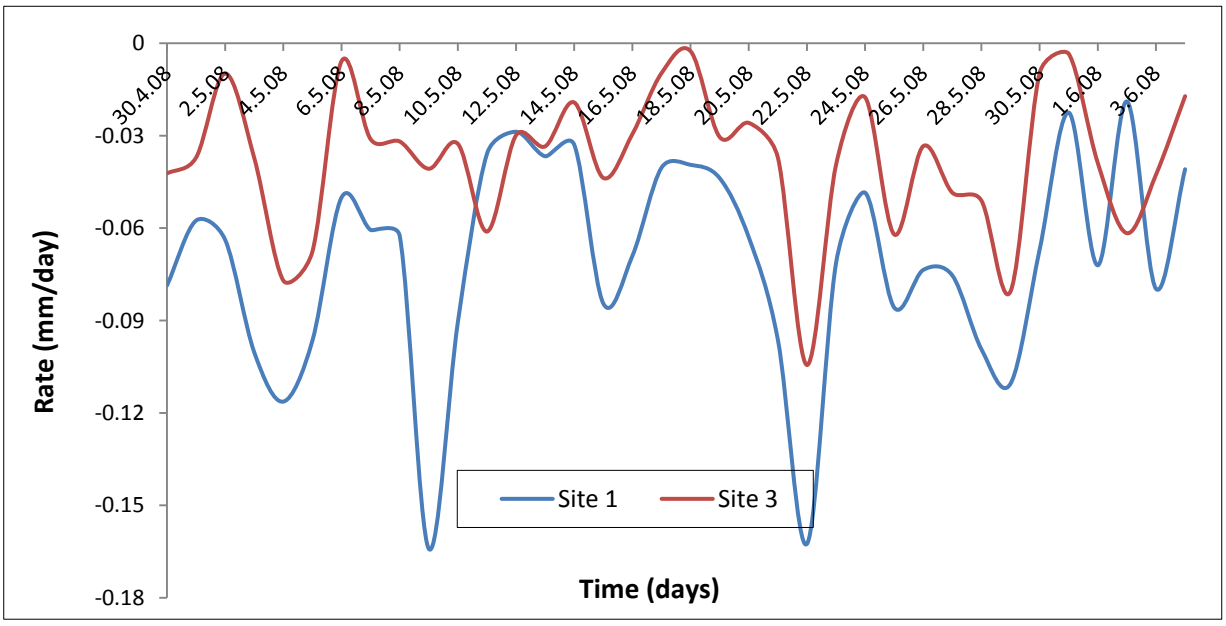

Figure 5.51 Effect of geometry (i.e. stub, roadway) and location zone (i.e. North, South) of sites on convergence rate at sites 1 and 3 between end of April and beginning of April 2008

As explained above, the difference in magnitude and rate of convergence recorded at the two sites is a result of effect of both sites geometry and location. This effect is also translated by the average daily working movement patterns (Figure 5.52).

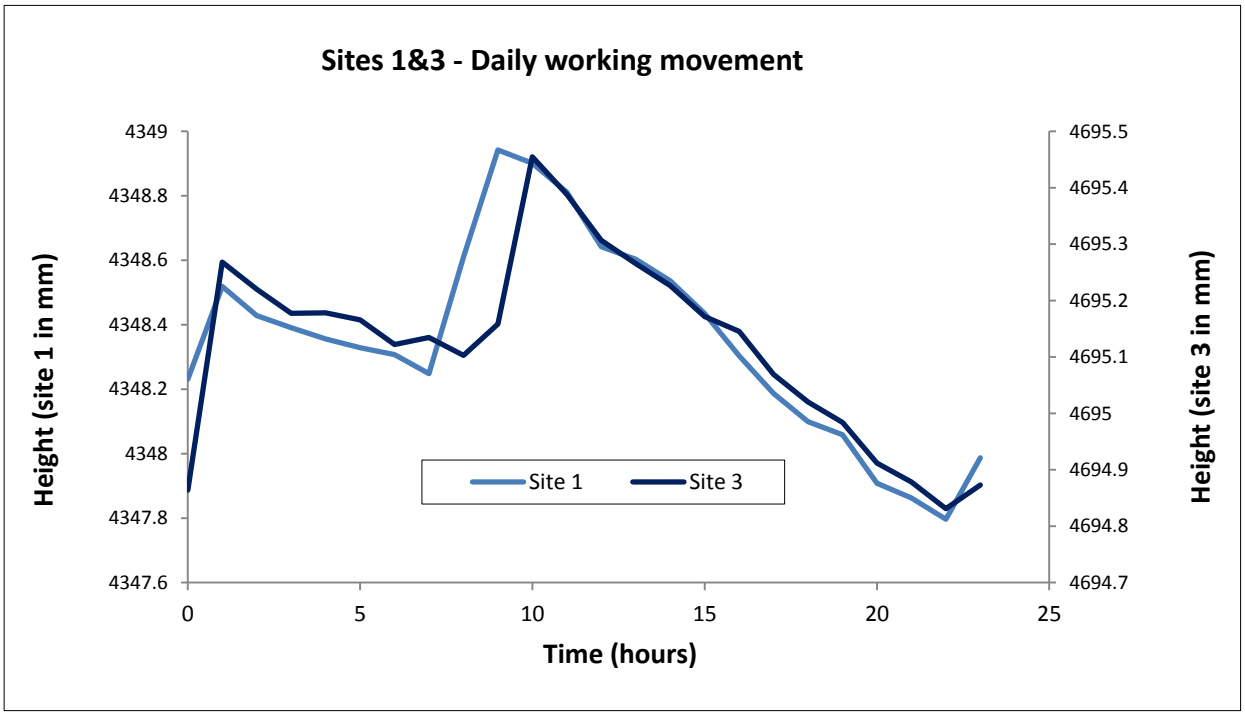

Figure 5.52 Mine workings movement over day at sites 1 and 3 between end of April and beginning of June 2008

Figure 5.52 indicates a minimum and maximum in the behaviour of workings at the two sites during day time. The maximum corresponds to the peak of movement which occurs at about 9:00 am and 11:00 am at site 1 and site 3, respectively. Meanwhile, the minimum point corresponds to the lowest value of movement recorded at each site at about 7:00 am and 8:00 am at sites 1 and 3, respectively. Convergence patterns obviously show that daily working behaviour at both sites is a function of the cooling system cycle at the mine as discussed above.

The analysis of magnitudes of convergence, rates of convergence and daily movement of mine workings at the three sites shows high convergence magnitude and rapid movement manifestation in the South than in the North over the two periods of measurement regardless of the geometry of the sites. Although the determination of the dominant controlling factors of working mechanics requires extensive data, it is believed

that the discrepancies observed in the magnitudes of convergence, rate of convergence and daily movement of working are attributed to the depth of the sites.

Beside the above controlling factors, floor heave also influences the patterns, magnitudes and rates of convergence of workings recorded at the monitoring sites; particularly at site 3 where milling of floor was carried out one month after instrumentation.

5.5 The reliability of the bespoke closuremeter

In order to evaluate the reliability of the bespoke closuremeter, two datasets are analyzed. The first dataset is of closuremeter-based workings movement at Panel 440 (i.e. site 2) and the second is of a built-in tape and spirit level-based dataset of workings movement at panel 416 (Figure 5.1). The latter is a continuous monitoring of workings convergence carried out by Boulby mine at ten stations along roadway between July 2005 and May 2008. The choice of the two panels is guided by their respective age (i.e. date of mining). Panel 440 was mined on 6th June 2005 (Table 5.1) and Panel 416 was mined on 17th June 2005 and the monitoring process began on 22nd July 2005.

The assessment of the reliability of the closuremeter is based on both the general trend of patterns of convergence and average convergence of workings at the two panels. The behaviour of working at Panel 416 was monitored over a period of about three years, with a large amount of data collected. However, only data of interest, i.e. covering measurement period between January and May 2008 and corresponding to that at Panel 440 were used in the assessment.

In addition, because of water inrush at Panel 416, only four stations (i.e. S1, S2, S3 and S4) whose positions given in Table 5.6 are retained for this process. Furthermore, because perceptible movement at site 2 is recorded between end of April and beginning of June 2008 (Figure 5.34), data covering this period are used.

Besides the assessment of the reliability of the bespoke closuremeter, pattern of convergence at Panel 416 is also used to explain the findings of the monitoring program

of mine workings mechanics at Boulby. Patterns of convergence at Panels 416 and 440 (i.e. site 2) are given in Figures 5.53 and 5.54, respectively.

Table 5.6 Positions of monitoring stations along roadway G at panel 416 (source Boulby Mine)

Stations	Estimated positions along the roadway (m)
1	30
2	105
3	125
4	207

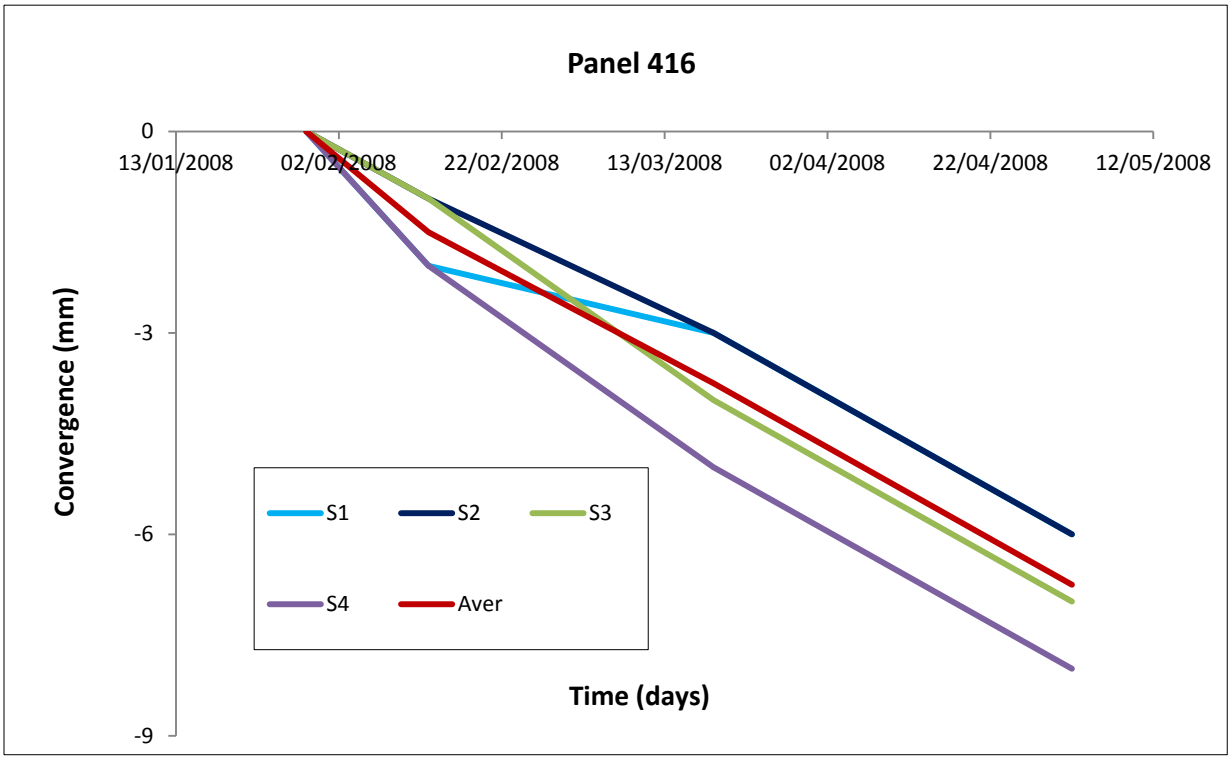

Figure 5.53 Convergence at four stations at panel 416 between January and May 2008

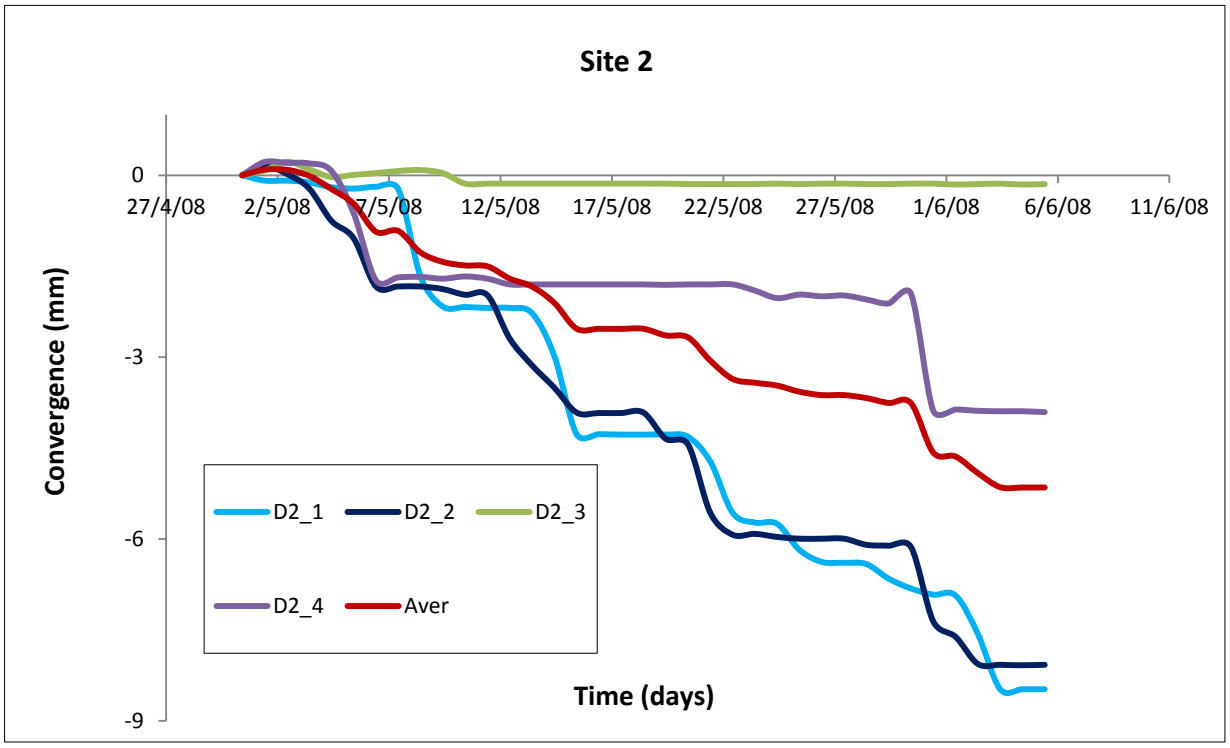

Figure 5.54 Convergence at site 2 between end of April and beginning of June 2008

Figures 5.53 and 5.54 show linear movement occurred at the both panels over the period of measurement. The smoothed trend of convergence patterns at Panel 440 is probably due to the monitoring process itself, including the monitoring instrument. In fact, monitoring process at this panel was continuous using a high resolution closuremeter, whereas at Panel 416 the monitoring process was discontinuous or episodic (i.e. measurements are taken periodically) using a relatively low resolution built-in tape and spirit level. Continuous monitoring allows small and short-term changes at Panel 440 to be recorded than the discontinuous process at Panel 416. More so, the sampling frequency of 5 minutes might also have contributed to the trend exhibited by the behaviour of working at this panel.

At the end of measurement, mine working closes over 6.75 mm and 5.15 mm at Panels 416 and 440, respectively. The slight discrepancy in the magnitudes of convergence at both sites might be due to the position of the stations or points at the sites. At Panel 416, all monitored points are located along the principal axis of the roadway, whereas at Panel 440 two monitored points are located at stubs and two other

along the roadway axis. Another additional influencing factor is the monitored area which could be estimated by the range between stations. At Panel 440, the maximum distance to data logger is 15 meters (Table 5.1) while at Panel 416 the minimum distance to the reference point is 30 meters (Table 5.5). From figures in Tables 5.1 and 5.6, it is obvious that the monitoring process at Panel 440 measures working movement within a relatively smaller area than that at Panel 416. The drop in the patterns of convergence noticed by the end of May 2008 at Panel 440 might be attributed to the crack observed on the floor during the period of measurement (Plate 5.4). Floor heave at this site induced a throw of about 2 cm wide across the roadway due to (i) the weight of the overburden, (ii) high temperatures and (iii) horizontal stresses. Fracture of floor might have also been exacerbated by the age of the site.

Plate 5.4 Crack on the floor across the roadway at site 2

In terms of rate, convergence at Panel 416 occurs at constant rate of magnitude approximately 0.085 mm/day and at Panel 440 the excavation closed up at lower rate than at Panel 440 (Figure 5.55).

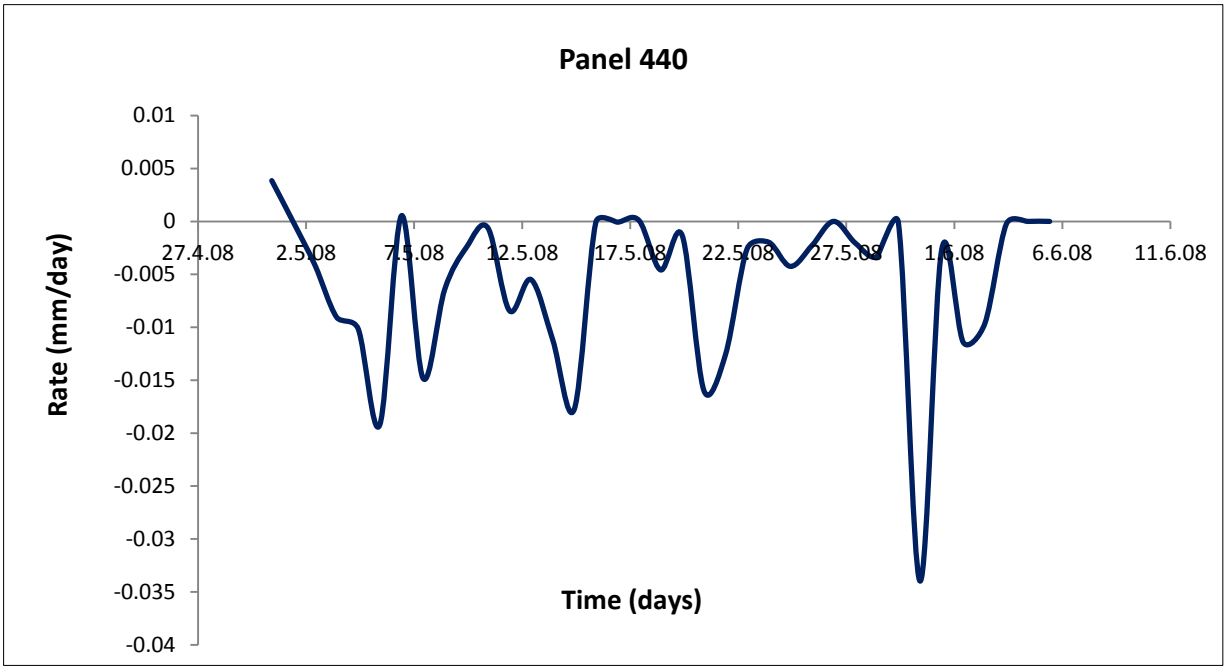

Figure 5.55 Convergence rate at site 2 between end of April and beginning of June 2008.

Comparable magnitudes of convergence recorded at both panels attest the reliability of the bespoke closuremeter in monitoring changes in the behaviour of mine working. Unlike the monitoring technique at Panel 416, Figure 5.55 shows that the bespoke closuremeter is capable of capturing short-term behaviour of working through measurement of small changes in the working behaviour which may unlikely be captured by the built-in tape and spirit level technique more suitable for long-term monitoring. The results also prove the dependency of convergence on the age of panels despite the magnitudes similarity.

The analysis of convergence patterns shows steady deformation of working over the periods of measurement in spite of the age, geometry and location of the sites. Although convergence patterns seem to disagree with the commonly accepted time-dependent behaviour of geomaterials, the findings are in good agreement with the creep behaviour of evaporite rocks. Indeed, by applying the evaporite rocks creep

model to the behaviour of mine working, patterns of convergence at all of the monitoring sites are identified to the secondary or steady stage of creep before roadway milling at site 3 (Figures 5.37-39).

Generally, geomaterials creep under sustained loading and yield excessively as the stress state is beyond a certain threshold. This time-dependent behaviour of geomaterials consists of four stages: (i) the instantaneous and recoverable elastic deformation which takes place once the material is excavated, (ii) transient or primary creep at an exponentially decaying rate, (iii) steady or secondary creep at constant rate and (iv) the unstable tertiary creep at an accelerating rate.

For underground excavations in potash and rocks salt, the long-term deformation (i.e. creep) of workings is controlled by the time-dependent properties of the rocks and other parameters including openings geometry and depth (Kwon and Wilson, 1999). The latter variable induces temperatures increase and flow of evaporite rocks, particularly of rock salt. Furthermore, deformation of excavation may continue for several months and even years after excavation before the complete closure of the openings.

Mine instrumentation allows measurement of displacement to provide information on the response of excavation to the mining of adjacent excavations and on the long-term stability of the openings during and after the excavation. Once the excavation of the opening has been completed, monitoring its behaviour ensures that no long-term instability is developing. Therefore, monitoring excavation creep calls for a long-term monitoring program from the beginning of the excavation process. A too late installation of instruments results in the loss of initial behaviour of workings.

For mine instrumentation took place several months after the sites were excavated (Table 5.1), neither the instantaneous nor the transient stages of creep were recorded because they occurred before the installation of the instruments at the sites. Additionally, because of the short-term monitoring program it was not possible to capture the accelerating creep stage. Hence, only the steady-state of creep has been monitored.

5.6 Summary and conclusion

In this chapter, we have discussed the results of short-term monitoring of excavation convergence, determined the factors which control the mechanics of mine working at Boulby potash mine and assessed the reliability of the bespoke closuremeter on the basis of patterns and magnitudes of convergence at four monitoring sites at Panel 416. From the findings, the following conclusions are drawn:

Convergence at the monitoring sites occurs gradually and linearly over the time of measurement. Deformation at the four sites is a function of the position of the monitored point at the site, age, geometry and location of the site. Convergence of working occurs inversely to the age of the monitoring sites. At all of sites, rapid movement develops along roadway than at stub. At site of stub type, rapid movement develops at point in close proximity to the roadway. Similar patterns and magnitudes of movement are recorded at sites of same age. In addition to the geometry and age of the sites, the geological variations in the near-seam at the sites might have also influenced the behaviour of the excavation at the sites.

In terms of magnitudes, higher magnitudes of convergence are recorded in the South than in the North of the mine. In this regard, although it is quite difficult to precisely determine the factor between the location and geometry of site which mostly controls the behaviour of working in the South and North, I firmly believe that the location of the sites significantly influences the convergence of working at Boulby mine as a result of the excavation depth and the resulting gradient of temperatures. Additionally, it is worth noting that floor heave also controls the patterns, magnitudes and rates of convergence at the monitoring sites.

Despite the slight discrepancies in the patterns of convergence at Panel 440 and Panel 416, similar magnitudes of convergence and also patterns of convergence rate at Panel 440 attest the reliability of the bespoke closuremeter in monitoring small changes in the working behaviour at Boulby mine.

When the factor of time interval between the excavation and instrumentation of the sites is considered, the linear trend displayed by the average convergence patterns

at all of the monitoring sites is identified with the steady or secondary stage of the creep behaviour of potash and salt rocks. Neither the instantaneous nor the transient stages of potash and salt creep behaviour were captured because of the relatively long time interval between the mining and the instrumentation of the sites.

Chapter 6
The FLAC 2D modelling approach

6.1 Introduction

In mining, numerical models are used to estimate the extent of potential instability in the rock surrounding underground excavations. This chapter describes the procedure of applying the 2D Fast Lagrangian Analysis of Continua (FLAC) code of the Finite Difference Method (FDM), used for the numerical simulation of the mine workings closure at Boulby mine. The fundamental components of the modelling process to be considered are:

1. Definition of a finite difference grid;
2. The constitutive behaviour and material properties; and
3. The boundary and initial conditions.

The finite difference grid spans the physical domain (i.e. geometry) of the problem being analyzed. The constitutive behaviour and associated material properties dictate or determine the response (e.g. deformation) of the model when disturbed (i.e. excavated). In the case under study the disturbance originates from potash removal. The boundary and initial conditions define the *in-situ* state of the problem (i.e. the conditions prevailing before disturbance – e.g. excavation is introduced) (Itasca, 2005).

After defining these conditions, the initial equilibrium state of the model was calculated. The model was then disturbed and the resulting response of the model evaluated.

6.2 The model geometry

A simplified conceptual model was used to represent the domain of the system under study. The geological formations which constitute the system were assumed to be homogeneous and isotropic. The modelled system was initially considered not to have structural features such as fractures and faults which may affect the strength of the rock mass with the assumption that Boulby structure is continuous (Kemeling, 2006; Talbot *et al*., 1982). A fault has been after incorporated within the structure which in addition to acting as plane of weakness when failure occurs will reduce the strength of the rock mass (Islam and Shinjo, 2009; Brody and Brown, 2006). The conceptualized model of the structure being analyzed is given in Figure 6.1 below. The thicknesses of layers in Figure 6.1 are those of strata given in Table 6.6 below (Sections 3.3.2 and 3.4.3).

6.3 Initial conditions for the Model

6.3.1 Model grid generation

The FLAC mesh 1400 m wide and 1400 m high representing a section of the structure of Boulby was generated for the numerical analysis. The determination of the size (or dimensions) of the mesh has been dictated by two main factors: the depth of the potash seam and the inclusion of all the overlying layers in the model. These are the main drivers of patterns of stress and deformation distribution through the overburden. A third main factor is related to the determination of the mesh boundaries. These artificial boundaries should be placed far away from the area of interest so that the behaviour in the area is not greatly affected to impair the outcomes of the analysis (Itasca, 2005). The potash seam is extracted at a depth of approximately 1,200 m below the surface (Figure 6.1). For the reliability of the modelling results the density of the zone of interest (i.e. potash) is chosen higher than the remaining zones of the structure. A mesh grid (i.e. density) of 10 m x 1 m is used for the zone of interest and of 10 m x 10 m for the remaining regions of grid model. The FLAC code used for the generation of the grid is provided in Appendix A.

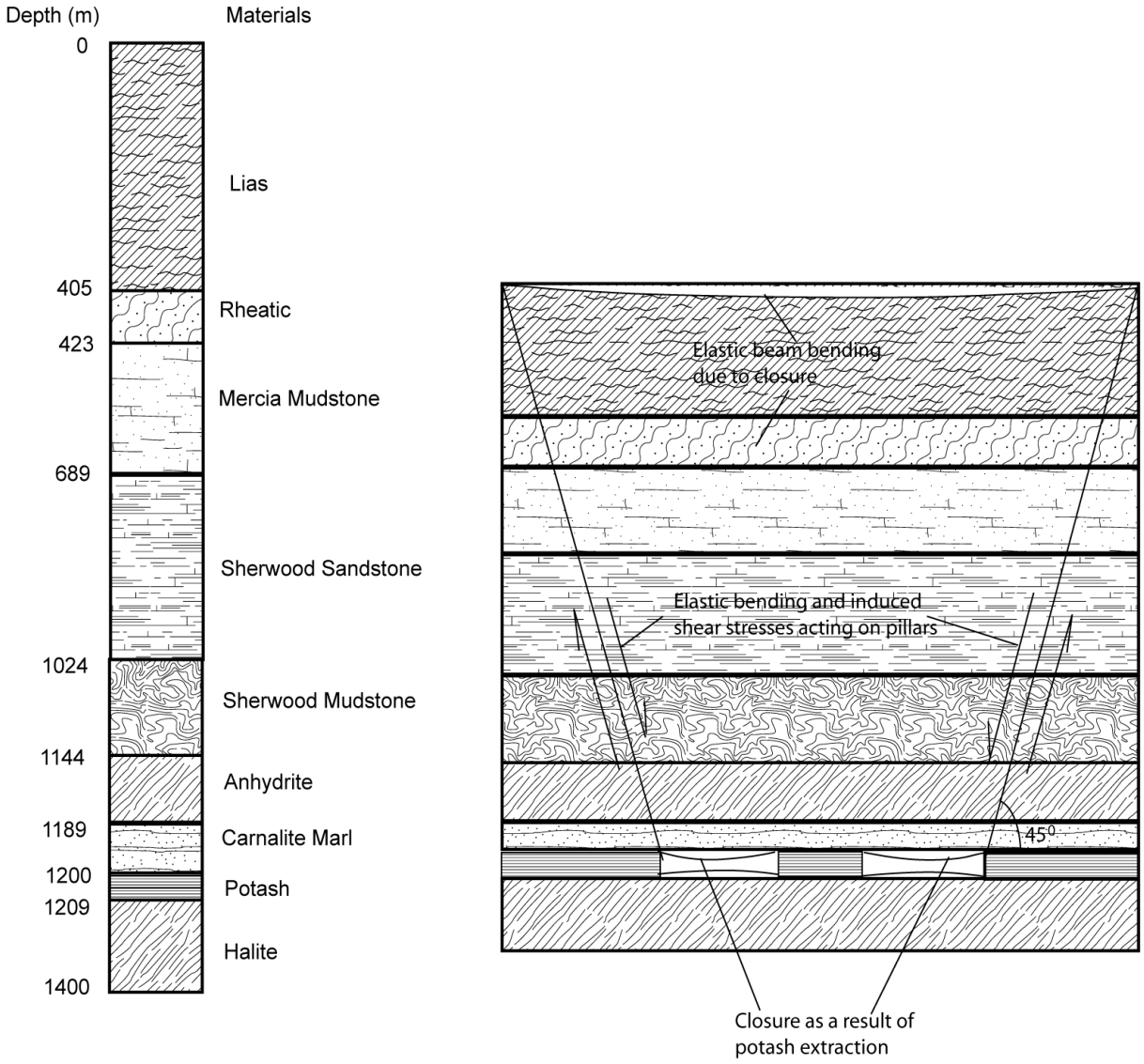

Figure 6.1 A simple conceptualized model of Boulby structure and a geological cross section showing the stratification above the excavations**.** Not to scale - Schematic only.

Because the production of potash is undertaken by excavating two roadways through the rocks as discussed in Section 3.3.1 a grid mesh with two excavations representing the underground layout was used for the numerical analysis (Figure 6.2).

6.3.1.1 Constitutive models

After generating the model grid, the necessary input parameters were assigned to the materials. The two main input variables are the material constitutive models and the associated mechanical properties.

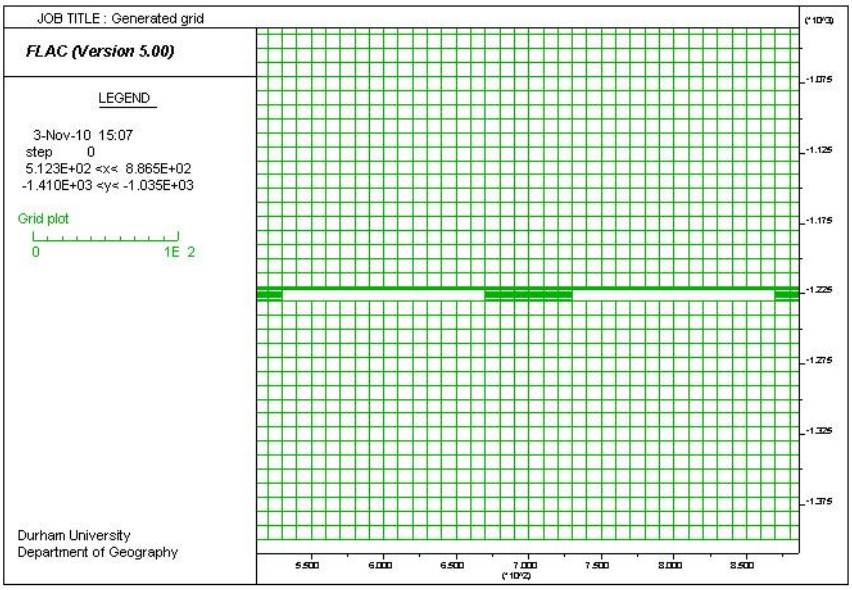

Figure 6.2 FLAC grid and the potash seam for the unfaulted structures

Three different models and failure criteria were used in this process for the characterization of the behaviour of the strata of Boulby structure. The Drucker-Prager model was used to characterize the behaviour of the Lias and Rheatic layers on the top, the Mohr-Coulomb was applied to the behaviour of Mercia Marl, Sherwood Sandstone, Sherwood Mudstone and Anhydrite on the middle and the strain-softening model for the evaporite layers on the bottom as an approximation to the creep behaviour of the rocks. The selection of these models was on the basis of rheological considerations of materials discussed in Section 3.6.1.

6.3.2 Boundary conditions for the model

After the grid was generated, the boundary conditions were applied. The left and right sides of the grid were fixed from the movement in the x-direction, and the bottom was

fixed in the y-direction. The FLAC 2D coding for setting boundary conditions for the model is provided in Appendix A.

6.3.3 Applying *in-situ* conditions

Prior to mining *in-situ* state of stress is always present. This fact should be taken into consideration within the modelling process in order to prevent the behaviour of the model from the influence of this state. This may be done by setting the initial conditions through the application for instance, of the predetermined *in-situ* stress, pore pressure to the model (Itasca, 2005). In this research the *in-situ* conditions applied to the model include stresses and pore water pressure. The properties of water present within Sherwood sandstone are given in Table 6.1. The vertical stress for each layer is estimated from equation 3.12. Whilst equation 2.4 computes the horizontal stresses for non evaporite strata the ratio 0.51 of horizontal to vertical stress (Section 3.6.3) is used to estimate the horizontal stress for carnalite marl, potash and halite strata (Hebblewhite, 1977). The stresses for each layer are given next to the geological sequence of the model.

Table 6.1 Water properties used for modelling (from: Zhang and Hiscock, 2010; Bahadori and Vuthaluru, 2009; Hitchmough *et al*., 2007; Caughill and Beddoes, 1996)

Density (Kg/m^3)	Bulk modulus (GPa)	Brine pressure (MPa)
1000	2.2	9.3

6.4 Models

Six models were generated to analyse the rock mass response to mining. The approach used was to progress from a simple model of the structure under consideration to one which better translates the more complex real situation at Boulby Mine. Given the presence of brine within the sandstone each model will contain the Sherwood sandstone layer to reflect the Boulby structure which is assumed to contain three types of material behaviour: the Drucker-Prager (DP) for lias and rheatic; Mohr-Coulomb (MC)

for mercia mudstone, sherwood sandstone, sherwood mudstone and anhydrite; and Strain-softening (SS) for carnalite marl, potash and halite strata above the potash seam. As a result, the models evolved from a three layers to a seven layers above the potash taking into consideration the fault. The last translates better a real world system in terms of patterns of maximum principal stress and vertical displacement distributions, as well as the effects of heterogeneous lithology and geological fault.

6.4.1 Progressing the models

I start by grouping the geological strata together to reduce the heterogeneity of the structure and then systematically separate the grouped strata out to increase the geological complexity hence, the heterogeneity of the structure by progressively adding layers to the first model. Tables 6.2-6.6, portraying the respective materials and estimated stress and thicknesses, describe generated models whose sequence of stratification runs from the top to bottom of the cross-section. While Table 6.2 represents the first model with three materials or layers above the potash seam, model 2 in Table 6.3 is obtained by adding a layer of Mercia mudstone on top of Sherwood sandstone. Subsequent models 3 to 5 are obtained by adding one more layer to the previous one. Model 6 is a duplicate of model 5 with a fault incorporated.

The calculated vertical stresses in Tables 6.2 to 6.6 are pressures generated by each geological unit and the differences in the vertical stress values is a function of different densities of different grouped geological materials. The horizontal stress in the final column is a calculated value based on Poisson's ratio, not *in situ* stress measurements. The deformation models applied to the strata throughout the succession are described in Section 3.6.1 and Tables 3.5 and 3.6.

Table 6.2 Materials and estimated stresses used for model 1 (Sections 3.3.2, 3.4.3 and 3.6.3)

Strata	Thickness (m)	Behaviour	Vertical stress (MPa)	Horizontal stress (MPa)
Lias	423	DP	-10.8	-2.7
Sherwood sandstone	721	MC	-28.5	-2.2
Carnalite marl	56	SS	-29.7	-15.1
Potash	9	SS	-29.9	-15.2
Halite	191	SS	-34.0	-17.4

Table 6.3 Materials and estimated stresses used for model 2 (Sections 3.3.2, 3.4.3 and 3.6.3)

Strata	Thickness (m)	Behaviour	Vertical stress (MPa)	Horizontal stress (MPa)
Lias	423	DP	-10.8	-2.7
Mercia mudstone	266	MC	-17.8	-1.6
Sherwood sandstone	455	MC	-29.0	-2.2
Carnalite marl	56	SS	-30.3	-15.4
Potash	9	SS	-30.4	-15.5
Halite	191	SS	-34.6	-17.6

Table 6.4 Materials and estimated stresses used for model 3 (Sections 3.3.2, 3.4.3 and 3.6.3)

Trata	Thickness (m)	Behaviour	Vertical stress (MPa)	Horizontal stress (MPa)
Lias	423	DP	-10.8	-2.7
Mercia mudstone	266	MC	-17.8	-1.6
Sherwood sandstone	335	MC	-26.1	-2.0
Sherwood mudstone	120	MC	-28.8	-2.2
Carnalite marl	56	SS	-30.0	-15.3
Potash	9	SS	-30.2	-15.4
Halite	191	SS	-34.3	-17.5

Table 6.5 Materials and estimated stresses used for model 4 (Sections 3.3.2, 3.4.3 and 3.6.3)

Strata	Thickness (m)	Behaviour	Vertical stress (MPa)	Horizontal stress (MPa)
Lias	405	DP	-10.3	-2.6
Rheatic	18	DP	-10.8	-0.6
Mercia mudstone	266	MC	-17.8	-1.5
Sherwood sandstone	335	MC	-26.0	-2.0
Sherwood mudstone	120	MC	-28.7	-2.2
Carnalite marl	56	SS	-30.0	-15.3
Potash	9	SS	-30.1	-15.4
Halite	191	SS	-34.3	-17.5

Table 6.6 Materials and estimated stresses used for model 5 (Sections 3.3.2, 3.4.3 and 3.6.3)

Strata	Thickness (m)	Behaviour	Vertical stress (MPa)	Horizontal stress (MPa)
Lias	405	DP	-10.3	-2.6
Rheatic	18	DP	-10.8	-0.6
Mercia mudstone	266	MC	-17.8	-1.5
Sherwood sandstone	335	MC	-26.0	-2.0
Sherwood mudstone	120	MC	-28.7	-2.2
Anhydrite	45	MC	-30.0	-8.5
Carnalite marl	11	SS	-30.2	-15.4
Potash	9	SS	-30.4	-15.5
Halite	191	SS	-34.5	-17.6

6.4.2 Final model: Model 6

This model obtained by incorporating a fault into model 5 allows assessing the effect of geological structure on the patterns of stress and displacement distribution due to the extraction of potash. The fault is considered to be a real interface which implies that one side of the structure may slide and/or open relative to one another (Itasca, 2005). It is

assumed to be a homogeneous single plane with a throw of 10 meters, equivalent to the width of a grid zone (Sheng and Reddish, 2005).

The Boulby mine has no known parameters for its fault. However, a coal mine within the region has a fault known to be of weathered, persistent and smooth surface (Hao and Azzam, 2005; Sheng and Reddish, 2005). This analogue was used for the analysis of the influence of fault on geomechanical processes. It is worth to state that the referred analogue may not reflect the reality at Boulby mine. Henceforth, the analysis has turned to the effects of fault on the distribution of stress and displacement in deep mining rather than the prediction of a practical case.

Given the small dips of beds at Boulby (Section 3.3.3) the fault inclination was not taken into consideration despite its influence on the plane of slip (Brady and Brown, 2006). For simplicity the fault dips down in the Northwest-Southeast direction up to the potash seam. Its parameters and the subsequent structure generated grid are given in Figure 6.3 and Table 6.7, respectively.

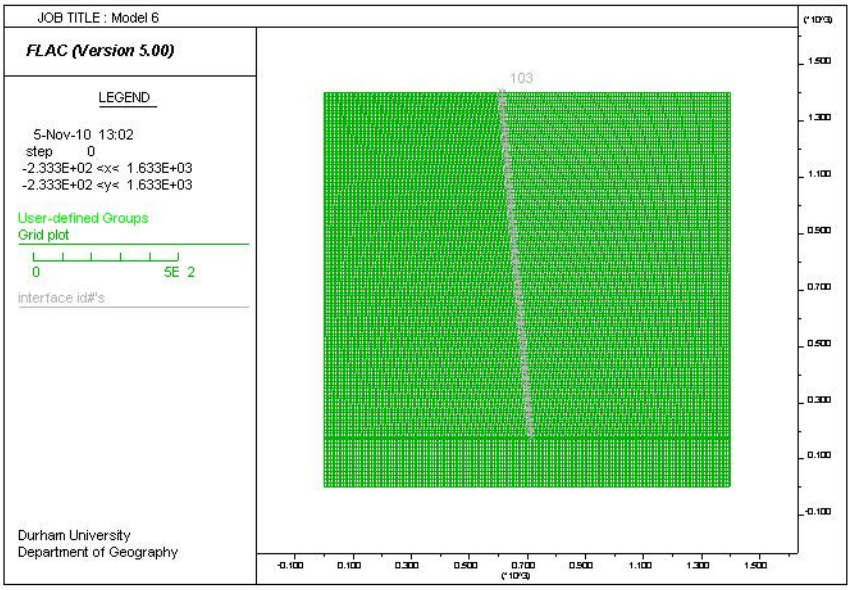

Figure 6.3 FLAC grid for the faulted structure (i.e. model 6)

Table 6.7 Fault parameters used for modelling (from: Hao and Azzam, 2005; Sheng and Reddish, 2005)

Normal stiffness (GPa/m)	Shear stiffness (GPa/m)	Friction (degrees)	Cohesion (MPa)
20	2	28	0.4

6.5 Properties of the overlying strata

The mechanical properties of rocks material used in the modelling process are from laboratory tests (including tensile, uniaxial and triaxial compressive tests carried out on Boulby rocks) and literature review on similar lithologies as discussed in Section 3.4. The mechanical parameters assigned to the Rheatic layer are deduced from the nature of its constitutive materials (i.e. mudstone, limestone, shale) (Howley, 2007) and also with respect to strength parameters of Lias.

The elastic deformability properties of materials are the bulk modulus (*K*) and the shear modulus (*G*). These parameters are related to each other through the stiffness or Young's modulus (*E*) and Poisson's ratio (*v*) as follows:

$$k = \frac{E}{3(1-2\nu)} \tag{6.1}$$

$$G = \frac{E}{2(1+\nu)} \tag{6.2}$$

The strength properties of materials are the internal angle of friction (Φ=phi) and the cohesion (C). The tensile strength limits may generally be calculated using the relation C/tan (Φ).

Values of parameters k_ϕ and ζ_ϕ for Lias and Rheatic strata are estimated from equation 3.5. The summarized parameters of strata used for modelling are presented in Table 6.8.

Table 6.8 Summary of the mechanical properties of strata used for modelling

STRATA	Geotechnical Parameters						Tensile Strength (MPa)
	Deformability		Strength				
	Bulk Modulus (GPa)	Shear Modulus (GPa)	Cohesion (MPa)		Friction (degrees)		
Drucker-Prager Materials							
			k_ϕ	ζ_ϕ			
Lias	9.17	12.55	0.024	0.768	33		3.9
Rheatic	4.81	6.2	0.094	0.819	35		4.24
Mohr-Coulomb Materials							
Mercia mudstone	13.51	15.76	6.0		41		2.76
Sherwood sandstone	11.55	12.60	11		45		5.20
Sherwood mudstone	10.53	12.70	26.0		44		6.86
Anhydrite	14.43	10.83	17.0		43		6.08
Strain-Softening Materials							
			Peak	Residual	Peak	Residual	
Carnalite marl	3.9	2.93	3.0	1.0	35	18	1.24
Potash	28.73	8.18	10.0	6.0	36	33	1.79
Halite	17.93	9.25	10.0	9.4	40	10	1.63

6.6 Calculating rock response

6.6.1 Excavating the panels

To finalize the analysis of the response of the model, three steps were undertaken: first, we considered the behaviour of materials as described in model 5 and brought it to its equilibrium state; second, we excavated the potash seam; and last we stepped the model and determined the number of stepping for the analysis.

The potash seam was excavated and two openings separated by a yielding pillar were made to reflect the two roadways in the mine working. In order to determine the

number of steps (i.e. timestep) for the model analysis, convergence of mine working was recorded as shown in Figure 6.4. Stepping the model resulted in an increase of convergence of workings at constant rate. The number of steps at which change in the pattern of convergence of working would have occurred, also known as the pattern inflection, was determined at a value of 55.4 mm. This value is the FLAC modelling predicted total closure of mine working and the referred number of steps is used for the numerical analysis.

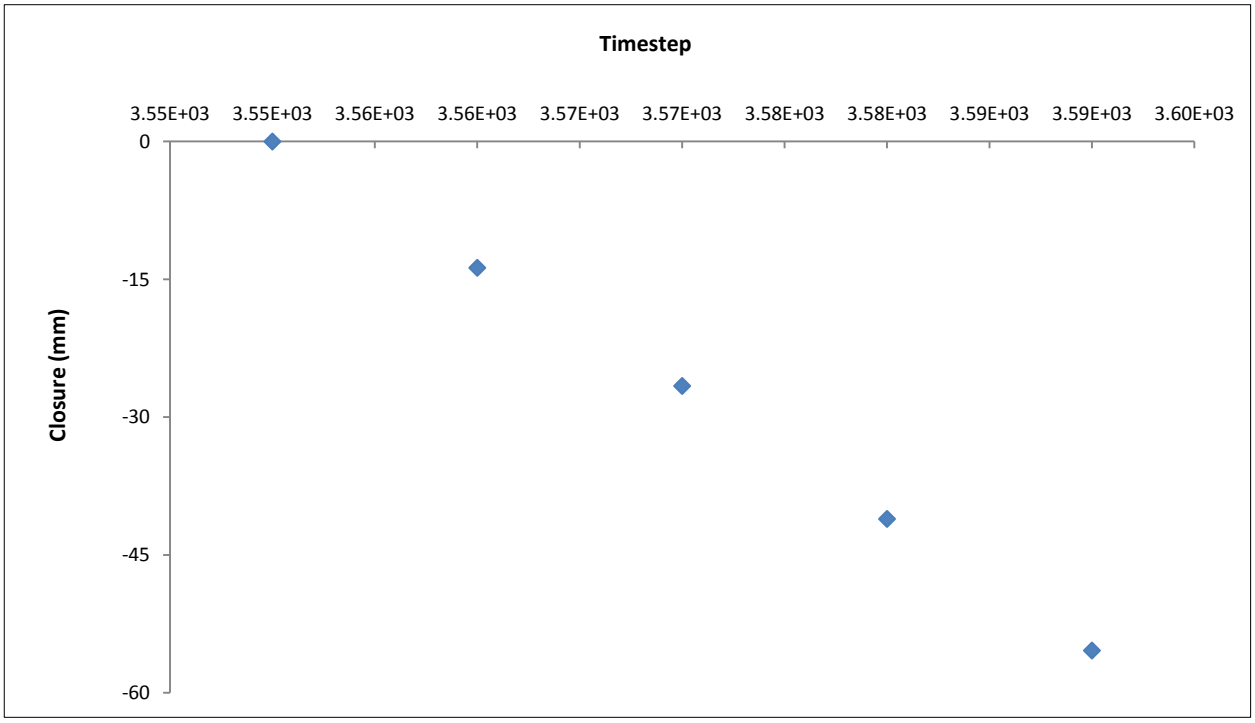

Figure 6.4 FLAC predicted total closure using laboratory data

Although this pattern is in agreement with the total closure exhibiting linear pattern as measured in the mine (see Section 5.4.2, Figure 5.31), in contrast its magnitude is less than the measured one of 75.9 mm over one month. This may be attributed to the effect of scaling or discontinuities, unaccounted in the modelling process.

Generally, laboratory data neither reflect the actual behaviour of the strata nor account for the effects of scale (Kwon and Wilson, 1999). Therefore, it is essential to consider the effects of scale and discontinuity within the structure. In rock mechanics,

empirical approaches are often used to scale laboratory properties to account for the discontinuities and heterogeneities present in a rock mass. The most used approach was developed by Bieniawski in 1978. It characterizes the deformability of a rock mass by the modulus of deformation E_m based upon the rock mass rating (RMR) (Equation 6.3), (Itasca, 2005).

$$E_m = 2(RMR) - 100 \quad (6.3)$$

For values of E_m between 1 and 10 GPa, equation 6.4 developed by Sarafim and Pereira (1983) is generally used.

$$E_m = 10 \exp \frac{(RMR - 10)}{40} \quad (6.4)$$

The strength of the rock mass may be estimated by the empirical rock mass strength criterion developed by Hoek and Brown (1980) and expressed as (Itasca, 2005):

$$\sigma_{1s} = \sigma_3 + (m\sigma_c\sigma_3 + s\sigma_c^2)^{1/2} \quad (6.5)$$

where: σ_{1s} = major principal stress at peak strength;

σ_3 = minor principal stress ;

m and *s* = constants depending on the rock properties and the extent to which it has been broken before being subjected to failure stresses ;

σ_c = uniaxial compressive strength of intact rock material.

The Mohr-Coulomb angle of friction and cohesion may also be determined from the Hoek-Brown criterion through expression which relates ϕ and c to *m* and *s* constants (Itasca, 2005).

Generally, the effects of scale are accounted by the stiffness (i.e. Young's - E modulus) or elastic deformability (i.e. *κ* and *G*) of the strata and the actual behaviour of strata at lower stresses is well reflected by the strength properties (i.e. cohesion and friction angle) values (Lee, 2005).

Another method for extrapolating laboratory results to field-scale properties (i.e. real cases) is a straight reduction of the stiffness and strength from laboratory tests of intact rock specimens (Lloyd *et al*., 1997). This approach of reducing and adjusting the elastic deformability and strength parameters of the layers is widely used to account for the scale effects, the presence of discontinuities and heterogeneity of strata at lower stresses. In mining activity, this approach enables analyzing the behavior of overlying strata and investigating into stress and strain distribution, and also modelling of closure of mine workings and ground subsidence. According to Itasca (2005), the adjustment of the stiffness causes the structure under study to be instable and consequently leads to the failure of the structure (Itasca, 2005).

Xie *et al*. (2009) adopted this approach to investigate into stress shell characteristics of surrounding rock in a fully mechanized top-coal caving face. They reduced the Young's modulus by half, the cohesion by one quarter, and the tensile strength to one tenth. The frictional angle was slightly reduced by 3-5 degrees whereas the Poisson's ratio was kept constant. Using this technique Mark *et al*., (2007) reduced the strength to 0.58 of the unconfined compressive strength in order to examine the response of a longwall entry owing to horizontal stress. Lee (2005) reduced the strength and stiffness properties of all strata by quarter, half and three-quarter to develop a numerical model of rocks failure mechanisms due to lateral displacement. Grgic *et al.*, (2003) reduced the strength of heterogeneous iron mine rock and weathered marls by 30 % and kept constant the elastic properties of the rocks to account for the scale effect for a better understand of both short- and long-term collapses of mines in Lorraine, France. Modelling the behaviour of panels at different depths below the surface at Boulby mine Caughill and Beddoes (1996) reduced the Young's modulus of all strata by a factor of 3 to account for scale effects while adjusting the cohesion and friction angle values to better reflect the behaviour of the strata at lower stress.

The present study uses this approach to produce dataset in Table 6.9 for modelling measured total closure and patterns of stress and displacement distribution by reducing data in Table 6.8 by dimensionless factors. Where necessary, materials parameters were adjusted.

The dataset was obtained by reducing Lias, Rheatic, Mercia mudstone, Sherwood sandstone, Sherwood mudstone and Anhydrite strata parameters by a factor of 4, Carnalite marl stratum parameters by a factor of 5/2 and Potash stratum parameters by a factor of 6/5. Using this dataset FLAC analysis predicted 75.2 mm of total closure of mine workings relatively equal to the measured total closure (Figure 5.31). The calibration approach is based on that most of mine workings convergence occurs at the start of the excavation. Additionally, this approach may be used for modelling the differences in the deformation at the start, immediately and after the excavation. The calibration plot is shown in Figure 6.5. The strata parameters and the resulting total closure are given in Table 6.9 and Figure 6.6.

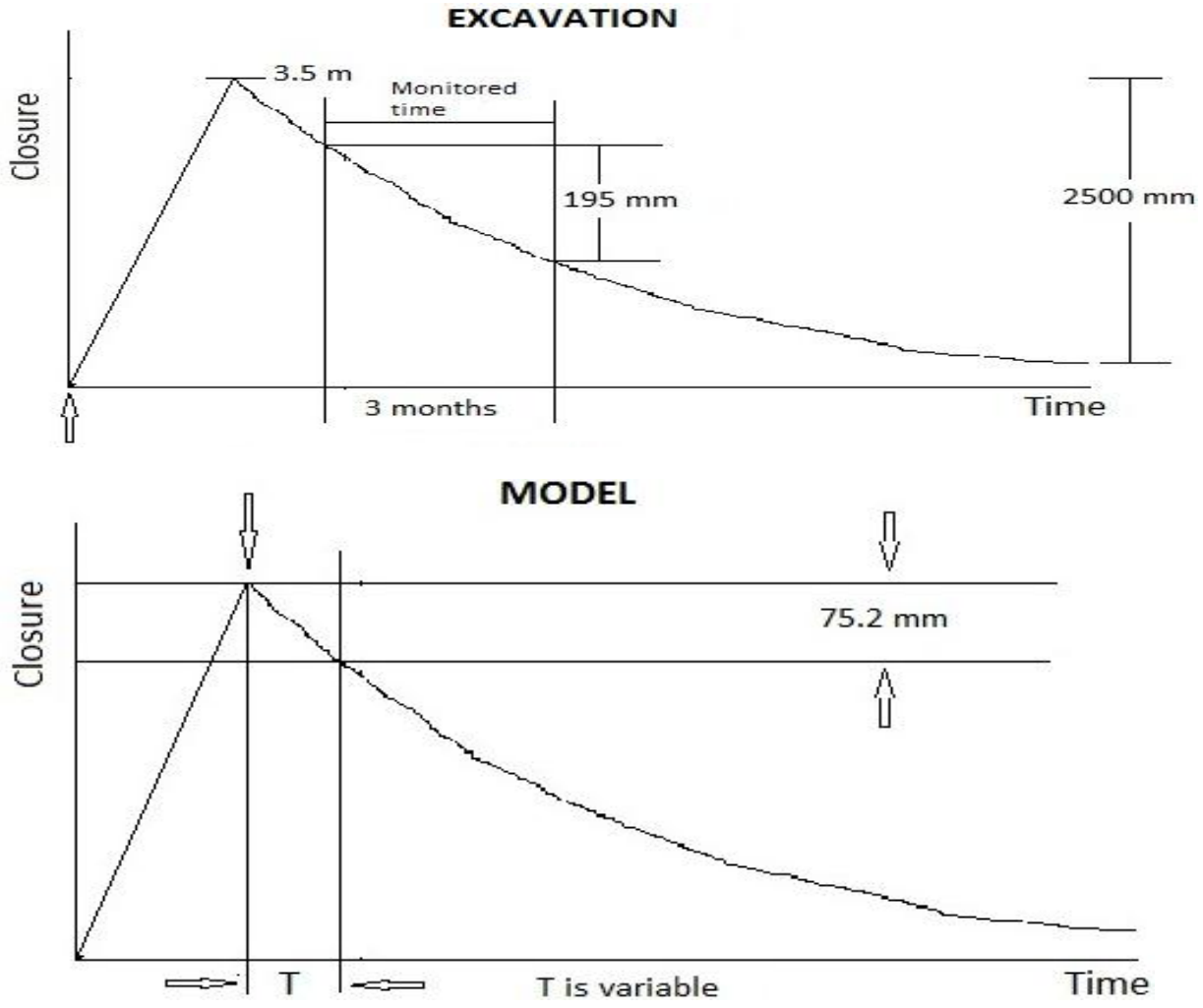

Figure 6.5 Calibration curves showing difference in the measured convergence (top) and predicted convergence (bottom). FLAC modelled convergence occurring at the start of excavation whereas the underground measurement took place after the excavation

Figure 6.5 portrays that the underground monitoring process (top) recorded the steady or secondary stage of creep behaviour of workings. The monitoring process failed to capture the instantaneous and first stages of the creep behaviour as a result of elapsed time between mining and instrumentation of sites. Over three months of measurements mine workings gradually and linearly closed over 195 mm, whereas the numerical analysis (bottom) predicted mine working convergence immediately after the excavation. Because the patterns trend and magnitude of measured convergence the models were based on the numeral analysis could not model stage I of the creep behaviour. Over the range of model period (T), the analysis predicted convergence of 75.2 mm, which is closer to the monitored data over the first month of measurement (Figure 5.31).

Table 6.9 Dataset of mechanical properties of strata used for modelling measured total closure, calibrated against monitored deformation

STRATA	Geotechnical Parameters						Tensile Strength (MPa)
	Deformability		Strength				
	Bulk Modulus (GPa)	Shear Modulus (GPa)	Cohesion (MPa)		Friction (degrees)		
Drucker-Prager Materials							
			k_ϕ	ζ_ϕ			
Lias	2.3	3.14	0.006	0.192	-		0.98
Rheatic	1.2	1.55	0.024	0.2	-		1.06
Mohr-Coulomb Materials							
Mercia mudstone	3.38	3.94	1.5		10.25		0.69
Sherwood sandstone	2.89	3.15	2.75		11.25		1.3
Sherwood mudstone	2.63	3.18	6.5		11		1.72
Anhydrite	3.61	2.71	4.25		10.75		1.52
Strain-Softening Materials							
			Peak	Residual	Peak	Residual	
Carnalite marl	1.56	1.17	1.2	0.4	14.0	7.2	0.5

Potash	23.94	6.82	8.33	5.0	30.0	27.5	1.49
Halite	17.93	9.25	10.0	9.4	40	10	1.63

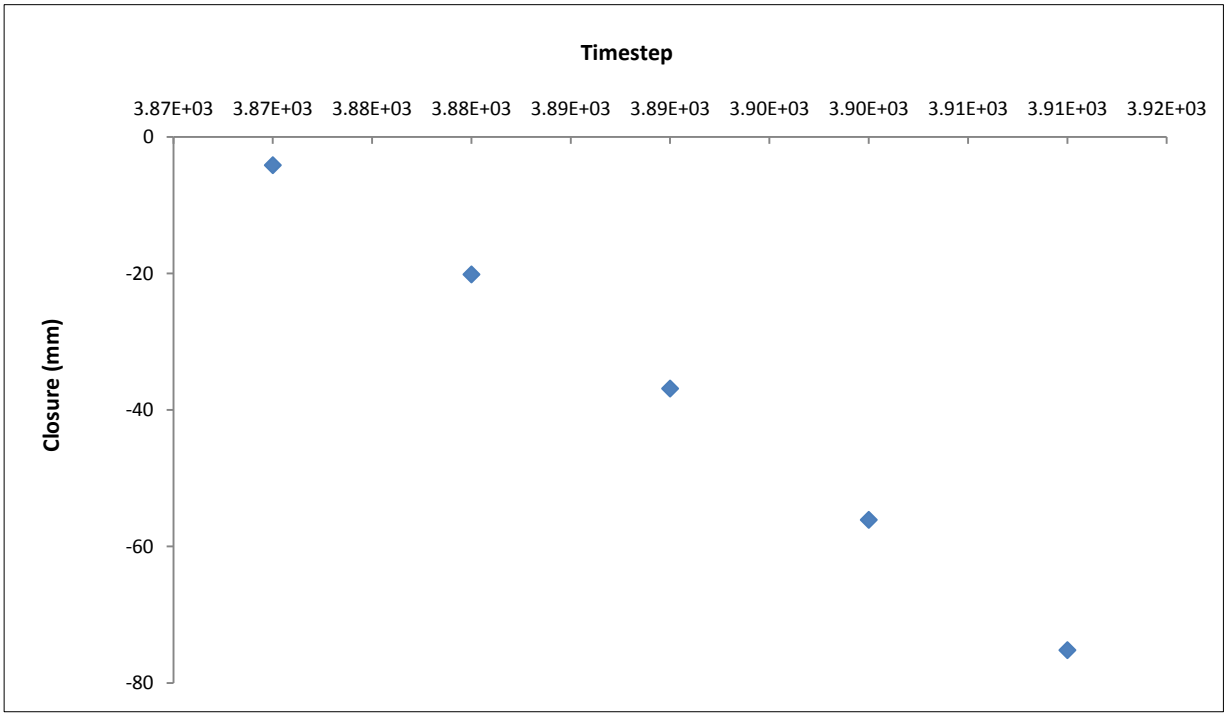

Figure 6.6 FLAC predicted total closure using data in Table 6.9

6.6.2 Analyzing model sensitivity

The physical meaning of model sensitivity would be better understood by using the minimum and maximum values of the variation range of material parameters in the analysis. However, because of the lack such values for some of material parameters and also of time for fully sensitivity analysis the constraint to force the models behaviour to be different from one another guided the determination of strata parameters values. Therefore, input material parameters were reduced by dimensionless factors as this approach has been used by others. Two datasets were generated to analyse the sensitivity of developed models of roof-to-floor closure, stress-displacement patterns distribution and resulting subsidence.

The first dataset was obtained by reducing strata parameters by a factor of 2 for Lias, Rheatic, Mercia mudstone, Sherwood sandstone and Sherwood mudstone; whilst strata parameters for subsequent Anhydrite, Carnalite marl and Potash are reduced by a factor of 6, 3/2 and 8/7, respectively. This dataset produced 78 mm of total closure, slightly higher than the measured convergence of mine workings (Figure 5.30). Figures 6.7, 6.8 and Table 6.10 describe the models.

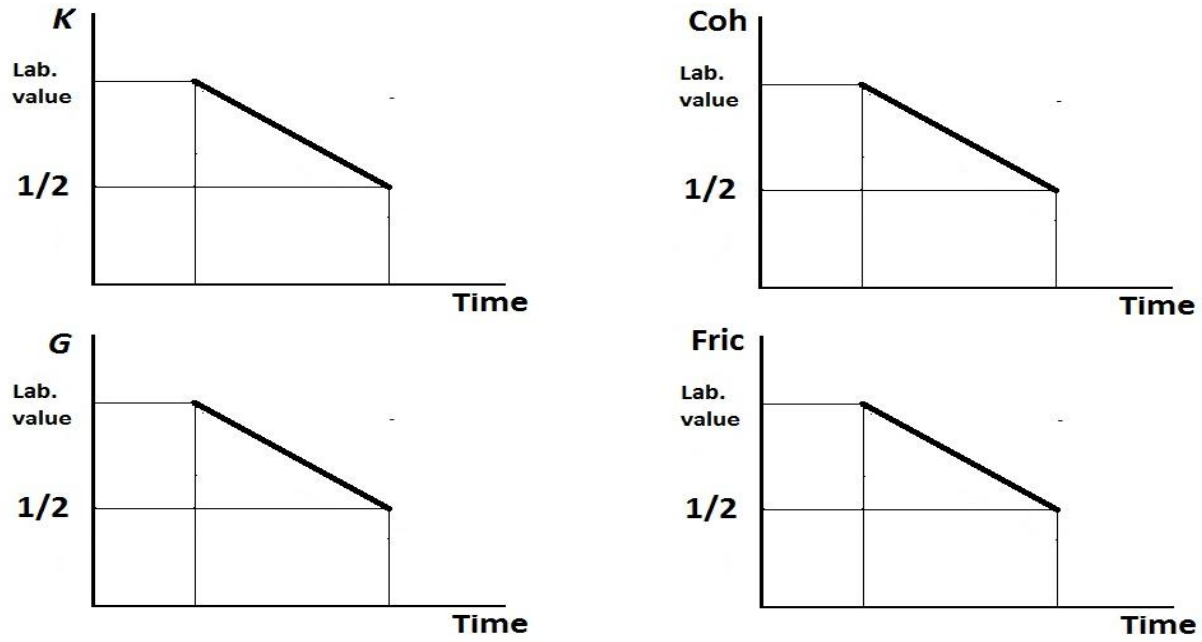

Figure 6.7 Depicted model 1 run with values of bulk modulus (*K*), shear modulus (*G*), cohesion (Coh) and frinction (Fric) of strata reduced by a factor of 2 for the sensitivity analysis

Table 6.10 First dataset of strata parameters used for analysing the sensitivity of developed models

STRATA	Geotechnical Parameters				Tensile Strength (MPa)
	Deformability		Strength		
	Bulk Modulus (GPa)	Shear Modulus (GPa)	Cohesion (MPa)	Friction (degrees)	
Drucker-Prager Materials					
			k_ϕ ζ_ϕ		

Lias	4.59	6.28	0.012	0.38	-		2.0
Rheatic	2.41	3.1	0.047	0.41	-		2.12
Mohr-Coulomb Materials							
Mercia mudstone	6.76	7.88	3.0		20.5		1.38
Sherwood sandstone	5.78	6.3	5.5		22.5		2.6
Sherwood mudstone	5.27	6.35	13.0		22.0		3.43
Anhydrite	2.41	1.81	2.83		7.17		1.01
Strain-Softening Materials							
			Peak	Residual	Peak	Residual	
Carnalite marl	2.6	1.95	2.0	0.67	23.33	12.0	0.83
Potash	25.14	7.16	8.75	5.25	31.5	28.86	1.57
Halite	17.93	9.25	10.0	9.4	40	10	1.63

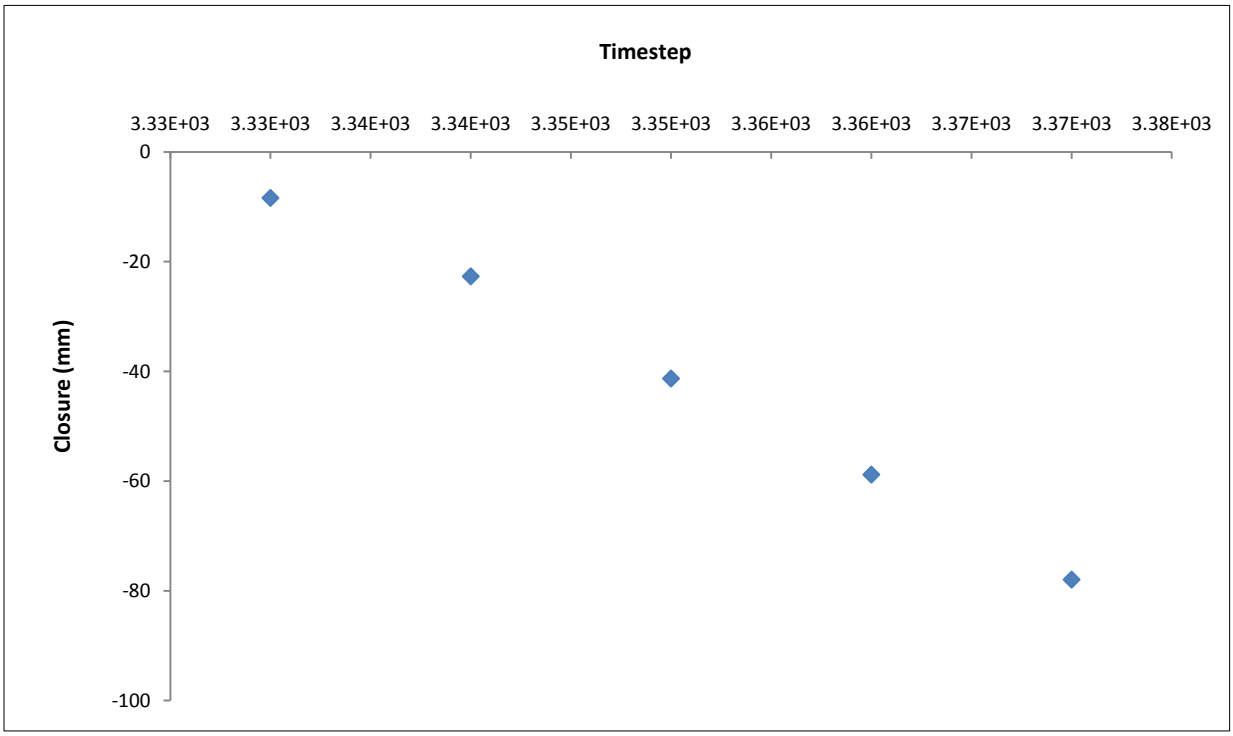

Figure 6.8 FLAC predicted total closure using data in Table 6.10

The second dataset was obtained by reducing strata parameters by a factor of 3 for Lias, Rheatic, Mercia mudstone, Sherwood sandstone, Sherwood mudstone and

Anhydrite; whilst strata parameters for subsequent Carnalite marl and Potash are reduced by a factor of 5/3 and 6/5, respectively. This dataset produced 76.1 mm of total closure, closer to the measured convergence of mine workings. Figures 6.9, 6.10 and Table 6.11 describe the models.

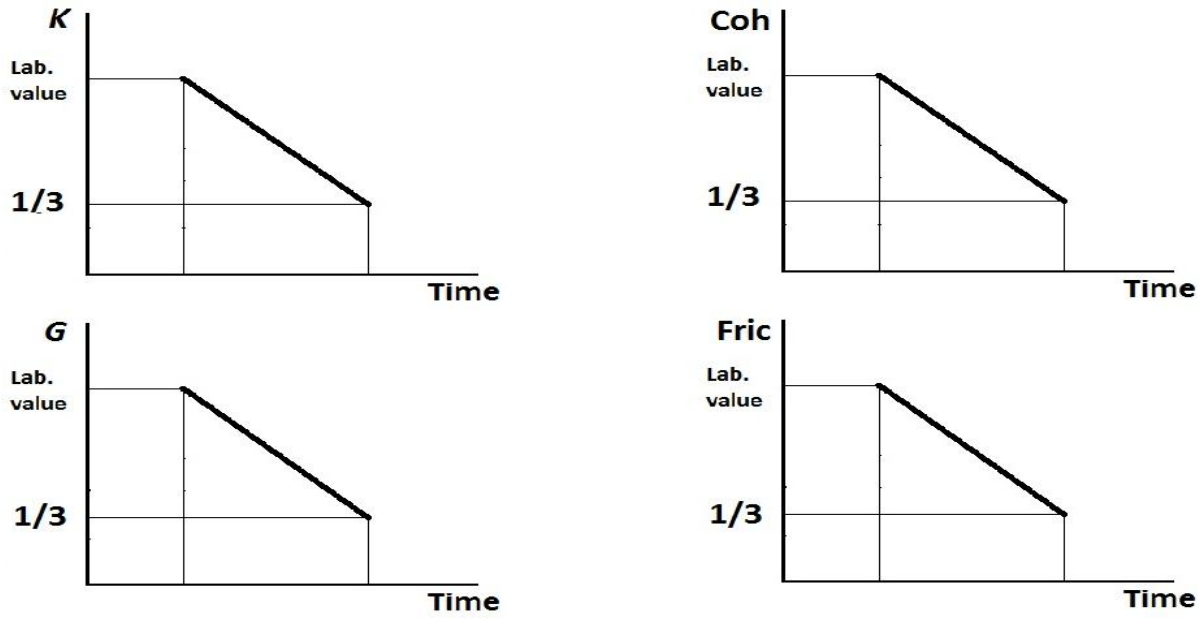

Figure 6.9 Depicted model 2 run with values of bulk modulus (*K*), shear modulus (*G*), cohesion (Coh) and frinction (Fric) of strata reduced by a factor of 3 for the sensitivity analysis

Table 6.11 Second dataset of strata parameters used for analysing sensitivity of developed models

STRATA	Geotechnical Parameters					Tensile Strength (MPa)
	Deformability		Strength			
	Bulk Modulus (GPa)	Shear Modulus (GPa)	Cohesion (MPa)		Friction (degrees)	
Drucker-Prager Materials						
			k_ϕ	ζ_ϕ		
Lias	3.06	4.18	0.008	0.26	-	1.3
Rheatic	1.6	2.1	0.031	0.27	-	1.41
Mohr-Coulomb Materials						

Mercia mudstone	4.5	5.25	2.0		13.67		0.92
Sherwood sandstone	3.85	4.2	3.67		15.0		1.73
Sherwood mudstone	3.51	4.23	8.67		14.67		2.29
Anhydrite	4.81	3.61	5.67		14.33		2.03
Strain-Softening Materials							
			Peak	Residual	Peak	Residual	
Carnalite marl	2.34	1.76	1.8	0.6	21	10.8	0.744
Potash	23.94	6.82	8.33	5.0	30.0	27.5	1.49
Halite	17.93	9.25	10.0	9.4	40	10	1.63

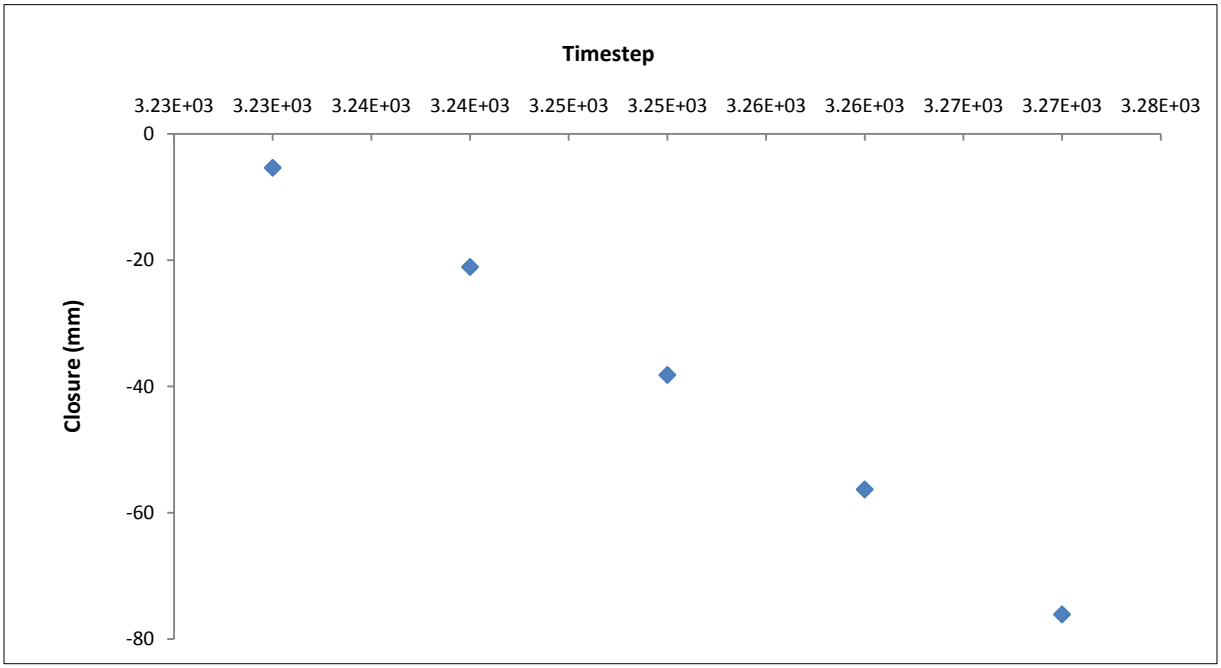

Figure 6.10 FLAC predicted total closure using data in Table 6.11

Figures 6.8 and 6.10 show that closure of excavation is not sensitive to the variation of material parameters. The excavation closes up at similar magnitudes regardless the reduction factor of material parameters. The slight difference in the magnitudes of closure is attributed to the fact that closure of underground excavation is primarly a function of behaviour of strata in the immediate roof and particularly of carnalite marl and potash (i.e. 2 m protective layer) in the present case. Such

discrepancy in the magnitudes of closure may be addressed by properly adjusting the mechanical parameters of these two layers.

For the discontinuous model (i.e. model 6) two analyses were performed. First, we considered a glue fault (i.e. no occurrence of sliding) whereas in the second analysis sliding of blocks of structure was allowed to occur. Values of excavations, yield pillar and potash left in place as a protective layer were obtained from the Boulby Mine (Table 6.12). These values were kept constant in all models for a simplified mine layout as shown in Figure 6.11.

Table 6.12 Excavations dimensions

Excavation specifications		
Width	Height	Thickness of potash left on place
8 m	7 m	2 m

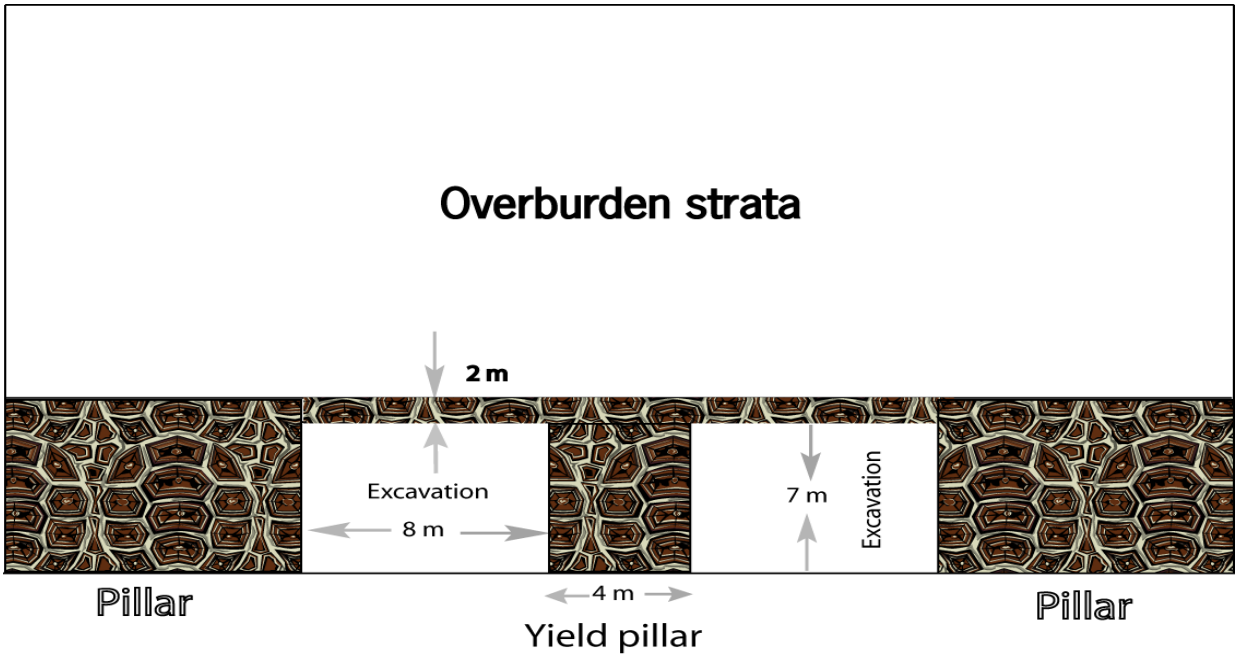

Figure 6.11 A simplified cross-sectional illustration of mine layout and the excavation specifications.

6.7 Summary and conclusion

The mechanical characteristics of the floor mine have control on the behaviour of the workings (Sections 2.2 and 2.3.2.2), the resulting stress and displacement distribution. At Boulby mine layer of potash is left on the floor of excavations at the start of mining in order to control floor heave. But in all of our models, the floor consists of hard halite rock. This is because the research is intended to investigate the geomechanical processes with emphasis on stress and displacement distribution throughout the overburden at the mine. Hence, this has limited effect on our analysis results.

A total of six models were developed to numerically simulate the behaviour of mine workings. Simulations were performed to examine patterns of stress and vertical displacement distribution in a real world system due to underground mining. The patterns of stress and displacement distribution through the structures were determined for each performed model.

The effects of the heterogeneity lithological properties and geological structure on the patterns of stress and displacement distributions were assessed. Additionally, the sensitivity of developed models of stress and displacement, total closure of mine workings and ground subsidence were analyzed. Furthermore, the effects of water within the structure on the patterns of stress and displacement, and ground subsidence were also examined.

At first, we measured at the mine the convergence of workings using the bespoke closuremeter. Then we plotted the pattern of subsidence of continuous survey occurred over the mine area using levelling technique.

With the modelling process, we were able to compare the above with the predicted convergence of workings and subsidence patterns obtained using simplistic and more realistic finite difference models. Further results of the modelling are discussed in Chapter 7.

Chapter 7
Results of modelling and analysis

7.1 Introduction

In this chapter we analyze the results of modelling from the FLAC 2D code. In Section 7.2, we examine the patterns of stress and displacement distribution versus the lithological heterogeneous properties and geological fault, including the nature of the fault. The sensitivity of the models to varying material parameters is also studied. Section 7.3 examines the patterns of total closure versus lithology, geological fault and their sensitivity to the variation of material parameters. Section 7.4 analyzes the ground subsidence, lithology and geological fault relationships, and also the sensitivity of the models. The patterns of predicted and measured ground subsidence are analyzed in Section 7.5. Section 7.6 evaluates the effect of water on stress, displacement and ground subsidence. A summary of the chapter is given in Section 7.7.

Datasets used are those in Tables 6.9, 6.10 and 6.11, unless otherwise specified. Taking advantage of symmetry of domain geometry in unfaulted structures, each result from convergence and subsidence analyses is referred only to one excavation.

7.2 Patterns of stress and displacement distribution

Excavating an underground opening in rock mass induces stress and strain redistribution which leads to the modification of the original properties of the rock mass near the excavation (Wong *et al*., 2008; Kwon *et al*., 2009). The induced stress may create zones of compressive or tensile stress which may locally exceed the rock strength (Martino and Chandler, 2004) and likely lead to the deterioration or damage of the structure (Bhalla *et al*., 2005).

As indicated in Chapter 6, dataset in Table 6.9 was used to obtain: the patterns of stress, the patterns of displacement, the magnitude of maximum stress and the magnitude of total displacement. These parameters are linked to the distribution under study.

7.2.1 Relationship with lithology

The analysis of the effect of lithological heterogeneity on stress and displacement distribution was conducted by plotting patterns of stress and vertical displacement for the five continuous models. Because we are interested in the behaviour of the whole structure (i.e. both rock skeleton intraparticle bonds and pore pressure are involved) and also given that the structure under investigation is undrained, its short term stability will be better assessed through the analysis of total stress distribution. A quantitative analysis of magnitudes of maximum stress and total displacement was done to characterize the effects of lithology and understand the mechanisms of failure of the overburden strata due to the extraction of potash. The patterns of stress and displacement distribution, and magnitudes for models 1-5 are shown in Figures 7.1-5 and Figure 7.6, respectively.

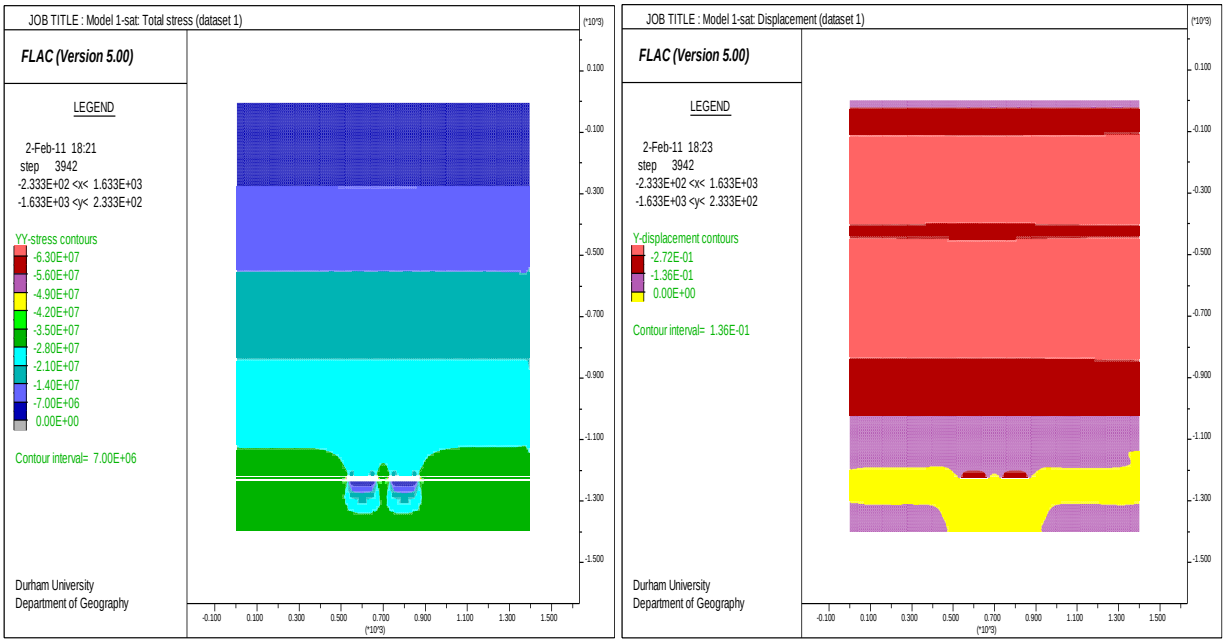

Figure 7.1 Patterns of total stress (Pa) left and vertical displacement (m) right distribution for model 1 for the lithology effect analysis

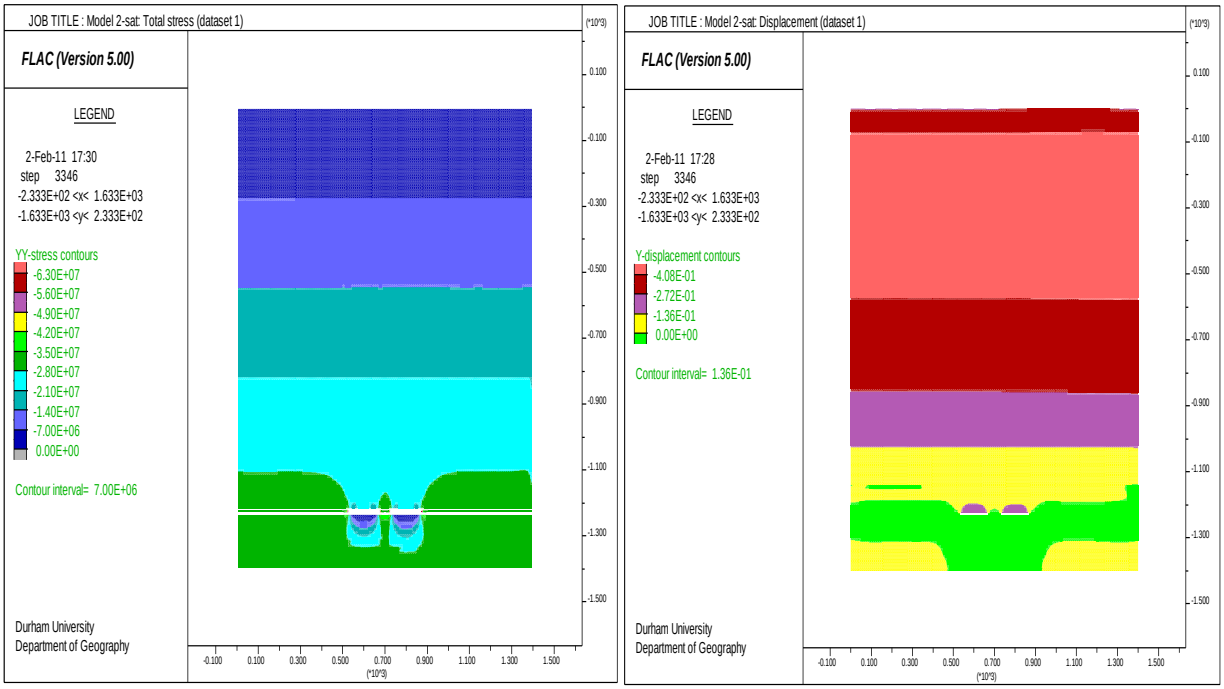

Figure 7.2 Patterns of total stress (Pa) left and vertical displacement (m) right distribution for model 2 for the lithology effect analysis

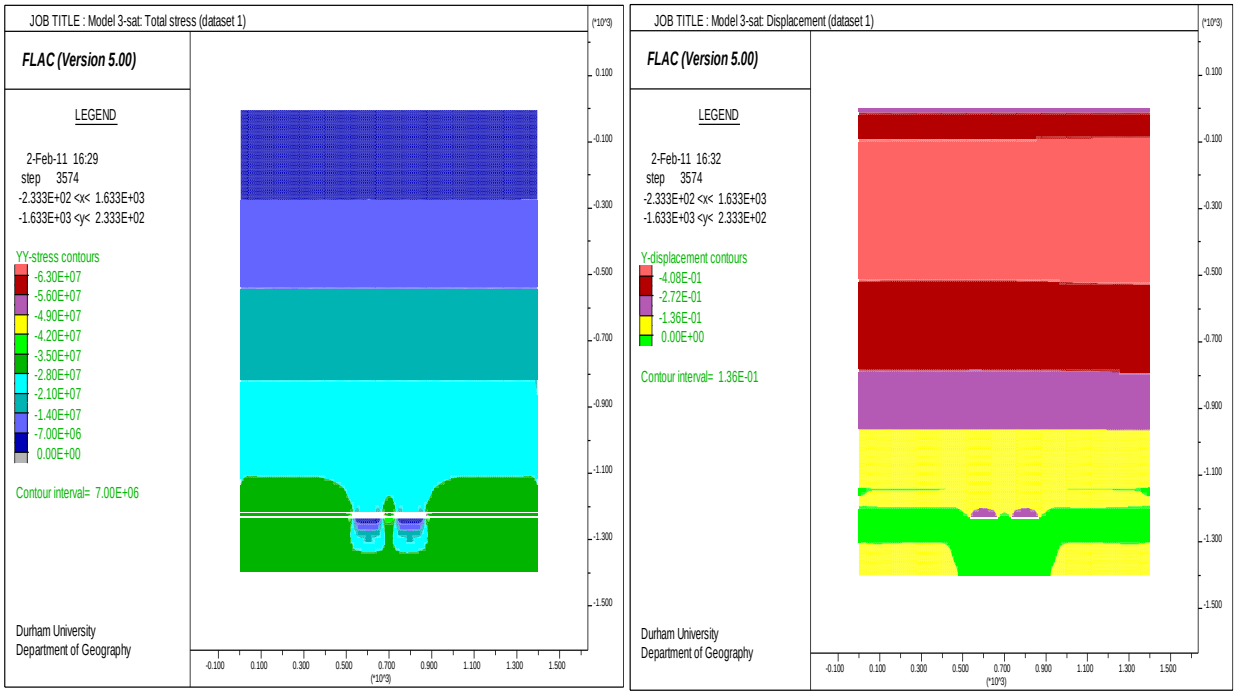

Figure 7.3 Patterns of total stress (Pa) left and vertical displacement (m) right distribution for model 3 for the lithology effect analysis

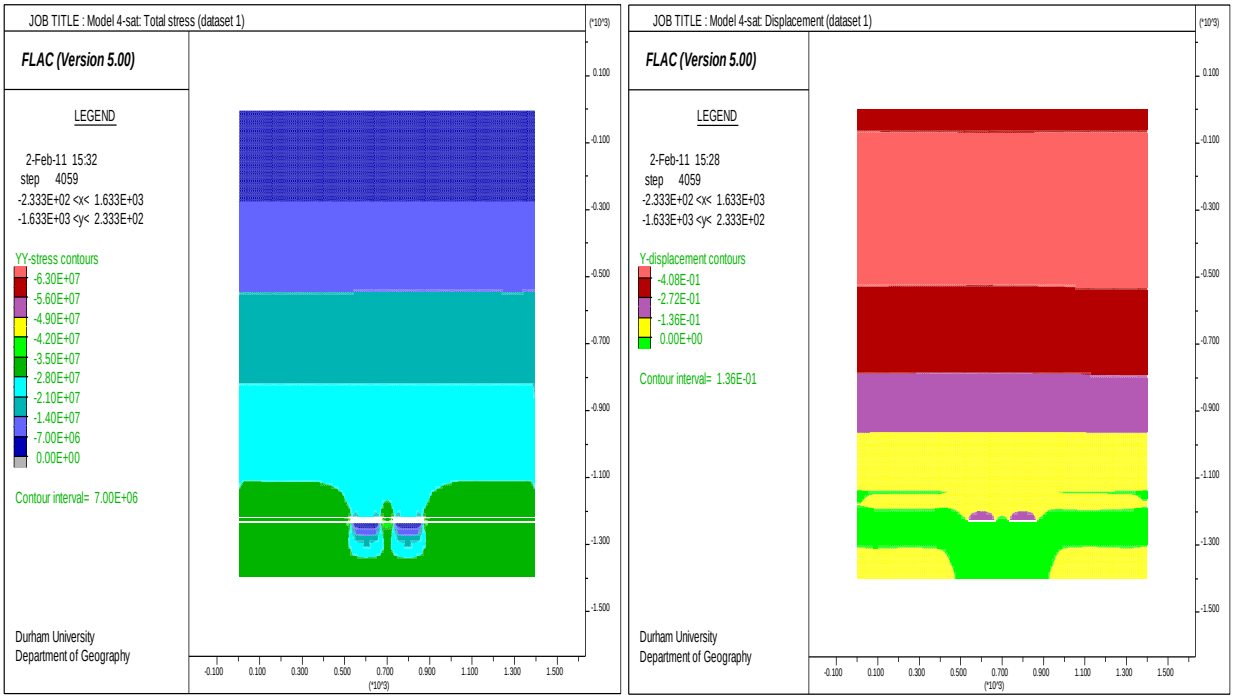

Figure 7.4 Patterns of total stress (Pa) left and vertical displacement (m) right distribution for model 4 for the lithology effect analysis

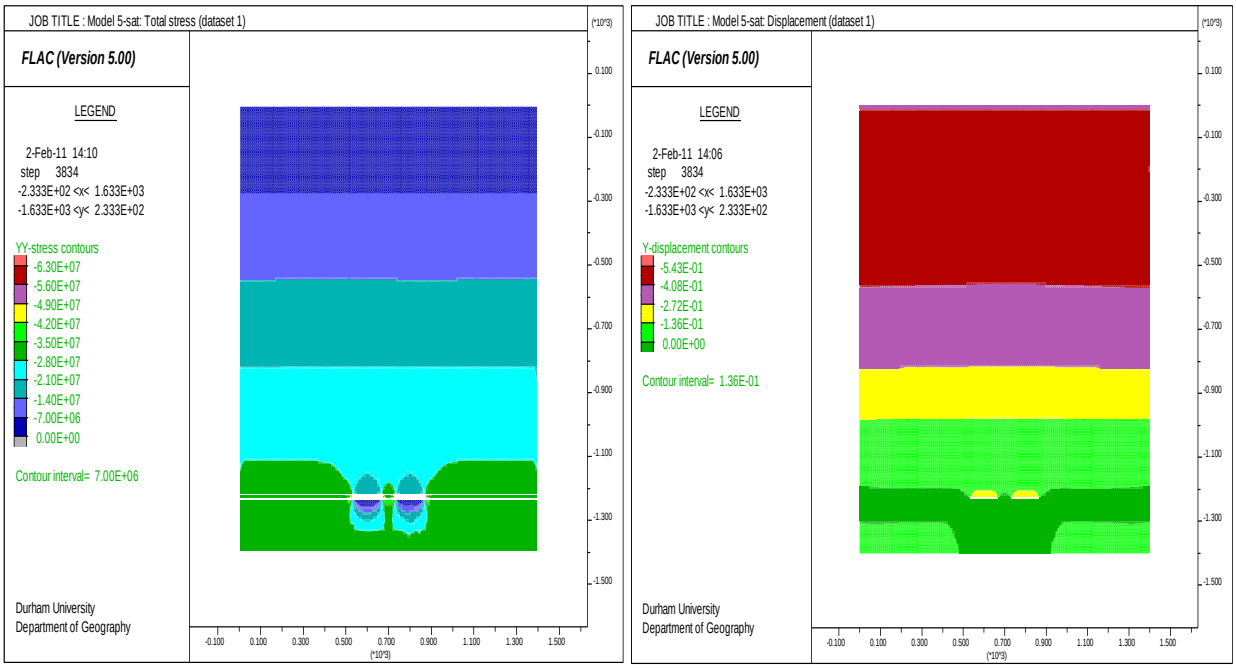

Figure 7.5 Patterns of total stress (Pa) left and vertical displacement (m) right distribution for model 5 for the lithology effect analysis

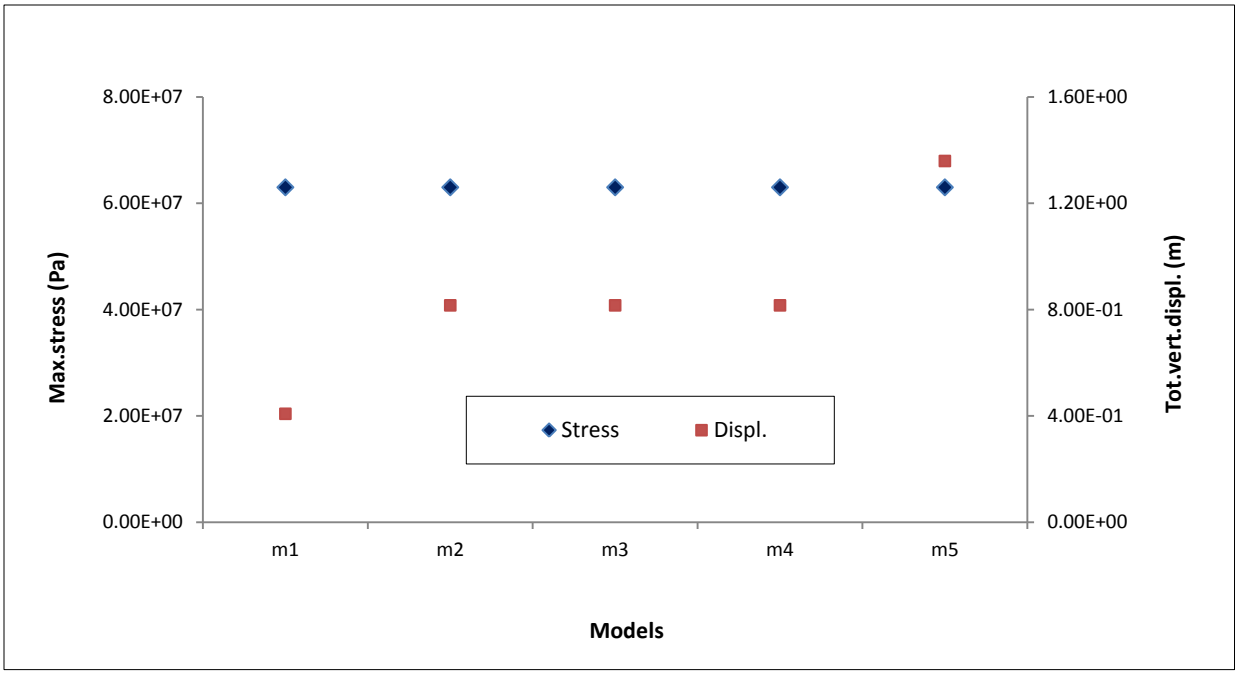

Figure 7.6 Relationship of magnitudes of maximum stress (Pa) and total displacement (m) with lithology using parameters in Table 6.9

The plots of total stress and associated displacement patterns (Figures 7.1-5) indicate the slight influence of lithology on stress and displacement distribution due to potash mining. The distribution of stress and displacement is mostly dependent of the behaviour of the strata in the overburden. The plots show the occurrence of gradient of stress and displacement within the structure with magnitude of stresses acting upon strata higher than the stress used in the analysis.

In all models, the hangingwall above the excavations alternatively dilates and compresses attempting to fill up the void caused by the shear stress (i.e. bending) induced in the potash layer. In the process, beds separate and voids are formed in the immediate “hangingwall” above the excavations. The maximum stress around the opening in all the structures increases and is greater than the estimated *in-situ* stress (Tables 6.2-6). This increase may be attributed to the time-dependent effect of the mining-induced stress which tends to exceed the stiffness and strength of materials. With the stiffness and strength of materials being exceeded, deformation of the structure occurs as a result of relaxation leading to the decrease of the stress within the structure.

The increase of maximum stress around the opening may also due to the increase of total vertical stress as a result of pore water pressure increase. Indeed, total vertical stress increase results in the rearrangement of solid particles to new positions closer together as water flows. However, given the no flowing state of water in the current research and the laterally confined Sherwood sandstone (i.e. lateral movement is restricted), particles do not rearrange and therefore no increase in the interparticle forces is possible. Since the pore water resists the particles rearrangement the pore water pressure is increased, and therefore the total vertical stress increase (Craig, 2004).

Given the similarity and low magnitude of convergence of mine workings, the extraction of potash resulted in same maximum stress acting at potash horizon. A scarcely perceptible ground movement develops on the surface with flatter trough of subsidence whose angle of draw may equal 45 degrees through all the structures, as measured at Boulby mine (Kemeling, 2006). The depth of the extraction and the overlying strata mechanics may have controlled the transmission of stress and deformation through the overburden upwards towards the surface.

For the model 1 the hangingwall consists of thick and dense strata, less deformation was induced by mining potash despite the significant beds separation displayed by the displacement pattern in Figure 7.1.

The plots of displacement show tensile movement occurring on the middle of cross-section while compressive deformation occurs at the edges of the cross-section. This can result in the shift of location of subsidence highest magnitude on the ground surface.

Mining potash induces maximum vertical stress acting around excavations higher than the stress used in the analysis. In all structures, the extraction of potash results in development of flat and shallow affected area on the surface. Although the density of the materials may have influenced the stress and displacement distribution, the constitutive behaviour of layer is the predominant factor that has controlled the stress and displacement redistribution within the structures. Another factor to consider is the

duration of model stepping (i.e. number of timesteps), though this does not translate from the analysis results. Further discussion of the findings is given in Chapter 8.

7.2.2 Relationship with fault

In order to evaluate the effect of geological fault on stress and displacement distribution, we plotted patterns of total stress and vertical displacement associated with the faulted structure. In addition, magnitudes of maximum stress and total displacement of both unfaulted and faulted structures were plotted together to quantify the effect of fault on stress and displacement. The distribution patterns and magnitudes of stress and displacement for both natures of fault are shown in Figures 7.7-9.

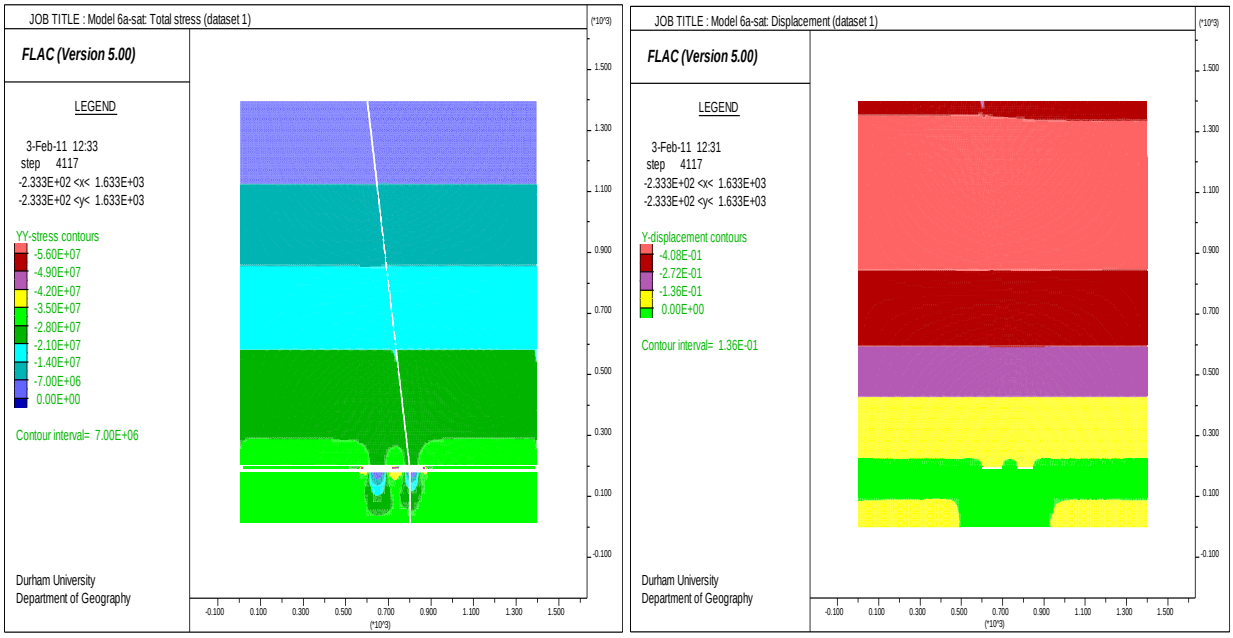

Figure 7.7 Patterns of total stress (Pa) left and vertical displacement (m) right distribution for model 6 with unglued (i.e. real) fault

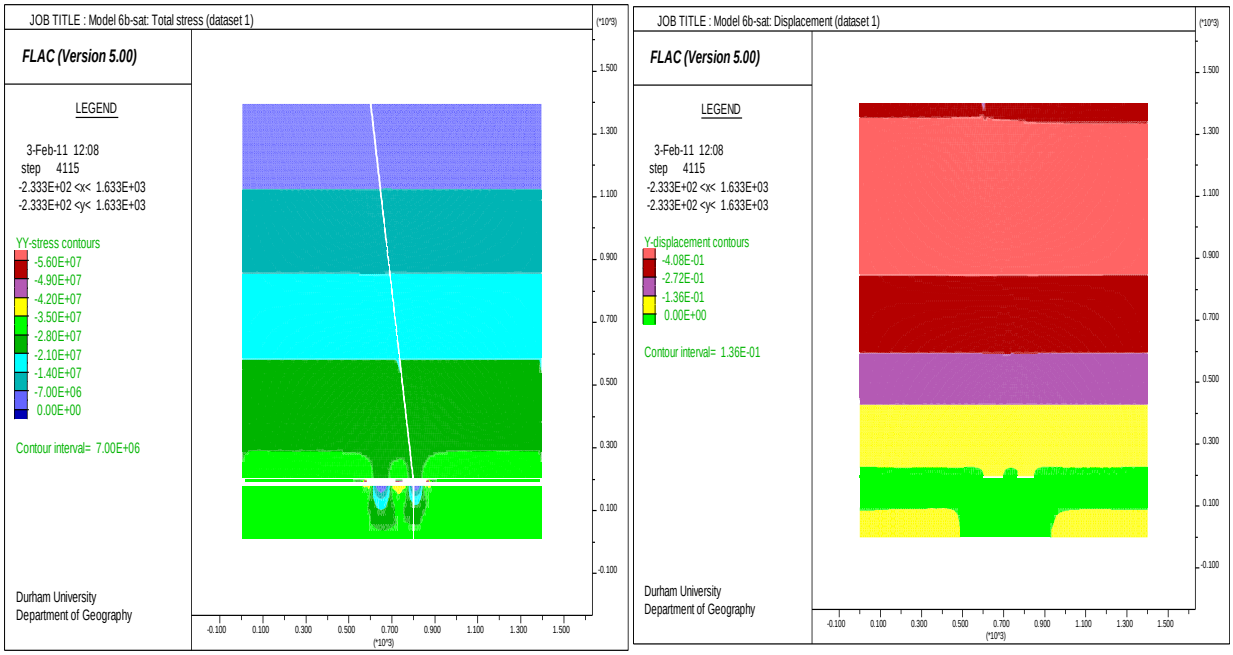

Figure 7.8 Patterns of total stress (Pa) left and vertical displacement (m) right distribution for model 6 with a glued fault

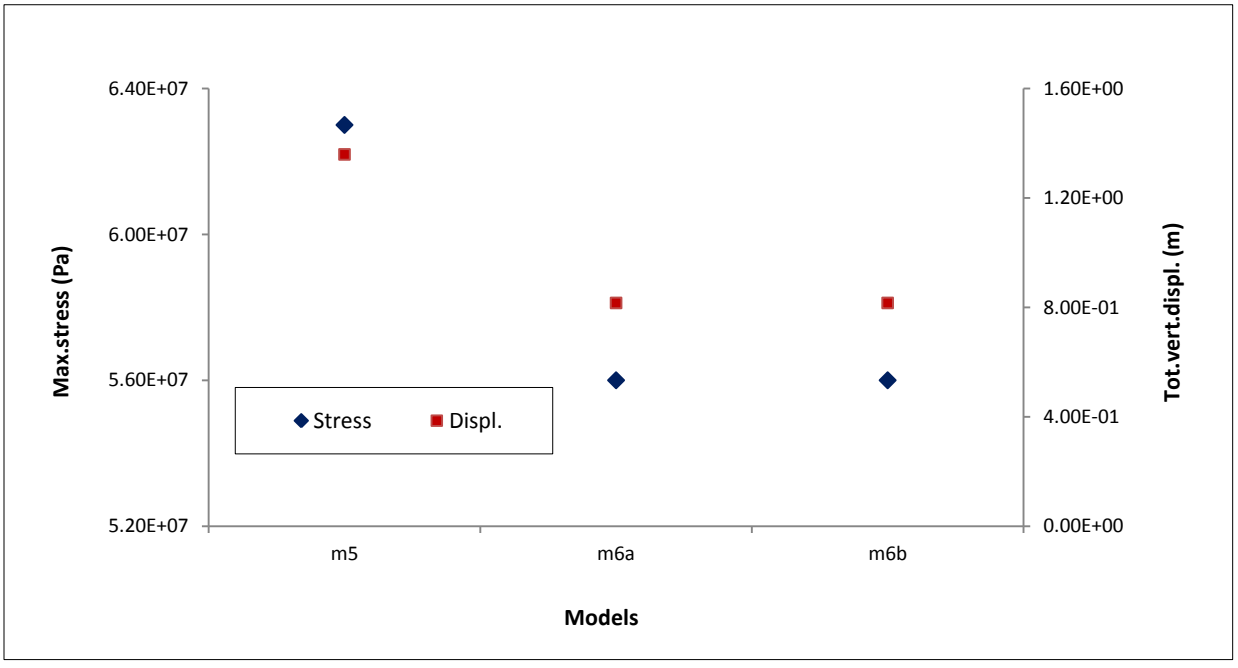

Figure 7.9 Influence of fault on maximum principal stress and displacement. m5 = continuous model, m6a= model with unglued fault, m6b=model with glued fault

Figures 7.7 and 7.8 portray a similarity in the effects of fault on the distribution patterns of stress and displacement. This suggests that the fault induces gradients of stress and displacement within the structure regardless whether the fault is real or glued.

In contrast to a continuous structure, the presence of fault yielded three results: it decreased the magnitude of maximum stress and total displacement; narrowed the stressed region above excavations and limited the tensile deformation of the structure within the saturated Sherwood sandstone zone (Figure 7.5).

One explanation of this may be the stiffness and strength of the fault which may have controlled deformation of the structure. Given that the mechanics of rock mass is driven by the mechanics of both geological fault and intact rock mining-induced stress may have been insufficient to exceed the strength and stiffness of the fault to induce either sliding of blocks of structure or movement along it.

An alternative explanation is that the fault might have acted as absorbent of deformation (The Geological Society, 2008). However, this effect may not be proven from the trend displayed by the patterns of displacement distribution related to the real fault (Figure 7.8). The findings are discussed in the chapter that follows.

7.2.3 Stress and displacement distribution sensitivity

The sensitivity of the models of stress and displacement distribution was analysed by varying the reduction dimensionless factors in the determination of the stiffness and strength of strata for model inputs. Based on the measured magnitude of convergence of mine workings, laboratory parameters of strata above the Anhydrite were successively reduced by a factor of 2 and 3. Thereafter, parameters of Anhydrite, Carnalite marl and Potash strata were reduced by appropriate factors (Tables 6.10 and 6.11).

The patterns of total stress and vertical displacement associated with the three datasets are plotted and given in Appendix B for comparative analysis. The plots show

a sensitivity of stress and displacement distribution to the variation of material parameters, though mining potash induces gradient of stress and displacement within all the structures. Nevertheless, their trends around the excavations vary with the stiffnesses and strengths of Carnalite marl and Potash.

For quantifying the sensitivity of stress and displacement models, we plotted in Figures 7.10 and 7.11 magnitudes of maximum stress and total vertical displacement related to the three datasets given in Tables 6.9-11.

Figures 7.10 Relationship of magnitudes of maximum stress (Pa) with lithology for sensitivity analysis using the three datasets

Figure 7.10 shows that the reduction of factors has limited sensitivity on the maximum stress. This is probably due to the low and similar magnitude of roof-to-floor closure of workings in all the structures these models were based on.

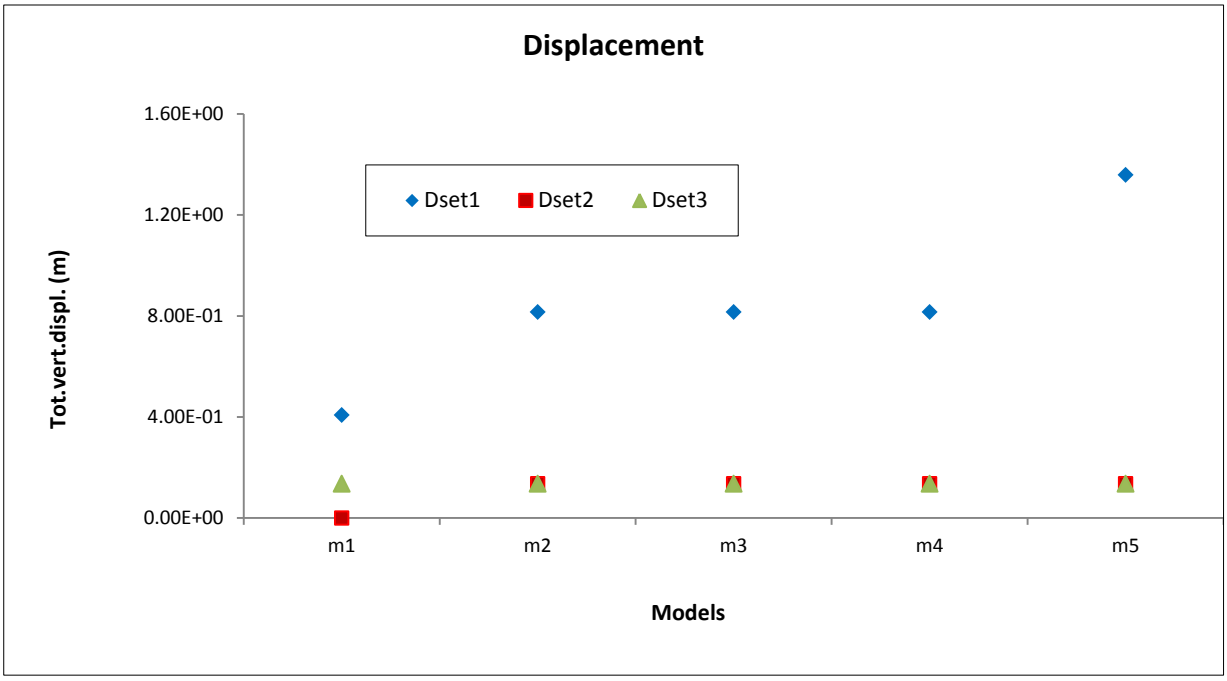

Figures 7.11 Relationship of magnitudes of total vertical displacement (m) with lithology for models sensitivity analysis using the three datasets

Figure 7.11 shows that the higher the reduction factor, the more the total vertical displacement. This trend infers a relationship between the stiffness and strength of the materials and the displacement within the structure. In other terms, the increase of the reduction factor of material parameters decreases the stiffness and strength of materials leading to the increase of deformation of structure as a result of relaxation of the stressed materials.

7.3 Patterns of convergence versus lithology and geological fault

The immediate roof characteristics, including lithology, compressive and/or tensile strength, strength and stiffness parameters are key drivers of mine roof closure (Singh, 2004; Jeremic, 1985).

In addition, yield pillar width, thicknesses and strength of the overlying layers and localized geological features also control the amount of closure in the immediate vicinity of the excavation (Lachenicht and Aswegen, 1999). The width of the excavation and the

width/depth ratio may also influence the deformation behaviour of the mine roof (Holzer, 1984).

The yielding of floor material under pressure and shear stress acting on the wall beneath the excavation results in floor heave (Brady and Brown, 2006) therefore, in the closure of mine workings.

7.3.1 Relationship with lithology

Total closure data recorded on the middle of the excavations in continuous models (i.e. models 1-5) are plotted (Figure 7.12).

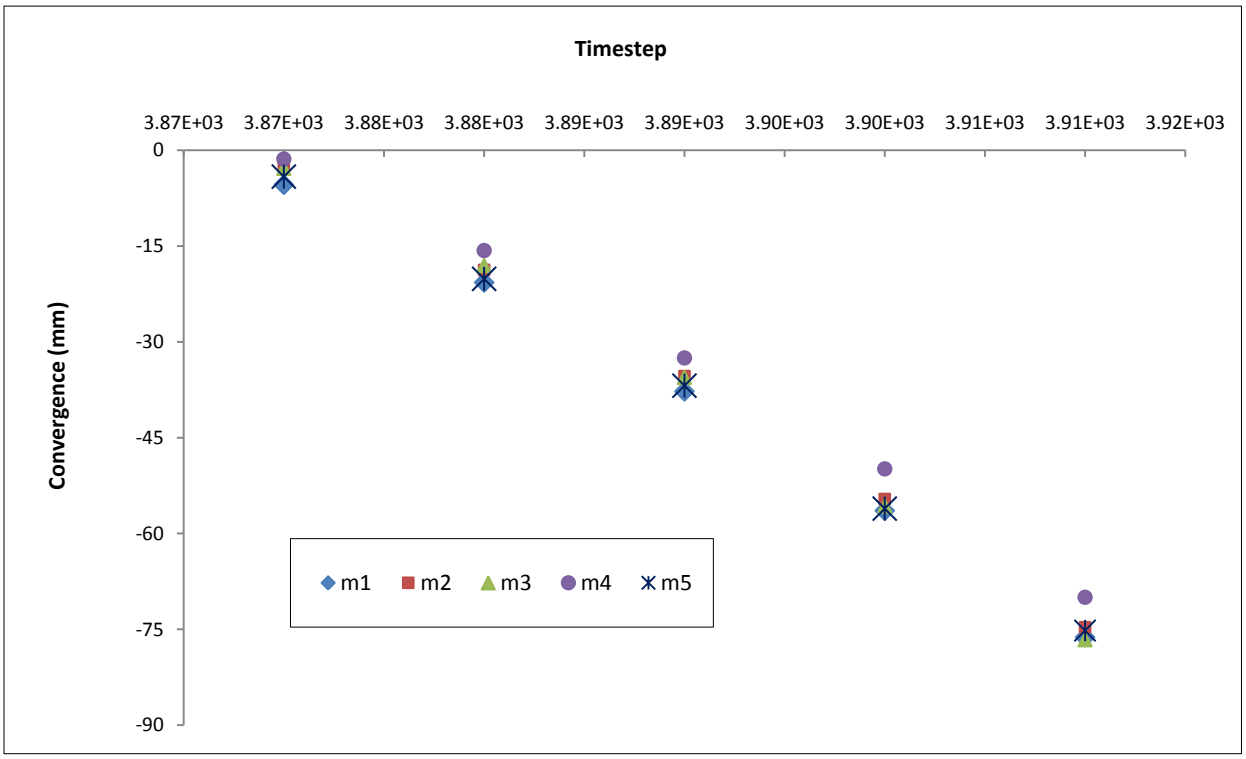

Figure 7.12 Effect of lithology on convergence of mine workings for models 1-5

This plot demonstrates limited dependency of closure of mine working on the lithological heterogeneity. Patterns of total closure in the five models exhibit similar linear trend, and the excavations closed up to relatively same magnitudes. Given that the floor in all five models is made of halite rock, the similarity in the patterns and

magnitudes of total closure demonstrates that closure of mine working is driven by the closure of mine roof which is mainly controlled by the behaviour of both the potash left in place as a protective layer and the Carnalite marl in the immediate roof.

7.3.2 Relationship with fault

The effects of discontinuities within structure on total closure were evaluated by comparing patterns of total closure in the continuous structure (i.e. model 5) with those in a discontinuous structure (i.e. model 6). Unlike in model 5 total closure on the middle of both excavations in model 6 was analyzed. The patterns of closure related to the real fault and glued fault are shown in Figures 7.13 and 7.14, respectively.

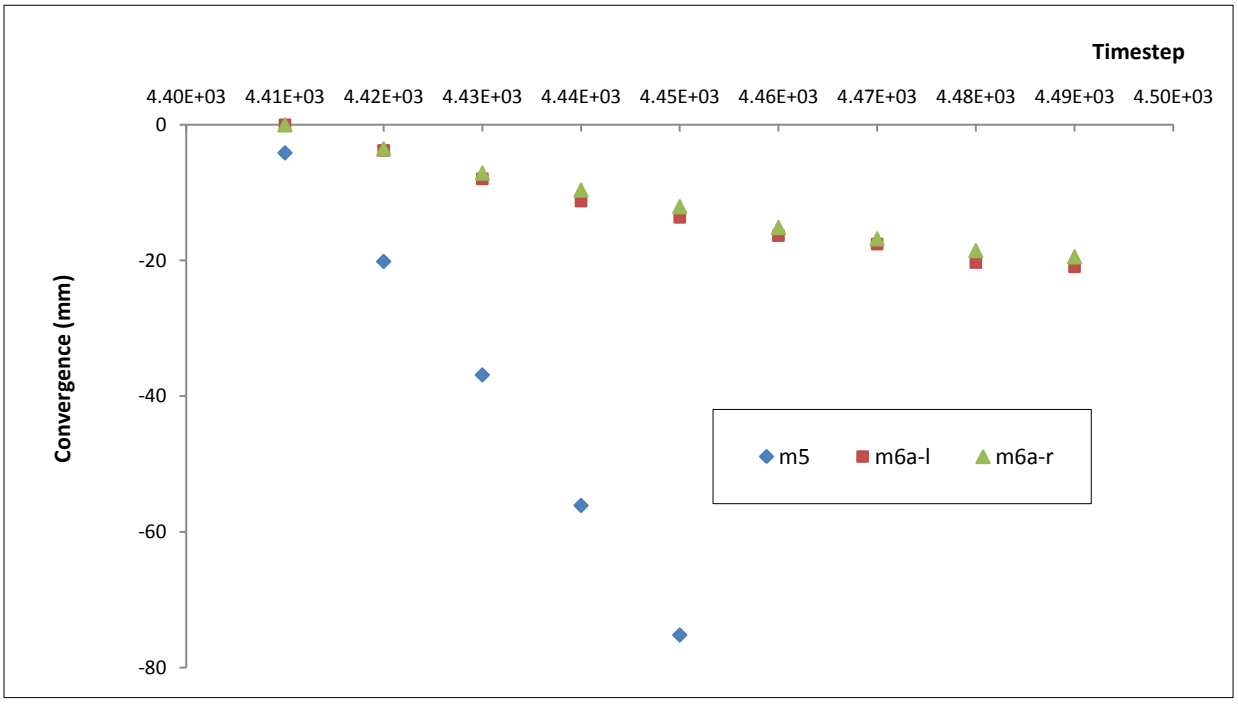

Figure 7.13 Effect real fault (i.e. separation and slipping may occur) “a” upon convergence of workings on the middle of excavation of left-hand (l) and excavation of right-hand (r) side

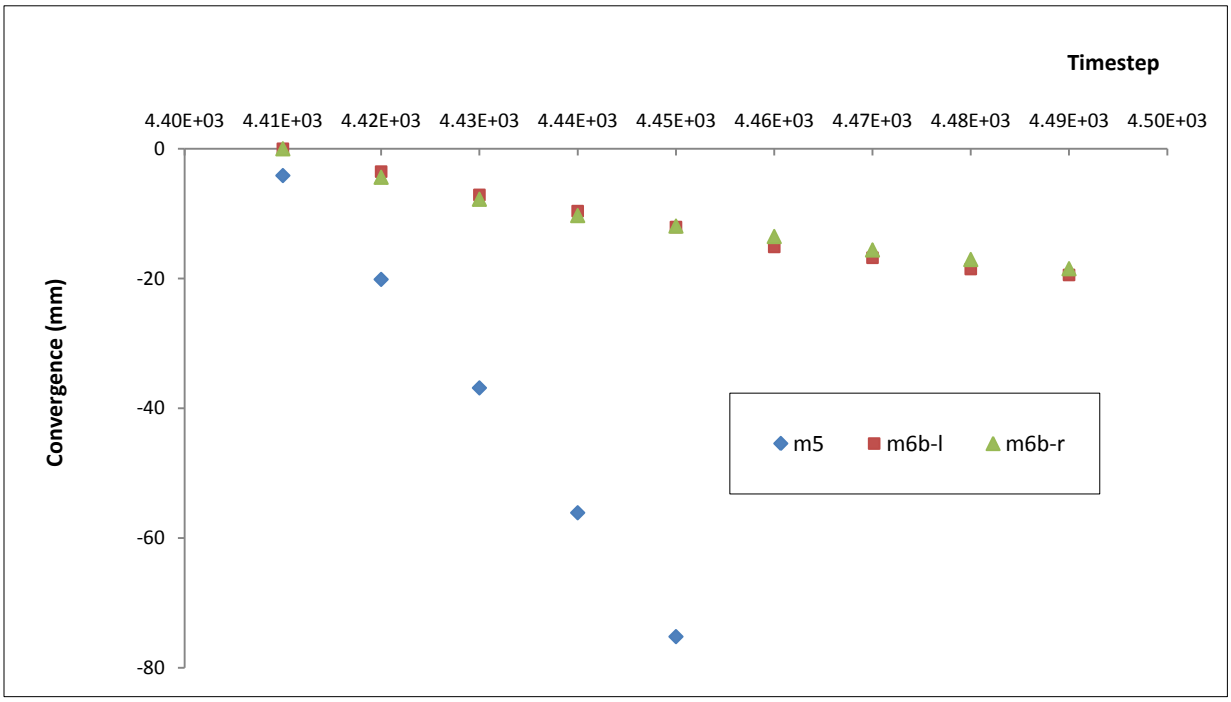

Figure 7.14 Effect of glued fault (i.e. separation and slipping will not occur) “b” upon convergence of workings on the middle of excavation of left-hand (l) and excavation of right-hand (r) side

From Figures 7.13 and 7.14**,** the effect of fault on the patterns and magnitudes of convergence of mine working is obvious. The closure of workings in discontinuous structure occurred more smoothly than in the continuous one. The fault decreases the magnitude and rate of closure on the middle of both excavations in disregard of its nature. This could be justified given the same characteristics of materials in the immediate roof and in the floor within these structures.

The assumption that the fault does not cross the potash seam and it extends up to the potash seam might have prevented mining-induced stress from exceeding the strength of the materials in the immediate roof which may have exacerbated deformation and failure of the materials in this zone. Therefore, this resulted in the low magnitudes of convergence of mine working recorded at the excavations.

7.3.3 Sensitivity for unfaulted structures

The sensitivity analysis of closure was conducted by plotting convergence of workings for each of datasets for the five unfaulted structures and is depicted in Figures 7.15-19.

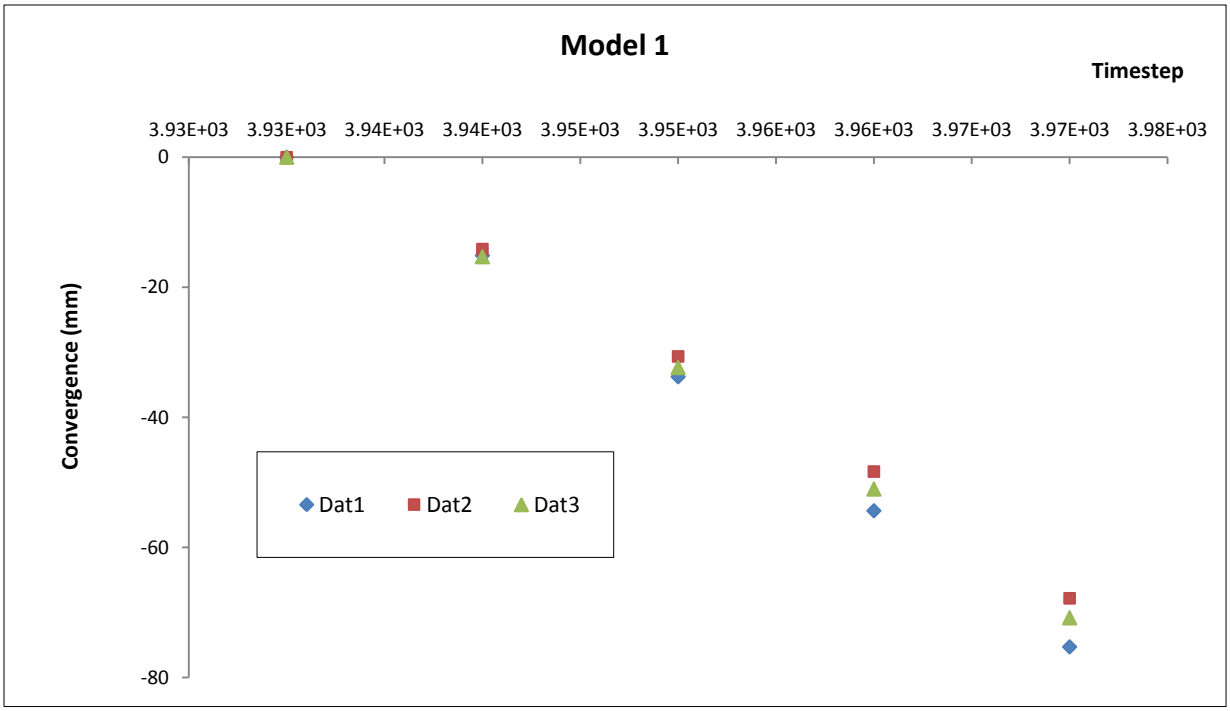

Figure 7.15 Convergence associated with the three datasets for model 1 for the analysis of sensitivity

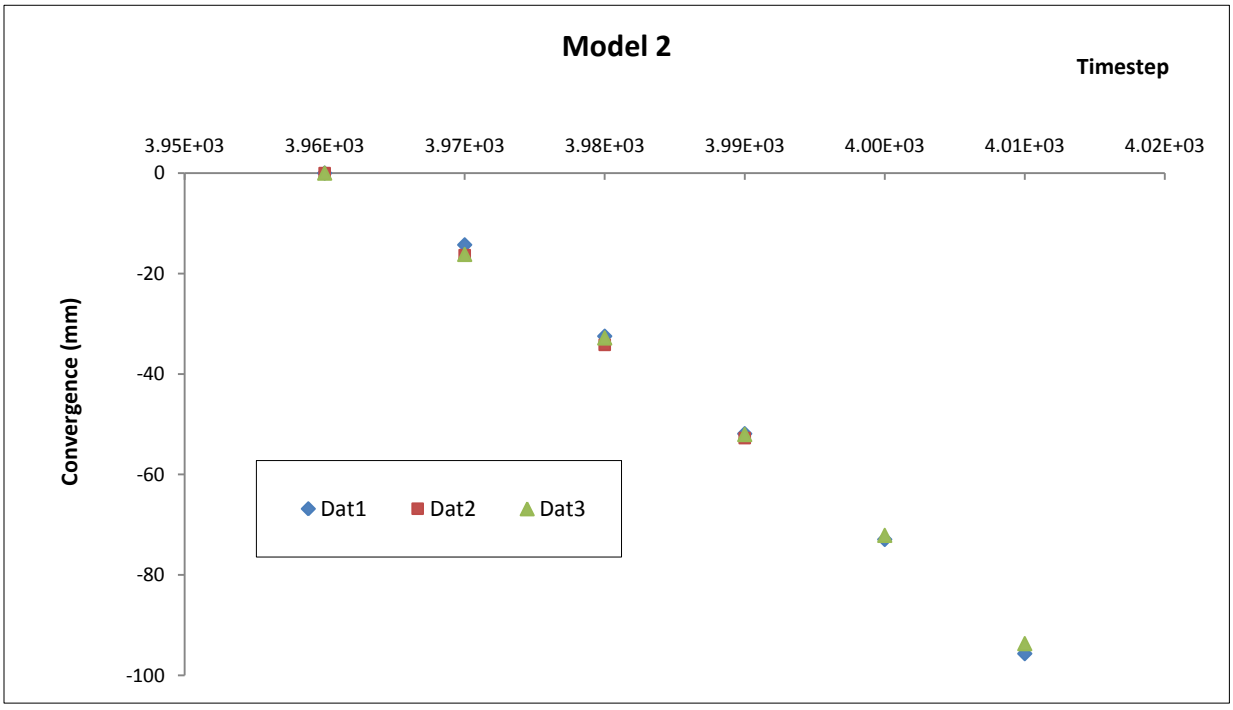

Figure 7.16 Convergence associated with the three datasets for model 2 for the analysis of sensitivity

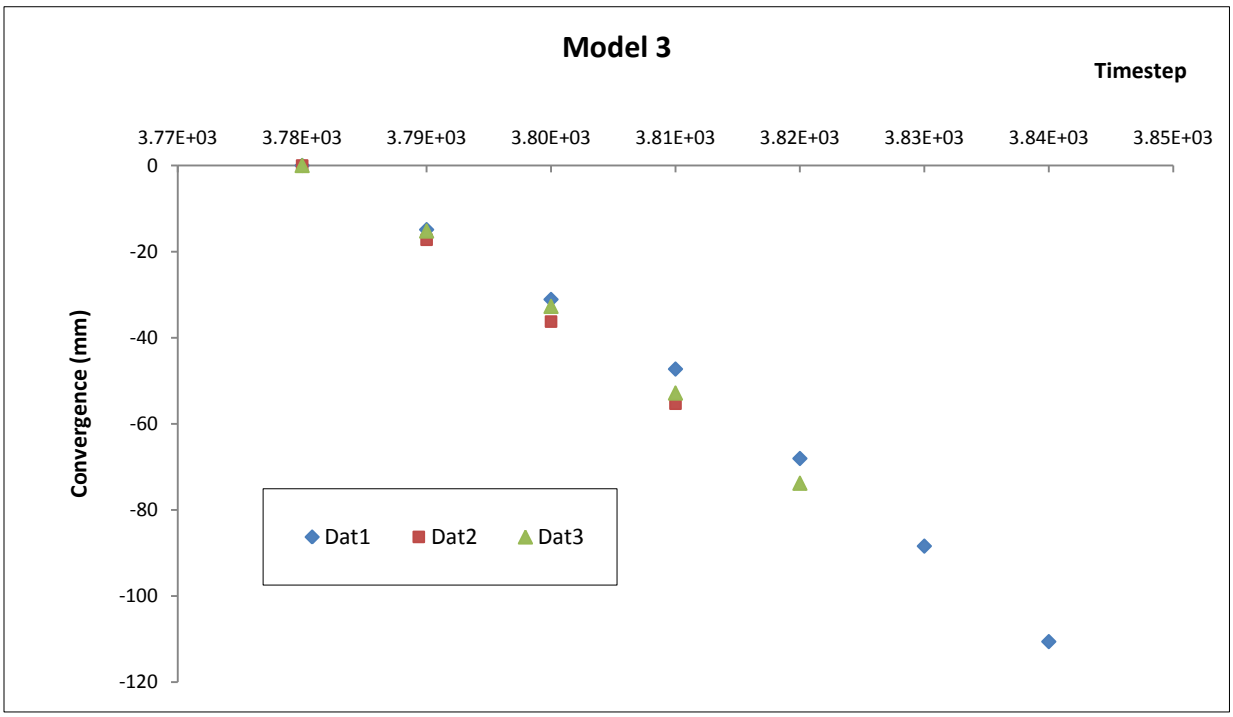

Figure 7.17 Convergence associated with the three datasets for model 3 for the analysis of sensitivity

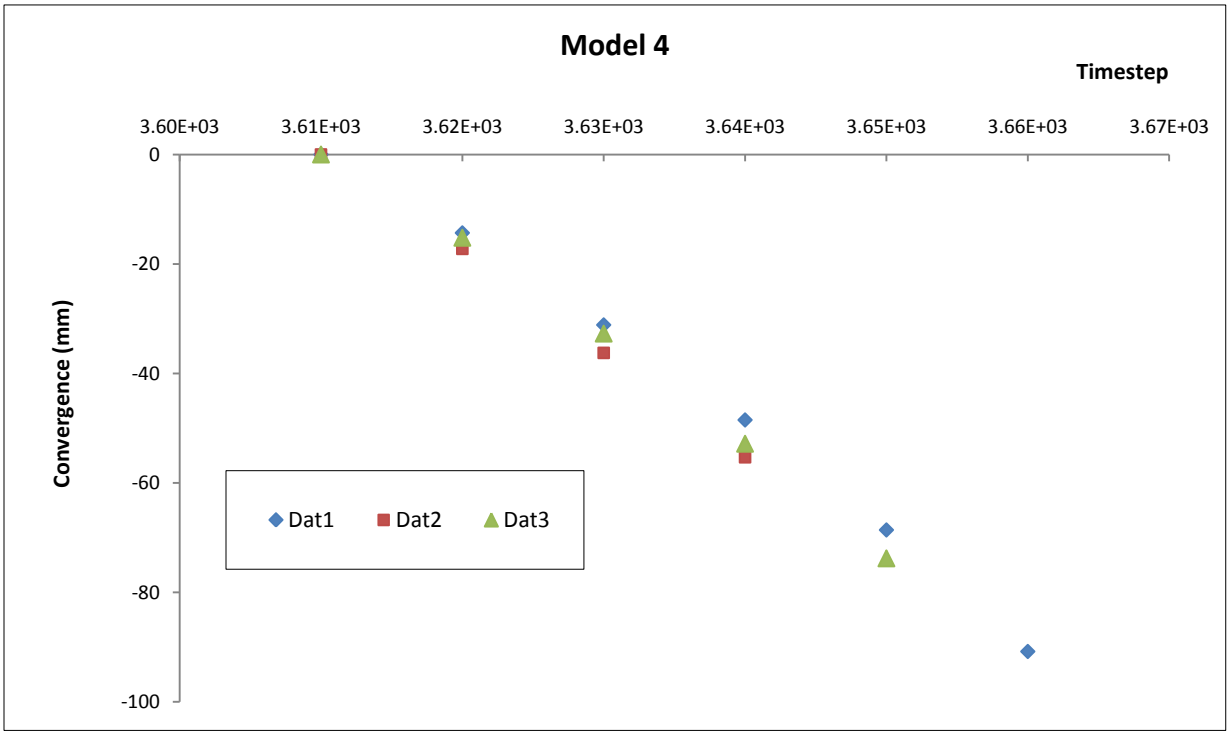

Figure 7.18 Convergence associated with the three datasets for model 4 for the analysis of sensitivity

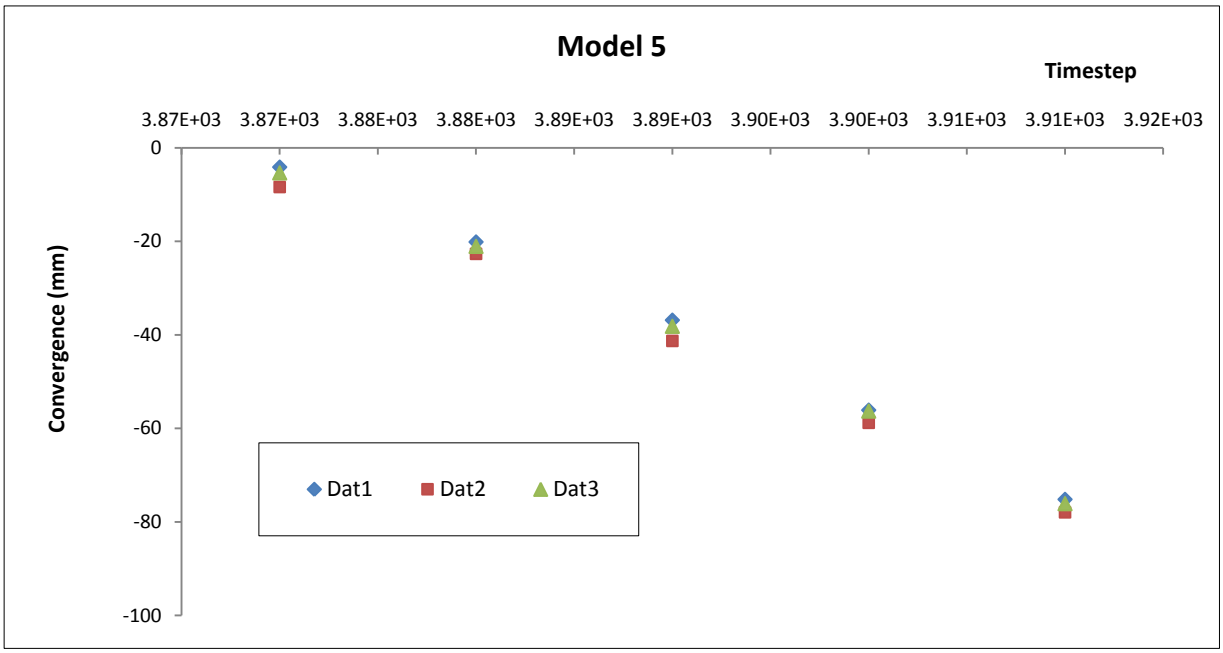

Figure 7.19 Convergence associated with the three datasets for model 5 for the analysis of sensitivity

Figures 7.15-19 show similar linear patterns of convergence for the five models. This implies that the convergence patterns are not sensitive to the variation of the parameters of materials in the range given in Tables 6.9-11, although the magnitudes are relatively sensitive.

The slight discrepancies in the magnitudes of total closure may be attributed to the mine roof closure which has higher contribution to the closure. Worth to note that the mine roof closure is primarily governed by the behaviour of Carnalite marl and Potash rocks in the immediate roof and to some extent the behaviour of Anhydrite layer.

7.4 Patterns of ground subsidence

Ground subsidence is a gradual settlement of the ground surface resulting from the readjustment of the overburden strata above the mine workings and the compressibility of individual rock layers owing to increasing overburden stress (Ma *et al*., 2006; Holzer, 1984). The patterns and rates of ground subsidence are greatly affected by several factors, among: the lithology (i.e. mechanical characteristics, bending resistance of

layers), hydrology, density and heterogeneity of the subsurface formations (Brady and Brown, 2006; Dunrud, 1984; Holzer, 1984). The following sections evaluate the dependency of patterns of time-dependent ground deformation on the lithological heterogeneity and geological structure.

7.4.1 Relationship with lithology

In the modelling process mining activity in all models was assumed to take place at the same depth. Therefore, the variable depth does not account in the analysis.

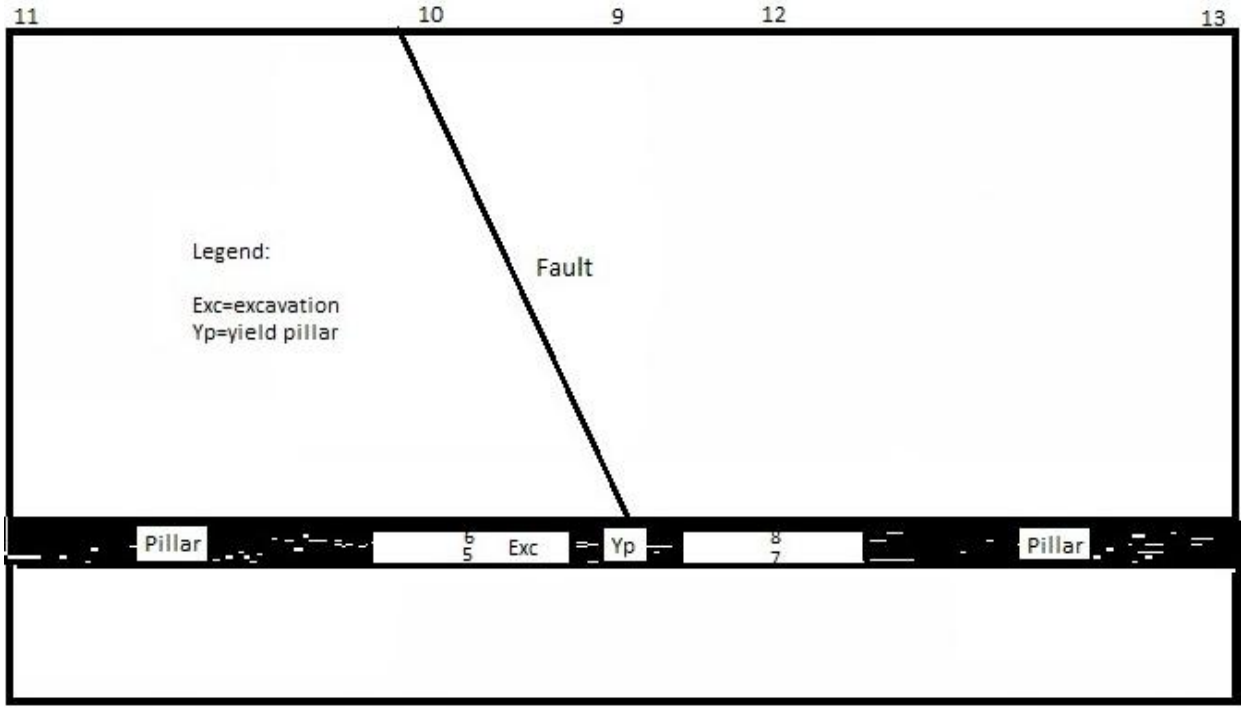

Figure 7.20 A simplified cross-section of Boulby structure with a geological fault showing the monitoring points on the surface – The fault does not cross the potash seam.

To investigate the effect of lithology upon the patterns of ground subsidence we consider the five unfaulted structures (i.e. models 1-5). Taking advantage of geometry domain symmetry, patterns of ground deformation of points shown in Figure 7.20 are plotted in Figures 7.21-23.

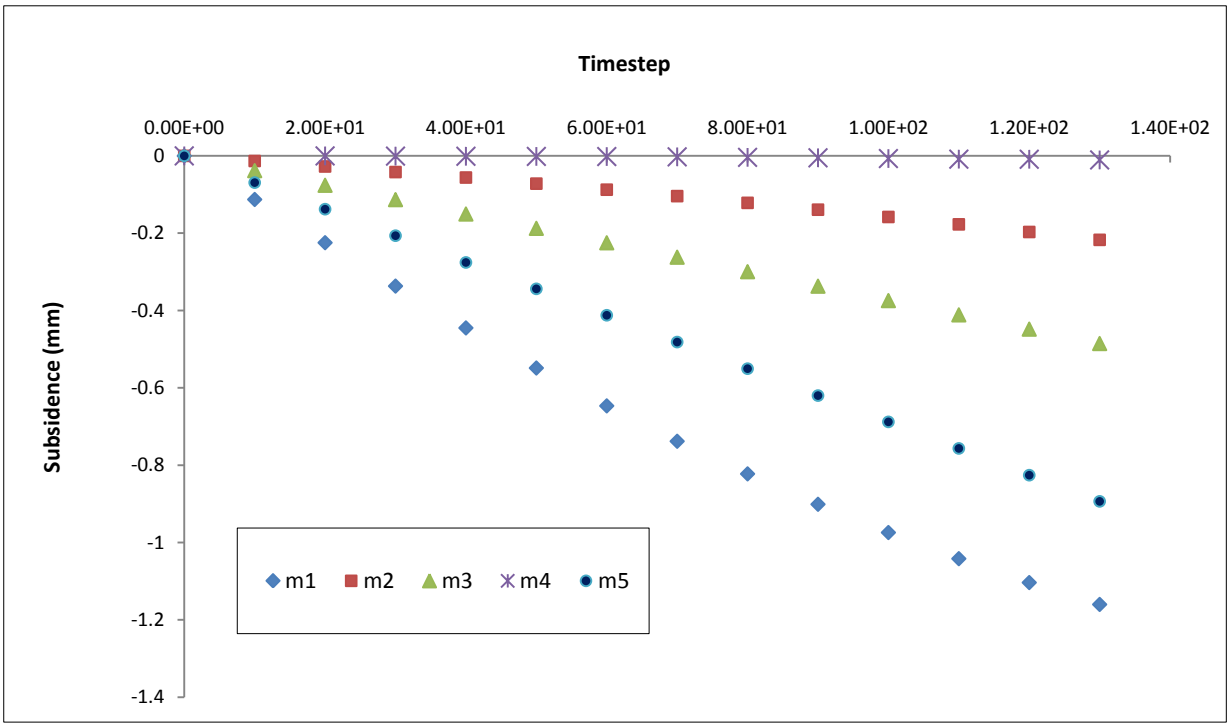

Figure 7.21 Effect of lithology on subsidence on the middle of cross-section of the unfaulted structures

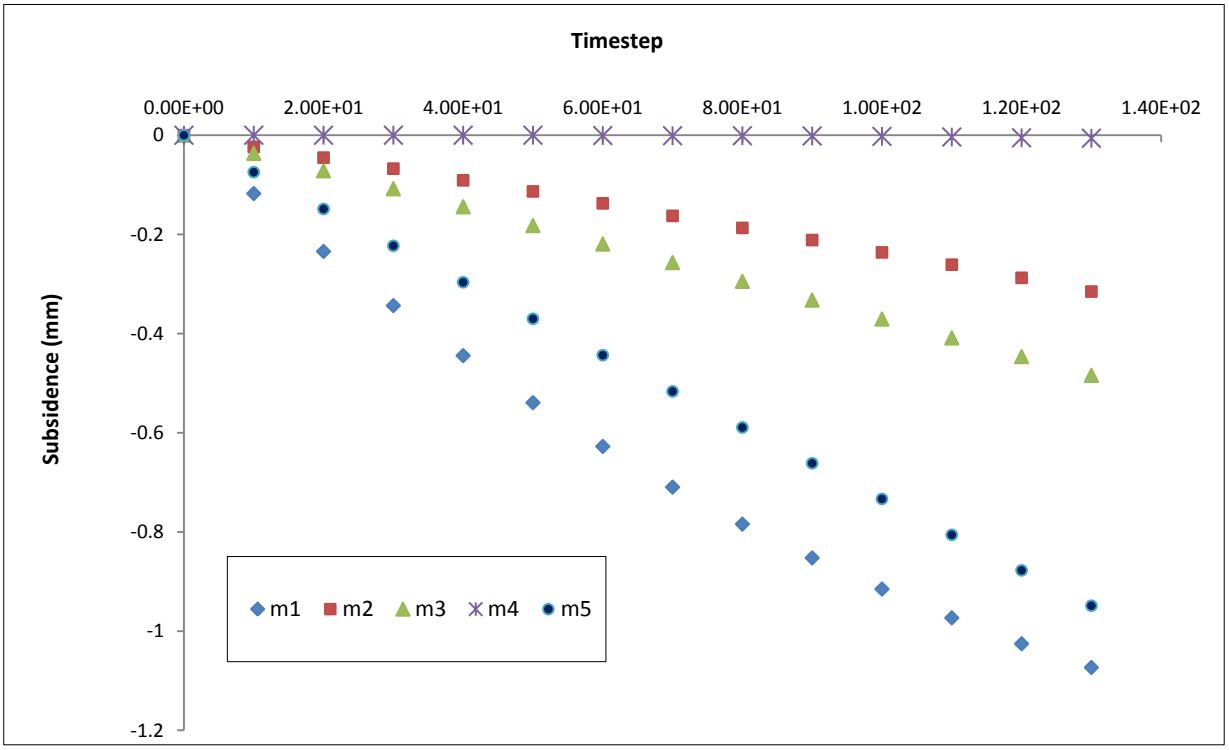

Figure 7.22 Effect of lithology on subsidence on the top of the excavation in unfaulted structures

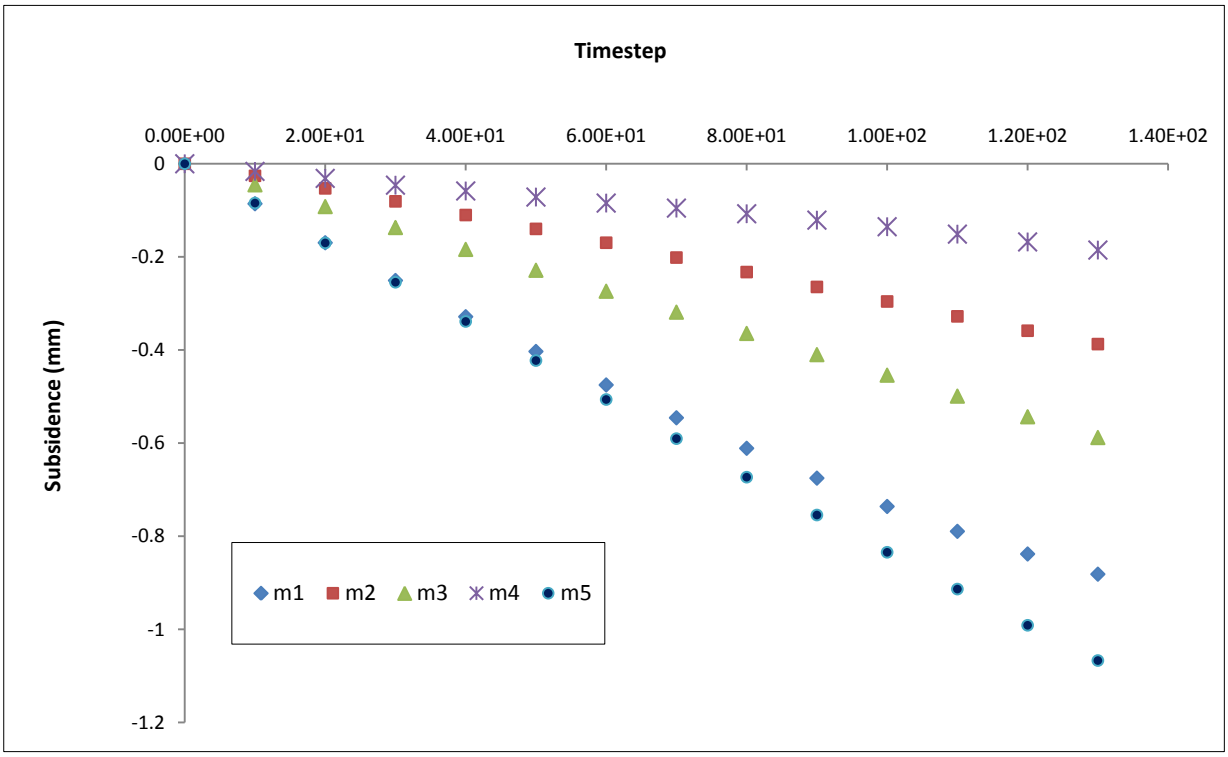

Figure 7.23 Effect of lithology on subsidence at the edge of cross-section in unfaulted structures

The patterns of ground deformation in Figures 7.21-23 show different trends of movement at the monitored points. In model 2, model 3 and model 5 ground deformation exhibit gradual linear trend whereas smooth non-linear patterns are displayed by the movement at the three monitored points in model 1. Ground movement in model 4 occurred gradually and linearly at the edge of cross-section while smooth ground subsidence was recorded on the middle of cross-section and top of the excavation (Figures 7.29-30).

The magnitudes and rates of ground subsidence are a function of the lithology. High magnitudes and rates of movement were recorded in model 1 and model 5 than in the three other models. The smallest rate of movement was recorded in model 4. The rate of movement in model 3 ranges between the rate of movement in models 1 and 5, and the rate of movement in model 2.

The discrepancies in the patterns, magnitudes and rates of ground movement at the monitored points illustrate the response of individual layers within the models to

changes in stress regime as a result of mining. Given the difference in the deformability parameters (i.e. bulk and shear moduli), strength parameters (i.e. cohesion and friction) and tensile strength of materials within the models, the structures differently responded to the removal of potash. Additionally, the thickness and density of these layers are also different. These factors are among those governing the occurrence, magnitude and rate of ground deformation on the surface wherever mining activity takes place and also at Boulby Mine (Lachenicht and Aswegen, 1998; Dunrud, 1984; Kratzsch, 1983).

An unexpected effect of material behaviour (i.e. constitutive behaviour of individual layer) is the increase of magnitude and rate of subsidence from the middle to the edge of the cross-section (i.e. rim of trough of subsidence). This suggests that tensile and compressive movement might have occurred on the middle and edge of cross-section (Figures 7.1-5), respectively.

7.4.2 Relationship with fault and nature of fault

A geological fault within a structure affects the profile, magnitude and rate of ground subsidence. This mainly depends on the location of the fault within the area undergoing ground deformation, the geometrical position of the fault relative to the mine workings (The Geological Society, 2008), and also its nature. Two cases of fault, real and glued, were investigated to evaluate the effects of discontinuities and their nature on the patterns, magnitudes and rates of ground deformation.

7.4.2.1 Relationship with fault

The effects of fault were investigated by plotting patterns of subsidence in faulted structure and unfaulted structure for comparative analysis. Patterns of ground subsidence on the middle of cross-section, top of excavation and the edge of cross-section on both sides of fault for the faulted structure related to the real fault are plotted in Figure 7.24 and those related to the glued fault are shown in Figure 7.25.

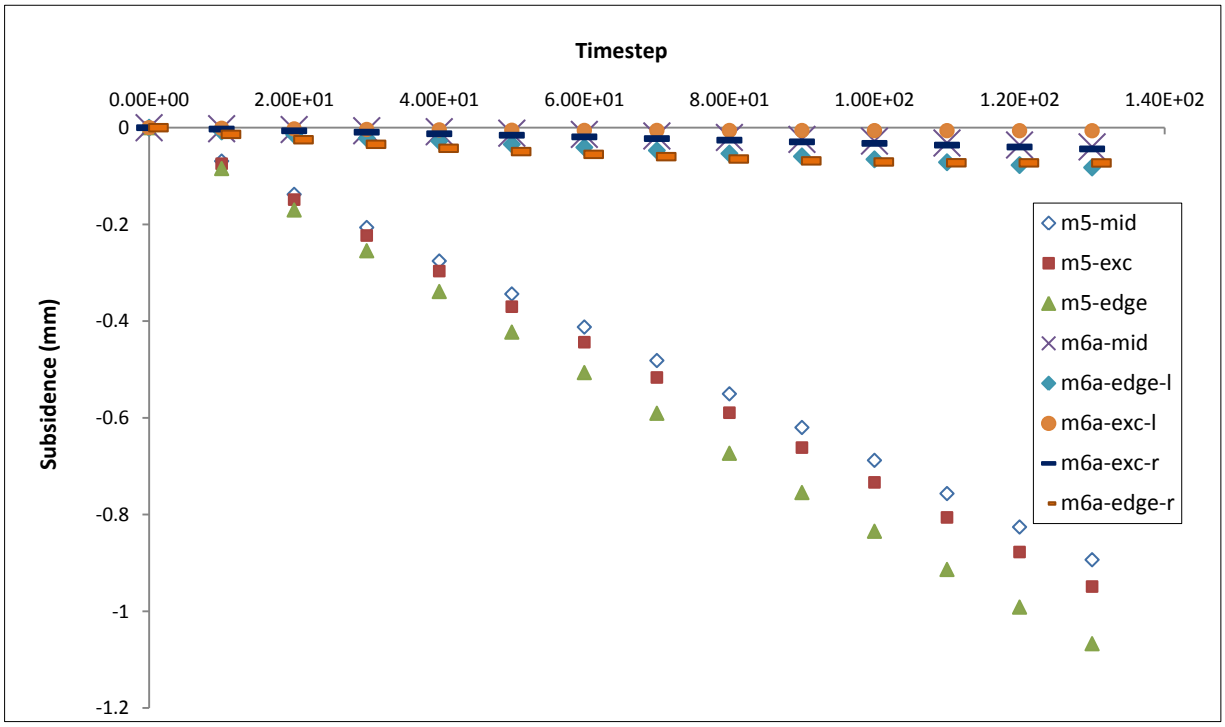

Figure 7.24 Effect of real fault (i.e. separation and sliding may occur) “a” on patterns of subsidence

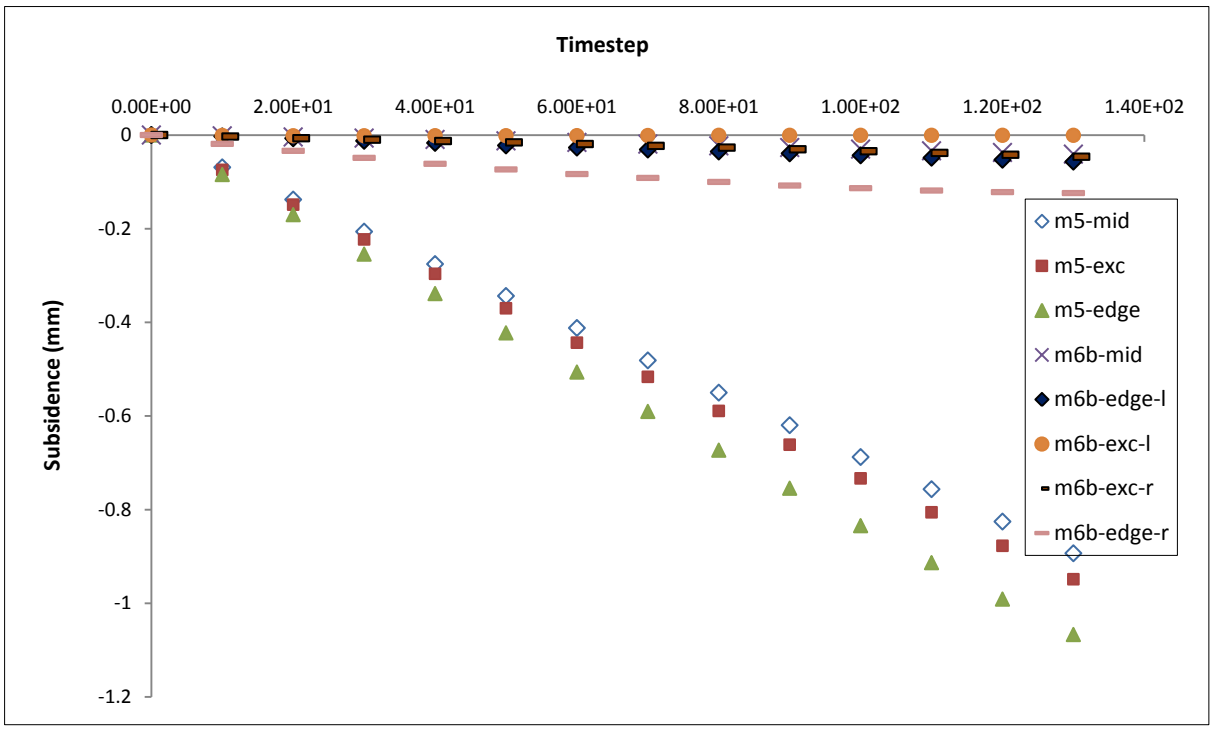

Figure 7.25 Effect of glued fault (i.e. separation and slipping won’t occur) “b” on patterns of subsidence

Figures 7.24-25 clearly illustrate the influence of fault on the patterns of subsidence, magnitudes and rate of subsidence at the monitored points. The fault disrupted the symmetrical occurrence of subsidence and significantly decreased the magnitude and rate of ground movement regardless its nature. The diagrams show that the glued fault has more effect on the magnitude and rate of subsidence. At some monitored points, particularly those situated on the right-hand side of the fault no noticeable movement was recorded at the monitored points. This would suggest that although deformation might have occurred on that side of the structure the analysis process could not record ground movement at these points on the surface given its low magnitude. The geometrical position of the fault relative to the monitoring points may have prevented deformation from readily propagating to these points.

7.4.2.2 Relationship with the nature of fault

The analysis of effect of nature of fault was carried out by plotting the patterns of ground movement related to both real and glued fault (Figure 7.26).

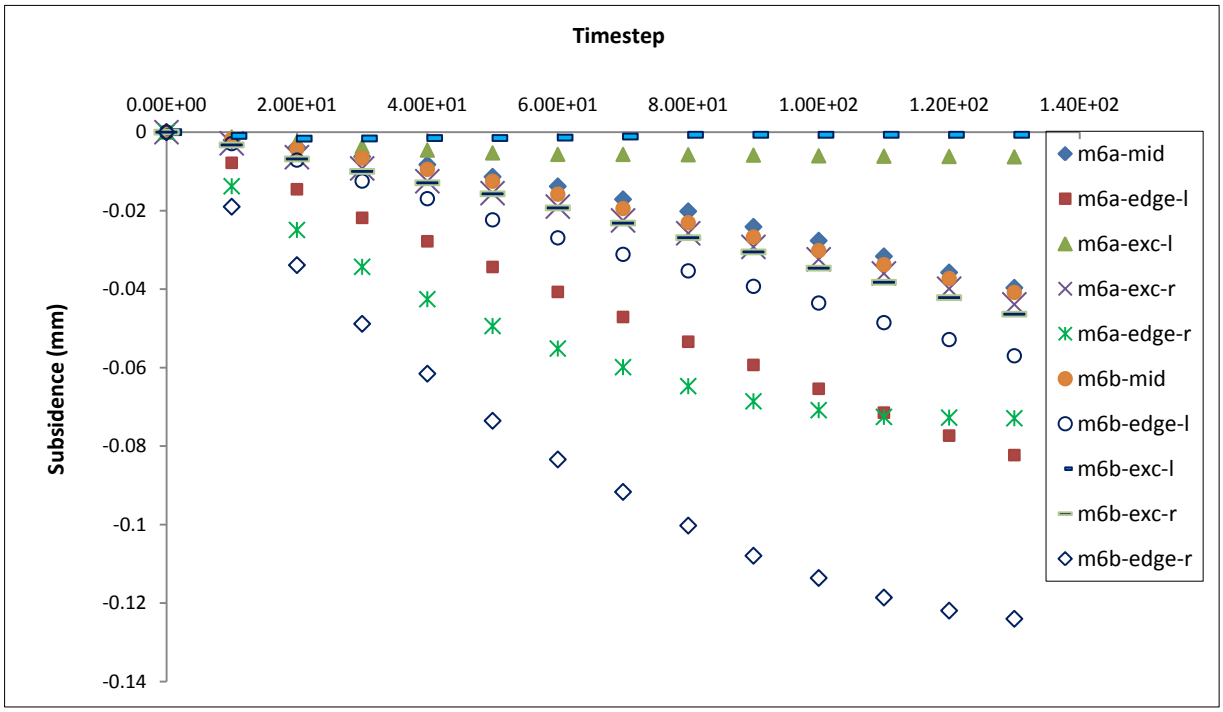

Figure 7.26 Relationship between real and glued fault and patterns of subsidence. M6a-=model with real fault, m6b=model with glued fault, mid=middle of cross-section, edge-l= left-hand edge, edge-r=right-hand edge, r-r=right-hand side exaction, r-l= left-hand side excavation

The nature of fault affects the patterns, magnitudes and rates of ground subsidence. The glued fault intensifies the smooth occurrence of subsidence at the edge on the right-hand side of cross-section. This fault also increases the magnitude and rate of subsidence at all of the monitored than the unglued fault. The low unglued fault-related magnitude and rate of subsidence might be attributed to the effect that the fault might have absorbed the mining-induced strain and deformation.

7.4.3 Ground subsidence sensitivity

Patterns of subsidence in model 5 associated with the three datasets (Table 6.9-11) are plotted in Figure 7.27 for the analysis of sensitivity.

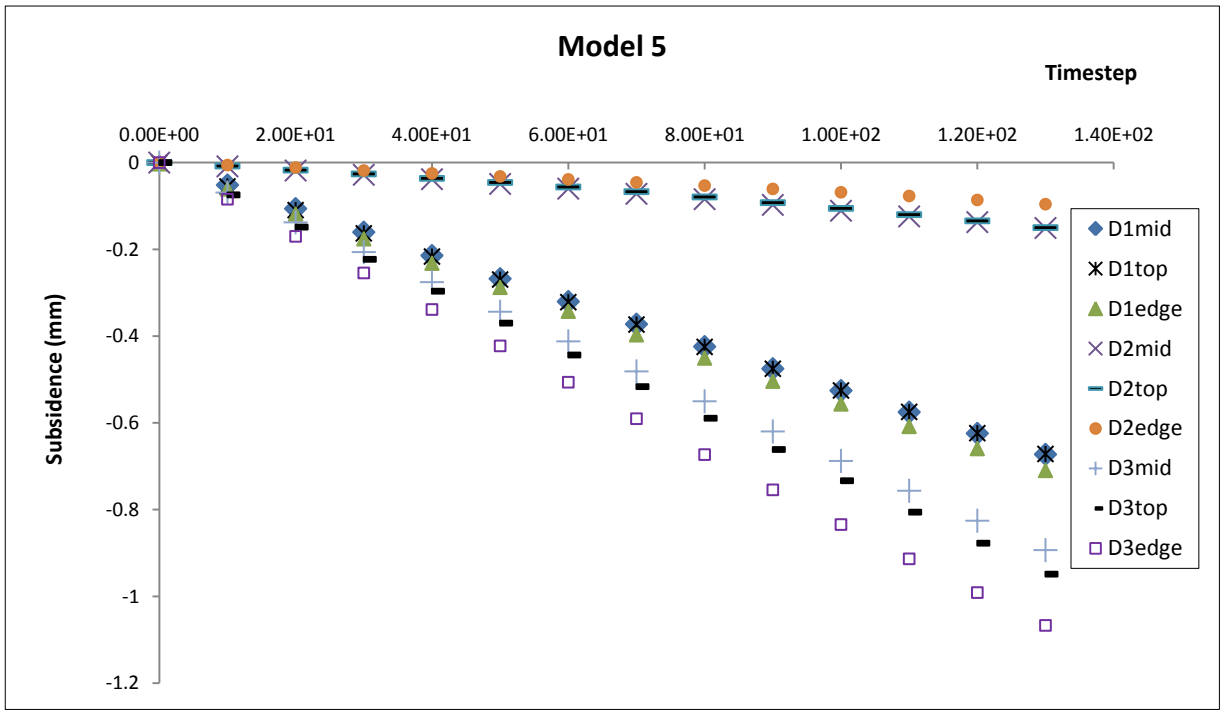

Figure 7.27 Relationship of ground subsidence with the variation of strata parameters in model 5 for the analysis of sensitivity, D1=dataset 1, D2=dataset 2 and D3=dataset 3

Figure 7.27 indicates that at the monitored points, the patterns of subsidence have limited sensitivity to the variation of material parameters, exhibiting a linear trend of movement. In the opposite, the associated magnitudes and rates are sensitive to the variation as a result of decrease of stiffness and strength of strata within the structures

(i.e. increase of reduction factor). Consequently, magnitudes and rates of subsidence at the monitored points are increased. The increase of magnitudes of subsidence from the centre to the edge of cross-section might be attributed to the different constitutive behaviour of the overlying strata which compose the structures. It may also be attributed to the low magnitude of horizontal stress used in the analysis resulting in the development of ground deformation more horizontally than vertically.

7.5 Predicted versus Measured ground subsidence

FLAC 2D "Predicted ground subsidence" was validated against Measured ground subsidence based on levelling survey at Boulby mine. The levelling data are from Boulby Mine annual surveys over the mine area and cover a period of twelve years between 1992 and 2004 (Kemeling, 2006). Ground movement in Staithes, where mine panels were constructed between September 1983 and December 1988, was analyzed. Pattern of subsidence at monitoring station 193 is shown in Figure 7.28.

As shown in Figure 7.20, the monitored points considered are located on the middle, top of excavation and at the edge of cross-section. Predicted ground subsidence at these points was plotted for unfaulted models 4 and 5 (Figures 7.29-31). For the faulted structure, we have plots 7.32-35.

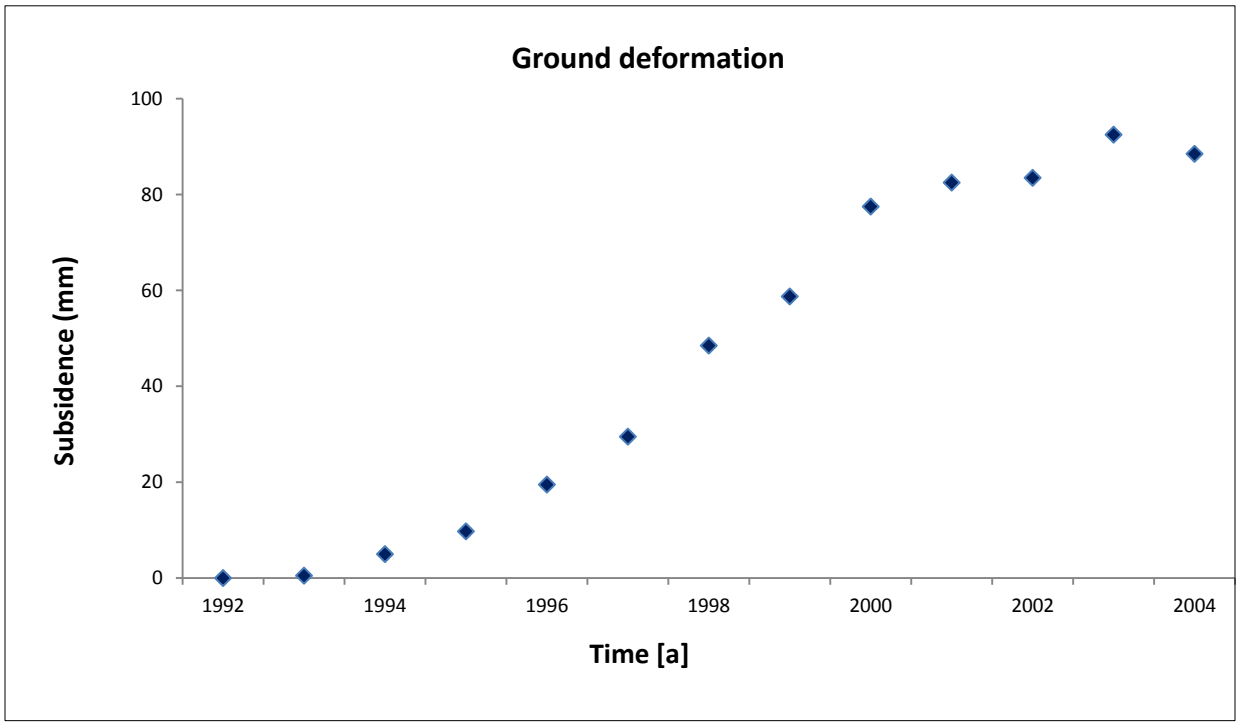

Figure 7.28 Levelling measured ground deformation at Boulby Mine from 1992 to 2004 at 193 monitoring station in Staithes (After Kemeling, 2006)

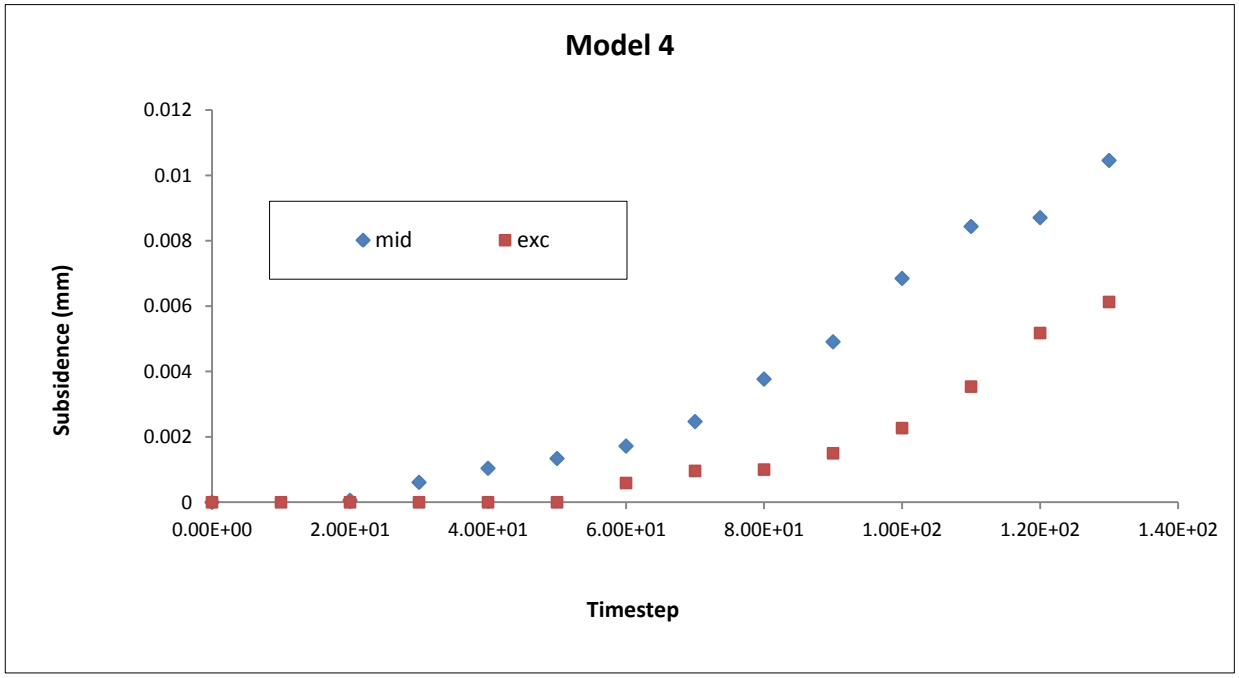

Figure 7.29 FLAC predicted subsidence on the middle of cross-section and top of excavation for model 4

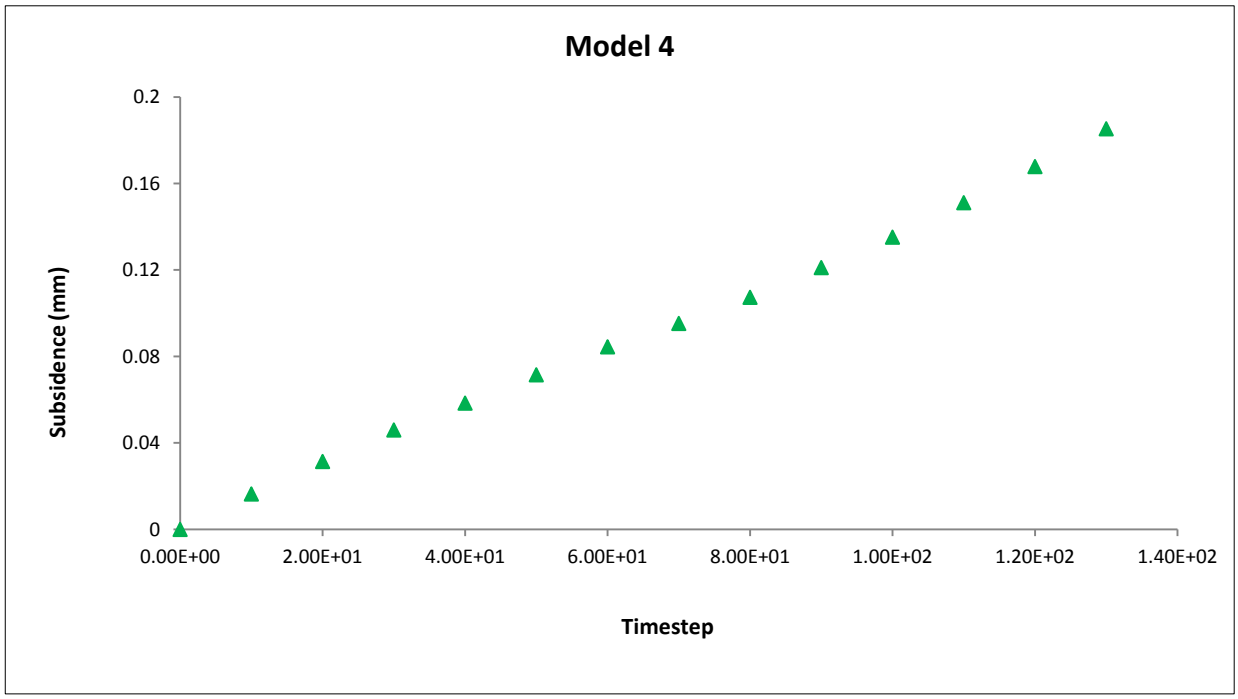

Figure 7.30 FLAC predicted subsidence at the edge of cross-section for model 4

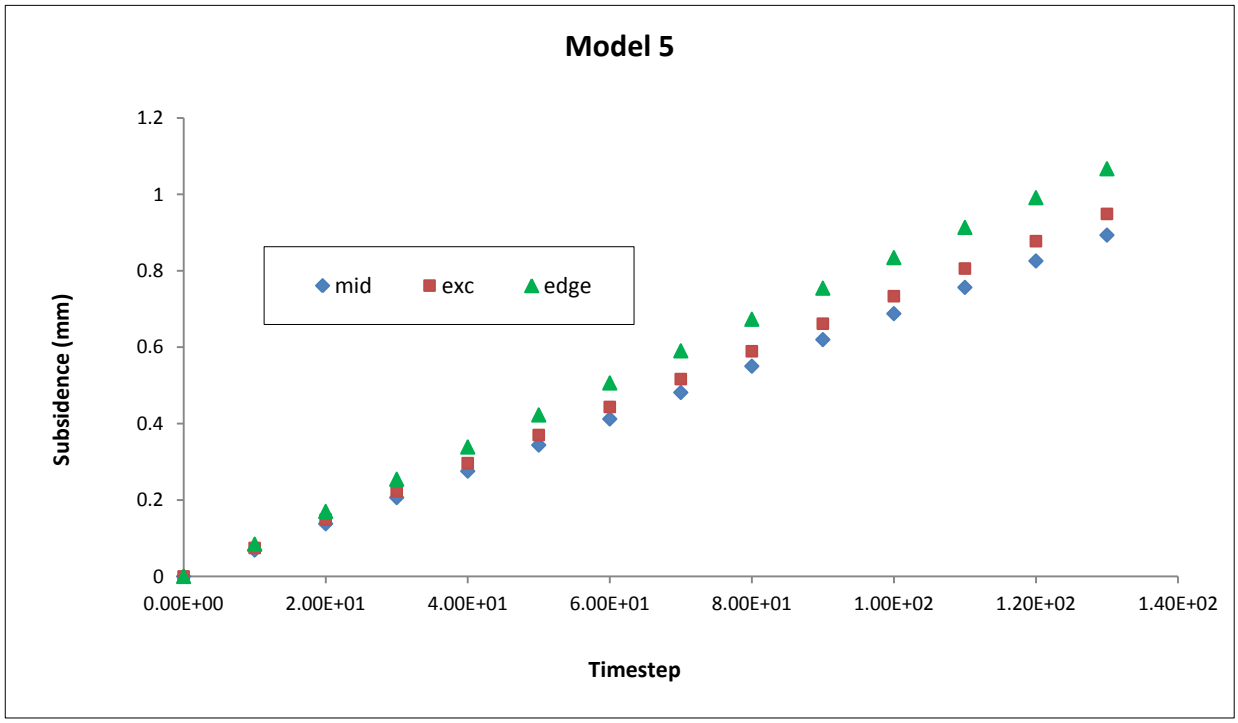

Figure 7.31 FLAC predicted subsidence on the middle of cross-section, top of excavation and at the edge of cross-section for model 5

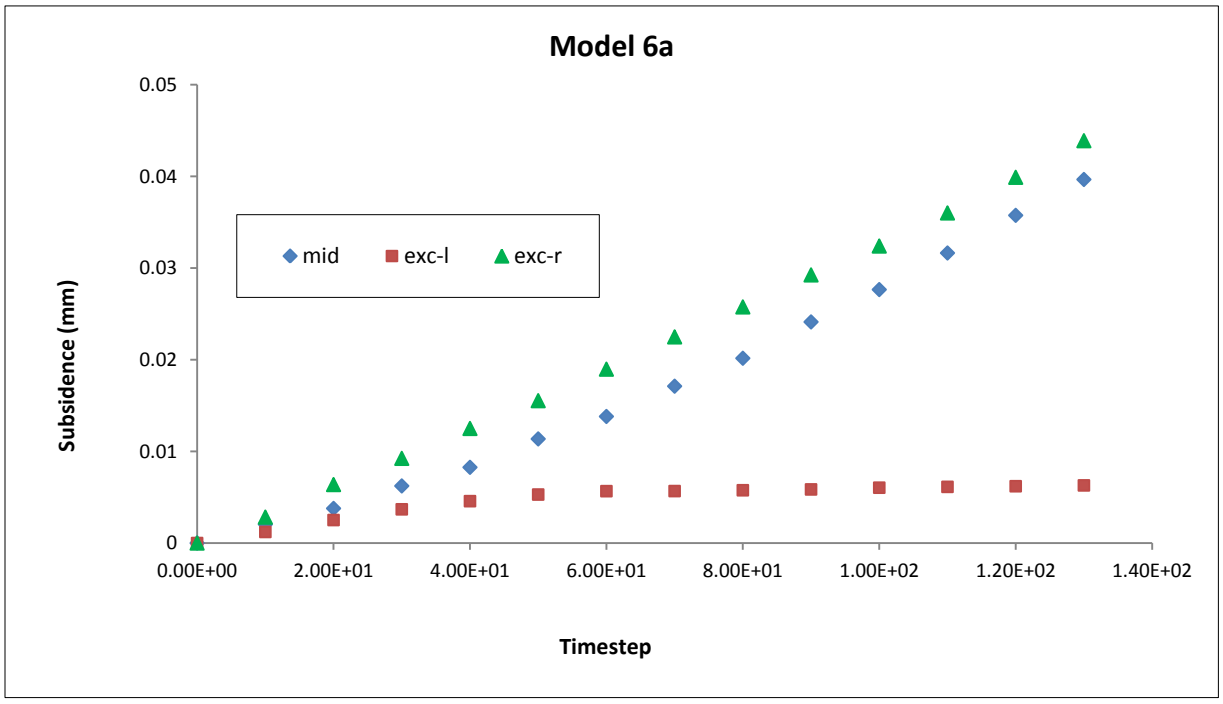

Figure 7.32 FLAC predicted subsidence on the middle of cross-section, the top of the left-(l) and right-(r) hand sides' excavations for the structure with real fault

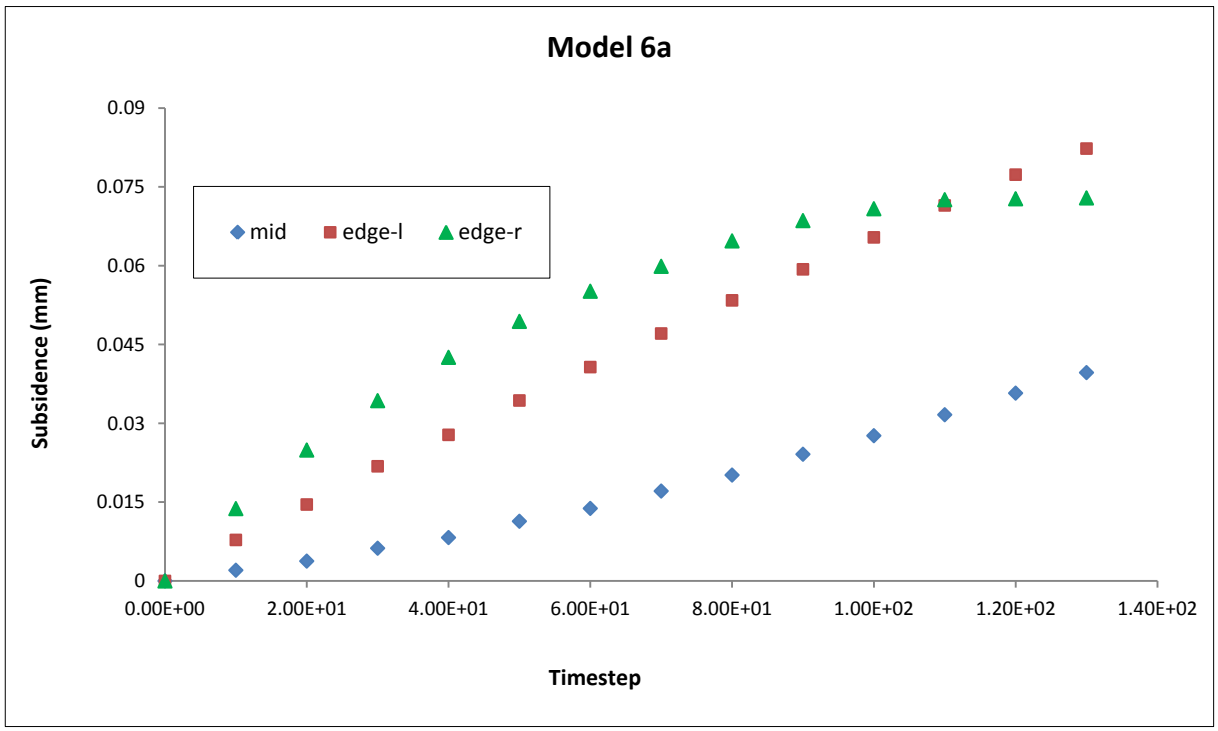

Figure 7.33 FLAC predicted subsidence on the middle of cross-section and at the left- and right-edges of cross-section for the structure with real fault

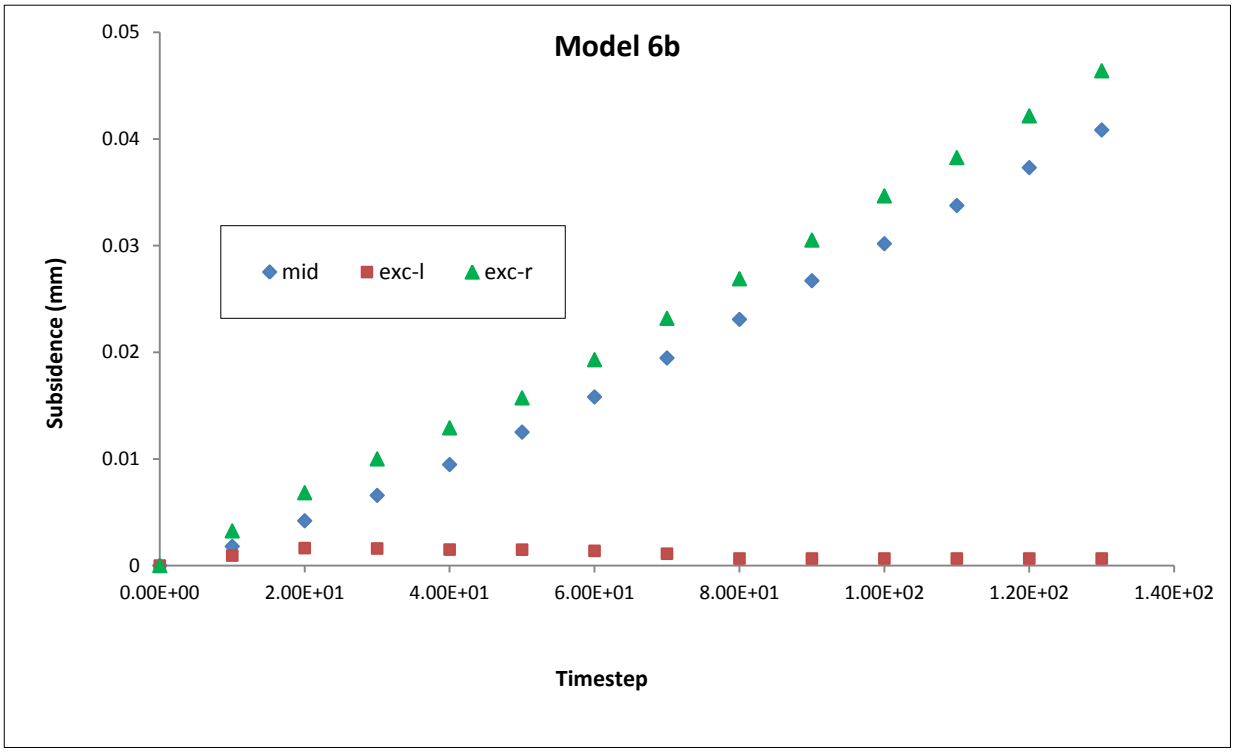

Figure 7.34 FLAC predicted subsidence on the middle of cross-section and the top of left-(l) and right-(r) hand sides' excavations for the structure with glued fault

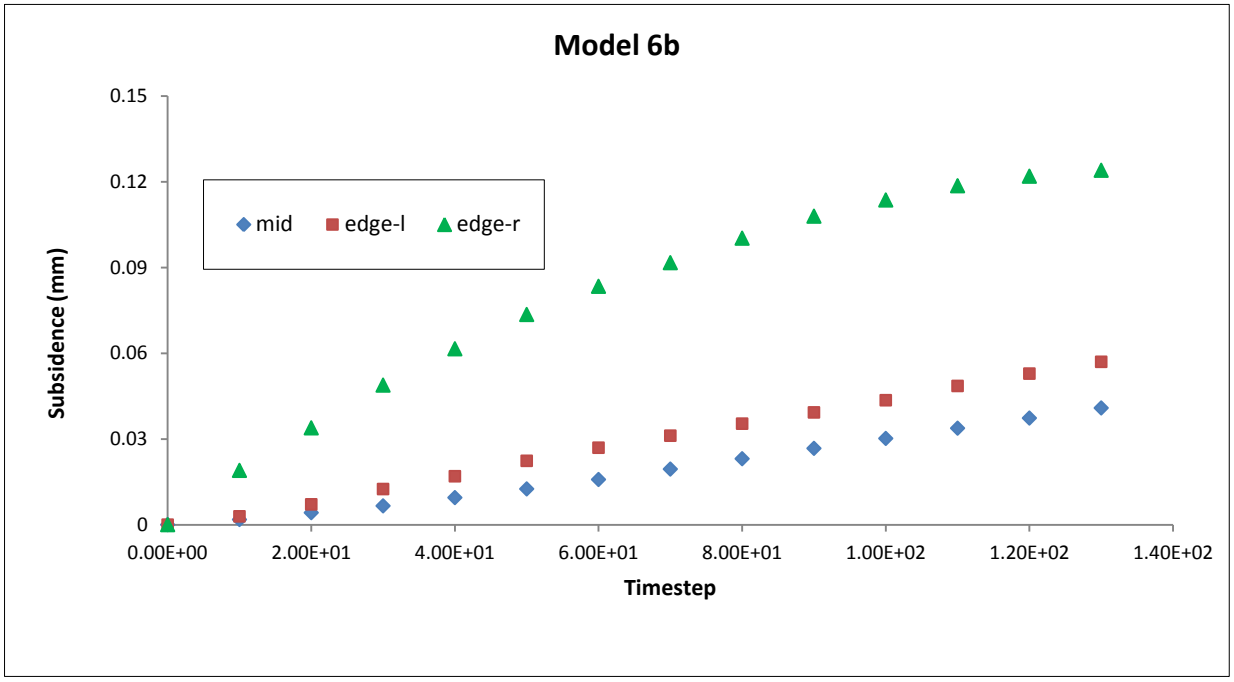

Figure 7.35 FLAC predicted subsidence on the middle of cross-section and at the left- and right-side edges of cross-section for the structure with glued fault

Predicted ground subsidence plots indicate two trends of movement in the investigated cases. In continuous model 4, smooth ground movement with increasing rate occurred on the middle of cross-section and the top of excavation whereas gradual and linear movement was recorded at the edge of the cross-section. In contrast, all monitored points in continuous model 5 gradually and linearly subsided at a rate higher than the rate of subsidence in model 4. Ground movement in discontinuous structures was linear on the middle of cross-section, top of excavation of right-hand side and also at the left-hand edge. At the right-hand edge and on top of excavation on the left-hand side of cross-section, ground movement was smooth for both real and glued faults with low rate of subsidence occurring on the top of excavation particularly in structure with glued fault.

When compared, predicted subsidence magnitudes in continuous structures are relatively higher than those in discontinuous structures. The fault within structure may have acted as either absorbent of mining-induced deformation or boundary of movement, decreasing the magnitude and rate of subsidence at the monitored points in disregard of the nature of the fault.

Predicted subsidence underestimates measured subsidence in both continuous and discontinuous structures regardless whether the fault is unglued or glued. This is because some of the factors which primarily govern ground subsidence were not taken into consideration in the predicted ground subsidence models. Such factors include the topography, number and type of discontinuities, and effect of proximity of newly excavated panels on pre-existing excavations. Additionally, despite water being present in the analyzed structure, its static (i.e. undrained analysis) nature may not reflect the actual nature of water at Boulby mine. Another fundamental factor which controls the magnitude and rate of predicted subsidence is the mechanical and rheological parameters of the strata within the models. Furthermore, the mechanics of strata may have also contributed to the low magnitudes of predicted ground subsidence.

7.6 Water effect analysis

Pore pressure is essential to the structure as an opposing component to stress exerted by the overlying strata. Reducing pore pressure either by withdrawal or flow of fluid leads to rock matrix stresses increase and reservoir bulk volume reduction. Consequently, the reservoir loses its supporting capacity of the earth stresses and displacements are induced within the reservoir; affecting the stress-strain regime within structures (Chang and Wang, 2006; Djaja *et al*., 2004).

It may also shape the profile of the trough of subsidence and control the magnitude and rate of subsidence. As a matter of fact, pore pressure negatively affects the strength of the structure either before or after excavation which may exacerbate the propagation of deformation and failure of materials towards the surface and therefore increase ground movement on the surface. Rock strength in the fault zone is much lower than that of continuous rocks (Islam *et al*., 2009). In the presence of water, rocks in faulted zones fail more easily increasing ground deformation.

The effects of water were analyzed through a comparative analysis of patterns and magnitudes of stress and displacement, subsidence and convergence associated with saturated and unsaturated structures. Both continuous and discontinuous structures and data in Table 6.9 were used. To characterise and understand the mechanisms of failure of the overburden due to water a quantitative analysis of magnitudes of maximum stress and total vertical displacement was undertaken.

7.6.1 Relationship with stress and displacement

Patterns of total stress and vertical displacement related to the saturated and unsaturated states for both continuous (i.e. model 5) and discontinuous (i.e. model 6) structures are plotted in Figures 7.36-37 and Figures 7.38-41, respectively. The magnitudes of maximum stress and total vertical displacement for both structures are given in Tables 7.1 and 7.2, respectively.

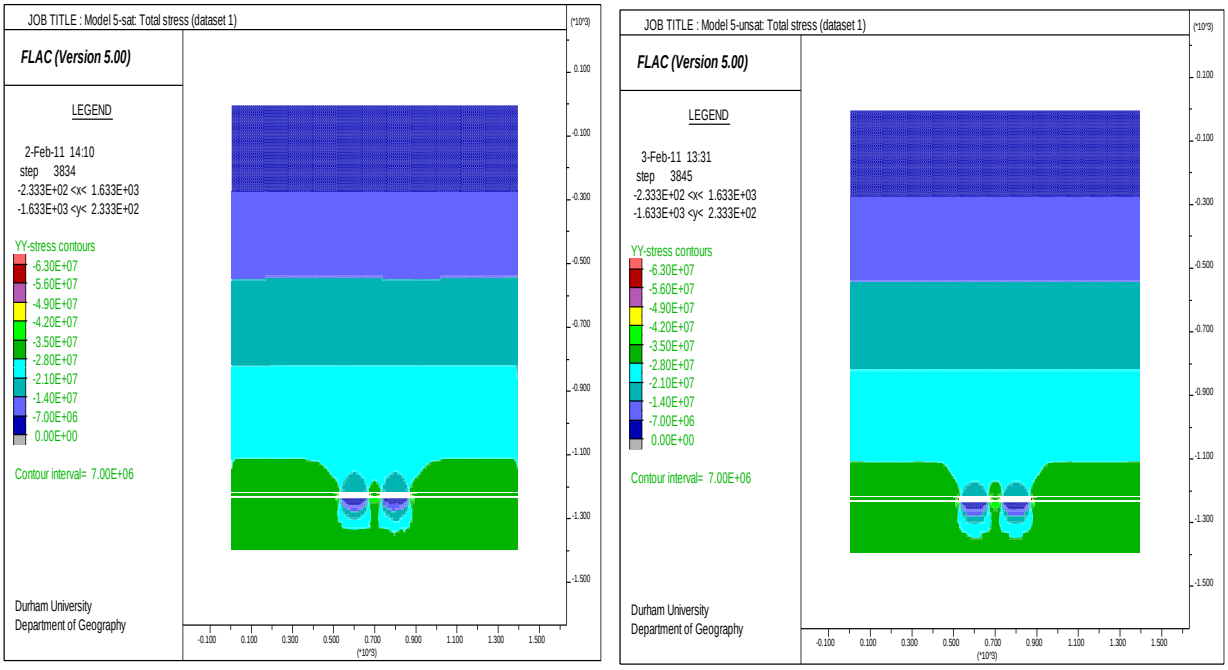

Figure 7.36 Effect of water on stress distribution for the continuous structure, left=saturated, right=unsaturated

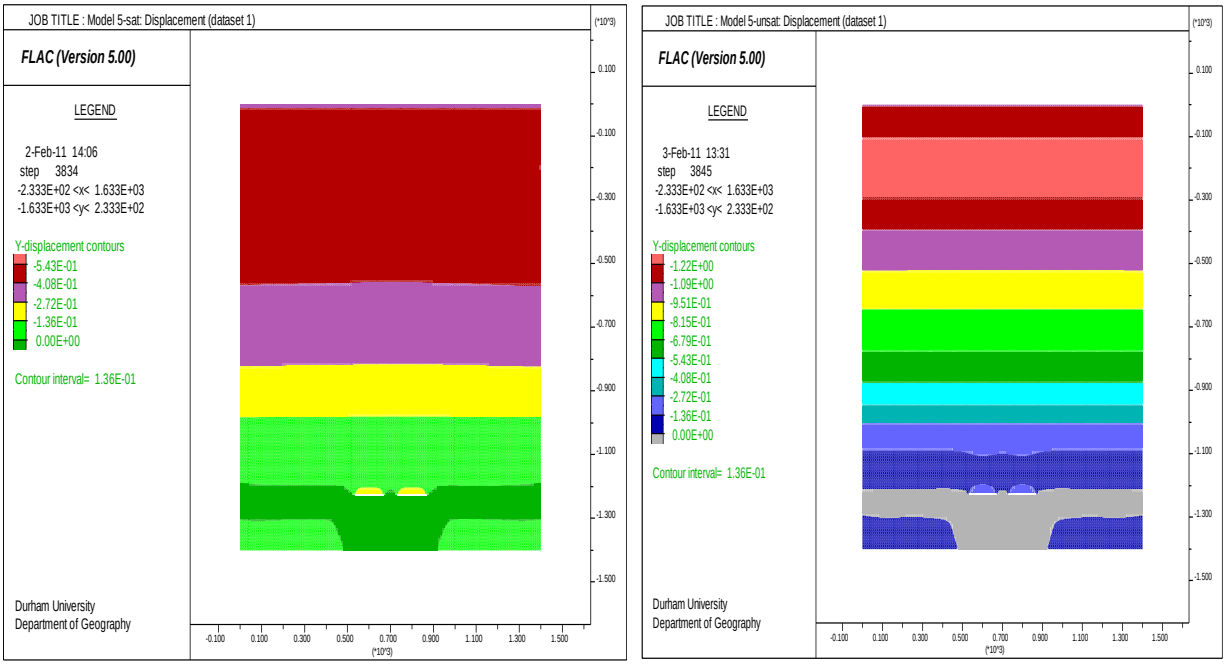

Figure 7.37 Effect of water on displacement distribution for the continuous structure, left=saturated, right=unsaturated

Table 7.1 Effect of water on magnitudes of maximum stress and total displacement for a continuous structure

Model	Maximum stress (MPa)	Tot. displacement (m)
Saturated	63	1.359
Unsaturated	63	6.114

Figures 7.36-37 and Table 7.1 translate the influence of water on the patterns and magnitudes of stress and displacement within the continuous structure. The presence of water slightly disrupts the linear stratification of stress within the structure, and induces tensile and compressive deformation on the middle and rib-side of the structure, respectively. Pore pressure may have transferred the weight of the overburden above the Sherwood sandstone stratum to the underlain strata, inducing stress around excavation similar to that in unsaturated structure. However, given its static nature, the pore pressure may have impeded deformation within the Sherwood sandstone leading to total deformation decrease within the saturated structure than within the unsaturated structure (Table 7.1.).

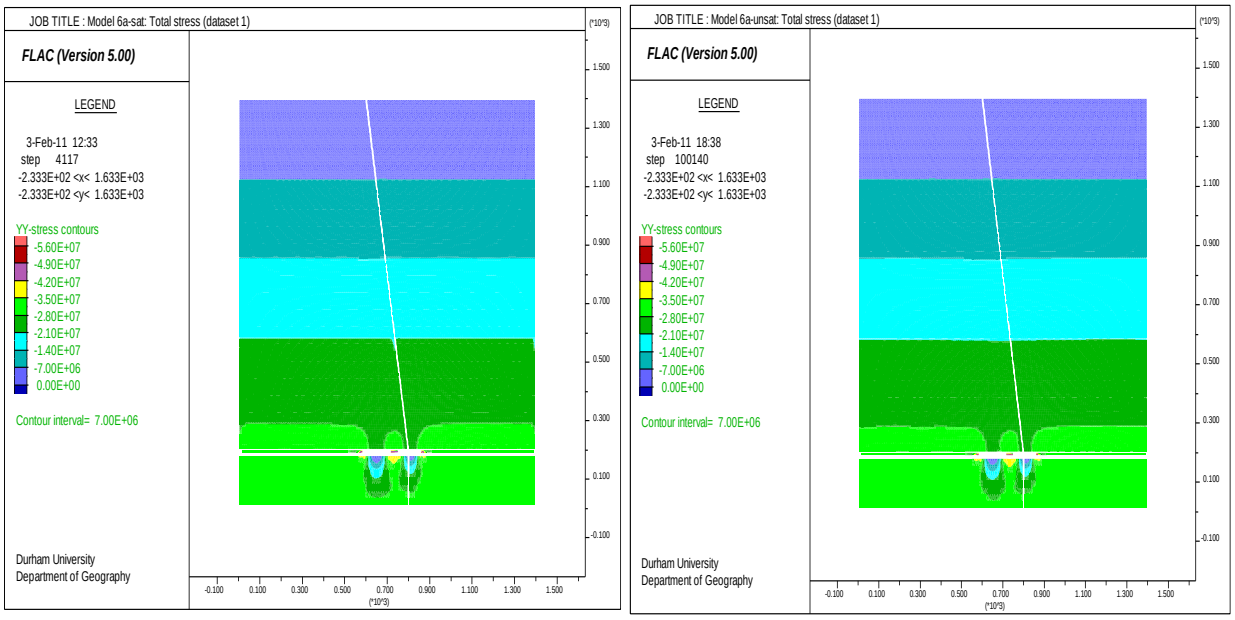

Figure 7.38 Effect of water on stress distribution for the discontinuous structure with unglued fault, left=saturated, right=unsaturated

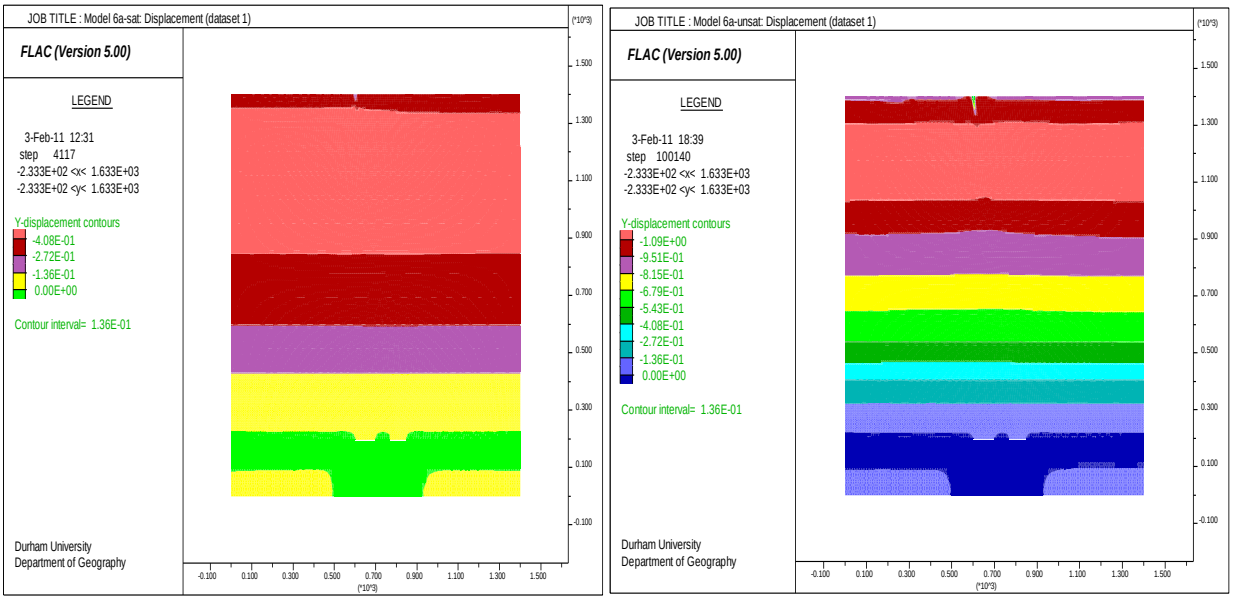

Figure 7.39 Effect of water on displacement distribution for the discontinuous structure with unglued fault, left=saturated, right=unsaturated

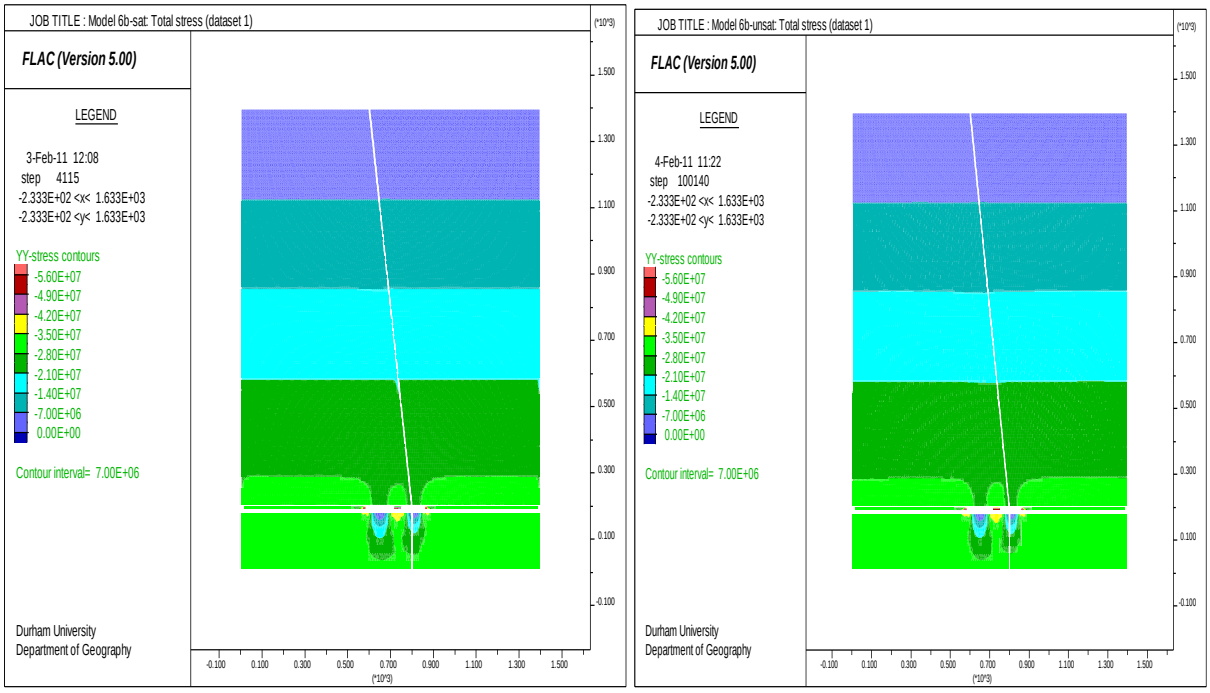

Figure 7.40 Effect of water on stress distribution for the discontinuous structure with glued fault, left=saturated, right=unsaturated

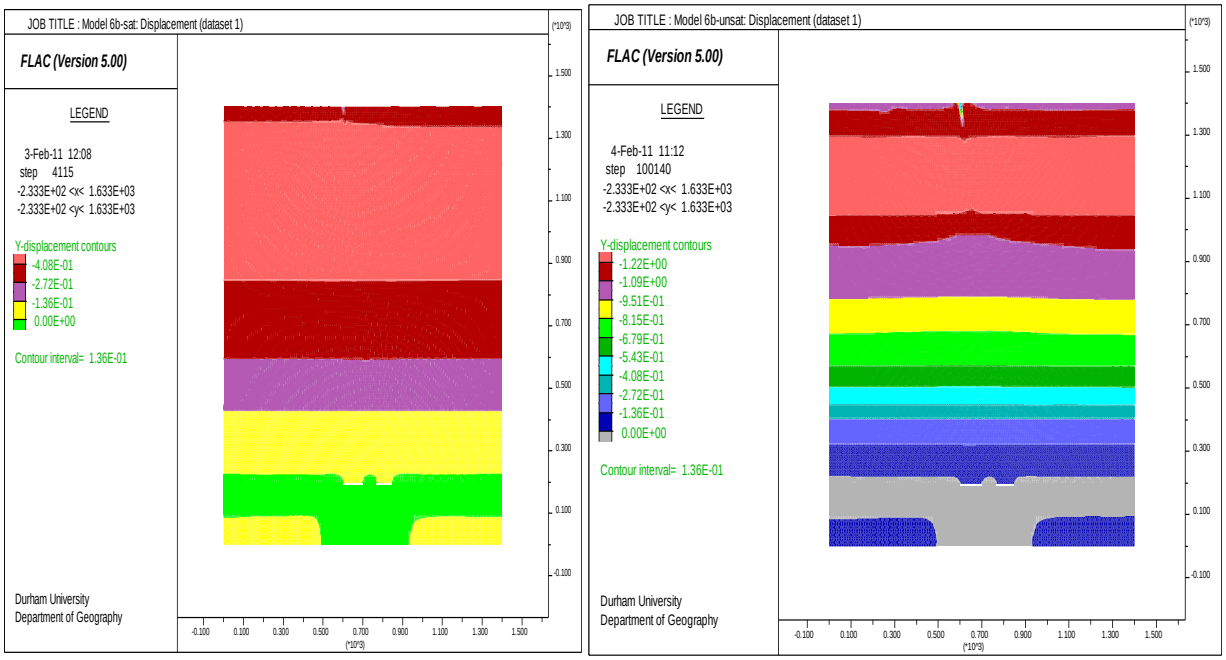

Figure 7.41 Effect of water on displacement distribution for the discontinuous structure with glued fault, left=saturated, right=unsaturated

Table 7.2 Effect of water on magnitudes of maximum stress and total displacement for discontinuous structure

Model	Maximum stress (MPa)		Tot. displacement (m)	
	Nature of fault		Nature of fault	
	Unglued	Glued	Unglued	Glued
Saturated	56	56	0.816	0.816
Unsaturated	56	56	4.894	6.114

Unlike in continuous structure pore pressure has limited effect on stress distribution within the discontinuous structure, whereas it affects the deformation distribution and decreases its magnitude in disregard of the nature of the fault. Pore pressure acted against mining-induced stress and prevented overburden strata from failing under under gravity. In other terms, the decrease of deformation within the saturated structures might be the fact that the fault acted as stress and deformation absorbent although pore pressure may have eased movement along fault.

7.6.2 Relationship with convergence

To examine the effect of water on convergence of mine workings, patterns of convergence of openings in continuous and discontinuous structures for both saturated and unsaturated states are depicted in Figure 7.42 and Figures 43-46, respectively.

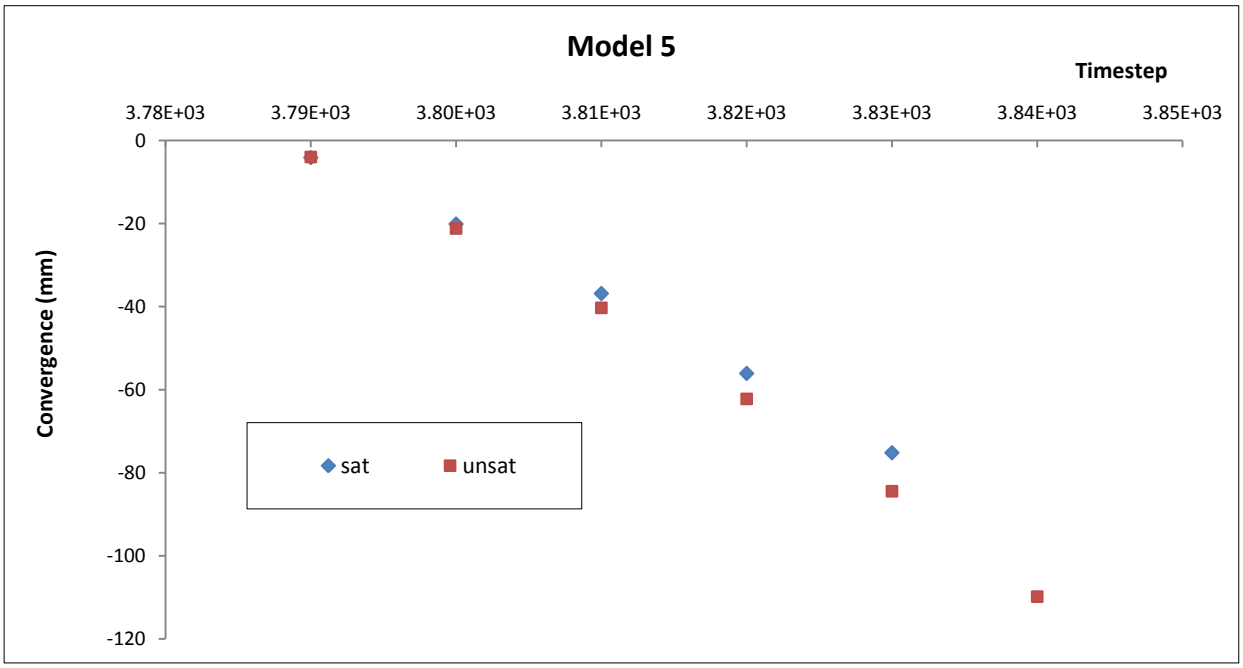

Figure 7.42 Effect of water on convergence on the middle of excavation of unfaulted structure

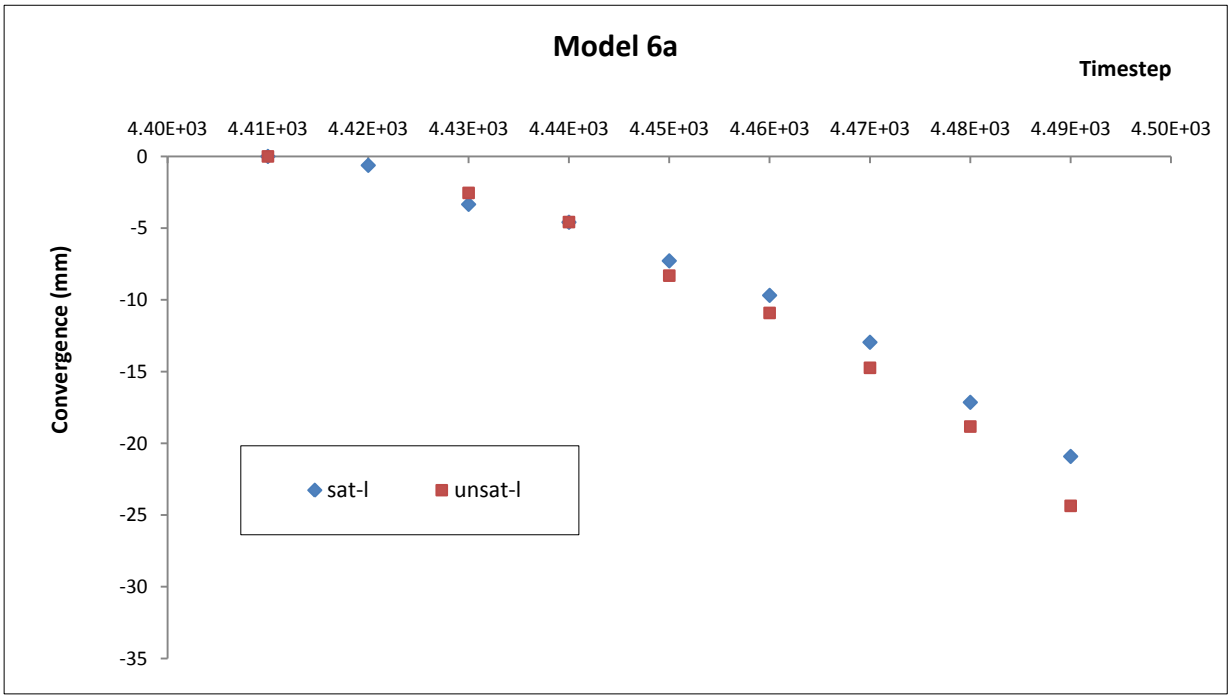

Figure 7.43 Effect of water on convergence on the middle of excavation on the left-hand side of structure with real fault

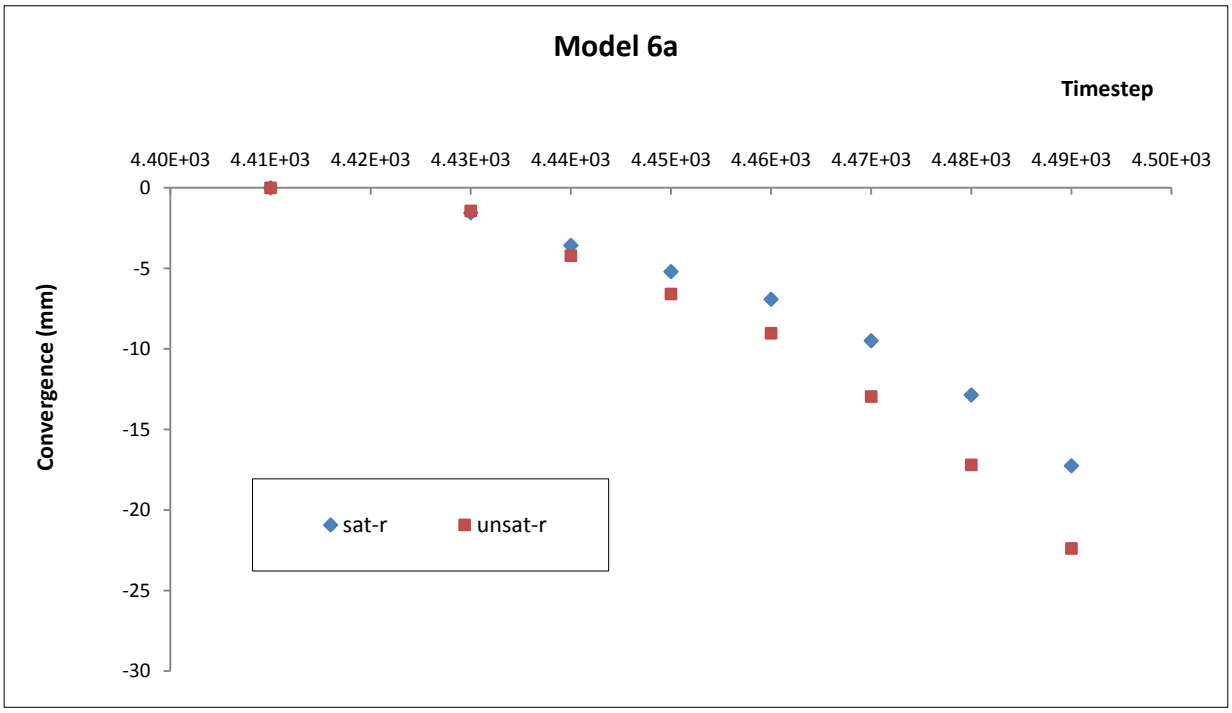

Figure 7.44 Effect of water on convergence on the middle of excavation on the right-hand side of structure with real fault

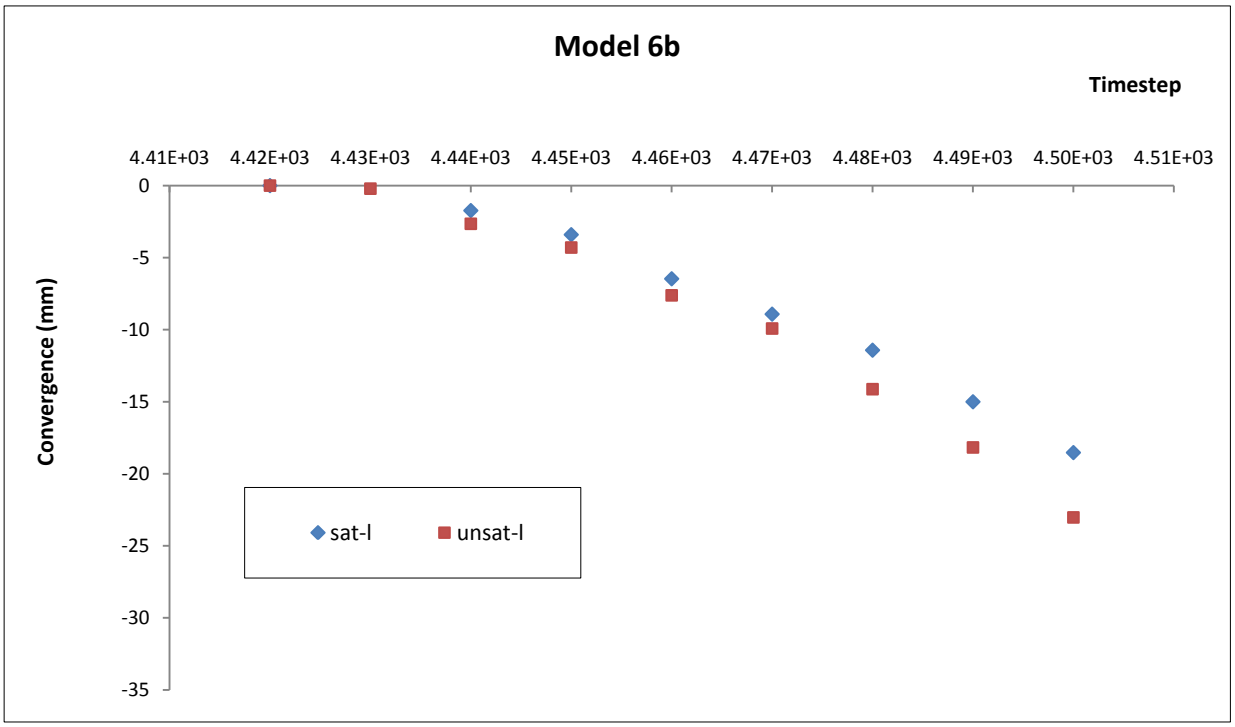

Figure 7.45 Effect of water on convergence on the middle of excavation on the left-hand side of structure with glued fault

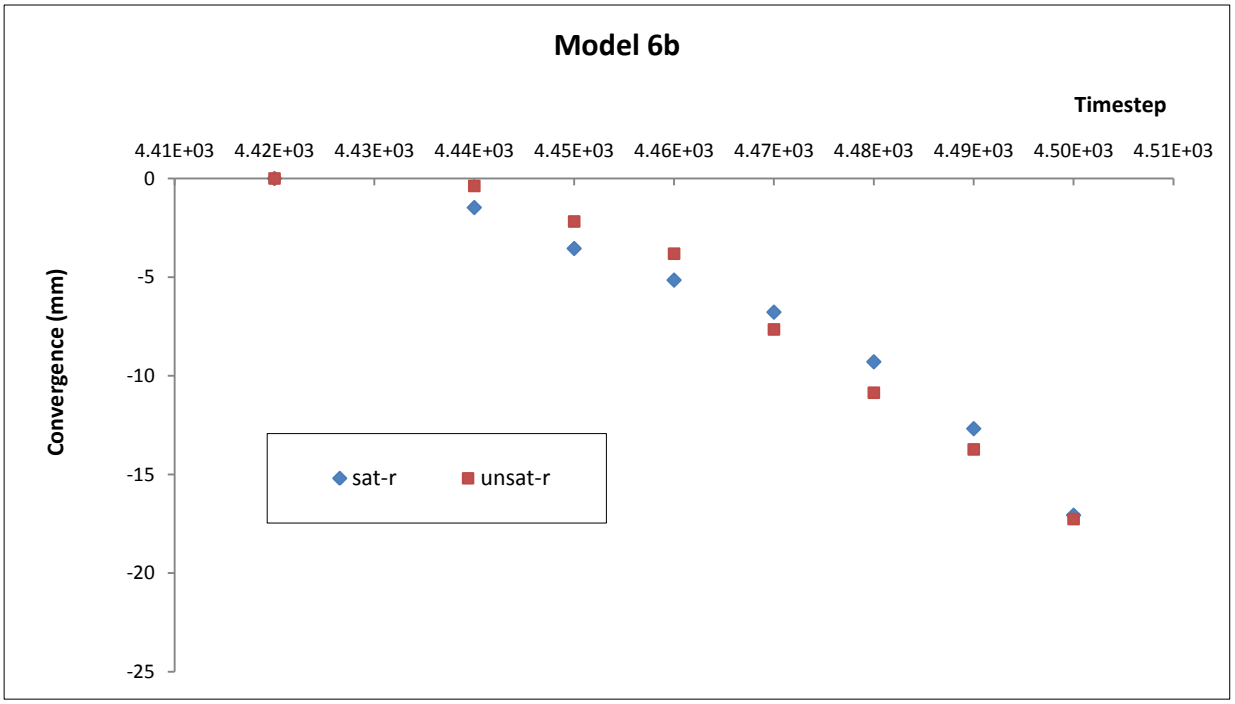

Figure 7.46 Effect of water on convergence on the middle of excavation on the right-hand side of structure with glued fault

The plots of convergence exhibit the dependency of convergence of mine workings on pore pressure. Whilst continuous structure-related convergence of workings occurred gradually and linearly, workings in discontinuous structures closed up gradually and smoothly after the potash extraction. Pore pressure slightly decreased the magnitude and rate of convergence of openings with no correlation of the nature of the fault.

Despite convergence of underground openings primarily depends upon the behaviour of the immediate roof, the pre- and post-excavation stress, particularly the horizontal stress, might have also controlled the closure of the workings in unsaturated structures (Section 2.3.2). As matter of fact, horizontal stress acting around the opening induces either slabbing and plastic flow of the mine roof or mine floor heave; sometimes both. In case of low stress, a sliding of delaminated roof is experienced. Whereas in the opposite (i.e. high stress), buckling of roof over the span occurs.

In saturated structures however, pore pressure might have carried part of the weight of the overburden alleviating the stress acting on both immediate roof and floor. Pore pressure might have also absorbed the mining-induced horizontal stress within the structure, resulting in a low magnitude of convergence of workings. The slight high magnitudes of convergence on the middle of excavation on the left-hand side could be attributed to the geometrical position of the fault relative to the excavations.

7.6.3 Relationship with subsidence

Saturated and unsaturated states-related subsidence patterns for the continuous structure are plotted in Figures 7.47-49. In discontinuous structures, patterns were plotted for points on the middle of cross-section and on both hand-sides of the fault (Figures 7.50-59).

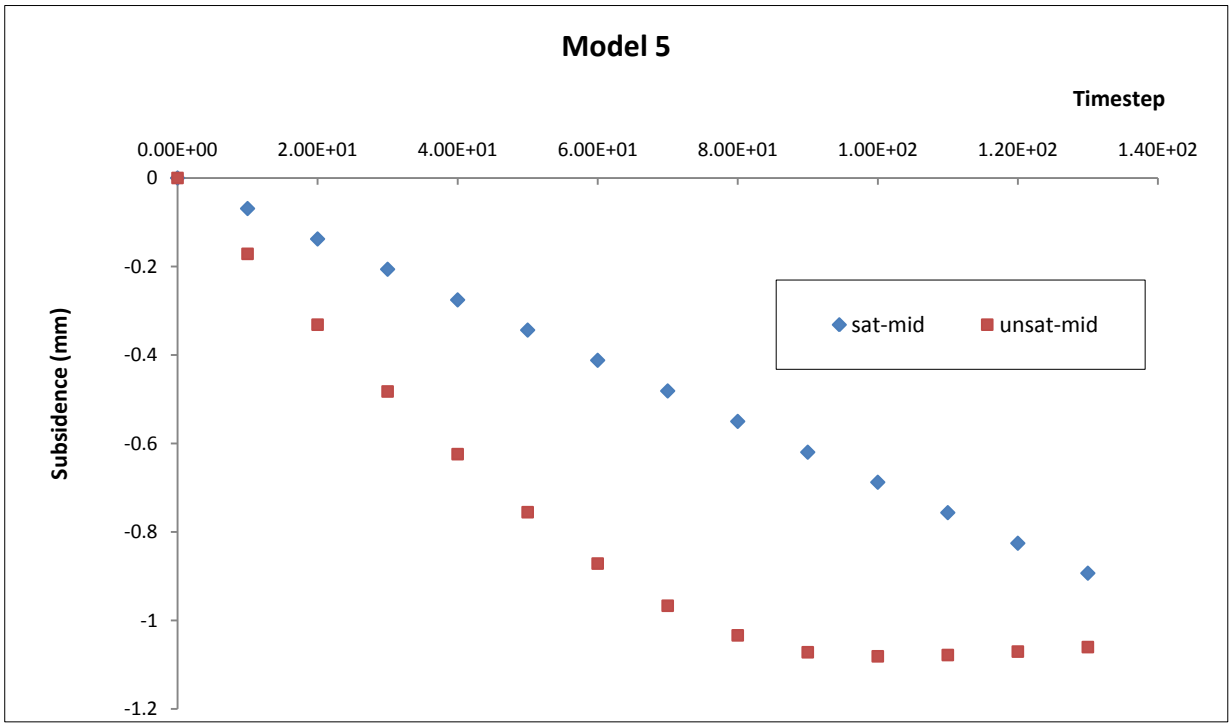

Figure 7.47 Effect of water on subsidence on the middle of cross-section of continuous structure

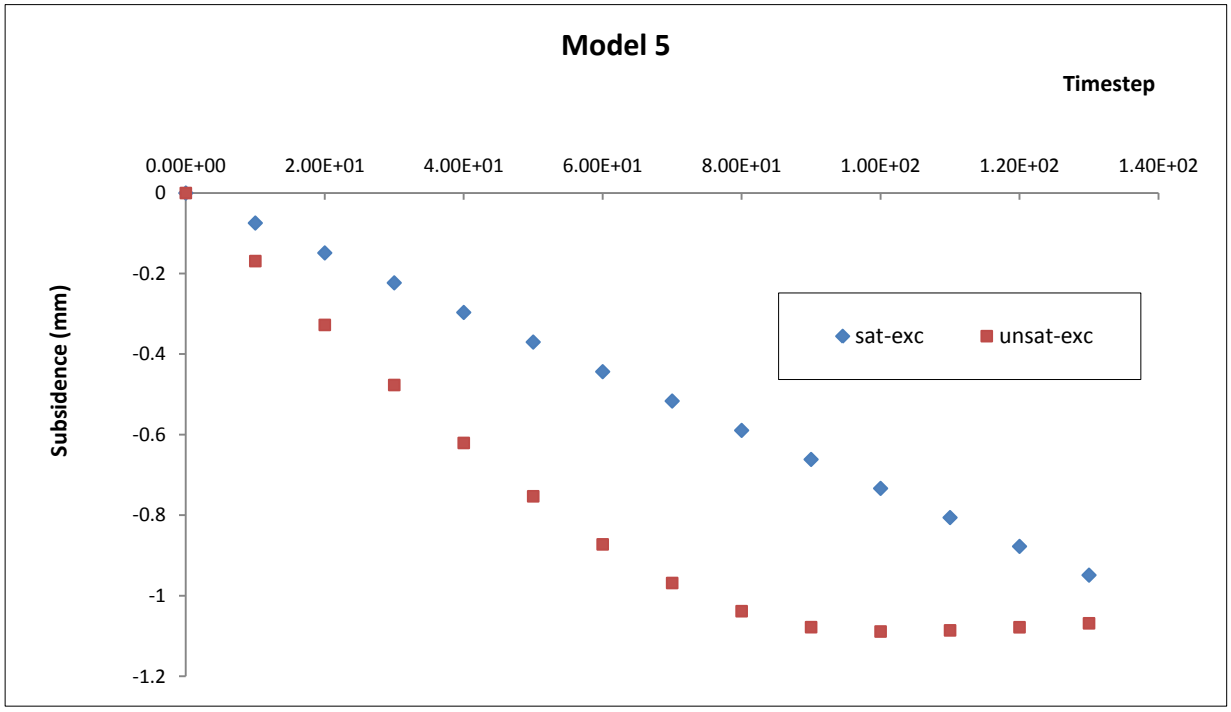

Figure 7.48 Effect of water on subsidence on the top of excavation in continuous structure

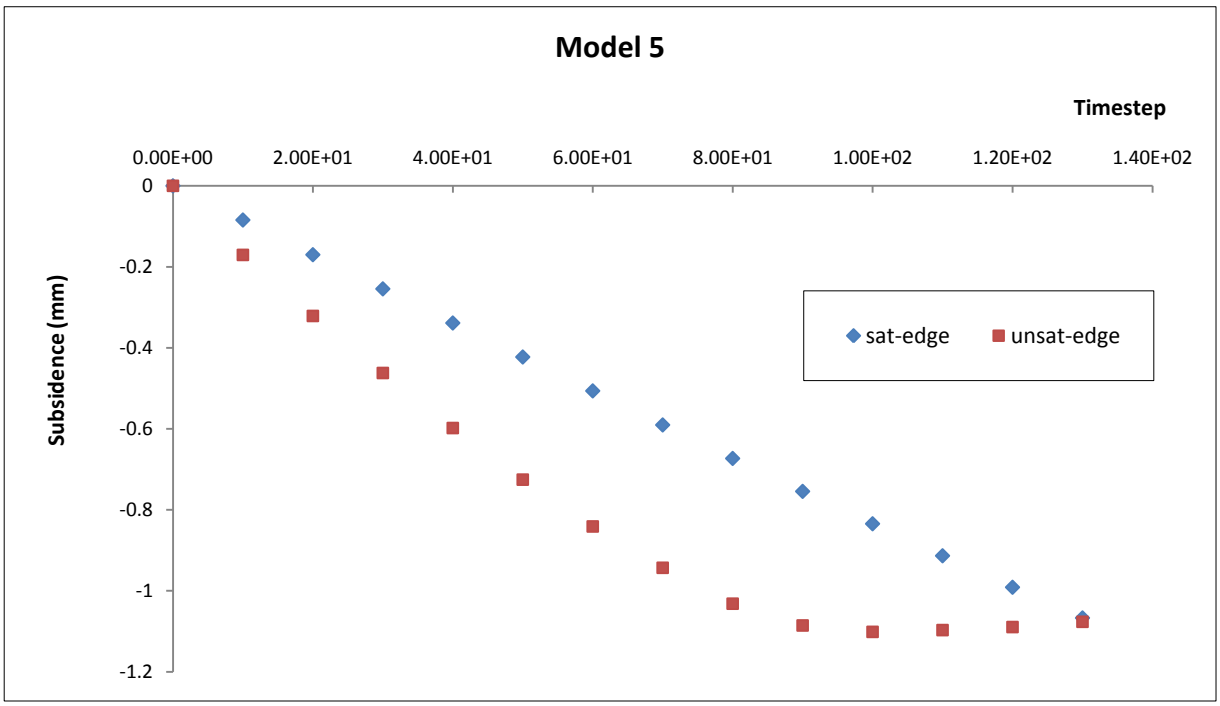

Figure 7.49 Effect of water on subsidence at the edge of cross-section of continuous structure

Figures 7.47-49 illustrate the effects of water on the patterns of ground subsidence. The water disrupts the smooth occurrence of ground deformation at the monitored points in the unsaturated structure and markedly decreases the magnitudes and rates of subsidence. This suggests that pore pressure supported the stress exerted by the overlying strata avoiding compaction and compression of matrix of rock and consequently, reduction of bulk volume of reservoir volume. The water also disrupts the symmetrical occurrence of ground deformation and decreases the magnitude of subsidence from the centre to the edge of cross-section than in unsaturated structure.

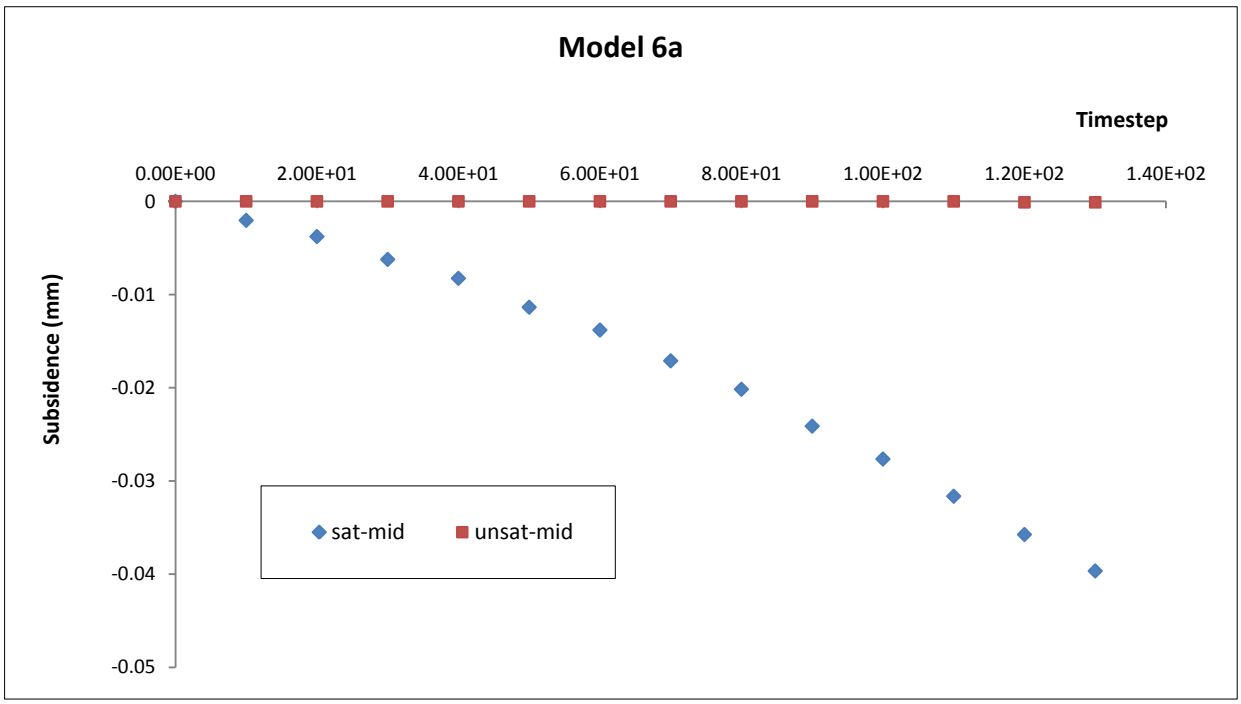

Figure 7.50 Effect of water on subsidence on the middle of cross-section of structure with real fault “a”

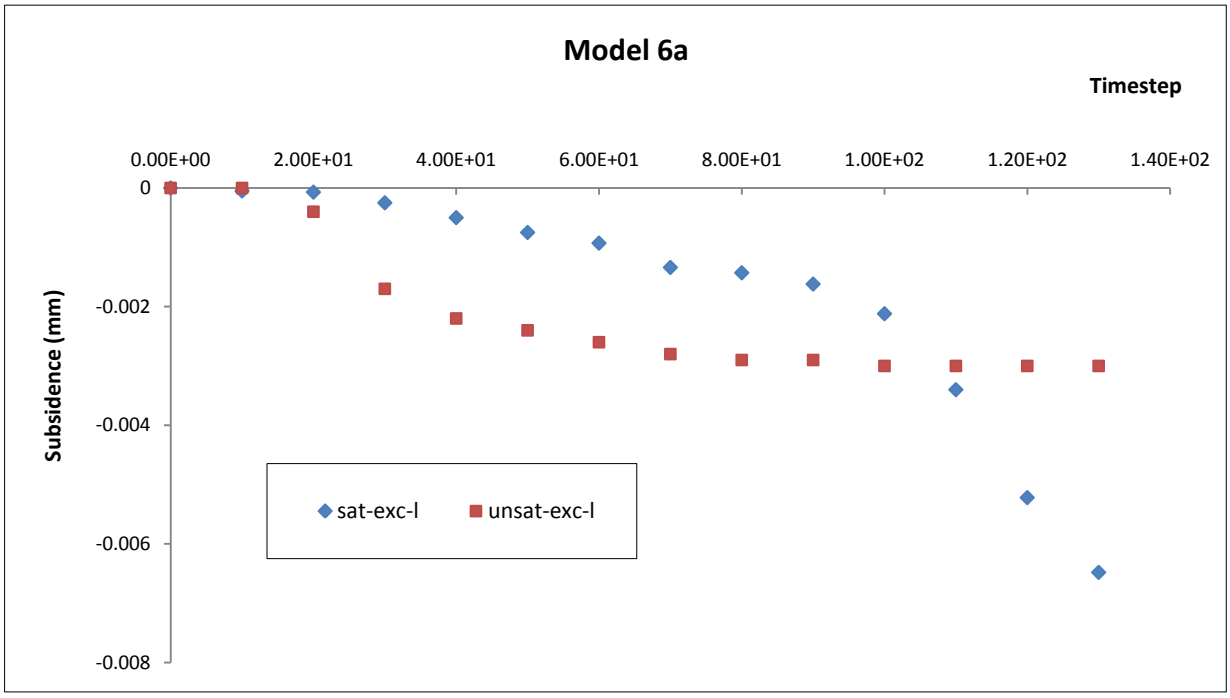

Figure 7.51 Effect of water on subsidence on top of excavation on the left-hand side of structure with real fault “a”

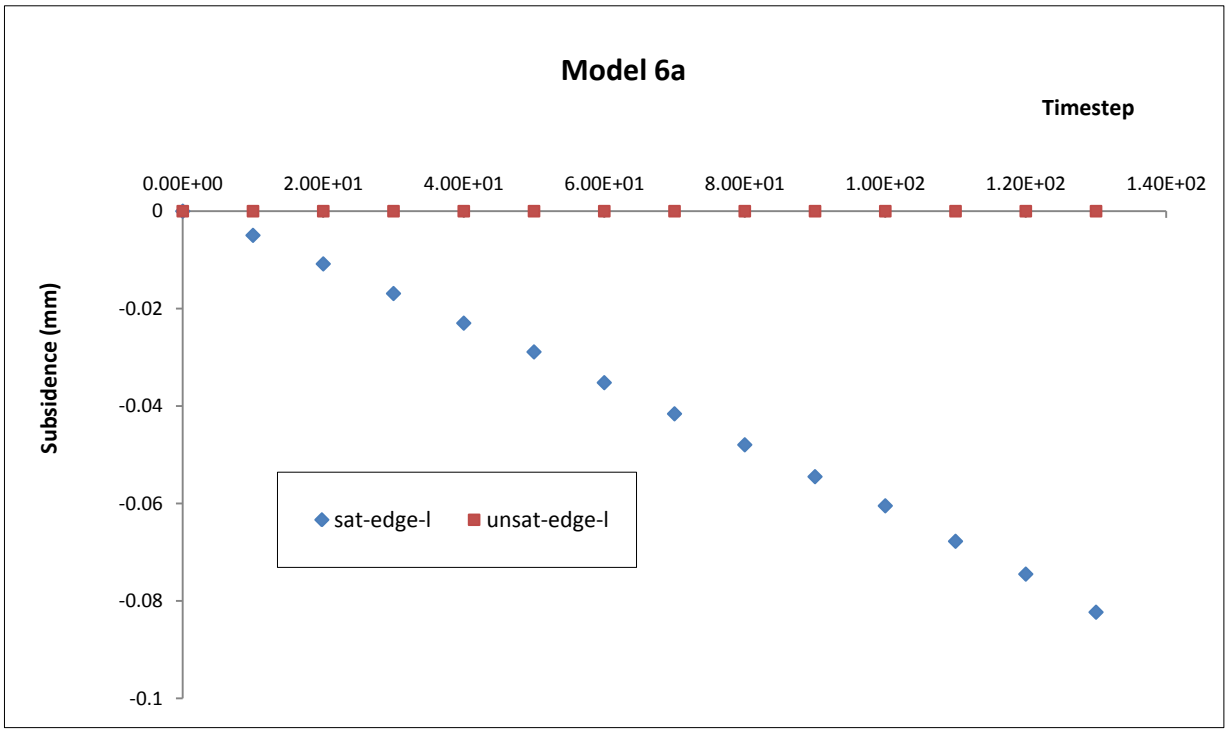

Figure 7.52 Effect of water on subsidence at the left-hand edge of cross-section of structure with real fault “a”

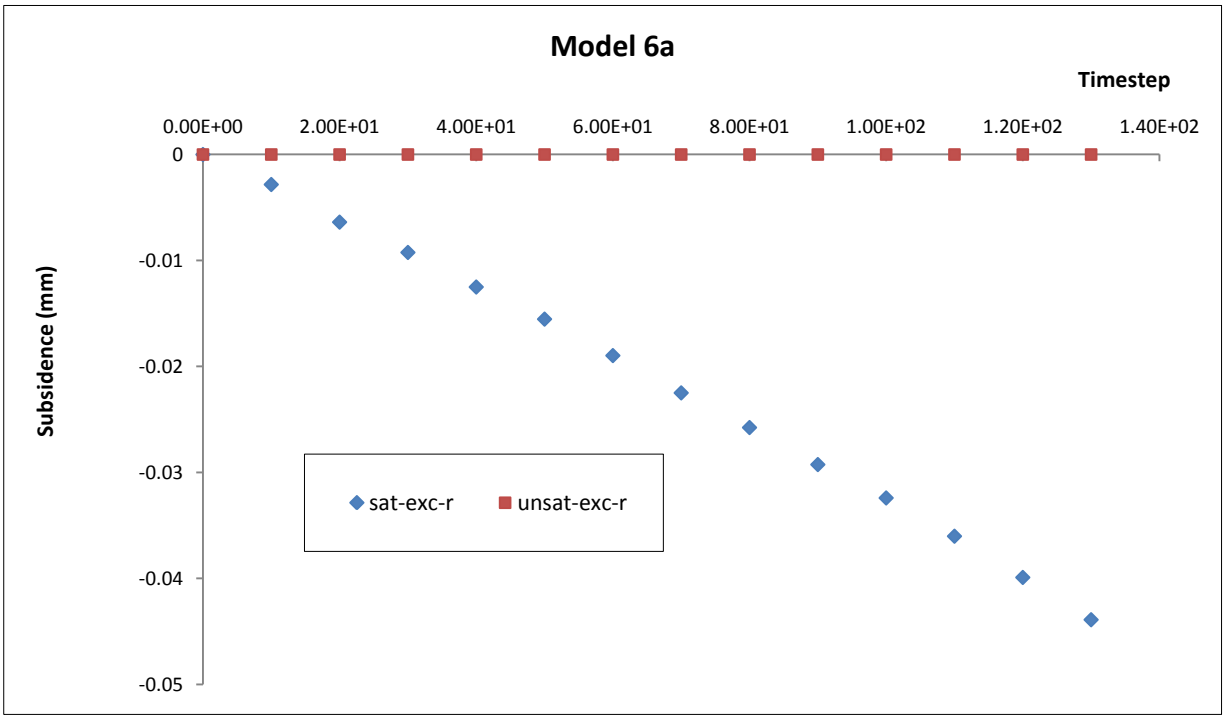

Figure 7.53 Effect of water on subsidence on the top of excavation on the right-hand side of structure with real fault “a”

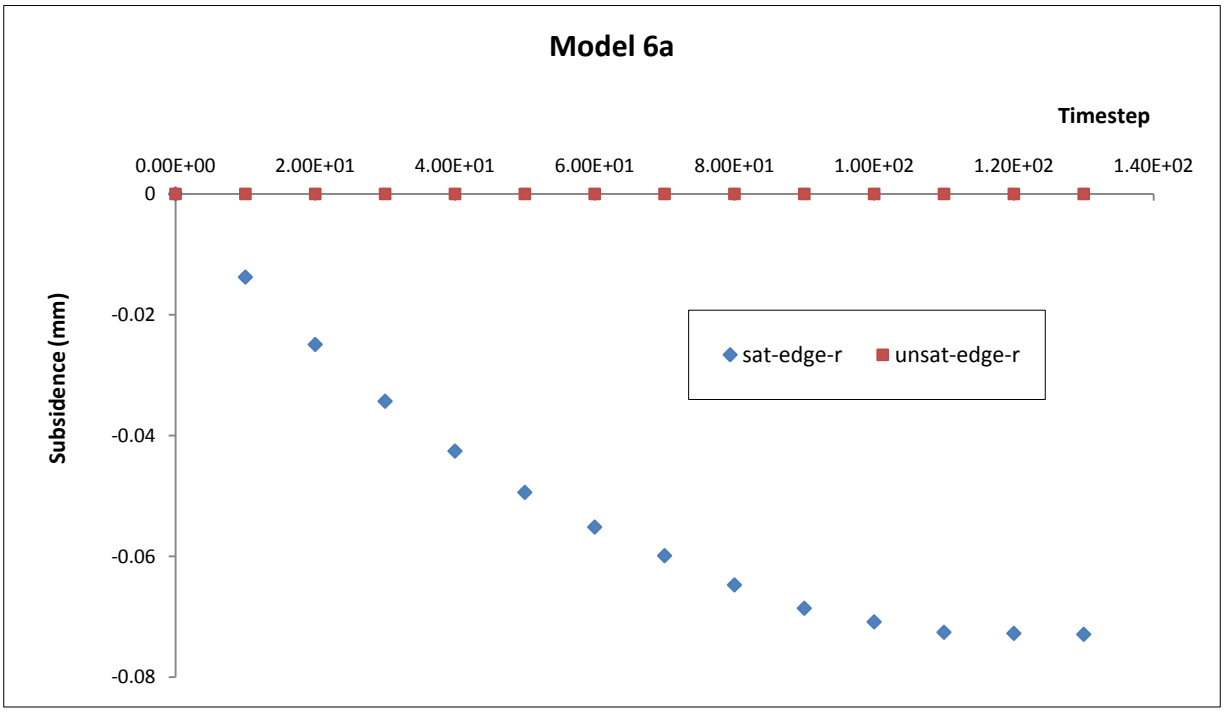

Figure 7.54 Effect of water on subsidence at the right-hand edge of structure with real fault “a”

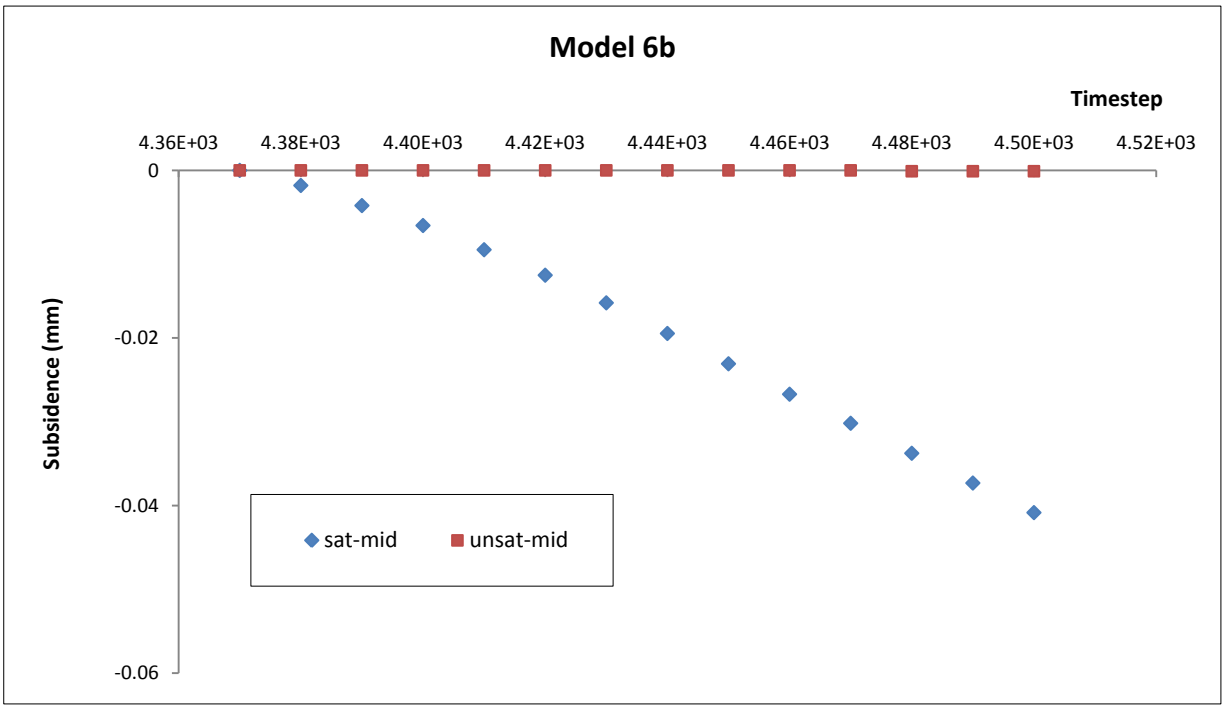

Figure 7.55 Effect of water on subsidence on the middle of cross-section of structure with glued fault “b”

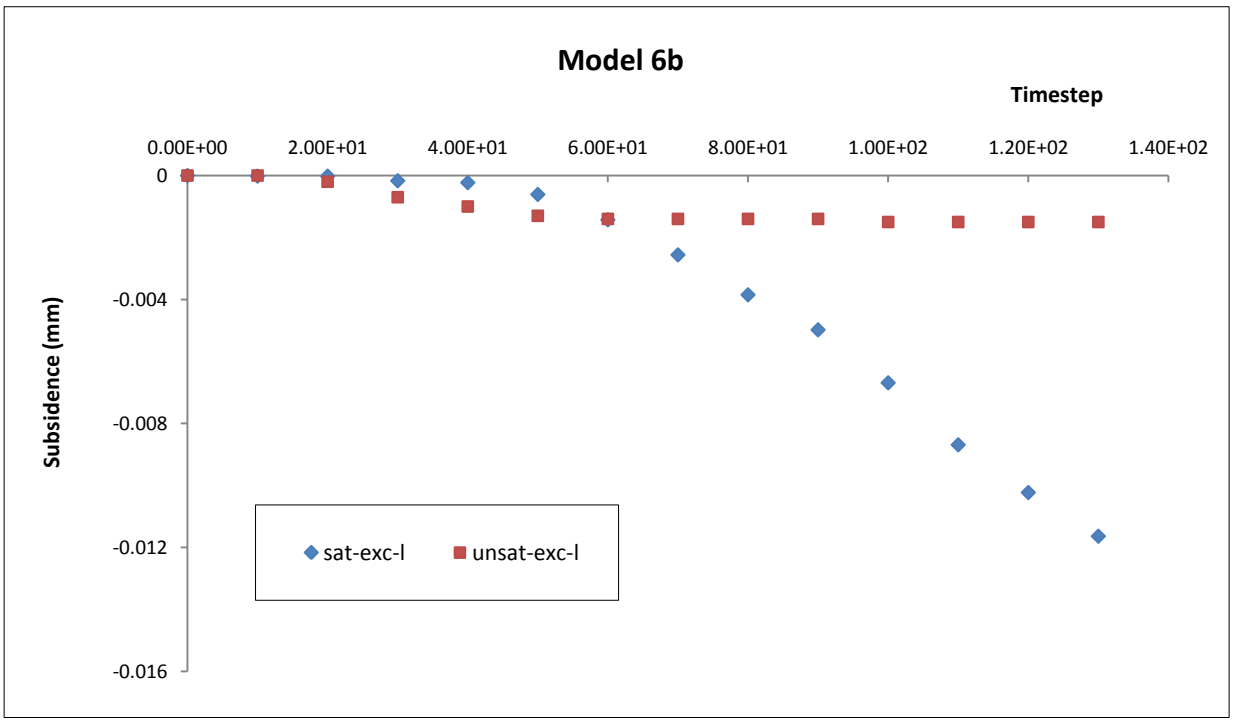

Figure 7.56 Effect of water on subsidence on top of excavation on the left-hand side of structure with glued fault “b”

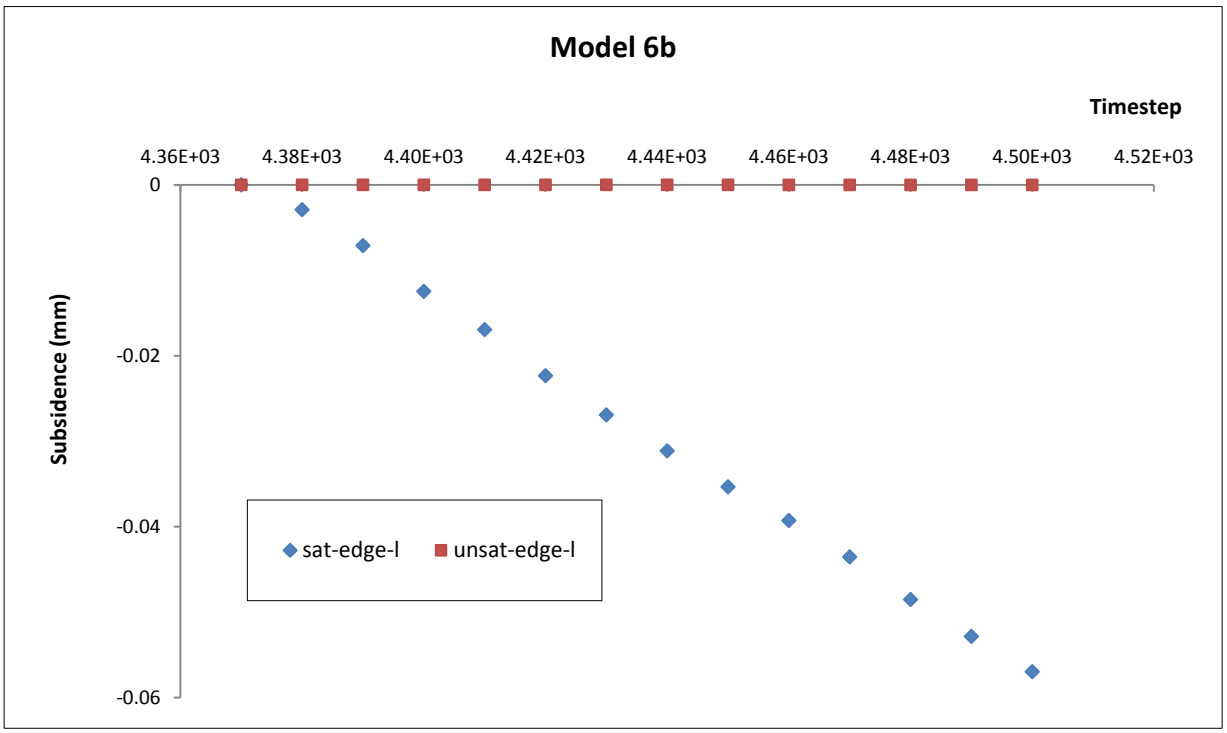

Figure 7.57 Effect of water on subsidence on the left-hand edge of cross-section of structure with glued fault “b”

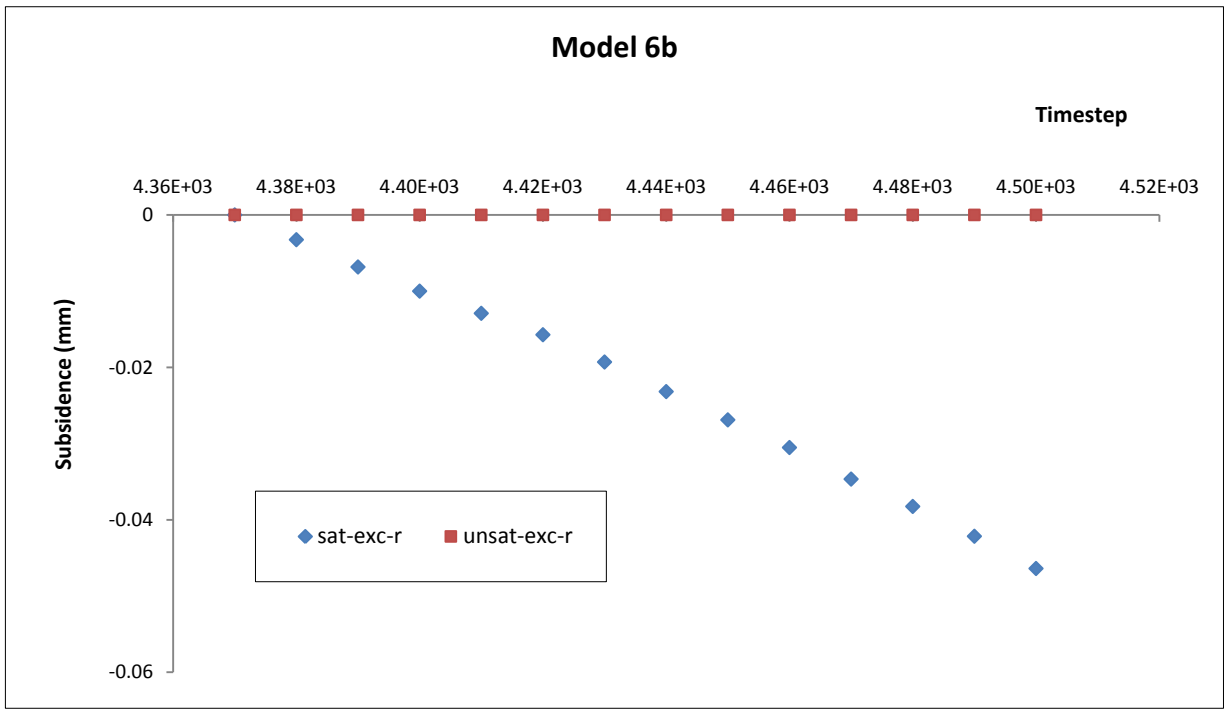

Figure 7.58 Effect of water on subsidence on the top of excavation on the right-hand side of structure with glued fault “b”

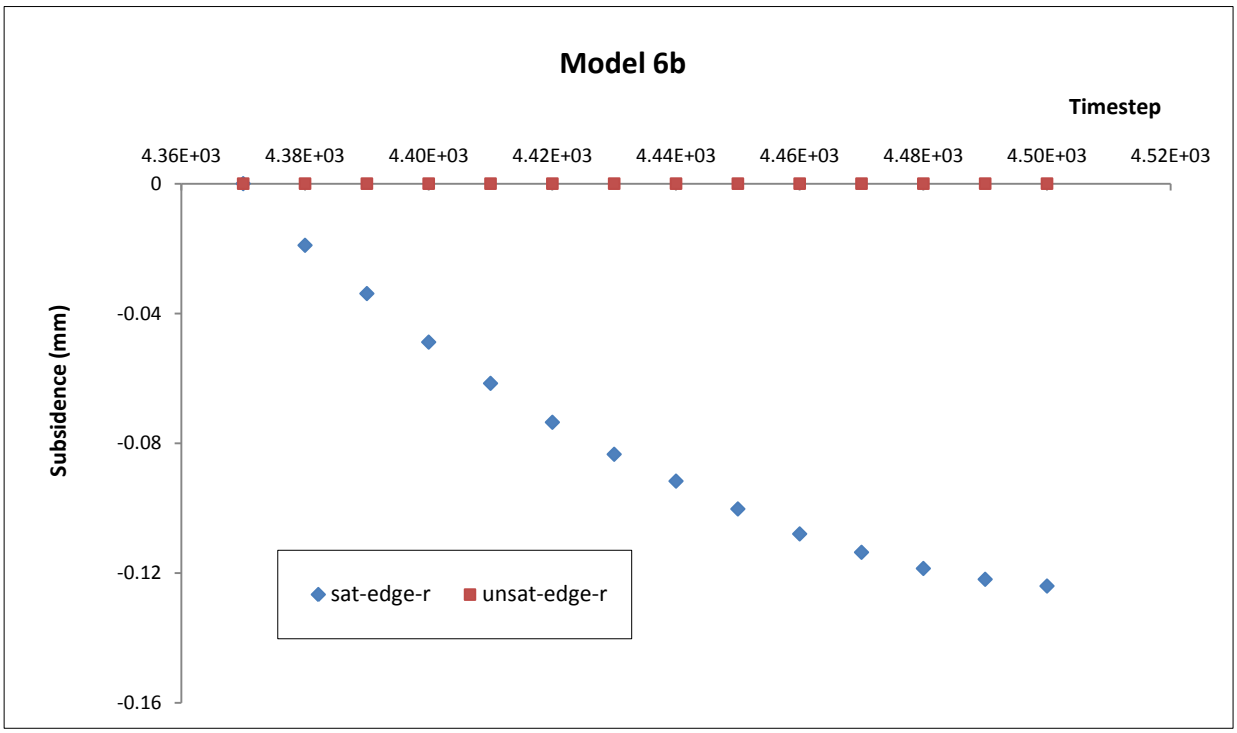

Figure 7.59 Effect of water on subsidence on the right-hand edge of cross-section of structure with glued fault “b”

Figures 7.50-59 portray the effect of water upon the patterns, magnitudes and rates of ground subsidence at the monitored points in the discontinuous structures. The water induces smooth and gradual patterns of subsidence at some of the points than the linear ones which occur at most of the monitored points in the unsaturated structure. For the magnitudes and rates of subsidence, they increase as a result of water regardless whether the fault is real or glued. Where non-linear movement occurs particularly on the top of left-hand side excavation, the water increases the rate of subsidence (Figures 7.51 and 7.56).

Pore pressure affects the strength of the structure and eases its failure along the fault, resulting in exacerbated deformation propagation upwards towards the surface leading to ground subsidence increase in saturated structure than in unsaturated structure.

The linear trend of subsidence with null magnitude observed at most of the monitoring points in the unsaturated structures may indicate the magnitude of deformation might have been lower to be perceptible on the surface. Whereas, the noticeable movement recorded on the top of excavations on the left-hand side is probably the result of the fault which might have exacerbated ground deformation at these points.

7.7 Summary and conclusion

A numerical analysis on the dependency of stress and displacement distribution, total closure and subsidence upon lithology, fault and water has been carried out using FLAC 2D models developed for the purpose (Chapter 6.). The models sensitivity has also been analysed.

Patterns of stress and displacement indicate a gradient distribution of stress and displacement within structures as a function of the lithological heterogeneity. In contrast, the results show that a geological fault has limited effect on stress and displacement redistribution patterns.

Patterns of convergence are not dependent upon the lithological heterogeneity but they are a function of the geological fault. Mine workings in continuous structures close gradually and linearly whereas, closure of workings in discontinuous structures occurred smoothly. Unlike convergence patterns, subsidence patterns are driven by both lithology and geological fault. The analysis predicts linear and non-linear ground subsidence for both continuous and discontinuous structures, depending on the monitored point. Pattern of measured subsidence show curved smooth trend at the monitored point.

As far as strata parameters variation (i.e. stiffness and strength) is concerned, the analysis has shown evidence of sensitivity on displacement within the structure and a limited sensitivity on the maximum stress.

In terms of magnitudes, predicted ground subsidence related to both unfaulted and faulted structures underestimates measured levelling technique-based subsidence. More so, unfaulted structures-associated predicted subsidence magnitudes are slightily higher than those of faulted structures.

Pore pressure induces linear patterns of subsidence in continuous structures and non-linear patterns in discontinuous structures particularly at the right-hand edge of the cross-section. It has the effect to increase magnitudes and rates of subsidence in discontinuous structures while decreasing the same in continuous structures.

As for the convergence of mine workings, the effect of water in continuous structures is to produce a linear trend. However, the trend turns to be curved and smooth in discontinuous structures. In both cases, resulted magnitudes and rates of convergence of mine workings decrease.

The analysis also shows that workings convergence is not sensitive to the lithological heterogeneity though the magnitude is sensitive. The patterns of subsidence are not sensitive to the variation of the material parameters and patterns of subsidence exhibit linear trend. The magnitudes and rates of subsidence are sensitive to the variation of materials and they increase with the increase of reduction factor.

Chapter 8
Discussion of the results

8.1 Introduction

In this chapter, we discuss variables which affect the patterns of stress and displacement distribution during the extraction of potash at Boulby mine. The combination of the behaviour of the materials and the more realistic FLAC 2D modelling tool of the Finite Difference Method permitted to quantify the effects of lithology and geological fault upon the stress and displacement and resulting subsidence.

8.2 Stress and displacement vs. lithology

The mining activity at Boulby mine is undertaken in a stratified rock and the mechanics of rocks which compose the structure govern the distribution and magnitudes of the induced stress and displacement. The distribution and magnitudes of stress and displacement are also dependent on the density (i.e. pressure) of strata and to some extent on the pore pressure of the brine within the Sherwood sandstone. Analysis of structures has enabled conclusions to be drawn over the effects of lithology and heterogeneous properties on the magnitudes of stress and displacement induced by the mining activity.

Potash excavation resulted in gradient of stresses and increase of stress acting around excavations in all structures than the virgin stress (Table 8.1) probably due to the stress used in the analysis (Table 6.2-6).

Based on the magnitudes of stress and displacement in Figure 7.6 and Table 8.1 patterns of stress and displacement distribution (Figures 7.1-5) may be arranged into three main groups. The first group is constituted of model 1 (Figure 7.1), the second

group comprises model 2 (Figure 7.2), model 3 (Figure 7.3) and model 4 (Figure 7.4) with equal values of stress and displacement, and the third group is that of model 5 (Figure 7.5).

Mining potash induced similar magnitudes of total and maximum vertical stresses in all models of the three groups. However, despite the similarity in the stress magnitudes mining potash induces different values of total displacement in the three groups with low value in model 1 of the first group. The highest magnitude of displacement occurs in model 5 of the third group (Table 8.1).

Table 8.1 Summary of magnitudes of stress and displacement as a function of the lithological heterogeneity

Models	Total vertical stress (MPa)	Total virgin stress (MPa)	Maximum vertical stress (MPa)	Virgin stress at seam level (MPa)	Total vertical displacement (m)
Model 1	319	133	63	29.9	0.408
Model 2	319	152.9	63	30.4	0.816
Model 3	319	178	63	30.2	0.816
Model 4	319	188	63	30.1	0.816
Model 5	319	218.7	63	30.4	1.359

The high density and thickness of Lias and Sherwood sandstone layers in the overburden might have played a major role in sustaining the stress generated by the removal of potash and therefore reducing failure and deformation of the structure. The cohesionless and frictionless state of Lias may have no or limited effect on the stress and displacement redistribution. Mining-induced shear stress (i.e. closure and damage) and flow of Carnalite marl into openings creates voids above excavations. Due to its thickness but also density, alternating tensile and compressive stresses acting on the hangingwall induced regions of tensile and compressive deformations within the overburden as displayed by patterns of displacement in Figure 7.1. Consequently, the lower part of the Sherwood sandstone fails in shear creating voids within the stratum. With time the overlying strata gradually fails downwards under its own weight leading to

the stress gradient with maximum stress around excavations higher than the stress used in the analysis (Table 8.1).

Patterns of stress in Figures 7.2-5 of model 2, model 3, model 4 and model 5 are similar to that associated with model 1. Unlike the similarty of stress patterns, displacement patterns are different and well defined in models of all the groups. Given the similarity of strata constitutive behaviour in the hangingwall of these structures and modelled as Mohr-Coulomb materials, the thickness and most importantly the density (i.e. pressure) of the strata again dictate the response of structures to mining. The introduction of Mercia mudstone in model 2 above the Sherwood sandstone increases the heterogeneity of the structure and the stress within. Consequently, resisting forces to mining-induced stress decrease resulting in structure prone to failure and deformation. Potash mining-induced shear around excavations causes failure of Sherwood sandstone under gravity and the weight of the overlying strata as Carnalite marl flows into excavations. This deformation gradually propagates towards surface through the Mercia mudstone and Lias strata resulting in the increase of magnitude of total displacement within the structure. However, because of the density and the mechanics of Mercia mudstone and Lias strata mining-induced stress was insufficient to exceed the strength of these strata. As a consequence, magnitude of total stress similar to that in model 1 is induced (Figure 7.2 and Table 8.1).

Stress and displacement distribution process in model 3 and model 4 is analogous to that in model 2. Sherwood mudstone incorporation in model 3 and Rheatic in model 4 increases the stress within the structures and their heterogeneity. The deformation that initiates at seam level in the two structures propagates towards the upper strata and the surface inducing values of total displacement equal to that induced in model 2 but twice that induced in model 1. As in model 2, given the low mining-induced stress to weaken the overburden strata, stress within the structures builds up to value comparable to stress in model 1 and model 2 with maximum stress higher than the stress at seam level (Table 8.1).

The third group of patterns of stress and displacement is within high magnitude deformation was induced. The excavation of potash resulted in well defined patterns of

displacement than in models in the two previous groups (Figure 7.5) as a result of the increase of heterogeneity hence, deformability and strength of the overburden strata despite the increase of the density of the structure.

Increase of structure heterogeneity due to Anhydrite incorporation in model 5 above the Carnalite marl weakened the structure, particularly the immediate roof zone. The Anhydrite stratum controlled the stress and displacement distribution within the structure though this distribution is somewhat similar to those of models in the second group. Flow of Carnalite marl into the openings led to development of shear stresses (i.e. bending) on the Anhydrite beam. With the loss of support below the Anhydrite, shear stresses might have concentrated onto the base of the beam. Owing to its high density, the Anhydrite beam acted against Carnalite marl downward movement and constrained this latter to detach from its host. Being highly deformed, Carnalite marl flowed non-linearly into excavations. As a result, the immediate materials distressed and deformed, leading to total displacement magnitude increase and the building-up of stress to that in the other structures (i.e. models 1-4) (Figure 7.6 and Table 8.1). Being unsupported, the hangingwall from the Anhydrite base gradually fell as intact block under its own weight. A shallow and flat affected area develops over the entire cross-section on the surface (Figure 7.5).

8.3 Stress and displacement vs. geological fault

Natural discontinuities (e.g. fault) behaviour is dominated by two main mechanisms: the sliding on the inclined surface at low normal loads (or stresses) and the inhibition of dilation and shearing along the geological fault at higher normal stresses. Both mechanisms develop in varying proportions during the deformation of structure (Brady and Brown, 2006; Jeremy, 1985). Relative movement of the two sides of fault is either elastic or nonelastic that is, the fault dilates at the onset of slip (Itasca, 2005).

Although being a plane of weakness, the fault has limited effect on the distribution of stress and deformation within the structure for both natures of fault (i.e. unglued and glued fault). Stress and displacement are linearly distributed between

excavations horizon and surface with a gradient akin that in continuous structure (i.e. model 5). The only major effect of the fault on the stress patterns is the narrowing of the stressed region above excavations. The fault also limited the tensile deformation of the structure within the saturated Sherwood sandstone region, as it occurred in continuous structure.

Unlike the stress and displacement distribution, the fault significantly affects the magnitudes of stress and displacement. The fault decreases the magnitudes of maximum stress and total displacement than in the continuous structure (Figure 7.9). Geological fault stiffness and strength might be the primarily controlling factors of the response of structure to mining. Neither sliding of blocks of structure each other nor movement along the fault occurred to induce structure deformation as mining-induced stress may have not exceeded its stiffness and strength. The high density and importantly the behaviour of the strata might have also contributed to the behaviour of the undermined structures. As matter of fact, the strain-softening nature of strata in the immediate roof suggests that deforming materials in this region will evolve from brittle softening as its cohesion decreases to gradual softening with the decrease of its internal friction (Section 3.6.1.3). Such apparently time-dependent process needs stress to build-up for the onset of deformation and failure of materials in the zone. This movement that initiates at the seam horizon gradually propagates upwards towards the surface through the upper strata. Furthermore, because materials in the intermediate and main zones (Kratzsch, 1983) are Mohr-Coulomb materials, this requires material shear strength to be exceeded for plastic deformation. This eases propagation of deformation upwards towards surface through materials in the surface zone of the structure. Moreover, although cohesionless and frictionless (i.e. prone to deform under low stress) strata in the surface zone of the structure are dense and thick. Again sufficient stress is needed to weaken these materials hence to effortlessness the transmission of the bottom-initiated deformation to the surface.

Hence, deformation and failure of materials within structures require stress to build-up to exceed both materials strength and fault strength and stiffness. This is obviously a long-term process. However, given that the current analysis of stress and

displacement is based on a short-term measurement of mine workings convergence mining-induced shear stress may have been insufficient to exceed the shear strength of materials and also the stiffness and strength of the fault to cause deformation and failure of materials in the overburden. Consequently, low magnitude of stress and displacement are induced within the structure than in continuous structure (Figure 7.9). Nevertheless, being highly stressed the overlying strata gradually failed as intact blocks under their own weight increasing the stress magnitudes around excavations hence, the whole structure total stress than the stress used in the analysis (Figures 7.7 and 7. 8, Table 8.1).

An alternative explanation could be the fault acted as stress and deformation absorbent. In fact, mining-induced shear stress might have exceeded the strengths of strata and also the strength and stiffness of the fault and induced deformation of structure. Additionally, sliding and movement of blocks of structures along fault might have occurred and also exacerbated deformation and failure of the structures. However, because of separation which eventually may have occurred along, the fault probably absorbed part of the induced stress and deformation (The Geological Society, 2008). As a result, magnitudes of stress and displacement in discontinuous structures decreased.

8.4 Patterns of convergence - lithology and fault relationship

8.4.1 Relationship with lithology

Lithology has no control on the patterns and rates of convergence of mine workings in continuous structures. Convergence of workings on the middle of the excavations in the five continuous structures occurs gradually and linearly at similar rate (Figure 7.12) despite the differences in the lithology accordingly, the mechanics of layers in the five models. Unlike the patterns, the magnitudes of convergence in the five models are slightly different. This would suggest that the workings behaviour has been driven by a factor other than the lithology and mechanics of the structures.

The structures of the five models consist of different materials which would respond in different manner (Table 6.13) to mining. Given that convergence of the excavation in the five structures occurs at similar rate this implies that convergence of mine workings was not governed the mechanics of the overburden.

Furthermore, because factors which may also have control on convergence of workings, including mine layouts (i.e. yield pillar width, abutment pillar, and roadway horizontal size), width/depth ratio and the floor rock mechanics in all five models are similar, mine workings convergence is mainly driven by the behaviour of the immediate roof. But, the immediate roof in models 1-4 consists of Carnalite marl and potash rocks (Tables 6.2-5) whereas in model 5 the immediate roof is made of Carnalite marl, potash rocks and part of Anhydrite rock (Table 6.6). The Carnalite marl which mostly constitutes the immediate roof in all models and whose thickness varies in model 5 is a weak rock prone to flow into excavations as a result of closure. Therefore, convergence of workings is primarily governed by the Potash protective layer left in place. With the loss of support, the 2 m of Potash protective layer deformed elasto-plastically in shear under its own weight closing up the excavations at similar rate.

8.4.2 Relationship with geological fault

The behaviour of workings underground mines in a discontinuous medium is a function not only of the Potash protective layer but also a function of the mechanics of the fault. Given the comparable characteristics of the rocks in the immediate roof and on floor in both continuous and discontinuous structures the fault, including its nature has controlled the convergence of the mine workings.

The fault decreased the magnitude and rate of convergence of workings in spite of its nature. It induced relatively smooth patterns of convergence of workings instead of the linear convergence patterns in continuous structures. In both cases of faults, convergence of excavations occurred at rather similar rate though the rate of convergence of the left-hand side excavation, particularly for the real fault, is slightly higher than that of the excavation on the right-hand side. A stressed region is induced

around the openings and in the immediate roof as this latter carries the overburden load but also a result of pressure arch. Consequently, low magnitudes of convergence are recorded at the two excavations (Figures 7.13-14).

An alternative explanation is that owing to its position above and up to the potash, the fault might restrain Carnalite marl to readily flow into the excavations a consequence of loss of support. Subsequently mine roof hence, mine workings closed up at low rate regardless the nature of the fault (Figures 7.13-14).

8.5 Ground subsidence-lithology and geological fault relationship

8.5.1 Relationship with lithology

Ground deformation in continuous models occurs at different rates (Figures 7.20-22) with the smallest rate of movement in model 2 and the highest rate of deformation in model 1 and model 5. The rate of movement in model 3 ranges between the rate of movement in models 1 and 5 and that in model 4.

Apart from movement in model 1 and model 4, ground deformation occurs gradually and linearly. Ground deformation in model 1 occurs smoothly at all the three monitored points. In model 4, two types of movement are recorded: a gradual and linear movement occurring at the edge of the cross-section and a smooth movement with increasing rate occurring on the middle of cross-section and the top of the excavation. The rate of deformation on the middle of cross-section is relatively similar to that on the top of excavation owing probably to the close proximity of the two points. An unexpected and surprising effect of lithology on ground subsidence is the increase of magnitude and rate of movement from the middle to the edge of the cross-section in model 3 and model 5. In the two others models however, the rate of movement gradually decreases from the middle to the edge of the cross-section (Figures 7.20-22). The constitutive behaviour of the materials within the structures might drive ground movement at the monitored points in these models.

Carnalite marl in models 1 and 2 flows into the openings as a result of loss of support. Consequently, the excavations closed up and shear stress may develop on the saturated sandstone. As the material weakens due to the brine pressure, the Sherwood sandstone fails under gravity in the attempt to fill up the voids created by the closure of excavations, and compresses under the weight of the overburden. Being cohesionless and of low friction, the hangingwall Lias in model 1 failed into the voids created by the compression of Sherwood sandstone. A flat and shallow deformed area is formed on the surface over the entire cross-section. With the incorporation of the dense Mercia mudstone layer above the Sherwood sandstone, the density and heterogeneity of the structure (i.e. model 2) increase as a result, the deformational behaviour of the structure is affected. Additionally, owing to its high cohesion and friction the Mercia mudstone might constrain the deformation that initiates at the mining horizon to propagate upwards towards the surface despite the brine within the Sherwood sandstone. As a result, low magnitudes and rates of ground deformation are recorded on the surface of this model. No noticeable trough of subsidence or deformed area develops on the surface of this model despite the low magnitude of subsidence recorded at the monitored points.

The dense, cohesive and friction Sherwood mudstone below the Sherwood sandstone (Tables 3.2 and 3.3) in model 3 increases the density of the structure, affecting the mechanics of the structure as the heterogeneity of the structure increases. The removal of support to Carnalite marl results in the concentration of shear stress on the base of Mercia mudstone beam as Carnalite marl flows into the excavations. Deformation of material initiates and propagates towards the saturated sandstone stratum. As in model 2, the Sherwood sandstone alternatively dilates and compresses creating a void on its top leaving the hangingwall Lias unsupported. With time this layer gradually fails under its own weight at relatively high rate than in model 2 filling up the voids created below. A flat and slightly deep deformed area is induced on the surface.

The introduction of Rheatic layer in model 4 also increases the density and slightly the heterogeneity of the structure and governs deformation and ground movement of and within the structure. As for the Mercia mudstone in model 2, the

presence of Rheatic layer in model 4 prevents deformation from propagating upwards the surface therefore, decreases the magnitude and rate of ground deformation at the monitored points. Again no appreciable deformed area develops on the surface.

Despite the incorporation of Anhydrite in model 5 significantly increases the density and heterogeneity of the structure, the decrease of thickness of Carnalite marl highly controlled ground movement which occurred within the structure. Unlike in the previous four models, convergence of excavations results in a considerable flow of marl into the openings causing shear stresses to develop on the Anhydrite beam. These shear stresses build up onto the base of Anhydrite beam, and then propagate laterally and upwards the Sherwood sandstone through the Sherwood mudstone layer. Structure deforms and beds eventually separate leading to gradual failure of the saturated Sherwood sandstone and the overlying strata, resulting in the rather high magnitude and rate of subsidence, and the occurrence of shallow and flat deformed area on the surface.

The discrepancies in the patterns, magnitudes and rates of ground movement recorded at the monitored points illustrate the response of individual layers within the models to changes in stress regime as a result of mining. The density, the pressure and the lithology heterogeneity of the models, including the deformational behaviour of the layers governed the stress and deformation redistribution and so; the occurrence, magnitudes and rates of ground subsidence on the surface.

8.5.2 Relationship with geological fault

The magnitude and rate of ground movement over an excavation in a discontinuous rock are a function of the position of the monitored points on the ground surface and also the nature of the fault. Of both natures of fault, a glued fault considerably decreases the amount and rate of subsidence at all the monitored points (Figure 7.26).

The fault disrupts the symmetrical occurrence of subsidence with respect to the central axis of the structure and significantly decreases of magnitude and rate of ground

movement regardless its nature (Figure 7.24-25). It shifts the locations of high rate of subsidence and increases the amount and rate of subsidence from the centre to the edge of the cross-section as in continuous structures. As a consequent, high ground movements are recorded at edges of the cross-section than on the top of excavations in close proximity to the fault regardless the nature of the fault.

The excavation of potash results in unbalanced movement of hangingwall and footwall owing to the difference in their weights. In the case of glued fault, given its close proximity to the fault material above the excavation on the right-hand side fails under gravity at relatively low rate. This movement gradually propagates vertically and laterally upwards towards the top of excavation and the edge on this side. In contrast, material on the left-hand side fails at relatively high rate owing to its direct exposure to mining-induced shear stress. The fault acts as boundaries controlling the lateral extent of ground deformation and trough of subsidence. Deformation and failure of structure are constrained to grow more laterally, the path of least resistance upwards towards the left-hand edge of cross-section than vertically.

In the case of real fault however, high rate of movement occurs at both edges of cross-section despite the slight higher magnitude of movement at the right-hand edge. Being far away from the fault deformation, including shear deformation of blocks material and movement along the fault readily propagate laterally towards the edges of the cross-section. Consequently, high magnitudes and rate of ground subsidence are recorded at these points than at points on the top of excavations and in close proximity to the fault. This also explains the high magnitude and rate of subsidence recorded on the top of excavation on the right-hand side than that on the left-hand side of cross-section.

Dipping from top-left to bottom-right the fault adversely controlled the propagation of deformation upwards towards the monitored points and therefore, the magnitudes and rates of ground subsidence at these points. The discrepancies in the magnitudes and rates of movement recorded at the monitored points could be attributed to the nature of the fault.

8.6 Predicted versus measured ground subsidence

Predicted ground subsidence generally occurs gradually and linearly at most of the monitored points over the undermined area in both continuous and discontinuous structures. At some monitored points however, particularly those situated at the right-hand edge in discontinuous structures ground movement occurred smoothly with decreasing rate of movement. This pattern of movement also occurred on the middle of the cross-section and the top of excavation in model 4. In contrast, measured ground subsidence (Figure 7.28) exhibits curved and smoothed pattern of ground movement.

The discrepancies in the patterns of predicted and measured subsidence are also corroborated by the magnitudes and rates of movement. Numerical analysis predicted low magnitudes of subsidence for both continuous (Figures 7.29-31) and discontinuous (Figures 7.32-35) structures than the leveling measured subsidence.

For the measured subsidence, several factors are involved in the profile, magnitude and rate of subsidence. Some of such factors are: the topography, the number of panels (old or newly excavated), the number and type of discontinuities within of structure. Geological discontinuities are ubiquitous in a body rock and affect the deformability and strength properties of the rock mass (Brady and Brown, 2006; Weijermars, 1998). Accordingly, they impact on the shape, magnitude and rate of ground subsidence (Section 7.4.2 and Section 8.4).

Pore pressure also contributed to the profile and magnitude of the levelling-based ground subsidence. Sherwood sandstone is a water reservoir which negatively affects the strength of the structure either before or after excavation to exacerbate deformation propagation and failure of materials toward the surface. In the presence of water, rocks in faulted zones fail more easily therefore, increases ground deformation. However, although water might be present in the analyzed structures its static state may not reflect the actual state of water at Boulby. As a matter of fact, the analysis considered water as static that is, prevented from flowing. Consequently, Sherwood sandstone strength might have not been highly affected. As a result, low magnitudes of predicted ground subsidence, particularly with the discontinuous structure are recorded.

Nevertheless, the presence of water within this structure may have shaped the curved and smooth profile of predicted ground subsidence.

An alternative explanation of low magnitudes of predicted ground subsidence could be the process of modelling itself, mostly in the behaviour of evaporite rocks (i.e. potash and Carnalite marl). A literature review indicates that the time-dependent behaviour of evaporite rocks is well described by creep model such as two component power law, time power law which would incorporate the effects of temperature and heat (Caughill and Beddoes, 1996) experienced by underground excavations in salt and potash rocks. In the present analysis, these materials have been modeled as strain-softening materials whose time-dependent deformation gradually evolves from the onset to the residual failure through the peak failure (Section 3.6.1). Given that predicted subsidence is based on a short-term monitoring of mine workings convergence this gradual deformation process of Carnalite marl and Potash rocks may have not occurred.

An additional explanation could be the factor of time between the FLAC predicted convergence the subsidence models were based on and the measured workings convergence. The present analysis examined ground deformation associated with mine workings convergence which occurs at the start of the excavation whereas underground measurements are those of steady stage of creep workings behaviour. This difference in time might have also influenced the patterns, magnitudes and rate of ground subsidence at the points on the surface although the analysis has considered that most of workings convergence takes place immediately after the excavation (Figure 6.5).

8.7 Summary and conclusion

This thesis has used the Fast Lagrangian Analysis of Continua code to analyze the effects of lithology and geological fault on stress and displacement distribution within the rock mass during deep Potash underground mining. The analysis has demonstrated a significant dependency of stress and displacement on structures heterogeneity degree, and therefore on the lithology of the structures.

Distribution and magnitudes of stress and displacement are function of geological fault and its nature (i.e. unglued and glued fault). Stress and displacement are asymmetrically distributed and their magnitudes decrease as the fault either decreases the structures strength or absorbs part of stress and displacement.

The lithology controls the patterns and magnitudes of stress and displacement. Mining potash results in more symmetrical distributed stress and displacement with respect to the principal axis of structures. Whilst the magnitude of displacement decreases owing to the increase of structures heterogeneity, stress magnitude, particularly around excavations increases probably due to the *in-situ* stress used in the analysis but also due to the total vertical stress increase a consequence of pore water pressure increase.

Subsidence profile and magnitude are also influenced by the lithology of the structures and geological fault. The magnitude and rate of ground movement increase with the increase of structure lithological heterogeneity. The presence of fault within structure and its nature not only control the patterns but also the magnitude and rate of ground movement depending on the position of the monitoring point.

Patterns, magnitudes and rates of convergence of mine workings on the middle of both excavations are mainly a function of the behaviour of the Potash protective layer in unfaulted models. In contrast, convergence of workings in faulted structures is driven in addition to the behaviour of the Potash protective layer by the mechanics of the geological fault and its nature within the undermined structures.

Convergence patterns are not sensitive to the lithological heterogeneity despite the analysis demonstrates that magnitude and rate of convergence are sensitivity to. Unlike the convergence, subsidence patterns are relatively sensitive to the variation of materials parameters, and the magnitude and rate of ground subsidence are more sensitive.

Both continuous and discontinuous structures-related predicted subsidence highly underestimate measured ground subsidence obtained with levelling technique despite subsidence magnitudes associated with continuous models are slightly higher

than those associated with the discontinuous models. Furthermore, the analysis predictes linear and smooth patterns of ground subsidence for both continuous and discontinuous structures depending on the monitoring point. The levelling-measured subsidence show curved and smothed trend of subsidence patterns.

Pore pressure affects the patterns, magnitudes and rate of subsidence for both continuous and discontinuous structures. Magnitude and rate of subsidence in continuous structure decrease, whereas they increase in discontinuous structures regarless of the fault nature. Pore pressure also decreases the magnitude of convergence and induces curved and smoothed patterns of convergence in the discontinuous structures. It has limited effect on the values in the continuous structure and induces linear patterns of convergence of mine workings.

Chapter 9
Conclusions

9.1 Summary of results

This study has investigated the reliability of comparatively simple cross-section models of mine workings convergence to real world settings. The summary of results is presented by re-examining the objectives of the research determined in Chapter 1, which I summarize below:

1. Short-term monitoring of the temporal and spatial patterns of mine workings convergence in order to:

Examine the effects of some variables: position of monitored points (i.e. along roadway or stub axis) at the site, location (i.e. North or South), geometry (i.e. roadway or stub) and age (i.e. date of excavationof sites) of the monitoring sites on patterns of mine workings convergence at Boulby mine.

A well designed monitoring scheme of workings movement might permit determination of factors which govern the workings behaviour, and therefore understanding the mechanism of short term deformation of workings in underground mines. A dataset has been produced from the monitoring of the behaviour of mine working at four selected sites within the mine taking into consideration the location of the sites relative to the center of the mine (i.e. the ‘man’ shaft), geometry or type and age of the sites using a specially designed closuremeter. Dataset analysis has demonstrated the influence of these variables on the magnitudes and rate of convergence though workings convergence occurred gradually and linearly at the monitoring sites. At all of sites more rapid movement occurs along roadway than along stub axis. Convergence magnitude is higher in the South than in the North of the mine mainly because of the depth of the site. In terms of age, magnitude and rate of convergence varied inversely to the age of the sites.

Concerning the factor of time interval between mining and instrumentation of site linear trends displayed by convergence patterns at all sites over the entire monitoring periods is identified with the steady state of creep of Potash and Salt rocks. However, given the relatively long interval of time between excavation and instrumentation of sites, the instantaneous and transient states of Potash and Salt creep behaviour were not recorded.

2. To analyze numerically the patterns of stress and displacement distribution in real world system using the Fast Lagrangian Analysis of Continua (FLAC 2D) code, and further:

(a) To investigate the effects of heterogeneity of lithology on stress and displacement distribution

Understanding the stress and displacement distribution process within rock mass around openings is a key factor in the stability of underground excavations and the occurrence of subsidence on the surface. Distribution of stress and displacement within undermined rock mass shows significant dependency on the stratigraphy of strata above the excavations. This is because layers above an excavation respond to mining activity according to their individual mechanical properties and also their constitutive behaviour.

Despite the gradient distribution of stress and displacement, the results indicate that this distribution highly depends on the heterogeneity of lithology and mostly the mechanical (i.e. constitutive) behaviour of the layers. Magnitude of vertical displacement increases with the increase of heterogeneity of the structure. Mining potash results in maximum stress acting around excavations higher than the stress used in the analysis probably as a result of strata response to mining activity.

(b) To investigate the effects of geological fault on stress and displacement distribution and magnitude and its nature (i.e. real or glued).

Geological fault within rock mass is a weak zone and significantly controls the local stress distribution and subsequent deformation. Slip along faults is of importance and controls stress and subsequent displacement distribution within the rock mass.

Although in discontinuous systems distribution of stress and displacement is governed by the normal and shear stiffnesses of the fault in addition to the mechanics of the intact rocks this study has demonstrated that the fault has limited effect on the patterns of stress and displacement despite their gradient occurrence. In contrast, the fault has significant effect on the magnitudes of stress and subsequent displacement in spite of the nature of the fault. This is probably due to the fact that mining-induced stress was insufficient to exceed the stiffness and strength of the fault, but also the strength of the overlying strata. Sliding of blocks of structure each other and movement along fault due to mining might have exacerbated deformation and failure of structure consequently; affected the stress and displacement within structure.

An alternative explanation is that the fault may have absorbed part of stress and displacement and therefore, decreased the magnitude of stress and displacement within the structures. Nevertheless, the mechanical behaviour of fault should be taken into consideration in the improvement of effects of discontinuities on the distribution and magnitudes of stress and displacement within rock mass.

3. To compare the patterns of level-measured subsidence with the patterns of predicted subsidence using the more simplistic and realistic finite difference models.

Ground subsidence profile, magnitude and rate of occurrence are governed by several factors: width, depth of excavation, width/depth ratio and the mechanics of the materials. This study has showed that besides the mechanics of layers and lithology the occurrence of ground subsidence is also governed by the presence of discontinuities within the undermined structure.

Analysis results validation showed slight desagreement in the trends of predicted and measured ground subsidence. Predicted ground deformation exhibited either linear or smooth movement of ground surface, whereas measured ground subsidence showed a curved and smoothed deformation of ground surface. This disagreement was also corroborated by the remarkable discrepancies in the magnitudes and rates of predicted and measured ground subsidence. The predicted subsidence associated with both continuous and discontinuous structures significantly underestimated the magnitudes of measured ground movement.

This disagreement is probably due to several factors. For the measured ground subsidence among controlling factors are: topography, number of panels (old or newly excavated), number and type of discontinuities within structures. In addition to these factors, is the state (i.e. undrained or drained) of pore pressure within the structure. Governing factors of predicted subsidence are mostly inherent to the process of modelling itself and may include the contitutive behaviour of strata particularly the strain-softening behaviour of evaporite rocks, the stiffness and strength of the fault and also the undrained state of water within the Sherwood sandstone. To improve prediction of subsidence, it is of relevance to consider the aforementioned factors with regard to the heterogeneity of the structure.

Nevertheless, the present study suggests that by properly adjusting the mechanical characteristics of the overburden and possibly of the fault, the simple cross-section models of mining subsidence may accurately match those of real world settings.

9.2 Summary of key findings

The key findings of this research are:

- Convergence of mine workings at depth occurred gradually and linearly over the time of measurement; and workings behaviour is a function of the position of the monitored point at the site, age, geometry and location of site. Rapid movement develops along roadway than along stub axis and at stub as well. At stub rapid

movement develops at point far away from the rib wall of excavations. Magnitude and rate of convergence decrease with the age of workings and are higher in the South than in the North as a result of depth of excavation.

- The distribution and magnitudes of stress and displacement are a function of the lithology and the mechanics of the overlying strata. They increase with the increase of heterogeneity of structures and decrease as a result of fault. In contrary, the fault has limited effect on the distribution of stress and displacement within the undermined structure although the lithology has significant control.

- There is a link between the zone of disturbance at the surface (i.e. affected surficial area) and the increase of heterogeneity of the overburden strata. Ground subsidence magnitude and rate of subsidence increase from the middle to the edge of the cross-section as a result of the lithology and mechanics of strata which constitute the structures.

- The fault acts as boundary controlling the lateral extent of ground deformation and trough of subsidence. As a consequence, deformation and failure of structure grow more laterally, the path of least resistance upwards towards than vertically to the surface with the fault nature as a key factor.

- Predicted convergence of workings is mainly governed by the 2 m of Potash left in the roof as protective layer and FLAC 2D predicted ground subsidence underestimated levelling-measured subsidence in both continuous and discontinuous structures.

9.3 Original contribution to knowledge

This study has undertaken to understand the short term behaviour of excavations in potash rocks by applying a strain-softening model to simulate the behaviour of the rock, providing detailed analyses of excavation convergence and the factors which govern stress and displacement distribution during deep active mining. Previously research in this field was based on the long-term behaviour of excavations in potash which the

results imply is more suitable for the analysis of the behaviour of excavations long after the mining has ceased. This has resulted in gap in our knowledge of the behaviour of these rocks, excavations and the transmission of the stress-displacement state through the overburden during deep active potash mining.

The characterization of the behaviour of excavations during active mining in potash rock is difficult because the short term behaviour of the excavations is a time-dependent process. Therefore, there is a need to approximate this behaviour of rocks by different but a more appropriate approach than long-term or creep approach and with a consideration of factors which might govern the convergence of opening and distribution of stress and displacement within the structure.

This study has used the strain-softening model as an approximation to the creep behaviour of excavations in potash rock at Boulby. It has combined the Mohr-Coulomb, Drucker-Prager and strain-softening models to characterize the behaviour of the overburden assumed to undergo short term deformation. A numerical analysis approach was used to understand the process of stress and displacement distribution involved in the failure of excavations in potash rock and the occurrence of ground subsidence during deep active mining at Boulby.

In addition, short term dataset of excavation convergence has been collected at selected points within the mine, using a specially designed closuremeter. The combination of the numerical analysis and short term excavation deformation enabled the understanding of the behaviour of salt, potash and carnalite marl rocks in relation with the behaviour of excavations at Boulby mine. Based on the findings the convergence of excavations at Boulby mine is mainly the result of the non-linear flow of the overlying carnalite marl into the mine workings in an attempt to achieve an equilibrium state of stress.

Although the analysis did not enable the capture of the first stage of the creep behaviour the results showed that the strain-softening model is a reasonable approximation of the creep behaviour. As a result, the study findings have permitted the determination of factors which govern the stress and displacement distribution, mine

excavation convergence and the occurrence of subsidence on surface due to mining activity.

However, although the study has produced significant results there is a clear need for future research for the improvement of the numerical process in the determination of controlling factors of the stress and subsequent displacement distribution during the extraction of potash at Boulby mine. This will contribute to our understanding on the behaviour of the Boulby complex system.

9.4 Modelling approach limitations

There are several constitutive models in rock mechanics suited to characterizing materials and analyzing the behaviour of overburden in underground mines. Each of the models is individually tailored to best suit a limited sub-set of material types. The behaviour shows the constitutive models tend to be designed to encompass either short-term behaviour of material under low stress or the long-term behaviour of strata under constant load. The currently available constitutive models differ markedly in the functionality they offer. This is a direct consequence of their being tailored for specific types of materials behaviour. Some models offer multiple functionality and encompass both elasto-plastic and visco-plastic failure of materials.

The present study applies the strain-softening approach to evaporite rocks behaviour particularly halite, potash and carnalite marl rocks aimed at analyzing controlling factors of stress and displacement, and ground subsidence during active deep potash mining. This approach intended to encompass both the short-term elasto-plastic and long-term creep behaviour of evaporite rocks in active deep potash mining.

However, the application of this approach to evaporite rocks may be inappropriate in that strain-softened materials fail more plastically as a result of weakening of the strengths of the rock masses. Consequently, stiffness-related elasto-plastic deformation may not occur within the loaded rock mass despite evaporite rocks that make up the roof and floor beams and pillars underground mines are likely

subjected to both short-term elasto-plastic and long-term visco-plastic deformation. Short-term elasto-plastic response of rock occurs due to stress change as result of mining, whereas long-term visco-plastic deformation of the rocks occurs as result of creep under static loading with the deterioration of their strengths.

Additionally, strain-softening modelled evaporite rocks pillars will provide more stability underground mine while creeping of the rocks will result in higher convergence rates of mine working, and creep behaviour of rock masses suits for predicting convergence and stability of roof beam and overlying strata underground mine. Therefore, the analysis results particularly patterns of stress and displacement distribution, and resulting subsidence may not reflect the actual trend of patterns of mine working convergence, stress and displacement distribution, and subsidence if creep model was applied to the evaporite rocks. Nevertheless, these results may be considered as the particular case of short-term elasto-plastic response of evaporite rocks due to stress change as a result of mining and hence, a starting point for further research. For this reason some recommendations are made in the following section for further research.

9.5 Recommendations for future research

This study has investigated factors governing the distribution of stress and displacement during deep mining at Boulby based on short-term behaviour of mine working. An important finding regarding the stress and strain distribution is that although the dependency of patterns and magnitudes of stress and displacement on the lithology however, there exists no straightforward linkage between the two variables. In addition, although it is generally accepted the influence of geological fault on stress and displacement, the study has showed that the presence of fault within structures has limited effect on the patterns and magnitudes of stress and displacement regardless its nature. Furthermore, the analysis has shown that there exists disagreement between predicted and measured ground subsidence in both patterns and magnitudes. This

would suggest that further research is needed for the improvement of the modelling process and recommendations should be made. These are:

(1) Sequential excavation of openings. Mining sequence significantly influences the stress distribution around and within the undermined rock. Therefore, sequential excavation of openings will allow stress and subsequent displacement due to the first excavated opening to develop, and then together with the effect of adjacent excavation on the behaviour of pre-existing excavation to be taken into consideration in the modelling process.

(2) The mechanical behaviour of strata. Evaporite rocks behaviour is time-dependent and may well characterized by creep model such as two component power law, time power law which incorporate the effects of temperature and heat experienced by underground excavations in salt and potash rocks. Although these rocks have adequately been characterized by the strain-softening model it still questionable in the effectiveness of this model. Therefore, comparative analysis of both creep and strain-softening models will help ascertain the efficiency of the strain-softening model in characterizing the behaviour of evaporite rocks.

(3) The scaling factors. In scaling the materials parameters to account for the effect of discontinuities and heterogeneity in the overburden care should be taken on the input data to reflect the actual behaviour of strata. Therefore laboratory parameters should be reduced by appropriate factors such modulus values may accommodate for instance strata bending, both size effects and subsidence mechanisms. In this regards, the behaviour of upper layers is of relevance. It still remains problematic to obtain highly accurate rock material properties due to the sample agility and deterioration in the extraction process.

(4) Effects of geological discontinuities. The behaviour of a rock mass subjected to changes in stress regime is governed by both the mechanical properties of the

intact rock material and the number and nature of the geological discontinuities present in the rock mass. However, although Boulby mine is considered as continuum medium as discussed in Chapter 3 and because geological faults are ubiquitous and are planes where sliding and dilation may occur according to the properties of the fault it is important to thoroughly investigate the effects of fault on the distribution and magnitudes of stress and displacement. In this regards, an appropriate approach should be used to accurately determine the fault parameters. Furthermore, a consideration of the heterogeneous nature of the fault may also give insight into the distribution of stress and displacement within Boulby mine.

(5) Effect of long-term closure of workings on stress and displacement distribution. The present FLAC models are associated with the closure of mine workings occurring at the start of the excavation and limited information is known on the distribution of stress and displacement related to the closure of workings immediately and/or after the excavation. For this, the FLAC models should be run until the differential workings convergence is minimal in order to analysis the stress and displacement distribution due to the complete closure of the mine workings.

(6) Future subsurface and ground subsidence monitoring using advanced techniques. Advanced mine roof monitoring techniques such as Optical reflector targets may help capture the 3D of the whole excavation deformation. The Global Positioning System (GPS) is an established technique in monitoring ground subsidence over large area and provides position information with accuracies to a few millimeters than any other surveying techniques of ground subsidence. With well designed monitoring scheme and network more accurate spatio-temporal patterns of ground deformation on the surface and mine roof behaviour subsurface may be obtained. The combination of GPS and the continuous levelling ground deformation at Boulby and mine workings closure will provide datasets of deformation of both surface and subsurface for the validation of

numerical modelling of gradual ground deformation process that takes place at Boulby mine.

(7) A new modelling approach that combines finite and discrete element codes-e.g. ELFEN. Such approach will better accommodate the continuous and discontinuous behaviour of both the mine workings and the overburden strata at Boulby mine.

References

Alvarez-Fernandez, M.I., Gonzalez-Nicieza, C., Menendez-Diaz, A., and Alvarez-Vigil, A.E., 2005. Generalization of the n-k influence function to predict mining subsidence. Engineering Geology 80, 1-36.

Aguado, M.B.D., and Gonzalez, C., 2009. Influence of the stress in a coal bump-prone deep coalbed: A case study. International Journal of Rock Mechanics & Mining Sciences 46, 333-345.

Akutagawa, S., Lee, J., Doba, N., Kitagawa, T., and Isogai, A., 2006. Identification and prediction of deformation behaviour around a shallow NATM tunnel using strain softening model. Tunnelling and Underground Space Technology 21, 6p.

Akcin, H., Degucci, T. and Kutoglu, H., 2006. Monitoring Mining Induced Subsidence Using GPS and InSAR, XXIII FIG Congress, Munich, Germany, October 8-13, 12p.

Alejano, L.R., Taboada, J., Garcia-Bastante, F., and Rodriguez, P., 2008. Multi-approach back-analysis of a roof bed collapse in a mining room excavated in stratified rock. International Journal of Rock Mechanics & Mining Sciences 45, 899-913.

Alejano, L.R., Ramirez-Oyanguren, P. and Taboada, J., 1999. FDM predictive methodology for subsidence due to flat and inclined coal seam mining. International Journal of Rock Mechanics and Mining Sciences 36, 475-491.

Alejano L.R., Rodriguez-Dono, A., Alonso, E., and Fdez.-Manin, G., 2009. Ground reaction curves for tunnels excavated in different quality rock masses showing several types of post-failure behaviour. Tunnelling and Underground Space Technology 24, 689-705.

Alkan, H., Cinar, Y., and Push, G., 2007. Rock salt dilatancy boundary from combined acoustic emission and triaxial compression tests. International Journal of Rock Mechanics and Mining Sciences 44, 108-119.

Amitrano, D. and Helmstetter, A., 2006. Brittle creep, damage and time-to-failure in rocks. Journal of Geophysical Research, vol.111, no B11, 28p.

Anderson, J.G.C., and Owen, T.R., 1980. The structure of the British Isles. Permagon Press Ltd., Oxford, 251p.

Annan, A.P., Davis, J.L., and Gendzwill, D., 1988. Radar sounding in potash mines, Saskatchewan, Canada. Geophysics, vol. 53, no 12, 1556-1564.

Apuani, T., Masetti, M. and Rossi, M., 2007. Stress-strain-time numerical modeling of a deep-seated gravitational slope deformation: Preliminary results. Quaternary International, vol. 171-172, 80-89.

Asanov, V.A., and Pan'kov, I.L., 2004. Deformation of salt rock joints in time. Journal of Mining Science, vol. 40, n^{o}. 4, 5p.

Aston, T.R.C., Tammemagi, H.Y. and Poon, A.W., 1987. A review and evaluation of empirical and analytical subsidence prediction techniques. Mining Science and Technology, 5, 59-69.

Atkins, W.S., 2005. Management of the abandoned salt mines at Carrickfergus, Co Antrim, 7p. http://www.detini.gov.uk/cgi-bin.

Bannister, A. and Baker, R., 1994. Solving Problems in Surveying. Longman House, Harlow, 346p.

Bannister, A. and Raymond, S., 1974. Surveying. The Pitman Press, Bath, 548p.

Barla, M., 2008. Numerical simulation of the swelling behaviour around tunnels based on special triaxial tests. Tunnelling and Underground Space Technology 23, 508-521.

Barnett, W.P. and Lorig, L., 2007. A model for stress-controlled pipe growth. Journal of Volcanology and Geothermal Research 159, 108-125.

Baryakh, A.A. and Samodelkina, N.A., 2005. Rheological analysis of geomechanical processes. Journal of Mining Science, Vol. 41, no. 6, 522-530.

Baryakh, A.A., Telgina, E.A., Samodelkina, N.A. and Devyatkov, S.Yu., 2005. Prediction of the intensive surface subsidence in mining potash series. Journal of Mining Science, Vol. 41, no. 4, 312-319.

Bell, F.G., 1981. A survey of the physical properties of some carbonate rocks. Bulletin of the International Association of Engineering Geology 24, 105-110.

Bell, F.G., 1981. Geotechnical properties of some evaporitic rocks. Bulletin of the International Association of Engineering Geology 24, 137-144.

Bell, F.G., 1994. A survey of the engineering properties of some anhydrite and gypsum from the north and midlands of England. Engineering Geology 38, 1-23.

Berest, P., Brouard, B., Feuga, B., and Karimi-Jafari, M., 2008. The 1873 collpase of the Saint-Maximilien panel at the Varangeville salt mine. International Journal of Rock Mechanics & Mining Sciences 45, 1025-1043.

Berest, P. and Brouard, B., 2003. Safety of salt caverns used for underground storage. Blow out; mechanical instability; seepage; cavern abandonment. Oil & Gas Science and Technology – Rev. IFP, vol. 58, no 3, 361-384.

Bhalla, S., Yang, Y.W., Zhao, J., and Soh, C.K., 2005. Structural health monitoring of underground facilities – Technological issues and challenges. Tunnelling and Underground Space Technology 20, 487-500.

Bigby, D., 2004. Mining innovations for instrumentation, Tunnels & Tunnelling International, UK, 3p.

Bigby, D., Kent, L., and Hurt, K., 2004. Safe application of mine roadway support systems. Research report 229, Staffordshire, UK, 208p.

Bigby, D., Lewis, D. and Luttig, F., 2003. Application of RMT's Remote reading telltale system to monitor roof movement during face retreat at west colliery, Germany. 22nd International conference on ground control in mining, USA, 10p.

Bigby, D. and DeMarco, M., 2001. Development of a remote reading dual-telltale system for monitoring mine roof deformation. 20th International conference on ground control in mining, USA, 10p.

Birtel, S., and Stockhert, B., 2007. Brittle failure and short-term ductile deformation at 500^{o}C – the record of quartz veins beneath an exhumed low-angle normal fault. Geophys. Res. Abstracts, Vol. 9, 05223, 2p.

Bizjak, K.F. and Zupancic, A., 2009. Site and laboratory investigation of the Slano blato landslide. Engineering Geology 105, 171-185.

Boidy, E., 2002. Modelisation numerique du comportement differe des cavites souterraines. PhD Thesis, University Joseph Fourier – Grenoble I, 320p.

Bond, J., Szostak-Chrzanowski, A. and Chrzanowski, A., 2007. Design of geodetic deformation monitoring schemes using deterministic modelling: an open pit mine example. In Proceedings of the 3rd International Symposium on Geo-information for disaster management, Ontario, 22p.

Boys, C., 1990. The geology of potash deposits at PCS Cory Mine, Saskatchewan. MSc thesis, University of Saskatchewan, Dept. of Geological Sciences, 238p.

Brady, B.H.G. and Brown, E.T., 2006. Rock Mechanics for underground mining. Springer, 3rd ed., 628p.

Bugden, A., Minney, D. and Altounyan, P., 2001. Improving roof control at a South African coal mine. 20th International conference on ground control in mining, USA, 10p.

Buzdar, S.A.R.K., 1968. A laboratory investigation into the mechanical properties of some sedimentary rocks with special reference to potash. PhD. Thesis, University of Newcastle upon Tyne, 179p.

Cai, M., 2008. Influence of stress path on tunnel excavation response –Numerical tool selection and modelling strategy. Tunnelling and Underground Space Technology 23, 618-628.

Cai, M., Kaiser, P.K., Tasaka, Y., Maejima, T., Morioka, H. and Minami, M. 2004. Generalized crack initiation and crack damage stress thresholds of brittle rock masses near underground excavations. International Journal of Rock Mechanics & Mining Sciences 41, 833-847.

Cai, M., Kaiser, P.K. and Martin, C.D., 2001. Quantification of rock mass damage in underground excavations from microseismic event monitoring. International Journal of Rock Mechanics & Mining Sciences 38, 1135-1145.

Cantieni, L., and Anagnostou, G., 2009. The interaction between yielding supports and squeezing ground. Tunnelling and Underground Space Technology 24, 309-322.

Caughill, D.L., and Beddoes, R.J., 1996. Rock mechanics initial evaluation report. Cleveland Potash Ltd., Golder Associates, 2402\REVREP.DOC, 22p.

Cela, J.J.L., 1998. Analysis of reinforced concrete structures subjected to dynamic loads with a viscoplastic Drucker-Prager model. Applied Mathematical Modelling 22, 495-515.

Celesco Transducer Products, Inc., 2007. Compact string pot, USA, 2p. http://www.celesco.com

Chandler, N., 2004. Developing tools for excavation design at Canada's Underground Research Laboratory. International Journal of Rock Mechanics & Mining Sciences 41, 1229-1249.

Chang, C.-C., 2000. Estimation of local subsidence using GPS and leveling combined data. Surveying and Land Information Systems, vol. 60, no 2, 85-94.

Chang, C.-C. and Wang, T.-N., 2006. GPS monitoring ground subsidence associated with seasonal underground water level decline: Case analysis for a section of Taiwan High Speed Rail. Surveying and Land Information Science, vol. 66, no 1, 45-54.

Chatterjee, R.S., Fruneau, B., Rudant, J.P., Roy, P.S., Frison, P.-Louis, Lakhera, R.C., Dadhwal, V.K. and Saha, R., 2006. Subsidence of Kolkata (Calcuta) City, India during the 1990s as observed from space by Differential Synthetic Aperture Radar Interferometry (D-InSAR) technique. Remote Sensing of Environment 102, 176-185.

Chrzanowski, A., Monahan, C., Roulston, B. and Szostak-Chrzanowski, A., 1997. Integrated monitoring and modelling of ground subsidence in potash mines. International Journal of Rock Mechanics & Mining Sciences 34, 16p.

Cook, R.F., 1974. Rock mechanics investigations associated with shaft excavations in deep evaporite deposit. PhD Thesis, University of Newcastle upon Tyne, 224p.

Coulthard, M.A., 1999. Applications of numerical modelling in underground mining construction. Geotechnical and Geological Engineering 17, 373-385.

Coulthard J.M., and Bell, F.G., 1993. The engineering geology of the Lower Lias clay at Blockley, Gloucestershire, UK. Geotechnical and Geological Engineering, 11, 185-201.

Coulthard, M.A., and Dutton, A.J., 1988. Numerical modelling of subsidence induced by underground mining. The 29th U.S. Symposium on Rock Mechanics (USRMS), June 13-15, Minneapolis, 8p. http://www.onepetro.org

CPL, Survey Dept., 2002. File: Subsidence Contracting, 6p.

Craig, R.F., 2004. Craig's Soil Mechanics. Abingdon, Oxon, UK, 447p.

Cristescu, N.D., 2002. Dilatancy as related to evolutive damage in Cristescu, N.D., Hardy, H. R., Simionescu, R.O. and Simionescu, Jr., Romania (eds). Basic and Applied Salt Mechanics: Proceedings of the Fifth Conference on the Mechanical Behaviour of Salt. A.A. Balkema, Netherlands, 466p.

Cristescu, N.D., Hardy, H. R., Simionescu, R.O. and Simionescu, Jr., 2002. Basic and applied salt mechanics: Proceedings of the Fifth Conference on the Mechanical Behaviour of Salt. A.A. Balkema, Netherlands, 466p.

Cristescu, N.D. and Hunsche, U., 1998. Time effects in rock mechanics. Chichester, 342p.

Crosta, G.B., Imposimato, S., and Roddeman, D., 2009. Numerical modelling of entrainment/deposition in rock and debris-avalanches. Engineering Geology 109, 135-145.

Crutzen, P.J., 2002. Geology of Mankind, 415:pp.23

Cui X., Miao, X., Wang, J. an, Yang, S., Liu, H., Song, Y., Liu, H., and Hu, X., 2000. Improved prediction of differential subsidence caused by underground mining. International Journal of Rock Mechanics and Mining Sciences 37, 615-627.

David, I.G., 1996. The Boulby Mine. Mineralogical Record, 7p. http://findarticles.com

Deng, H., 2000. Predicting the extent of rock failure/loosening above underground excavations in massive and jointed rock. MSc Thesis, Dept. of Civil & Geological Engineering, University of Manitoba, 166p.

Dhawan, K.R., Singh, D.N., and Gupta, I.D., 2004. Three-dimensional element analysis of underground caverns. Technical Notes. International Journal of Geomechanics 4, 224-228.

Diederichs, M.S., Kaiser, P.K. and Eberhardt, E., 2004. Damage initiation and propagation in hard rock during tunnelling and the influence of near-face stress rotation. International Journal of Rock Mechanics & Mining Sciences 41, 785-812.

Djaja, R., Rais, J., Abidin, H.Z. and Wedyanto, K., 2004. Land subsidence of Jakarta Metropolitan Area. 3rd FIG Regional Conference, Indonesia, 14p.

D'Onofrio, D. and Frame, J., 2003. The Yolo country GPS subsidence network, 20p. www.yolowra.org/YSN2002

Dubey, R.K., and Gairola, V.K., 2008. Influence of structural anisotropy on creep of rocksalt from Simla Himalaya, India: An experimental approach. Journal of Structural Geology 30, 710-718.

Dunrud, C.R., 1984, in Coal mine subsidence – western United States. Geological Society of America. Reviews in Engineering Geology, vol. VI, 43p.

Duzgun, H.S.B., 2005. Analysis of roof fall hazards and risk assessment for Zonguldak coal basin underground mines. International Journal of Coal Geology 64, 104-115.

Eberhard, E., 2001. Numerical modeling of three-dimension stress rotation ahead of an advancing tunnel face. International Journal of Rock Mechanics & Mining Sciences 38, 499-518.

Eberhardt, E., Stead, D. and Stimpson, B., 1999. Effects of sample disturbance on the stress-induced microfracturing characteristics of brittle rock. Can. Geotech. J. 36:239-250.

Ercikdi, B., Kesimal, A., Cihangir, F., Deveci, H., and Alp, I., 2009. Cemented paste backfill of sulphide-rich tailings: Importance of binder type and dosage. Cement & Concrete Composites 31, 268-274.

Erickson, S.G., Strayer, L.M., and Suppe, J., 2004. Numerical modelling of hinge-zone migration in fault-bend folds. Thrust tectonics and hydrocarbon systems: AAPG Memoir 82, 438-452.

Esterhuizen, G.S., Dolinar, D.R., Ellenberger, J.L., Prosser, L.J. and Iannacchione, A.T., 2007. Roof instability issues in underground limestone mines in the Unites States. Proceedings of the 26th International Conference on Ground Control in Mining. In Peng, S.S., Mark, C., Finfinger, G., Tadolini, S., Khair, A.W., Heasley, K. and Luo, Y., eds., Morgantown, 336-343.

Fabre, G., and Pellet, F., 2006. Creep and time-dependent damage in argillaceous rocks. International Journal of Rock Mechanics & Mining Sciences 43, 950-960.

Fairhurst, C., 2003. Stress estimation in rock: a brief history and review. International Journal of Rock Mechanics & Mining Sciences 40, 957-973.

Flint Hire & Supply Ltd., 2008. Pulleys, London, 9p. http:/www.flints.co.uk

Foley, J.M.S., 2006. An analysis of cavern stability and hydraulic fractures in relation to natural gas storage in limestone formations. MSc Thesis, Graduate School, Clemson University, 367p.

Fossum, A.F., and Fredrich, J.T., 2002. Salt mechanics primer for near-salt and sub-salt deepwater Gulf of Mexico field developments, Sanda Report, SAND2002-2063, Sanda National Laboratories, California, 67p.

Fredlund, D.G., Zhang, Z.M., and MacDonald, K., 1993. Analyses for the stability of potash tailings plies. Canadian Geotechnical Journal 30, 491-505.

Fuenkajorn, K., and Archeeploha, S., 2009. Prediction of cavern configurations from subsidence data. Engineering Geology 110, 21-29.

Fuenkajorn, K. And Phueakphum, D., 2010. Effects of cyclic loading on mechanical properties of Maha Sarakham salt. Engineering Geology 112, 43-52.

Fujimitsu, Y., Ehara, S., Oki, R., and Kanou, R., 2008. Numerical model of the hydrothermal system beneath Unzen Volcano, Japan. Journal of Volcanology and Geothermal Research 175, 35-44.

Ghafoori, M., Lashkaripour, G.R., Sadeghi, H., and Tarighi Azali, S., 2006. Comparison of predicted and actual behaviour and engineering geological characterization of the Kallet tunnel, Iran. The Geological Society of London, 2006, IAEG, no 809, 8p.

Ghoreychi, M., and Daupley, X., 2003. Mechanical-transport processes in salt: consequences for abandonment of underground exploitations. ISRM 2003-Technology roadmap for rock mechanics, South African Institute of Mining and Metallurgy, 6p.

Gilbride, L.J., Free, K.S. and Kehrman, R., 2005. Modelling block cave subsidence at the Molycorp, Inc., Questa Mine- A case study. American Rock Mechanics Association, 40th U.S. Symposium on Rock Mechanics: Rock Mechanics for Energy, Mineral and Infrastructure Development in the Northern Regions, Anchorage, Alaska, 14p.

Gledan, J., 2004. Development of low cost GPS strategies for deformation monitoring. PhD thesis, School of civil engineering and geosciences, University of Newcastle upon Tyne, 216p.

Gray, R.E. and Bruhn, R.W.,1984, in Coal mine subsidence – eastern United States. Geological Society of America. Reviews in Engineering Geology, vol. VI, 23p.

Habimana, J., Labiouse, V., and Descoeudres, F., 2002. Geomechanical characterisation of cataclastic rocks: experience from the Cleuson-Dixence project. International Journal of Rock Mechanics & Mining Sciences 39, 677-693.

Hajiabdolmajid, V., Kaiser, P.K. and Martin, C.D., 2002. Modelling brittle failure of rock. International Journal of Rock Mechanics & Mining Sciences 39, 731-741.

Halabura, S.P., and Hardy, M.P., 2007. An overview of the geology of solution mining of potash in Saskatchewan. Solution mining research Institute. Technical Meeting Halifax, Nova Scotia, 18p.

Hallert, B., 1960. Photogrammetry. Basic Principles and General Survey. McGraw W-Hill, New York, 340p.

Hamiel, Y., Katz, O., Lyakhovsky, V., Reches, Z. and Fialko, Y., 2006. Stable and unstable damage evolution in rocks with implications to fracturing of granite. Geophys. J. Int., doi:10.1111/j.1365-246X.2006.03126.x, 12p.

Hao, Y.H., and Azzam, R., 2005. The plastic zones and displacements around underground openings in rock masses containing a fault. Tunnelling and Underground Space Technology 20, 49-61.

Hart, R., 2003. Enhancing rock stress understanding through numerical analysis. International Journal of Rock Mechanics & Mining Sciences 40, 1089-1097.

Hartman, H.L., and Mutmansky, J.M., 2002. Introductory – Mining Engineering, 2nd ed. John Wiley and Sons, Inc., Hoboken, New Jersey, 570p.

Hebblewhite, B.K., 1977. Underground potash mine design based on rock mechanics principles and measurements. PhD Thesis, University of Newcastle upon Tyne, 460p.

Henk, A., 2006. Stress and strain during fault-controlled lithospheric extension – insights from numerical experiments. Tectonophysics 415, 39-55.

Henk, A. and Nemcok, M., 2008. Stress and fracture prediction in inverted half-graben structures. Journal of Structural Geology 30, 81-97.

Herrera, G., Tomas, R., Lopez-Sanchez, J.M., Delgado, J., Mallorqui, J.J., Duque, S. and Mulas, J., 2007. Advanced DInSAR analysis on mining areas: La Union case study (Murcia, SE Spain). Engineering Geology 90, 148-159.

Hesselbo, S.P., 2008. Sequence stratigraphy and inferred relative sea-level change from the onshore British Jurassic. Proceedings of the Geologists' Association, 119, 19-34.

Highley, D., Bloodworth, A., and Bate, R., 2006. Potash, Mineral Planning Factsheet, British Geological Survey, 6p.

Hoek, E., Kaiser, P.K. and Bawden, W.F., 1995. Support of underground excavations in hard rock. A.A. Balkema/Rotterdam/Brookfield, 215p.

Hofer, D., and Kamlah, M., 2005. Drucker-Prager-Cap creep modelling of pebble beds in fusion blankets. Fusion Engineering and Design 73, 105-117.

Holzer, 1984, in Coal mine subsidence – western United States. Geological Society of America. Reviews in Engineering Geology, vol. VI, 43p.

Hood, M., Ewy, R.T. and Riddle, L.R., 1983. Empirical methods of subsidence prediction – A case study from Illinois. *Inter. Jour. of Rock Mech. Min. Sci. & Geomech. Abstr.* 20, no 4, 153-170.

http://diqky.blogspot.com/2009/02/room-and-pillar , accessed on 08/09/2009

Howley, I., 2007. Working with drillers. The Do's and Don'ts. GSHPA, 13p. www.loopmastereurope.co.uk , accessed on 07/02/2011

Hu, Y., Zhang, K. and Liu, G., 2005. Deformation Monitoring and Analysis Using Regional GPS Permanent Tracking Station Networks. FIG Working Week 2005 and GSDI-8, Cairo, Egypt, April 16-21, 15p.

Hubert-Ferrari, A., King, G., Manighetti, I., Armijo, R., Meyer, B., and Tappommier P., 2003. Long-term elasticity in the continental lithosphere; modeling the Aden Ridge propagation and the Anatolian extrusion process. *Geophys. J. Int*. 153, 111-132.

Hudec, M.R., and Jackson, M.P.A., 2007. Terra infirma: Understanding salt tectonics. Earth-Science Reviews 82, 1-28.

Hurn, J., 1993. Differential GPS Explained. Trimble Navigation, Sunnyvale, 55p.

Hurn, J., 1989. GPS – A guide to the Next Utility. Trimble Navigation, Sunnyvale, 76p.

Iannacchione, A.T., Bajpayee, T.S. and Edwards, J.L., 2005. Forecasting roof falls with monitoring technologies – A look at the Moonee Colliery Experience, NIOSH Mining Document, 8p. http://www.cdc.gov/niosh/mining/pubs

ICL Fertilizers, 2007, 2p. http://www.mining-technology.com/projects/boulby.

Islam, Md. R., Hayashi, D., and Kamruzzaman, A.B.M., 2009. Finite element modelling of stress distributions and problems for multi-slice longwall mining in Bangladesh, with special reference to the Barapukuria coal mine. International Journal of Coal Geology 78, 91-109.

Janssen, V., 2002. GPS volcano deformation monitoring. GPS Solutions 6, 128-130.

Janssen, V., Roberts, C., Rizos, C. and Abidin, H.Z., 2002. Low-cost GPS-based volcano deformation monitoring at Mt. Papandayan, Indonesia. Journal of Volcanology and Geothermal Research 115, 139-151.

Jarosz, A. and Shepherd, L., 2002. Is ISAR Interferometry Able to Detect Slope Deformations of Open Pit Mines? Curtin University, Western Australian School of Mines, Mine Surveying Program, Australian, 9p.

Jeremic, M.L., 1994. Rock mechanics in salt mining. A.A. Balkema, Rotterdam, 532p.

Jeremic, M.L., 1985. Strata Mechanics in Coal Mining. A.A. Balkema, Rotterdam, 566p.

Jiang, Y., Li, B., and Yamashita, Y., 2009. Simulation of cracking near a large underground cavern in a discontinuous rock mass using the expanded distinct element method. International Journal of Rock Mechanics & Mining Sciences 46, 97-106.

Jing, L. and Hudson, J.A., 2002. Numerical methods in rock mechanics. International Journal of Rock Mechanics & Mining Sciences 39, 409-427.

Jumikis, A.R., 1983.Rock mechanics. T.T.P. Clausthal-Zellerfield, Germany, 613p.

Johnson, A., 2001. A brief introduction to the Geology of the Hartlepool Area. Geotrans-Online, 19p.

Karakul, H., Ulusay, R., and Isik, N.S., 2010. Empirical models and numerical analysis for assessing strength anisotropy based on block punch index and uniaxial

compression tests. International Journal of Rock Mechanics & Mining Sciences 47, 657-665.

Karakus, M., and Fowell, R.J., 2005. Back analysis for tunnelling induced ground movements and stress redistribution. Tunnelling and Underground Space Technology 20, 514-524.

Karmis, M. and Agioutantis, Z., 1999. On the paper FDM predictive methodology for subsidence due to flat and inclined coal seam mining; L.R. Alejano, P. Ramirez-Oyanguren, J. Taboada, International Journal of Rock Mechanics and Mining Sciences 36, 475-491. International Journal of Rock Mechanics and Mining sciences 36, 1095-1097.

Kavvadas, M.J., 2003. Monitoring and modeling ground deformations during tunneling. Proceedings, 11th FIG Symposium on deformation measurements. Santorini, Greece, 19p.

Kelsall, P.C. and Nelson, J.W., 1985. Geologic and engineering characteristics of Gulf region salt domes applied to underground storage and mining. In *Proc. Of 6th Int. Symp. on Salt*, The Salt Institute, Virginia, Vol. 1, 519-542.

Kemeling, I., 2006. Modelling ground surface deformation, with persistent scatter radar interferometry. PhD thesis, Department of Geography, Durham University, 252p.

Kennedy M., 2002.The global positioning system and GIS: An Introduction, 2nd edition. Taylor & Francis Inc., London and New York, 345p.

Kim, M.-Hyung, Inoue, J. and Horii, H., 2004. Flow analysis of jointed rock masses based on excavation-induced transmissivity change of rough joints. International Journal of Rock Mechanics & Mining Sciences 41, 959-974.

Kinakin, D., and Stead, D., 2005. Analysis of the distributions of stress in natural ridge forms: implications for the deformation mechanisms of rock slopes and the formation of sacking. Geomorphology 65, 85-100.

Klayvimut, K., Wetchasat, K., and Fuenkajorn, K., 2007. Preliminary study of geomechanical performance of Maha Sarakham salt for nuclear waste repository. www.geocities.com/aekgeo/sut/nuclear_waste_repository

Kontogianni, V. A. and Stiros, S.C., 2005. Induced deformation during tunnel excavation: Evidence from geodetic monitoring. Engineering Geology 79, 115-126.

Kontogianni, V.A., and Stiros, S.C., 2002. Predictions and observations of convergence in shallow tunnels: case histories in Greece. Engineering Geology 63, 333-345.

Kratzsch, H., 1983. Mining Subsidence Engineering. Springer-Verlag, Berlin Heidelberg New York, 543 p.

Kumar, R., Sharma, K.G., and Varadarajan, A., 2008. Effect of strain softening on tunnel behaviour. World Tunnel Congres – Underground Faculties for Better Environment and Safety – India, 10p.

Kushwaha, A., and Banerjee, G., 2005. Exploitation of developed coal mine pillars by shortwall mining-a case example. International Journal of Rock Mechanics & Mining Sciences 42, 127-136.

Kwon, S., Lee, C.S., Cho, S.J., Jeon, S.W., and Cho, W.J., 2009. An investigation of the excavation damaged zone at the KAERI underground research tunnel. Tunnelling and Underground Space Technology 24, 1-13.

Kwon, S. And Wilson, J.W., 1999. Deformation mechanism of the underground excavations at the WIPP site. Rock Mech. Rock Engng. 32, 101-122.

Lachenicht, R., and Aswegen van, G., 1999. An investigation into the processes leading to water ingress in response to mining at Cleveland Potash Ltd. Report 6: Final report. CLEVREP00200, 33P.

Lee, J.W., 2005. Development of a numerical model of rock failure mechanisms associated with the impact of lateral displacement. MSc Thesis, University of Wollongong, 137p.

Lei, X., Kusunose, K., Rao, M.V.M.S., Nishizawa, O. and Satoh, T., 2000. Quasi-static fault growth and cracking in homogeneous brittle rock under triaxial compression using acoustic emission monitoring. Journal of Geophysical research, 105, no B3, 6127-6139.

Li, T., Cai, M.F., and Cai, M., 2007. A review of mining-induced seismicity in China. International Journal of Rock Mechanics & Mining Sciences 44, 1149-1171.

Li, X., Wang, S.J., Liu, T.Y., and Ma, F.S., 2004. Engineering geology, ground surface movement and fissures induced by underground mining in the Jinchuan Nickel Mine. Engineering Geology 76, 93-107.

Liang W., Yang, C., Zhao, Y., Dusseault, M.B., and Liu, J., 2007. Experimental investigation of mechanical properties of bedded salt rock. International Journal of Rock Mechanics & Mining Sciences 44, 400-411.

Lim, M., 2006.Coastal cliff evolution with reference to Staithes, North Yorkshire. PhD thesis, Department of Geography, Durham University, 376p.

Lloyd, P.W., Mohammad, N. and Reddish, D.J., 1997. Surface subsidence prediction techniques for UK coalfields – An innovative numerical modelling approach. Mining Congress of Turkey, Guyaguler, 14p.

Ma, R., Wang, Y., Ma, T., Sun, Z., and Yan, S., 2006. The effect of stratigraphic heterogeneity on areal distribution of land subsidence at Taiyuan, northern China. Environ Geol 50, 551-568.

Mandak, P.K., Singh, R., Maiti, J., Singh, A.K., Kumar, R. and Sinha, A., 2008. Underpinning-based simultaneous extraction of contiguous sections of a thick coal seam under weak and laminated parting. International Journal of Rock Mechanics & Mining Sciences 45, 11-28.

Mark, C., Gale, W., Oyler, D., and Chen, J., 2007. Case history of the response of a longwall entry subjected to concentrated horizontal stress. International Journal of Rock Mechanics & Mining Sciences 44, 210-221.

Martin, C.D., and Christiansson, R., 2009. Estimating the potential for spalling around a deep nuclear waste repository in crystalline rock. International Journal of Rock Mechanics & Mining Sciences 46, 219-228.

Martin, J.C. and Serdengecti, S., 1984. Subsidence over oil and gas fields. Geological Society of America, Reviews in Engineering Geology, vol. VI, 12p.

Martino, J.B., and Chandler, N.A., 2004. Excavation-induced damage studies at the Underground Research Laboratory. International Journal of Rock Mechanics & Mining Sciences 41, 1413-1426.

Matsuki, K., Nakama, S., and Sato, T., 2009. Estimation of regional stress by FEM for a heterogeneous rock mass with a large fault. International Journal of Rock Mechanics & Mining Sciences 46, 31-50.

McLellan, P., Hawkes, C., Steadman, E.N., and Harju, J.A., 2008. Geomechanical testing and modelling of reservoir and cap rock integrity in an acid EOR/sequestration project, Zama, Alberta, Canada. Energy Procedia 00, 8p.

Meckel, T.A., 2008. An attempt to reconcile subsidence rates determined from various techniques in southern Louisiana. Quaternary Science Reviews 27, 1517-1522.

Meglis, I.L., Chow, T., Martin, C.D. and Young, R.P., 2004. Assessing in situ microcrack damage using ultrasonic velocity tomography. International Journal of Rock Mechanics & Sciences 42, 25-34.

Miao, M., McDonnell, J., Vuckovic, L., and Hawkins, C.S., 2010. Poisson's ratio and porosity of carbon nanotube dry-spun yarns. Carbon 48, 2802-2811.

Mine, J.K., 1978. The Potash deposits and their associates in the area of the Boulby Mine, Cleveland, University of Edinburgh, Edinburgh, 506p.

Minkley, W., Menzel, W., Konietzky, H. and Kamp, L. te, 2001. A visco-elasto-plastic softening model and its application for solving static and dynamic stability problems in potash mining, in *FLAC and Numerical Modeling in Geomechanics - 2001 (2nd International FLAC Conference, Lyon, France, October 2001)*, 21-27, Balkema, Rotterdam.

Miralles, L., Sans, M., Gali, S., and Santanach, P., 2001. 3-D rock salt fabrics in a shear zone (Sura Anticline, South-Pyrenees). Journal of Structural Geology 23, 675-691.

Mitchell, A.R. and Griffiths, D.F., 1987. The finite difference method in partial differential equations. John Willey & Sons, Chichester, 272p.

Mitra, R., 2006. Imaging of stress in rock samples using numerical modelling and laboratory tomography. PhD Thesis, Faculty of the Virginia Polytechnic Institute and State University, 189p.

Miura, K., Okui, Y., and Horii, H., 2003. Micromechanics-based prediction of creep failure of hard rock for long-term safety of high-level radioactive waste disposal system. Mechanics of Materials 35, 587-601.

Moller, S.C., and Vermeer, P.A., 2008. On numerical simulation of tunnel installation. Tunnelling and Underground Space Technology 23, 461-475.

Monaghan, W.D., and Trevits, M.A., 2004. Application of ground penetrating radar to evaluate the extent of polyurethane grout infiltration for mine roof control – a case study. http://www.cdc.gov/niosh/mining/pubs/pdfs/aogprte.pdf

Mousavi, S.M., Shamsai, A., Hesham M., El-N. and Khamehchian, 2001. A GPS-based monitoring program of land subsidence due to groundwater withdrawal in Iran. Can. J. Civ. Eng. 28, 452-464.

Narasimhan, T.N. and Goyal, K.P., 1984. Subsidence due to geothermal fluid withdrawal. Geological Society of America. Reviews in Engineering Geology, vol. VI, 32p.

NCB, 1966. Subsidence Engineers' Handbook, National Coal Board – Production Department, 130p.

North Yorkshire Geodiversity Partnership, 2006. Your Dales Rocks, Draft Local Geodiversity Action Plan, 45p. http://www.nygp.org.uk

Onset HOBO Data Loggers, 2005. Onset Computer Corporation, MAN-U12-006, 2P. http://www.onsetcomp.com

Ordnance Survey, 2007. A guide to coordinate systems in Great Britain. An introduction to mapping coordinate systems and the USE of GPS datasets with Ordnance Survey mapping, 46p

Patchet, S.J., 1970. Rock mechanics studies associated with the development of a deep potash mine. Ph.D. Thesis, University of Newcastle upon Tyne, 337p.

Petley, D.N., Higuchi, T., Petley, D.J., Bulmer, M.H. and Carey, J., 2005. The development of progressive landslide failure in cohesive materials, Geology, 33, 201-204.

Petley, D.N., Mantovani, F., Bulmer, M.H. and Zannoni, A., 2005. The use of surface monitoring data for the interpretation of landslide movement patterns. Geomorphology 66, 133-147.

Petley, D.N. and Allison, R.J., 1997. The mechanics of deep-seated landslides. Earth surface processes and landforms, 22, 747-758.

Phienwej, N., Thakur, P.K. and Cording, E.J., 2007. Time-dependent response of tunnels considering creep effect. International Journal of Geomechanics, vol. 7, no 4, 11p.

Phillipson, S.E., 2008. Texture, mineralogy, and rock strength in horizontal stress-related coal mine roof falls. International Journal of Coal Geology 75, 175-184.

Picher mining field, Northeast OKLAHOMA subsidence evaluation report, 2006, Oklahoma, USA, 149p.

Poliakov, A.N.B., Podladchikov, Y., and Talbot, C., 1993. Initiation of salt diapirs with frictional overburdens: numerical experiments. Tectonophysics 228, 199-210.

Popp, T., and Salzer, K., 2007. Anisotropy of seismic and mechanical properties of Opalinus clay during triaxial deformation in a multi-anvil apparatus. Physics and Chemistry of the Earth 32, 879-888.

Raucoules, D., Colesanti, C. and Carnec, C., 2007. Use of SAR interferometry for detecting and assessing ground subsidence. C.R. Geoscience 339, 289-302.

Raynaud, S., Ngan-Tillard, D., Desrues, J., and Mazerolle, F., 2008. Brittle-to-ductile transition in Beaucaire marl from triaxial tests under the CT-scanner. International Journal of Rock Mechanics & Mining Sciences 45, 653-671.

Rayner, D.H., and Hemingway, J.E., 1974. The geology and mineral resources of Yorkshire, Maney nd son ltd., Leeds, 405p.

Rawson, P.F., and Wright, J.K., 2000. The Yorkshire Coast. Geologists' Association Guide, v.34. Dinkyprint, London, 130p.

Rothenburg, L., Carvalho, A. L.P. Jr., and Dusseault, M.B., 2007. Performance of a mining panel over tachyhydrite in Taquari-Vassouras potash mine. Mechanical Behaviour of Salt – Understanding of THMC Processes in Salt, 305-314.

Rousakis, T.C., Karabinis, A.I., Kiousis, P.D., and Tepfers, R., 2008. Analytical modelling of plastic behaviour of uniformly FRP confined concrete members. Composites: Part B 39, 1104-113.

Santos, M.C., Gemael, C., Blake, B., Faggion, P., Krueger, C.P., Ferreira, L.D.D., Soares, M. and Szostak-Chrzanowski, A., 2001. Stage 1 of subsidence monitoring of the area surrounding Salto Caxias Power dam, in Brazil. FIG 10th International Symposium on Deformation Measurements, Orange, California, 89-97.

Schleinig, J.P. and Lukas, V., 2007. Monitoring of roof stability in salt mines. The Mechanical Behaviour of Salt – Understanding of THMC processes in Salt, 315-320.

Scrutton, C., 1994. Yorkshire rocks and landscape. A field guide. Yorkshire Geological Society, Maryport, Cumbria, 224p.

Sepehr, K., and Stimpson, B., 1988. Induced seismicity in potash mining – a finite element study. International Journal of Mining and Geological Engineering 6, 27-40.

Shahriar, K., Amoushahi, S., and Arabzadeh, M., 2009. Prediction of surface subsidence due to inclined very shallow coal seam mining. Coal Operators' Conference, The *AusIMM IIlawara Branch*, 11p. http://ro.uow.edu.au/coal/93

Shao, J.T., Chau, K.T., and Feng, X.T., 2006. Modeling of anisotropic damage and creep deformation in brittle rocks. International Journal of Rock Mechanics and Mining Sciences 43, 582-592.

Shao, J.F., Zhu, Q.Z., and Su, K., 2003. Modelling of creep in rock materials in terms of material degradation. Computers and Geotechnics 30, 549-555.

Sharan, S.K., 2005. Exact and approximate solutions for displacements around circular openings in elasto-brittle-plastic Hoek-Brown rock. International Journal of Rock Mechanics & Mining Sciences 42, 542-549.

Shen, B., King, A., and Guo, H., 2008. Displacement, stress and seismicity in roadway roofs during mining-induced failure. International Journal of Rock Mechanics & Mining Sciences 45, 672-688.

Shen, S.L. Hu, Y.S., and Hong, Z.S., 2006. Estimation of land subsidence based on groundwater flow model. Marine Georesources and Geotechnology, 24, 149-167.

Sheng Y., and Reddish D., 2005. Assessment of the water inflow to the mine workings by numerical modeling. Post-Mining 2005, Nancy, 10p. http://gisos.ensg.inpl-nancy-2005.

Shin H., Santamarina, J. C., and Cartwright, J.A., 2008. Contraction-driven shear failure in compacting uncemented sediments. The Geological Society of America, v. 36 no 12, 931-934.

Simms, M.J., Chidlaw, N., Morton, N., and Page, K.N., 2004. British Lower Jurassic Stratigraphy. Geological Conservation Review Series, v. 30. Joint Nature Conservation Committee, Peterborough, 458p.

Singh, R., Mandal, P.K., Singh, A.K., Kumar, R., Maiti, J. and Ghosh, A.K., 2008. Upshot of strata movement during underground mining of a thick coal seam below hilly terrain. International Journal of Rock Mechanics and Mining Sciences, vol. 45, no 1, 29-46.

Singh, R., 2004. Staggered development of a thick coal seam for full height working in a single lift by the blasting gallery method. International Journal of Rock Mechanics & Mining Sciences 41, 745-759.

Singh, B., and Goel, R.K., 1999. Rock mass classification: a practical approach in civil engineering. Elsevier Science Ltd., Kidlington, Oxford, 267p.

Sneed, M., Ikehara, M.E., Galloway, D.L. and Amelung, F., 2001. Detection and measurement of land subsidence using global positioning system and Interferometry synthetic aperture radar, Coachella Valleyr, California, 1996-1998. U.S. Geological survey, Sacramento, 26p.

Soltanzadeh, H., and Hawkes, C.D., 2009. Assessing fault reactivation tendency within and surrounding porous reservoirs during fluid production or injection. International Journal of Rock Mechanics & Mining Sciences 46, 1-7.

Spratt, D.A. and Harrison, B.J.D. (Editors), 1989. The North York Moors Landscape Heritage. The North York Moors National Park, 458p.

Stille, H., and Palmstrom, A., 2008. Ground behaviour and rock mass composition in underground excavations. Tunnelling and Underground Space Technology 23, 46-64.

Stiros, S.C. and Kontogianni, V.A., 2009. Coulomb stress changes: From earthquakes to underground excavation failures. International Journal of Rock Mechanics & Mining Sciences 46, 182-187.

Stiros, S., and Kontogianni, V., 2009. Mean deformation tensor and mean deformation ellipse of an excavated tunnel section. International Journal of Rock Mechanics & Mining Sciences 46, 1306-1314.

Stockburger, D.W., 1996. Introductory statistics: Concepts, models, and applications. The Psychology Department at Missouri State University, 8p. http://www.psychstat.missouristate.edu

Stramondo, S., Bozzano, F., Marra, F., Wegmuller, U., Cinti, F.R., Moro, M. and Saroli, M., 2008. Subsidence induced by urbanization in the city of Rome detected by advanced InSAR technique and geotechnical investigations. Remote Sensing of Environment 112, 3160-3172.

Swift, G.M., and Reddish, D.J., 2005. Underground excavations in rock salt. Geotechnical and Geological Engineering 23, 17-42.

Szostak-Chrzanowski, A., Chrzanowski, A. and Massiera, M., 2005. Use of deformation monitoring results in solving geotechnical problems – case studies. Engineering Geology 79, 3-12.

Szostak-Chrzanowski, A., Chrzanowski, A., and Massiera, M., 2003. Use of geodetic monitoring measurements in solving geomechanical problems in structural and mining engineering. Proceedings, 11th FIG Symposium of deformation measurements, Santorini, Greece, 8p.

Szwedzicki, T., 2003. Rock mass behaviour prior to failure. International Journal of Rock Mechanics & Mining Sciences 40, 573-584.

Talbot, C., Aftabi, P., and Chemia, Z., 2009. Potash in a salt mushroom at Hormoz Island, Hormoz Strait, Iran. Ore Geology Reviews 35, 317-332.

Talbot, C.J., Tully, C.P., and Woods, P.J.E., 1982. The structural geology of Boulby (Potash) mine, Cleveland, United Kingdom. Tectonophysics, 85, 167-204.

Tan, W.L., and Ranjith, P.G., 2003. Numerical analysis of pipe reinforcement in soft ground tunnelling, 10p. www.ce.washington.edu/em03/proceedings

The Geological Society, 2008. Fault Reactivation: Diagnostic Characteristics, 5p. www.ukgeohazards.info.

Tiwari, R.P., and Rao, K.S., 2006. Post failure behaviour of a rock mass under the influence of triaxial and true triaxial confinement. Engineering Geology 84, 112-129.

Tondi, E., Antonellini, M., Aydin, A., Marchegiani, L., and Cello, G., 2006. The role of deformation bands, stylolites and sheared stylolites in fault development in carbonate grainstones of Majella Mountain, Italy. Journal of Structural Geology 28, 376-391.

Urai, J.L. and Spiers, C.J., 2007. The effect of grain boundary water on deformation mechanisms and rheology of rocksalt during long-term deformation. Proceedings of the 6th conference on the mechanical behaviour of salt, 'SaltMech6', Hannover, 9p.

Utada, H., Takahashi, Y., Morita, Y., Koyama, T., Kagiyama, T., 2007. Active system for monitoring volcanic activity: A case study of the Izu-Oshima Volcano, Central Japan. Journal of Volcanology and Geothermal Research 164, 217-243.

Wakai, F., and Nikolic, S.Z., 2011. Effect of grain boundary slinding on shear viscosity and viscous Poisson's ratio in macroscopis shrinkage during sintering. Acta Materialia 59, 774-784.

Wang, G.Y., You, G., Shi, B., Yu, J., and Tuck, M., 2009. Long-term land subsidence and strata compression in Changzhou, China. Engineering Geology 104, 109-118.

Wang, G., 2004. A new constitutive creep-damage model for salt rock and its characteristics. International Journal of Rock Mechanics & Mining Sciences, 41, 7p.

Wang, H.F. and Anderson, M.P., 1982. Introduction to groundwater finite difference and finite element methods. Freeman, W.H. and Company, San Francisco, 237p.

Wang, H., and Ge, M., 2008. Acoustic emission/microseismic source location analysis for a limestone mine exhibiting high horizontal stresses. International Journal of Rock Mechanics & Mining Sciences 45, 720-728.

Wang, C., Wang, Y., and Lu, S., 2000. Deformational behaviour of roadways in soft rocks in underground coal mines and principles for stability control. International Journal of Rock Mechanics and Mining Sciences 37, 937-946.

Wang, S., Yin, X., Tang, H., and Ge, X., 2010. A new approach for analyzing circular tunnel in strain-softening rock masses. International Journal of Rock Mechanics & Mining Sciences 47, 170-178.

Wang, S.J., Wang, Y.Q., and Yang, S.Z., 2008. Study for lengthways ground subsidence induced by subsurface construction of metro. Proceedings of 2008 International Conference on Construction & Real Estate Management, 1&2, 807-810.

Ward, K.T. and Johnson, G.R., 2007. Geospatial methods provide timely and comprehensive urban forest information. Urban Forestry & Urban Greening 6, 15-22.

Watanabe, M., Enoki, M., and Kishi, T., 2003 Fracture behaviour of ceramic coatings during thermal cycling evaluated by acoustic emission method using laser interferometers. Materials Science and Engineering A 359, 368-374.

Weijermars, R., 1997. Principles of rock mechanics. Alboran Science Publishing, Saudi Arabia, 360p.

Whittles, D.N., Lowndes, I.S., Kingman, S.W., Yates. C. and Jobling, S., 2006. Influence of geotechnical factors on gas flow experienced in a UK longwall coal mine panel. International Journal of Rock Mechanics & Mining Sciences 43, 369-387.

Wiles, T.D., 2006. Reliability of numerical modelling predictions. International Journal of Rock Mechanics & Mining Sciences 43, 454-472.

Wolf, K.-H. and Bruining, H., 2007. Modelling the interaction between underground coal fires and their roof rocks. Fuel 86, 2761-2777.

Wong, H., Morvan, M., Deleruyelle, F. and Leo C.J., 2008. Analytical study of mine closure behaviour in a poro-elastic medium. Computers and Geotechnics 35, 645-654.

Wongsaroj, J., Soga, K. and Mair, R.J., 2007. Modelling of long-term ground response to tunnelling under St James's Park, London. Geotechnique 57, 75-90.

Wright, J., 1982. Ground and air survey for field scientists. Clarendon Press, Oxford, 327p.

Xianbin, Y. and Carlos, D da G., 2002. Stability analyses of underground room and pillar stopes by means of convergence. 8th Congresso Nacional de Geotechnica, Lisboa, 10p. http://cegeo.ist.utl.pt

Xiao-gang, H., Ren-wei, Z., Xiao-dong, P., Yong, S., Bo-gen, T. and Hua-shan, H., 2008. Numerical simulation for determining three zones in the goaf at a fully-mechanized coal face. J China Univ Mining & Technol 18, 0199-0203.

Xie, G.X., Chang, J.C., and Yang, K., 2009. Investigations into stress shell characteristics of surrounding rock in fully mechanized top-coal caving face. International Journal of Rocks Mechanics & Mining Sciences 46, 172-181.

Xiong, W., XiaoGang, W., QingWei, D., ZhiXin, J., NengXiong, X. and YanDong, S., 2008. Analysis of elastoplasticity and rheology due to mining subsidence. Sci China Ser D-Earth, vol. 51, no. 6, 826-836.

Zhang, Y., and Mitri, H.S., 2008. Elastoplastic stability analysis of mine haulage drift in the vicinity of mined stopes. International Journal of Rock Mechanics & Mining Sciences 45, 574-593

Zangerl, C., Eberhardt, E., Evans, K.F., and Loew, S., 2008. Consolidation settlements above deep tunnels in fractured crystalline rock: Part 2-Numerical analysis of the Gotthard highway tunnel case study. International Journal of Rock Mechanics and Mining Sciences, 45, 1211-1225.

Zhao, J., 2000. Applicability of Mohr-Coulomb and Hoek-Brown strength criteria to the dynamic strength of brittle rock. International Journal of Rock Mechanics and Mining Sciences, 37, 1115-1121.

Zhi.-hua. L., Lin-ming, D., Cai-ping, L., Zong-long, M., and An-ye, C., 2008. Study on fault induced rock bursts, J China Univ Mining & Technol 18, 0321-0326.

Zolochevsky, A., and Voyiadjis, G.Z., 2005. Theory of creep deformation with kinematic hardening for materials with different properties in tension and compression. International Journal of Plasticity 21, 435-462.

Yu, T, Teng, J.G., Wong, Y.L., and Dong, S.L., 2010. Finite element modelling of confined concrete: Drucker-Prager type plasticity model. Engineering Structures 32, 665-679.

Appendix A

FLAC Codes of generated grids

A. For assessing floor heave

```
flac: config cppudm
 Special FLAC configuration:
   cppudm-s allowed
flac: ; Initial model
flac: grid 90 90
flac: gen 0,-1500 0,0 1500,0 1500,-1500 i=1,91 j=1,91 ratio 1.0,1.0
flac: m e
flac: ; Final model
flac: ; Perform grid modification to fit the problem domain
flac: m n i=81,91 j=1,91;Not useful
flac: m n j=10; Create sub-grid of 9 layers of 1 meter each - region1
flac: m n j=30; Removed layer to be replaced by region 1 - region 2
flac: ; Moving region 1 to region 2 location
flac: gen 0,-1016.66669 0,-1000 1500,-1000 1500,-1016.66669 i=1,91 j=1,10 rat 1.0,1.0
flac: ; Perform attachment of relocated regions
flac: attach aside from 1,30 to 81,30 bside from 1,1 to 81,1
flac: attach aside from 1,31 to 81,31 bside from 1,10 to 81,10
flac: ; Assigning materials behaviour
flac: group 'Rock:Halite' notnull j 11 29
flac: model ss notnull group 'Rock:Halite'
flac: model ss i 1 80 j 11 29
flac: prop density=2200.0 bulk=6E9 shear=3.1E9 i 1 80 j 11 29
```

flac: prop cohesion=3.33E6 friction=13.33 dilation=0.0 tension=0.54e6 i 1 80 j 11 29

flac: prop ctab 1 ftab 2 i 1 80 j 11 29

flac: table 1 0,3.55e6 0,3.13e6

flac: table 2 0,13.33 0,3.33

flac: group 'Rock:Potash' notnull j 1 9

flac: model ss notnull group 'Rock:Potash'

flac: m ss i 1 80 j 1 9

flac: prop density=2100.0 bulk=9.58E9 shear=2.73E9 i 1 80 j 1 9

flac: prop cohesion=3.33E6 friction=12.0 dilation=0.0 tension=0.6e6 i 1 80 j 1 9

flac: prop ctab 1 ftab 2 i 1 80 j 1 9

flac: table 1 0,3.33e6 0,2.0e6

flac: table 2 0,12 0,11

flac: group 'Rock:Carnalite Marl' notnull j 31 42

flac: model ss notnull group 'Rock:Carnalite Marl'

flac: m ss i 1 80 j 31 42

flac: prop density=2300.0 bulk=1.3E9 shear=0.98E9 i 1 80 j 31 42

flac: prop cohesion=1e6 friction=11.67 dilation=0.0 tension=0.41e6 i 1 80 j 31 42

flac: prop ctab 1 ftab 2 i 1 80 j 31 42

flac: table 1 0,1e6 0,0.33e6

flac: table 2 0,11.67 0,6

flac: group 'Rock:Anhydrite' notnull j 43 50

flac: model ss notnull group 'Rock:Anhydrite'

flac: m ss i 1 80 j 43 50

flac: prop density=2800.0 bulk=4.81E9 shear=3.61E9 i 1 80 j 43 50

flac: prop cohesion=5.67E6 friction=14.33 dilation=0.0 tension=2.03e6 i 1 80 j 43 50

flac: prop ctab 1 ftab 2 i 1 80 j 43 50

flac: table 1 0,5.67e6 0,2.17e6

flac: table 2 0,14.33 0,5.33

```
flac: group 'Rock:Upper Halite' notnull j 51 90
flac: model ss notnull group 'Rock:Upper Halite'
flac: prop density=2200.0 bulk=4.1E9 shear=3.1E9 i 1 80 j 51 90
flac: prop cohesion=5.33E6 friction=11.67 dilation=0.0 tension=0.53e6 i 1 80 j 51 90
flac: prop ctab 1 ftab 2 i 1 80 j 51 90
flac: table 1 0,5.33e6 0,3.13e6
flac: table 2 0,11.67 0,3.33
flac: ; Initial conditions
flac: ini syy -25.5e6 i 1 80 j 51 90
flac: ini syy -25.7e6 i 1 80 j 43 50
flac: ini syy -25.95e6 i 1 80 j 31 42
flac: ini syy -26.1e6 i 1 80 j 1 9
flac: ini syy -26.2e6 i 1 80 j 11 29
flac: ini sxx -13.0e6 i 1 80 j 51 90
flac: ini sxx -13.1e6 i 1 80 j 43 50
flac: ini sxx -13.26e6 i 1 80 j 31 42
flac: ini sxx -13.3e6 i 1 80 j 1 9
flac: ini sxx -13.36e6 i 1 80 j 11 29
flac: ini szz -13.0e6 i 1 80 j 51 90
flac: ini szz -13.1e6 i 1 80 j 43 50
flac: ini szz -13.26e6 i 1 80 j 31 42
flac: ini szz -13.3e6 i 1 80 j 1 9
flac: ini szz -13.36e6 i 1 80 j 11 29
flac: ; Boundary conditions
flac: fix x i 1
flac: fix x i 81
flac: fix x y j 11
flac: ; apply gravity
```

flac: set grav=9.81

flac: ; Checking solving equilibrium state - histories

flac: his unbal

flac: his ydis i 1 j 91

flac: his ydis i 40 j 91

flac: his ydis i 81 j 91

flac: ; Equilibrium solving

flac: solve

flac: ; Excavating material

flac: m n i 31 38 j 1 7

flac: ; group 'null' i 31 38 j 1 7

flac: ; group delete 'null'

flac: m n i 43 50 j 1 7

flac: ; group 'null' i 43 50 j 1 7

flac: ; group delete 'null'

flac: ; Plotting histories

flac: history 5 ydisp i=35, j=8

flac: history 6 ydisp i=35, j=30

flac: history 7 ydisp i=47, j=8

flac: history 8 ydisp i=47, j=30

flac: ; Stepping model after excavating

flac: step 200

B. For analyzing stress and displacement distribution

B.1 Unfaulted structures

B.1.1 Saturated structures

MODEL 1

flac: !

flac: config gwflow cppudm

Special FLAC configuration:

groundwater flow

cppudm-s allowed

flac: grid 150,150

flac: gen (0.0,-1500.0) (0.0,0.0) (1500.0,0.0) (1500.0,-1500.0) ratio 1.0,1.0 i=1,151 j=1,151

flac: model elastic

flac: ;Perform grid modification to fit the problem domain

flac: model null i=141,151 j=1,151;Not useful

flac: model null j=10; Create sub-grid of 9 layers of 1 metre high each - region 1

flac: model null j=28; Removed layer to be replaced by region 1 - region 2

flac: ; Moving region 1 to region 2 location

flac: gen (0.0,-1230.0) (0.0,-1220.0) (1500.0,-1220.0) (1500.0,-1230.0) ratio 1.0,1.0 i=1,151 j=1,10

flac: ; Perform attachments of relocated regions

flac: attach aside from 1,28 to 141,28 bside from 1,1 to 141,1

flac: attach aside from 1,29 to 141,29 bside from 1,10 to 141,10

flac: group 'Rock:Lias' notnull j 108 150

flac: model drucker group 'Rock:Lias'

flac: prop density=2600.0 bulk_mod=2.3E9 shear_mod=3.14E9 kshear=0.006e6 qdil=0.0 qvol=0.192 tension=0.98E6 group 'Rock:Lias'

flac: group 'Rock:Sherwood sandstone' notnull j 36 107

flac: model mohr notnull group 'Rock:Sherwood sandstone'

flac: prop density=2500.0 bulk=2.89E9 shear=3.15E9 cohesion=2750000.0 friction=11.25 dilation=0.0 tension=1300000.0 notnull group 'Rock:Sherwood sandstone'

flac: group 'Rock:Carnalite marl' notnull j 29 35

flac: model ss notnull group 'Rock:Carnalite marl'

flac: m ss i 1 140 j 29 35

flac: prop density=2300.0 bulk=1.56E9 shear=1.17E9 i 1 140 j 29 35

flac: prop cohesion=1.2E6 friction=14 dilation=0.0 tension=0.5e6 i 1 140 j 29 35

flac: prop ctab 1 ftab 2 i 1 140 j 29 35

flac: table 1 0,1.2e6 0,0.4e6

flac: table 2 0,14 0,7.2

flac: group 'Rock:Potash' notnull j 1 9

flac: model ss notnull group 'Rock:Potash'

flac: m ss i 1 140 j 1 9

flac: prop density=2100.0 bulk=23.94E9 shear=6.82E9 i 1 140 j 1 9

flac: prop cohesion=8.33E6 friction=30 dilation=0.0 tension=1.49e6 i 1 140 j 1 9

flac: prop ctab 1 ftab 2 i 1 140 j 1 9

flac: table 1 0,8.33e6 0,5e6

flac: table 2 0,30 0,27.5

flac: group 'Rock:Halite' notnull j 11 27

flac: model ss notnull group 'Rock:Halite'

flac: m ss i 1 140 j 11 27

flac: prop density=2200.0 bulk=17.93E9 shear=9.25E9 i 1 140 j 11 27

flac: prop cohesion=10E6 friction=40 dilation=0.0 tension=1.63e6 i 1 140 j 11 27

flac: prop ctab 1 ftab 2 i 1 140 j 11 27

flac: table 1 0,10e6 0,9.4e6

flac: table 2 0,40 0,10

flac: ini syy -10.8e6 i 1 140 j 108 150

flac: ini syy -28.5e6 i 1 140 j 36 108

flac: ini syy -29.7e6 i 1 140 j 29 36

flac: ini syy -29.9e6 i 1 140 j 1 9

flac: ini syy -34.0e6 i 1 140 j 11 27

flac: ini sxx -2.7e6 i 1 140 j 108 150

flac: ini sxx -2.2e6 i 1 140 j 36 108

flac: ini sxx -15.1e6 i 1 140 j 29 36

flac: ini sxx -15.2e6 i 1 140 j 1 9

flac: ini sxx -17.4e6 i 1 140 j 11 27

flac: ini szz -2.7e6 i 1 140 j 108 150

flac: ini szz -2.2e6 i 1 140 j 36 108

flac: ini szz -15.1e6 i 1 140 j 29 36

flac: ini szz -15.2e6 i 1 140 j 1 9

flac: ini szz -17.4e6 i 1 140 j 11 27

flac: ; Assigning boundary conditions

flac: fix x i 1 j 11 151

flac: fix x i 141 j 11 151

flac: fix x y i 1 141 j 11

flac: ; Undrained analysis

flac: set flow=off

flac: water bulk = 2.2e9

flac: apply pp=9.3e6 i 1 141 j 36 108

flac: fix sat i 1 141 j 36 108

flac: ; apply gravity

flac: set grav=9.81

flac: ; Checking solving equilibrium state - histories

flac: his unbal

flac: his ydis i 1 j 151

flac: his ydis i 70 j 151

flac: his ydis i 141 j 151

flac: solve

flac: ; Excavating material

flac: model null i 54 67 j 1 7

flac: group 'null' i 54 67 j 1 7

flac: group delete 'null'

flac: model null i 74 87 j 1 7

flac: group 'null' i 74 87 j 1 7

flac: group delete 'null'

flac: history 5 ydisp i=61, j=28

flac: history 6 ydisp i=61, j=8

flac: history 7 ydisp i=81, j=28

flac: history 8 ydisp i=81, j=8

flac: history 9 ydisp i=70,j=151

flac: history 10 ydisp i=61, j=151

flac: history 11 ydisp i=30, j=151

flac: history 12 ydisp i=1, j=151

flac: history 13 ydisp i=80, j=151

flac: history 14 ydisp i=109, j=151

flac: history 15 ydisp i=141, j=151

flac: step 140

MODEL 2

flac: !

flac: config gwflow cppudm

Special FLAC configuration:

groundwater flow

cppudm-s allowed

flac: grid 150,150

flac: gen (0.0,-1500.0) (0.0,0.0) (1500.0,0.0) (1500.0,-1500.0) ratio 1.0,1.0 i=1,151 j=1,151

flac: model elastic

flac: ;Perform grid modification to fit the problem domain

flac: model null i=141,151 j=1,151;Not useful

flac: model null j=10; Create sub-grid of 9 layers of 1 metre high each - region 1

flac: model null j=28; Removed layer to be replaced by region 1 - region 2

flac: ; Moving region 1 to region 2 location

flac: gen (0.0,-1230.0) (0.0,-1220.0) (1500.0,-1220.0) (1500.0,-1230.0) ratio 1.0,1.0 i=1,151 j=1,10

flac: ; Perform attachments of relocated regions

flac: attach aside from 1,28 to 141,28 bside from 1,1 to 141,1

flac: attach aside from 1,29 to 141,29 bside from 1,10 to 141,10

flac: group 'Rock:Lias' notnull j 108 150

flac: model drucker group 'Rock:Lias'

flac: prop density=2600.0 bulk_mod=2.3E9 shear_mod=3.14E9 kshear=0.006e6 qdil=0.0 qvol=0.192 tension=0.98E6 group 'Rock:Lias'

flac: group 'Rock:Mercia mudstone' notnull j 82 107

flac: model mohr notnull group 'Rock:Mercia mudstone'

flac: prop density=2700.0 bulk=3.38E9 shear=3.94E9 cohesion=1500000.0 friction=10.25 dilation=0.0 tension=690000.0 notnull group 'Rock:Mercia mudstone'

flac: group 'Rock:Sherwood sandstone' notnull j 36 81

flac: model mohr notnull group 'Rock:Sherwood sandstone'

flac: prop density=2500.0 bulk=2.89E9 shear=3.15E9 cohesion=2750000.0 friction=11.25 dilation=0.0 tension=1300000.0 notnull group 'Rock:Sherwood sandstone'

flac: group 'Rock:Carnalite marl' notnull j 29 35

flac: model ss notnull group 'Rock:Carnalite marl'

flac: m ss i 1 140 j 29 35

flac: prop density=2300.0 bulk=1.56E9 shear=1.17E9 i 1 140 j 29 35

flac: prop cohesion=1.2E6 friction=14 dilation=0.0 tension=0.5e6 i 1 140 j 29 35

flac: prop ctab 1 ftab 2 i 1 140 j 29 35

flac: table 1 0,1.2e6 0,0.4e6

flac: table 2 0,14 0,7.2

flac: group 'Rock:Potash' notnull j 1 9

flac: model ss notnull group 'Rock:Potash'

flac: m ss i 1 140 j 1 9

flac: prop density=2100.0 bulk=23.94E9 shear=6.82E9 i 1 140 j 1 9

flac: prop cohesion=8.33E6 friction=30 dilation=0.0 tension=1.49e6 i 1 140 j 1 9

flac: prop ctab 1 ftab 2 i 1 140 j 1 9

flac: table 1 0,8.33e6 0,5e6

flac: table 2 0,30 0,27.5

flac: group 'Rock:Halite' notnull j 11 27

flac: model ss notnull group 'Rock:Halite'

flac: m ss i 1 140 j 11 27

flac: prop density=2200.0 bulk=17.93E9 shear=9.25E9 i 1 140 j 11 27

flac: prop cohesion=10E6 friction=40 dilation=0.0 tension=1.63e6 i 1 140 j 11 27

flac: prop ctab 1 ftab 2 i 1 140 j 11 27

flac: table 1 0,10e6 0,9.4e6

flac: table 2 0,40 0,10

flac: ; Initial conditions

flac: ini syy -10.8e6 i 1 140 j 108 150

flac: ini syy -17.8e6 i 1 140 j 82 108

flac: ini syy -29.0e6 i 1 140 j 36 82

flac: ini syy -30.3e6 i 1 140 j 29 36

flac: ini syy -30.4e6 i 1 140 j 1 9

flac: ini syy -34.6e6 i 1 140 j 11 27

flac: ini sxx -2.7e6 i 1 140 j 108 150

flac: ini sxx -1.6e6 i 1 140 j 82 108

flac: ini sxx -2.2e6 i 1 140 j 36 82

flac: ini sxx -15.4e6 i 1 140 j 29 36

flac: ini sxx -15.5e6 i 1 140 j 1 9

flac: ini sxx -17.6e6 i 1 140 j 11 27

flac: ini szz -2.7e6 i 1 140 j 108 150

flac: ini szz -1.6e6 i 1 140 j 82 108

flac: ini szz -2.2e6 i 1 140 j 36 82

flac: ini szz -15.4e6 i 1 140 j 29 36

flac: ini szz -15.5e6 i 1 140 j 1 9

flac: ini szz -17.6e6 i 1 140 j 11 27

flac: ; Assigning boundary conditions

flac: fix x i 1 j 11 151

flac: fix x i 141 j 11 151

flac: fix x y i 1 141 j 11

flac: ; Undrained analysis

flac: set flow=off

flac: water bulk = 2.2e9

flac: apply pp=9.3e6 i 1 141 j 36 82

flac: fix sat i 1 141 j 36 82

flac: ; apply gravity

flac: set grav=9.81

flac: ; Checking solving equilibrium state - histories

flac: his unbal

flac: his ydis i 1 j 151

flac: his ydis i 70 j 151

flac: his ydis i 141 j 151

flac: solve

flac: ; Excavating material

flac: model null i 54 67 j 1 7

flac: group 'null' i 54 67 j 1 7

flac: group delete 'null'

flac: model null i 74 87 j 1 7

flac: group 'null' i 74 87 j 1 7

flac: group delete 'null'

flac: history 5 ydisp i=61, j=28

flac: history 6 ydisp i=61, j=8

flac: history 7 ydisp i=81, j=28

flac: history 8 ydisp i=81, j=8

flac: history 9 ydisp i=70,j=151

flac: history 10 ydisp i=61, j=151

flac: history 11 ydisp i=30, j=151

flac: history 12 ydisp i=1, j=151

flac: history 13 ydisp i=80, j=151

flac: history 14 ydisp i=109, j=151

flac: history 15 ydisp i=141, j=151

flac: step 140

MODEL 3

flac: !

flac: config gwflow cppudm

Special FLAC configuration:

groundwater flow

cppudm-s allowed

flac: grid 150,150

flac: gen (0.0,-1500.0) (0.0,0.0) (1500.0,0.0) (1500.0,-1500.0) ratio 1.0,1.0 i=1,151 j=1,151

flac: model elastic

flac: ;Perform grid modification to fit the problem domain

flac: model null i=141,151 j=1,151;Not useful

flac: model null j=10; Create sub-grid of 9 layers of 1 metre high each - region 1

flac: model null j=28; Removed layer to be replaced by region 1 - region 2

flac: ; Moving region 1 to region 2 location

flac: gen (0.0,-1230.0) (0.0,-1220.0) (1500.0,-1220.0) (1500.0,-1230.0) ratio 1.0,1.0 i=1,151 j=1,10

flac: ; Perform attachments of relocated regions

flac: attach aside from 1,28 to 141,28 bside from 1,1 to 141,1

flac: attach aside from 1,29 to 141,29 bside from 1,10 to 141,10

flac: group 'Rock:Lias' notnull j 108 150

flac: model drucker group 'Rock:Lias'

flac: prop density=2600.0 bulk_mod=2.3E9 shear_mod=3.14E9 kshear=0.006e6 qdil=0.0 qvol=0.192 tension=0.98E6 group 'Rock:Lias'

flac: group 'Rock:Mercia mudstone' notnull j 82 107

flac: model mohr notnull group 'Rock:Mercia mudstone'

flac: prop density=2700.0 bulk=3.38E9 shear=3.94E9 cohesion=1500000.0 friction=10.25 dilation=0.0 tension=690000.0 notnull group 'Rock:Mercia mudstone'

flac: group 'Rock:Sherwood sandstone' notnull j 48 81

flac: model mohr notnull group 'Rock:Sherwood sandstone'

flac: prop density=2500.0 bulk=2.89E9 shear=3.15E9 cohesion=2750000.0 friction=11.25 dilation=0.0 tension=1300000.0 notnull group 'Rock:Sherwood sandstone'

flac: group 'Rock:Sherwood mudstone' notnull j 36 47

flac: model mohr notnull group 'Rock:Sherwood mudstone'

flac: prop density=2300.0 bulk=2.63E9 shear=3.18E9 cohesion=6500000.0 friction=11.0 dilation=0.0 tension=1720000.0 notnull group 'Rock:Sherwood mudstone'

flac: group 'Rock:Carnalite marl' notnull j 29 35

flac: model ss notnull group 'Rock:Carnalite marl'

flac: m ss i 1 140 j 29 35

flac: prop density=2300.0 bulk=1.56E9 shear=1.17E9 i 1 140 j 29 35

flac: prop cohesion=1.2E6 friction=14 dilation=0.0 tension=0.5e6 i 1 140 j 29 35

flac: prop ctab 1 ftab 2 i 1 140 j 29 35

flac: table 1 0,1.2e6 0,0.4e6

flac: table 2 0,14 0,7.2

flac: group 'Rock:Potash' notnull j 1 9

flac: model ss notnull group 'Rock:Potash'

flac: m ss i 1 140 j 1 9

flac: prop density=2100.0 bulk=23.94E9 shear=6.82E9 i 1 140 j 1 9

flac: prop cohesion=8.33E6 friction=30 dilation=0.0 tension=1.49e6 i 1 140 j 1 9

flac: prop ctab 1 ftab 2 i 1 140 j 1 9

flac: table 1 0,8.33e6 0,5e6

flac: table 2 0,30 0,27.5

flac: group 'Rock:Halite' notnull j 11 27

flac: model ss notnull group 'Rock:Halite'

flac: m ss i 1 140 j 11 27

flac: prop density=2200.0 bulk=17.93E9 shear=9.25E9 i 1 140 j 11 27

flac: prop cohesion=10E6 friction=40 dilation=0.0 tension=1.63e6 i 1 140 j 11 27

flac: prop ctab 1 ftab 2 i 1 140 j 11 27

flac: table 1 0,10e6 0,9.4e6

flac: table 2 0,40 0,10

flac: ; Initial conditions

flac: ini syy -10.8e6 i 1 140 j 108 150

flac: ini syy -17.8e6 i 1 140 j 82 108

flac: ini syy -26.1e6 i 1 140 j 48 82

flac: ini syy -28.8e6 i 1 140 j 36 48

flac: ini syy -30.0e6 i 1 140 j 29 36

flac: ini syy -30.2e6 i 1 140 j 1 9

flac: ini syy -34.3e6 i 1 140 j 11 27

flac: ini sxx -2.7e6 i 1 140 j 108 150

flac: ini sxx -1.6e6 i 1 140 j 82 108

flac: ini sxx -2.0e6 i 1 140 j 48 82

flac: ini sxx -2.2e6 i 1 140 j 36 48

flac: ini sxx -15.3e6 i 1 140 j 29 36

flac: ini sxx -15.4e6 i 1 140 j 1 9

flac: ini sxx -17.5e6 i 1 140 j 11 27

flac: ini szz -2.7e6 i 1 140 j 108 150

flac: ini szz -1.6e6 i 1 140 j 82 108

flac: ini szz -2.0e6 i 1 140 j 48 82

flac: ini szz -2.2e6 i 1 140 j 36 48

flac: ini szz -15.3e6 i 1 140 j 29 36

flac: ini szz -15.4e6 i 1 140 j 1 9

flac: ini szz -17.5e6 i 1 140 j 11 27

flac: ; Assigning boundary conditions

flac: fix x i 1 j 11 151

flac: fix x i 141 j 11 151

flac: fix x y i 1 141 j 11

flac: ; Undrained analysis

flac: set flow=off

flac: water bulk = 2.2e9

flac: apply pp=9.3e6 i 1 141 j 48 82

flac: fix sat i 1 141 j 48 82

flac: ; apply gravity

flac: set grav=9.81

flac: ; Checking solving equilibrium state - histories

flac: his unbal

flac: his ydis i 1 j 151

flac: his ydis i 70 j 151

flac: his ydis i 141 j 151

flac: solve

flac: ; Excavating material

flac: model null i 54 67 j 1 7

flac: group 'null' i 54 67 j 1 7

flac: group delete 'null'

flac: model null i 74 87 j 1 7

flac: group 'null' i 74 87 j 1 7

flac: group delete 'null'

flac: history 5 ydisp i=61, j=28

flac: history 6 ydisp i=61, j=8

flac: history 7 ydisp i=81, j=28

flac: history 8 ydisp i=81, j=8

flac: history 9 ydisp i=70,j=151

flac: history 10 ydisp i=61, j=151

flac: history 11 ydisp i=30, j=151

flac: history 12 ydisp i=1, j=151

flac: history 13 ydisp i=80, j=151

flac: history 14 ydisp i=109, j=151

flac: history 15 ydisp i=141, j=151

flac: step 140

MODEL 4

flac: !

flac: config gwflow cppudm

Special FLAC configuration:

groundwater flow

cppudm-s allowed

flac: grid 150,150

flac: gen (0.0,-1500.0) (0.0,0.0) (1500.0,0.0) (1500.0,-1500.0) ratio 1.0,1.0 i=1,151 j=1,151

flac: model elastic

flac: ;Perform grid modification to fit the problem domain

flac: model null i=141,151 j=1,151;Not useful

flac: model null j=10; Create sub-grid of 9 layers of 1 metre high each - region 1

flac: model null j=28; Removed layer to be replaced by region 1 - region 2

flac: ; Moving region 1 to region 2 location

flac: gen (0.0,-1230.0) (0.0,-1220.0) (1500.0,-1220.0) (1500.0,-1230.0) ratio 1.0,1.0 i=1,151 j=1,10

flac: ; Perform attachments of relocated regions

flac: attach aside from 1,28 to 141,28 bside from 1,1 to 141,1

flac: attach aside from 1,29 to 141,29 bside from 1,10 to 141,10

flac: group 'Rock:Lias' notnull j 110 150

flac: model drucker group 'Rock:Lias'

flac: prop density=2600.0 bulk_mod=2.3E9 shear_mod=3.14E9 kshear=0.006e6 qdil=0.0 qvol=0.192 tension=0.98E6 group 'Rock:Lias'

flac: group 'Rock:Rheatic' notnull j 108 109

flac: model drucker group 'Rock:Rheatic'

flac: prop density=2500.0 bulk_mod=1.2E9 shear_mod=1.55E9 kshear=0.024e6 qdil=0.0 qvol=0.2 tension=1.06E6 group 'Rock:Rheatic'

flac: group 'Rock:Mercia mudstone' notnull j 82 107

flac: model mohr notnull group 'Rock:Mercia mudstone'

flac: prop density=2700.0 bulk=3.38E9 shear=3.94E9 cohesion=1500000.0 friction=10.25 dilation=0.0 tension=690000.0 notnull group 'Rock:Mercia mudstone'

flac: group 'Rock:Sherwood sandstone' notnull j 48 81

flac: model mohr notnull group 'Rock:Sherwood sandstone'

flac: prop density=2500.0 bulk=2.89E9 shear=3.15E9 cohesion=2750000.0 friction=11.25 dilation=0.0 tension=1300000.0 notnull group 'Rock:Sherwood sandstone'

flac: group 'Rock:Sherwood mudstone' notnull j 36 47

flac: model mohr notnull group 'Rock:Sherwood mudstone'

flac: prop density=2300.0 bulk=2.63E9 shear=3.18E9 cohesion=6500000.0 friction=11.0 dilation=0.0 tension=1720000.0 notnull group 'Rock:Sherwood mudstone'

flac: group 'Rock:Carnalite marl' notnull j 29 35

flac: model ss notnull group 'Rock:Carnalite marl'

flac: m ss i 1 140 j 29 35

flac: prop density=2300.0 bulk=1.56E9 shear=1.17E9 i 1 140 j 29 35

flac: prop cohesion=1.2E6 friction=14 dilation=0.0 tension=0.5e6 i 1 140 j 29 35

flac: prop ctab 1 ftab 2 i 1 140 j 29 35

flac: table 1 0,1.2e6 0,0.4e6

flac: table 2 0,14 0,7.2

flac: group 'Rock:Potash' notnull j 1 9

flac: model ss notnull group 'Rock:Potash'

flac: m ss i 1 140 j 1 9

flac: prop density=2100.0 bulk=23.94E9 shear=6.82E9 i 1 140 j 1 9

flac: prop cohesion=8.33E6 friction=30 dilation=0.0 tension=1.49e6 i 1 140 j 1 9

flac: prop ctab 1 ftab 2 i 1 140 j 1 9

flac: table 1 0,8.33e6 0,5e6

flac: table 2 0,30 0,27.5

flac: group 'Rock:Halite' notnull j 11 27

flac: model ss notnull group 'Rock:Halite'

flac: m ss i 1 140 j 11 27

flac: prop density=2200.0 bulk=17.93E9 shear=9.25E9 i 1 140 j 11 27

flac: prop cohesion=10E6 friction=40 dilation=0.0 tension=1.63e6 i 1 140 j 11 27

flac: prop ctab 1 ftab 2 i 1 140 j 11 27

flac: table 1 0,10e6 0,9.4e6

flac: table 2 0,40 0,10

flac: ; Initial conditions

flac: ini syy -10.3e6 i 1 140 j 110 150

flac: ini syy -10.8e6 i 1 140 j 108 110

flac: ini syy -17.8e6 i 1 140 j 82 108

flac: ini syy -26.0e6 i 1 140 j 48 82

flac: ini syy -28.7e6 i 1 140 j 36 48

flac: ini syy -30.0e6 i 1 140 j 29 36

flac: ini syy -30.1e6 i 1 140 j 1 9

flac: ini syy -34.3e6 i 1 140 j 11 27

flac: ini sxx -2.6e6 i 1 140 j 108 150

flac: ini sxx -0.6e6 i 1 140 j 108 110

flac: ini sxx -1.5e6 i 1 140 j 82 108

flac: ini sxx -2.0e6 i 1 140 j 48 82

flac: ini sxx -2.2e6 i 1 140 j 36 48

flac: ini sxx -15.3e6 i 1 140 j 29 36

flac: ini sxx -15.4e6 i 1 140 j 1 9

flac: ini sxx -17.5e6 i 1 140 j 11 27

flac: ini szz -2.6e6 i 1 140 j 108 150

flac: ini szz -0.6e6 i 1 140 j 108 110

flac: ini szz -1.5e6 i 1 140 j 82 108

flac: ini szz -2.0e6 i 1 140 j 48 82

flac: ini szz -2.2e6 i 1 140 j 36 48

flac: ini szz -15.3e6 i 1 140 j 29 36

flac: ini szz -15.4e6 i 1 140 j 1 9

flac: ini szz -17.5e6 i 1 140 j 11 27

flac: ; Assigning boundary conditions

flac: fix x i 1 j 11 151

flac: fix x i 141 j 11 151

flac: fix x y i 1 141 j 11

flac: ; Undrained analysis

flac: set flow=off

flac: water bulk = 2.2e9

flac: apply pp=9.3e6 i 1 141 j 48 82

flac: fix sat i 1 141 j 48 82

flac: ; apply gravity

flac: set grav=9.81

flac: ; Checking solving equilibrium state - histories

flac: his unbal

flac: his ydis i 1 j 151

flac: his ydis i 70 j 151

flac: his ydis i 141 j 151

flac: solve

flac: ; Excavating material

flac: model null i 54 67 j 1 7

flac: group 'null' i 54 67 j 1 7

flac: group delete 'null'

flac: model null i 74 87 j 1 7

flac: group 'null' i 74 87 j 1 7

flac: group delete 'null'

flac: history 5 ydisp i=61, j=28

flac: history 6 ydisp i=61, j=8

flac: history 7 ydisp i=81, j=28

flac: history 8 ydisp i=81, j=8

flac: history 9 ydisp i=70,j=151

flac: history 10 ydisp i=61, j=151

flac: history 11 ydisp i=30, j=151

flac: history 12 ydisp i=1, j=151

flac: history 13 ydisp i=80, j=151

flac: history 14 ydisp i=109, j=151

flac: history 15 ydisp i=141, j=151

flac: step 140

MODEL 5

flac: !

flac: config gwflow cppudm

Special FLAC configuration:

groundwater flow

cppudm-s allowed

flac: grid 150,150

flac: gen (0.0,-1500.0) (0.0,0.0) (1500.0,0.0) (1500.0,-1500.0) ratio 1.0,1.0 i=1,151 j=1,151

flac: model elastic

flac: ;Perform grid modification to fit the problem domain

flac: model null i=141,151 j=1,151;Not useful

flac: model null j=10; Create sub-grid of 9 layers of 1 metre high each - region 1

flac: model null j=28; Removed layer to be replaced by region 1 - region 2

flac: ; Moving region 1 to region 2 location

flac: gen (0.0,-1230.0) (0.0,-1220.0) (1500.0,-1220.0) (1500.0,-1230.0) ratio 1.0,1.0 i=1,151 j=1,10

flac: ; Perform attachments of relocated regions

flac: attach aside from 1,28 to 141,28 bside from 1,1 to 141,1

flac: attach aside from 1,29 to 141,29 bside from 1,10 to 141,10

flac: group 'Rock:Lias' notnull j 110 150

flac: model drucker group 'Rock:Lias'

flac: prop density=2600.0 bulk_mod=2.3E9 shear_mod=3.14E9 kshear=0.006e6 qdil=0.0 qvol=0.192 tension=0.98E6 group 'Rock:Lias'

flac: group 'Rock:Rheatic' notnull j 108 110

flac: model drucker group 'Rock:Rheatic'

flac: prop density=2500.0 bulk_mod=1.2E9 shear_mod=1.55E9 kshear=0.024e6 qdil=0.0 qvol=0.2 tension=1.06E6 group 'Rock:Rheatic'

flac: group 'Rock:Mercia mudstone' notnull j 82 108

flac: model mohr notnull group 'Rock:Mercia mudstone'

flac: prop density=2700.0 bulk=3.38e9 shear=3.94e9 cohesion=1.5e6 friction=10.25 dilation=0.0 tension=0.69e6 notnull group 'Rock:Mercia mudstone'

flac: group 'Rock:Sherwood sandstone' notnull j 48 82

flac: model mohr notnull group 'Rock:Sherwood sandstone'

flac: prop density=2500.0 bulk=2.89E9 shear=3.15E9 cohesion=2.75E6 friction=11.25 dilation=0.0 tension=1.3e6 notnull group 'Rock:Sherwood sandstone'

flac: group 'Rock:Sherwood mudstone' notnull j 36 48

flac: model mohr notnull group 'Rock:Sherwood mudstone'

flac: prop density=2300.0 bulk=2.63E9 shear=3.18E9 cohesion=6.5E6 friction=11 dilation=0.0 tension=1.72e6 notnull group 'Rock:Sherwood mudstone'

flac: group 'Rock:Anhydrite' notnull j 32 36

flac: model mohr notnull group 'Rock:Anhydrite'

flac: prop density=2800.0 bulk=3.61E9 shear=2.71E9 cohesion=4.25E6 friction=10.75 dilation=0.0 tension=1.52e6 notnull group 'Rock:Anhydrite'

flac: group 'Rock:Carnalite marl' notnull j 29 31

flac: model ss notnull group 'Rock:Carnalite marl'

flac: m ss i 1 140 j 29 31

flac: prop density=2300.0 bulk=1.56E9 shear=1.17E9 i 1 140 j 29 31

flac: prop cohesion=1.2E6 friction=14 dilation=0.0 tension=0.5e6 i 1 140 j 29 31

flac: prop ctab 1 ftab 2 i 1 140 j 29 31

flac: table 1 0,1.2e6 0,0.4e6

flac: table 2 0,14 0,7.2

flac: group 'Rock:Potash' notnull j 1 9

flac: model ss notnull group 'Rock:Potash'

flac: m ss i 1 140 j 1 9

flac: prop density=2100.0 bulk=23.94E9 shear=6.82E9 i 1 140 j 1 9

flac: prop cohesion=8.33E6 friction=30 dilation=0.0 tension=1.49e6 i 1 140 j 1 9

flac: prop ctab 1 ftab 2 i 1 140 j 1 9

flac: table 1 0,8.33e6 0,5e6

flac: table 2 0,30 0,27.5

flac: group 'Rock:Halite' notnull j 11 27

flac: model ss notnull group 'Rock:Halite'

flac: m ss i 1 140 j 11 27

flac: prop density=2200.0 bulk=17.93E9 shear=9.25E9 i 1 140 j 11 27

flac: prop cohesion=10E6 friction=40 dilation=0.0 tension=1.63e6 i 1 140 j 11 27

flac: prop ctab 1 ftab 2 i 1 140 j 11 27

flac: table 1 0,10e6 0,9.4e6

flac: table 2 0,40 0,10

flac: ; Initial conditions

flac: ini syy -10.3e6 i 1 140 j 110 150

flac: ini syy -10.8e6 i 1 140 j 108 110

flac: ini syy -17.8e6 i 1 140 j 82 108

flac: ini syy -26.0e6 i 1 140 j 48 82

flac: ini syy -28.7e6 i 1 140 j 36 48

flac: ini syy -30.0e6 i 1 140 j 32 36

flac: ini syy -30.2e6 i 1 140 j 29 31

flac: ini syy -30.4e6 i 1 140 j 1 9

flac: ini syy -34.5e6 i 1 140 j 11 27

flac: ini sxx -2.6e6 i 1 140 j 110 150

flac: ini sxx -0.6e6 i 1 140 j 108 110

flac: ini sxx -1.5e6 i 1 140 j 82 108

flac: ini sxx -2e6 i 1 140 j 48 82

flac: ini sxx -2.2e6 i 1 140 j 36 48

flac: ini sxx -8.5e6 i 1 140 j 32 36

flac: ini sxx -15.4e6 i 1 140 j 29 31

flac: ini sxx -15.5e6 i 1 140 j 1 9

flac: ini sxx -17.6e6 i 1 140 j 11 27

flac: ini szz -0.6e6 i 1 140 j 108 110

flac: ini szz -1.5e6 i 1 140 j 82 108

flac: ini szz -2e6 i 1 140 j 48 82

flac: ini szz -2.2e6 i 1 140 j 36 48

flac: ini szz -8.5e6 i 1 140 j 32 36

flac: ini szz -15.4e6 i 1 140 j 29 31

flac: ini szz -15.5e6 i 1 140 j 1 9

flac: ini szz -17.6e6 i 1 140 j 11 27

flac: ; Assigning boundary conditions

flac: fix x i 1 j 11 151

flac: fix x i 141 j 11 151

flac: fix x y i 1 141 j 11

flac: ; Undrained analysis

flac: set flow=off

flac: water bulk = 2.2e9

flac: apply pp=9.3e6 i 1 141 j 48 82

flac: fix sat i 1 141 j 48 82

flac: ; apply gravity

flac: set grav=9.81

flac: ; Checking solving equilibrium state - histories

flac: his unbal

flac: his ydis i 1 j 151

flac: his ydis i 70 j 151

flac: his ydis i 141 j 151

flac: solve

flac: ; Excavating material

flac: model null i 54 67 j 1 7

flac: group 'null' i 54 67 j 1 7

flac: group delete 'null'

flac: model null i 74 87 j 1 7

flac: group 'null' i 74 87 j 1 7

flac: group delete 'null'

flac: history 5 ydisp i=61, j=28

flac: history 6 ydisp i=61, j=8

flac: history 7 ydisp i=81, j=28

flac: history 8 ydisp i=81, j=8

flac: history 9 ydisp i=70,j=151

flac: history 10 ydisp i=61, j=151

flac: history 11 ydisp i=30, j=151

flac: history 12 ydisp i=1, j=151

flac: history 13 ydisp i=80, j=151

flac: history 14 ydisp i=109, j=151

flac: history 15 ydisp i=141, j=151

flac: step 140

B.1.3 Unsaturated structure

MODEL 5

flac: !

flac: config cppudm

Special FLAC configuration:

cppudm-s allowed

flac: grid 150,150

flac: gen (0.0,-1500.0) (0.0,0.0) (1500.0,0.0) (1500.0,-1500.0) ratio 1.0,1.0 i=1,151 j=1,151

flac: model elastic

flac: ;Perform grid modification to fit the problem domain

flac: model null i=141,151 j=1,151;Not useful

flac: model null j=10; Create sub-grid of 9 layers of 1 metre high each - region 1

flac: model null j=28; Removed layer to be replaced by region 1 - region 2

flac: ; Moving region 1 to region 2 location

flac: gen (0.0,-1230.0) (0.0,-1220.0) (1500.0,-1220.0) (1500.0,-1230.0) ratio 1.0,1.0 i=1,151 j=1,10

flac: ; Perform attachments of relocated regions

flac: attach aside from 1,28 to 141,28 bside from 1,1 to 141,1

flac: attach aside from 1,29 to 141,29 bside from 1,10 to 141,10

flac: group 'Rock:Lias' notnull j 110 150

flac: model drucker group 'Rock:Lias'

flac: prop density=2600.0 bulk_mod=4.59E9 shear_mod=6.28E9 kshear=0.012e6 qdil=0.0 qvol=0.038 tension=2.0E6 group 'Rock:Lias'

flac: group 'Rock:Rheatic' notnull j 108 110

flac: model drucker group 'Rock:Rheatic'

flac: prop density=2500.0 bulk_mod=2.414E9 shear_mod=3.1E9 kshear=0.047e6 qdil=0.0 qvol=0.41 tension=2.12E6 group 'Rock:Rheatic'

flac: group 'Rock:Mercia mudstone' notnull j 82 108

flac: model mohr notnull group 'Rock:Mercia mudstone'

flac: prop density=2700.0 bulk=6.76e9 shear=7.88e9 cohesion=3e6 friction=20.5 dilation=0.0 tension=1.38e6 notnull group 'Rock:Mercia mudstone'

flac: group 'Rock:Sherwood sandstone' notnull j 48 82

flac: model mohr notnull group 'Rock:Sherwood sandstone'

flac: prop density=2500.0 bulk=5.78E9 shear=6.3E9 cohesion=5.5E6 friction=22.5 dilation=0.0 tension=2.6e6 notnull group 'Rock:Sherwood sandstone'

flac: group 'Rock:Sherwood mudstone' notnull j 36 48

flac: model mohr notnull group 'Rock:Sherwood mudstone'

flac: prop density=2300.0 bulk=5.27E9 shear=6.35E9 cohesion=13E6 friction=22 dilation=0.0 tension=3.43e6 notnull group 'Rock:Sherwood mudstone'

flac: group 'Rock:Anhydrite' notnull j 32 36

flac: model mohr notnull group 'Rock:Anhydrite'

flac: prop density=2800.0 bulk=2.41E9 shear=1.81E9 cohesion=2.83E6 friction=7.17 dilation=0.0 tension=1.01e6 notnull group 'Rock:Anhydrite'

flac: group 'Rock:Carnalite marl' notnull j 29 31

flac: model ss notnull group 'Rock:Carnalite marl'

flac: m ss i 1 140 j 29 31

flac: prop density=2300.0 bulk=2.6E9 shear=1.95E9 i 1 140 j 29 31

flac: prop cohesion=2E6 friction=23.33 dilation=0.0 tension=0.83e6 i 1 140 j 29 31

flac: prop ctab 1 ftab 2 i 1 140 j 29 31

flac: table 1 0,2e6 0,0.67e6

flac: table 2 0,23.33 0,12

flac: group 'Rock:Potash' notnull j 1 9

flac: model ss notnull group 'Rock:Potash'

flac: m ss i 1 140 j 1 9

flac: prop density=2100.0 bulk=25.14E9 shear=7.16E9 i 1 140 j 1 9

flac: prop cohesion=8.75E6 friction=31.5 dilation=0.0 tension=1.57e6 i 1 140 j 1 9

flac: prop ctab 1 ftab 2 i 1 140 j 1 9

flac: table 1 0,8.75e6 0,5.25e6

flac: table 2 0,31.5 0,28.86

flac: group 'Rock:Halite' notnull j 11 27

flac: model ss notnull group 'Rock:Halite'

flac: m ss i 1 140 j 11 27

flac: prop density=2200.0 bulk=17.93E9 shear=9.25E9 i 1 140 j 11 27

flac: prop cohesion=10E6 friction=40 dilation=0.0 tension=1.63e6 i 1 140 j 11 27

flac: prop ctab 1 ftab 2 i 1 140 j 11 27

flac: table 1 0,10e6 0,9.4e6

flac: table 2 0,40 0,10

flac: ; Initial conditions

flac: ini syy -10.3e6 i 1 140 j 110 150

flac: ini syy -10.8e6 i 1 140 j 108 110

flac: ini syy -17.8e6 i 1 140 j 82 108

flac: ini syy -26.0e6 i 1 140 j 48 82

flac: ini syy -28.7e6 i 1 140 j 36 48

flac: ini syy -30.0e6 i 1 140 j 32 36

flac: ini syy -30.2e6 i 1 140 j 29 31

flac: ini syy -30.4e6 i 1 140 j 1 9

flac: ini syy -34.5e6 i 1 140 j 11 27

flac: ini sxx -2.6e6 i 1 140 j 110 150

flac: ini sxx -0.6e6 i 1 140 j 108 110

flac: ini sxx -1.5e6 i 1 140 j 82 108

flac: ini sxx -2e6 i 1 140 j 48 82

flac: ini sxx -2.2e6 i 1 140 j 36 48

flac: ini sxx -8.5e6 i 1 140 j 32 36

flac: ini sxx -15.4e6 i 1 140 j 29 31

flac: ini sxx -15.5e6 i 1 140 j 1 9

flac: ini sxx -17.6e6 i 1 140 j 11 27

flac: ini szz -0.6e6 i 1 140 j 108 110

flac: ini szz -1.5e6 i 1 140 j 82 108

flac: ini szz -2e6 i 1 140 j 48 82

flac: ini szz -2.2e6 i 1 140 j 36 48

flac: ini szz -8.5e6 i 1 140 j 32 36

flac: ini szz -15.4e6 i 1 140 j 29 31

flac: ini szz -15.5e6 i 1 140 j 1 9

flac: ini szz -17.6e6 i 1 140 j 11 27

flac: ; Assigning boundary conditions

flac: fix x i 1 j 11 151

flac: fix x i 141 j 11 151

flac: fix x y i 1 141 j 11

flac: ; apply gravity

flac: set grav=9.81

flac: ; Checking solving equilibrium state - histories

flac: his unbal

flac: his ydis i 1 j 151

flac: his ydis i 70 j 151

flac: his ydis i 141 j 151

flac: solve

flac: ; Excavating material

flac: model null i 54 67 j 1 7

flac: group 'null' i 54 67 j 1 7

flac: group delete 'null'

flac: model null i 74 87 j 1 7

flac: group 'null' i 74 87 j 1 7

flac: group delete 'null'

flac: history 5 ydisp i=61, j=28

flac: history 6 ydisp i=61, j=8

flac: history 7 ydisp i=81, j=28

flac: history 8 ydisp i=81, j=8

flac: history 9 ydisp i=70,j=151

flac: history 10 ydisp i=61, j=151

flac: history 11 ydisp i=30, j=151

flac: history 12 ydisp i=1, j=151

flac: history 13 ydisp i=80, j=151

flac: history 14 ydisp i=109, j=151

flac: history 15 ydisp i=141, j=151

flac: step 140

B.2 Faulted structures

B.2.1 Saturated structures

B.2.1.1 Unglued (i.e. real) fault

flac: !

local> !startstate Model6-fault.sav

flac: config gwflow cppudm

Special FLAC configuration:

groundwater flow

cppudm-s allowed

flac: grid 170,153

flac: gen 0.0,0.0 0.0,191.0 800.0,191.0 800.0,0.0 i 1 73 j 1 9

flac: model elastic i=1,72 j=1,8

flac: gen 800.0,0.0 800.0,191.0 1400.0,191.0 1400.0,0.0 i 74 146 j 1 9

flac: model elastic i=74,145 j=1,8

flac: gen 0.0,191.0 0.0,200.0 800.0,200.0 800.0,191.0 i 147 171 j 1 19

flac: model elastic i=147,170 j=1,18

flac: gen 800.0,191.0 800.0,200.0 1400.0,200.0 1400.0,191.0 i 147 171 j 20 38

flac: model elastic i=147,170 j=20,37

flac: gen 0.0,200.0 0.0,1400.0 600.0,1400.0 800.0,200.0 i 1 73 j 10 154

flac: model elastic i=1,72 j=10,153

flac: gen 800.0,200.0 600.0,1400.0 1400.0,1400.0 1400.0,200.0 i 74 146 j 10 154

flac: model elastic i=74,145 j=10,153

flac: attach aside from 1 9 to 73 9 bside from 147 1 to 171 1

flac: attach aside from 147 19 to 171 19 bside from 1 10 to 73 10

flac: attach aside from 74 9 to 146 9 bside from 147 20 to 171 20

flac: attach aside from 147 38 to 171 38 bside from 74 10 to 146 10

flac: attach aside from 73,9 to 73,1 bside from 74,9 to 74,1

flac: attach aside from 171,19 to 171,1 bside from 147,38 to 147,20

flac: interface 103 aside from 73,154 to 73,10 bside from 74,154 to 74,10

flac: group 'Rock:Lias' notnull i 1 72 j 105 153

flac: model drucker group 'Rock:Lias'

flac: prop density=2600.0 bulk_mod=2.3E9 shear_mod=3.14E9 kshear=0.006e6 qdil=0.0 qvol=0.192 tension=0.98E6 group 'Rock:Lias'

flac: group 'Rock:Lias' notnull i 74 145 j 105 153

flac: model drucker group 'Rock:Lias'

flac: prop density=2600.0 bulk_mod=2.3E9 shear_mod=3.14E9 kshear=0.006e6 qdil=0.0 qvol=0.192 tension=0.98E6 group 'Rock:Lias'

flac: group 'Rock:Rheatic' notnull i 1 72 j 103 105

flac: model drucker group 'Rock:Rheatic'

flac: prop density=2500.0 bulk_mod=1.2E9 shear_mod=1.55e9 kshear=0.024e6 qdil=0.0 qvol=0.2 tension=1.06E6 group 'Rock:Rheatic'

flac: group 'Rock:Rheatic' notnull i 74 145 j 103 105

flac: model drucker group 'Rock:Rheatic'

flac: prop density=2500.0 bulk_mod=1.2E9 shear_mod=1.55e9 kshear=0.024e6 qdil=0.0 qvol=0.2 tension=1.06E6 group 'Rock:Rheatic'

flac: group 'Rock:Mercia mudstone' i 1 72 j 71 103

flac: model mohr group 'Rock:Mercia mudstone'

flac: prop density=2700.0 bulk=3.38E9 shear=3.94E9 cohesion=1500000.0 friction=10.25 dilation=0.0 tension=690000.0 group 'Rock:Mercia mudstone'

flac: group 'Rock:Mercia mudstone' i 74 145 j 71 103

flac: model mohr group 'Rock:Mercia mudstone'

flac: prop density=2700.0 bulk=3.38E9 shear=3.94E9 cohesion=1500000.0 friction=10.25 dilation=0.0 tension=690000.0 group 'Rock:Mercia mudstone'

flac: group 'Rock:Sherwood sandstone' i 1 72 j 31 71

flac: model mohr group 'Rock:Sherwood sandstone'

flac: prop density=2500.0 bulk=2.38E9 shear=3.15E9 cohesion=2750000.0 friction=11.25 dilation=0.0 tension=1300000.0 group 'Rock:Sherwood sandstone'

flac: group 'Rock:Sherwood sandstone' i 74 145 j 31 71

flac: model mohr group 'Rock:Sherwood sandstone'

flac: prop density=2500.0 bulk=2.38E9 shear=3.15E9 cohesion=2750000.0 friction=11.25 dilation=0.0 tension=1300000.0 group 'Rock:Sherwood sandstone'

flac: group 'Rock:Sherwood mudstone' i 1 72 j 16 31

flac: model mohr group 'Rock:Sherwood mudstone'

flac: prop density=2300.0 bulk=2.63E9 shear=3.18E9 cohesion=6500000.0 friction=11.0 dilation=0.0 tension=1720000.0 group 'Rock:Sherwood mudstone'

flac: group 'Rock:Sherwood mudstone' i 74 145 j 16 31

flac: model mohr group 'Rock:Sherwood mudstone'

flac: prop density=2300.0 bulk=2.63E9 shear=3.18E9 cohesion=6500000.0 friction=11.0 dilation=0.0 tension=1720000.0 group 'Rock:Sherwood mudstone'

flac: group 'Rock:Anhydrite' i 1 72 j 11 16

flac: model mohr group 'Rock:Anhydrite'

flac: prop density=2800.0 bulk=3.61E9 shear=2.71E9 cohesion=4250000.0 friction=10.75 dilation=0.0 tension=1520000.0 group 'Rock:Anhydrite'

flac: group 'Rock:Anhydrite' i 74 145 j 11 16

flac: model mohr group 'Rock:Anhydrite'

flac: prop density=2800.0 bulk=3.61E9 shear=2.71E9 cohesion=4250000.0 friction=10.75 dilation=0.0 tension=1520000.0 group 'Rock:Anhydrite'

flac: group 'Rock:Carnalite marl' notnull i 1 72 j 10 11

flac: model ss notnull group 'Rock:Carnalite marl'

flac: m ss i 1 72 j 10 11

flac: prop density=2300.0 bulk=1.56E9 shear=1.17E9 i 1 72 j 10 11

flac: prop cohesion=1.2E6 friction=14 dilation=0.0 tension=0.5e6 i 1 72 j 10 11

flac: prop ctab 1 ftab 2 i 1 72 j 10 11

flac: table 1 0,1.2e6 0,0.4e6

flac: table 2 0,14 0,7.2

flac: group 'Rock:Carnalite marl' notnull i 74 145 j 10 11

flac: model ss notnull group 'Rock:Carnalite marl'

flac: m ss i 74 145 j 10 11

flac: prop density=2300.0 bulk=1.56E9 shear=1.17E9 i 74 145 j 10 11

flac: prop cohesion=1.2E6 friction=14 dilation=0.0 tension=0.5e6 i 74 145 j 10 11

flac: prop ctab 1 ftab 2 i 74 145 j 10 11

flac: table 1 0,1.2e6 0,0.4e6

flac: table 2 0,14 0,7.2

flac: group 'Rock:Potash' notnull i 147 170 j 1 18

flac: model ss notnull group 'Rock:Potash'

flac: m ss i 147 170 j 1 18

flac: prop density=2100.0 bulk=23.94E9 shear=6.82E9 i 147 170 j 1 18

flac: prop cohesion=8.33E6 friction=30 dilation=0.0 tension=1.49e6 i 147 170 j 1 18

flac: prop ctab 1 ftab 2 i 147 170 j 1 18

flac: table 1 0,8.33e6 0,5e6

flac: table 2 0,30 0,27.5

flac: group 'Rock:Potash' notnull i 147 170 j 20 37

flac: model ss notnull group 'Rock:Potash'

flac: m ss i 147 170 j 20 37

flac: prop density=2100.0 bulk=23.94E9 shear=6.82E9 i 147 170 j 20 37

flac: prop cohesion=8.33E6 friction=30 dilation=0.0 tension=1.49e6 i 147 170 j 20 37

flac: prop ctab 1 ftab 2 i 147 170 j 20 37

flac: table 1 0,8.33e6 0,5e6

flac: table 2 0,30 0,27.5

flac: group 'Rock:Halite' notnull i 1 72 j 1 8

flac: model ss notnull group 'Rock:Halite'

flac: m ss i 1 72 j 1 8

flac: prop density=2200.0 bulk=17.93E9 shear=9.25E9 i 1 72 j 1 8

flac: prop cohesion=10E6 friction=40 dilation=0.0 tension=1.63e6 i 1 72 j 1 8

flac: prop ctab 1 ftab 2 i 1 72 j 1 8

flac: table 1 0,10e6 0,9.4e6

flac: table 2 0,40 0,10

flac: group 'Rock:Halite' notnull i 74 145 j 1 8

flac: model ss notnull group 'Rock:Halite'

flac: m ss i 74 145 j 1 8

flac: prop density=2200.0 bulk=17.93E9 shear=9.25E9 i 74 145 j 1 8

flac: prop cohesion=10E6 friction=40 dilation=0.0 tension=1.63e6 i 74 145 j 1 8

flac: prop ctab 1 ftab 2 i 74 145 j 1 8

flac: table 1 0,10e6 0,9.4e6

flac: table 2 0,40 0,10

flac: ; Initial conditions

flac: ini syy -10.3e6 i 1 145 j 105 153

flac: ini syy -10.8e6 i 1 145 j 103 105

flac: ini syy -17.8e6 i 1 145 j 71 103

flac: ini syy -26.0e6 i 1 145 j 31 71

flac: ini syy -28.7e6 i 1 145 j 16 31

flac: ini syy -30.0e6 i 1 145 j 11 16

flac: ini syy -30.2e6 i 1 145 j 10 11

flac: ini syy -30.4e6 i 147 170 j 1 37

flac: ini syy -34.5e6 i 1 145 j 1 8

flac: ini sxx -2.6e6 i 1 145 j 105 153

flac: ini sxx -0.6e6 i 1 145 j 103 105

flac: ini sxx -1.5e6 i 1 145 j 71 103

flac: ini sxx -2e6 i 1 145 j 31 71

flac: ini sxx -2.2e6 i 1 145 j 16 31

flac: ini sxx -8.5e6 i 1 145 j 11 16

flac: ini sxx -15.4e6 i 1 145 j 10 11

flac: ini sxx -15.5e6 i 147 170 j 1 37

flac: ini sxx -17.6e6 i 1 145 j 1 8

flac: ini szz -2.6e6 i 1 145 j 105 153

flac: ini szz -0.6e6 i 1 145 j 103 105

flac: ini szz -1.5e6 i 1 145 j 71 103

flac: ini szz -2e6 i 1 145 j 31 71

flac: ini szz -2.2e6 i 1 145 j 16 31

flac: ini szz -8.5e6 i 1 145 j 11 16

flac: ini szz -15.4e6 i 1 145 j 10 11

flac: ini szz -15.5e6 i 147 170 j 1 37

flac: ini szz -17.6e6 i 1 145 j 1 8

flac: ; Assigning boundary conditions

flac: fix x i 1

flac: fix x i 146

flac: fix x y i 1 146 j 1

flac: ; Undrained analysis

flac: set flow=off

flac: water bulk = 2.2e9

flac: apply pp=9.3e6 i 1 73 j 31 71

flac: apply pp=9.3e6 i 74 146 j 31 71

flac: fix sat i 1 146 j 31 71

flac: ; apply gravity

flac: set grav=9.81

flac: ; Checking solving equilibrium state - histories

flac: his unbal

flac: his ydis i 1 j 154

flac: his ydis i 85 j 154

flac: his ydis i 145 j 154

flac: ; Assiging interface properties - Unbonded interface

flac: interface 103 unglued kn=2.0E10 ks=2.0E9 cohesion=400000.0 dilation=0.0 friction=28.0 tbond=0.0 bslip=Off

flac: interface 103 unglued kn=2.0E10 ks=2.0E9 cohesion=400000.0 dilation=0.0 friction=28.0 tbond=0.0 bslip=Off

flac: solve

flac: model null i 165 j 1 14

flac: group 'null' i 165 j 1 14

flac: group delete 'null'

flac: model null i 166 j 1 14

flac: group 'null' i 166 j 1 14

flac: group delete 'null'

flac: model null i 167 j 1 14

flac: group 'null' i 167 j 1 14

flac: group delete 'null'

flac: model null i 170 j 1 14

flac: group 'null' i 170 j 1 14

flac: group delete 'null'

flac: model null i 147 j 20 33

flac: group 'null' i 147 j 20 33

flac: group delete 'null'

flac: model null i 148 j 20 33

flac: group 'null' i 148 j 20 33

flac: group delete 'null'

flac: history 5 ydisp i=61, j=9

flac: history 6 ydisp i=167, j=15

flac: history 7 ydisp i=73, j=9

flac: history 8 ydisp i=147, j=34

flac: history 9 ydisp i=85, j=154

flac: history 10 ydisp i=77, j=154

flac: history 11 ydisp i=1, j=154

flac: history 12 ydisp i=75, j=154

flac: history 13 ydisp i=92, j=154

flac: history 14 ydisp i=146, j=154

flac: step 140

B.2.1.2 Glued fault

flac: !

flac: config gwflow cppudm

Special FLAC configuration:

groundwater flow

cppudm-s allowed

flac: grid 170,153

flac: gen 0.0,0.0 0.0,191.0 800.0,191.0 800.0,0.0 i 1 73 j 1 9

flac: model elastic i=1,72 j=1,8

flac: gen 800.0,0.0 800.0,191.0 1400.0,191.0 1400.0,0.0 i 74 146 j 1 9

flac: model elastic i=74,145 j=1,8

flac: gen 0.0,191.0 0.0,200.0 800.0,200.0 800.0,191.0 i 147 171 j 1 19

flac: model elastic i=147,170 j=1,18

flac: gen 800.0,191.0 800.0,200.0 1400.0,200.0 1400.0,191.0 i 147 171 j 20 38

flac: model elastic i=147,170 j=20,37

flac: gen 0.0,200.0 0.0,1400.0 600.0,1400.0 800.0,200.0 i 1 73 j 10 154

flac: model elastic i=1,72 j=10,153

flac: gen 800.0,200.0 600.0,1400.0 1400.0,1400.0 1400.0,200.0 i 74 146 j 10 154

flac: model elastic i=74,145 j=10,153

flac: attach aside from 1 9 to 73 9 bside from 147 1 to 171 1

flac: attach aside from 147 19 to 171 19 bside from 1 10 to 73 10

flac: attach aside from 74 9 to 146 9 bside from 147 20 to 171 20

flac: attach aside from 147 38 to 171 38 bside from 74 10 to 146 10

flac: attach aside from 73,9 to 73,1 bside from 74,9 to 74,1

flac: attach aside from 171,19 to 171,1 bside from 147,38 to 147,20

flac: interface 103 aside from 73,154 to 73,10 bside from 74,154 to 74,10

flac: group 'Rock:Lias' notnull i 1 72 j 105 153

flac: model drucker group 'Rock:Lias'

flac: prop density=2600.0 bulk_mod=2.3E9 shear_mod=3.14E9 kshear=0.006e6 qdil=0.0 qvol=0.192 tension=0.98E6 group 'Rock:Lias'

flac: group 'Rock:Lias' notnull i 74 145 j 105 153

flac: model drucker group 'Rock:Lias'

flac: prop density=2600.0 bulk_mod=2.3E9 shear_mod=3.14E9 kshear=0.006e6 qdil=0.0 qvol=0.192 tension=0.98E6 group 'Rock:Lias'

flac: group 'Rock:Rheatic' notnull i 1 72 j 103 105

flac: model drucker group 'Rock:Rheatic'

flac: prop density=2500.0 bulk_mod=1.2E9 shear_mod=1.55e9 kshear=0.024e6 qdil=0.0 qvol=0.2 tension=1.06E6 group 'Rock:Rheatic'

flac: group 'Rock:Rheatic' notnull i 74 145 j 103 105

flac: model drucker group 'Rock:Rheatic'

flac: prop density=2500.0 bulk_mod=1.2E9 shear_mod=1.55e9 kshear=0.024e6 qdil=0.0 qvol=0.2 tension=1.06E6 group 'Rock:Rheatic'

flac: group 'Rock:Mercia mudstone' i 1 72 j 71 103

flac: model mohr group 'Rock:Mercia mudstone'

flac: prop density=2700.0 bulk=3.38E9 shear=3.94E9 cohesion=1500000.0 friction=10.25 dilation=0.0 tension=690000.0 group 'Rock:Mercia mudstone'

flac: group 'Rock:Mercia mudstone' i 74 145 j 71 103

flac: model mohr group 'Rock:Mercia mudstone'

flac: prop density=2700.0 bulk=3.38E9 shear=3.94E9 cohesion=1500000.0 friction=10.25 dilation=0.0 tension=690000.0 group 'Rock:Mercia mudstone'

flac: group 'Rock:Sherwood sandstone' i 1 72 j 31 71

flac: model mohr group 'Rock:Sherwood sandstone'

flac: prop density=2500.0 bulk=2.38E9 shear=3.15E9 cohesion=2750000.0 friction=11.25 dilation=0.0 tension=1300000.0 group 'Rock:Sherwood sandstone'

flac: group 'Rock:Sherwood sandstone' i 74 145 j 31 71

flac: model mohr group 'Rock:Sherwood sandstone'

flac: prop density=2500.0 bulk=2.38E9 shear=3.15E9 cohesion=2750000.0 friction=11.25 dilation=0.0 tension=1300000.0 group 'Rock:Sherwood sandstone'

flac: group 'Rock:Sherwood mudstone' i 1 72 j 16 31

flac: model mohr group 'Rock:Sherwood mudstone'

flac: prop density=2300.0 bulk=2.63E9 shear=3.18E9 cohesion=6500000.0 friction=11.0 dilation=0.0 tension=1720000.0 group 'Rock:Sherwood mudstone'

flac: group 'Rock:Sherwood mudstone' i 74 145 j 16 31

flac: model mohr group 'Rock:Sherwood mudstone'

flac: prop density=2300.0 bulk=2.63E9 shear=3.18E9 cohesion=6500000.0 friction=11.0 dilation=0.0 tension=1720000.0 group 'Rock:Sherwood mudstone'

flac: group 'Rock:Anhydrite' i 1 72 j 11 16

flac: model mohr group 'Rock:Anhydrite'

flac: prop density=2800.0 bulk=3.61E9 shear=2.71E9 cohesion=4250000.0 friction=10.75 dilation=0.0 tension=1520000.0 group 'Rock:Anhydrite'

flac: group 'Rock:Anhydrite' i 74 145 j 11 16

flac: model mohr group 'Rock:Anhydrite'

flac: prop density=2800.0 bulk=3.61E9 shear=2.71E9 cohesion=4250000.0 friction=10.75 dilation=0.0 tension=1520000.0 group 'Rock:Anhydrite'

flac: group 'Rock:Carnalite marl' notnull i 1 72 j 10 11

flac: model ss notnull group 'Rock:Carnalite marl'

flac: m ss i 1 72 j 10 11

flac: prop density=2300.0 bulk=1.56E9 shear=1.17E9 i 1 72 j 10 11

flac: prop cohesion=1.2E6 friction=14 dilation=0.0 tension=0.5e6 i 1 72 j 10 11

flac: prop ctab 1 ftab 2 i 1 72 j 10 11

flac: table 1 0,1.2e6 0,0.4e6

flac: table 2 0,14 0,7.2

flac: group 'Rock:Carnalite marl' notnull i 74 145 j 10 11

flac: model ss notnull group 'Rock:Carnalite marl'

flac: m ss i 74 145 j 10 11

flac: prop density=2300.0 bulk=1.56E9 shear=1.17E9 i 74 145 j 10 11

flac: prop cohesion=1.2E6 friction=14 dilation=0.0 tension=0.5e6 i 74 145 j 10 11

flac: prop ctab 1 ftab 2 i 74 145 j 10 11

flac: table 1 0,1.2e6 0,0.4e6

flac: table 2 0,14 0,7.2

flac: group 'Rock:Potash' notnull i 147 170 j 1 18

flac: model ss notnull group 'Rock:Potash'

flac: m ss i 147 170 j 1 18

flac: prop density=2100.0 bulk=23.94E9 shear=6.82E9 i 147 170 j 1 18

flac: prop cohesion=8.33E6 friction=30 dilation=0.0 tension=1.49e6 i 147 170 j 1 18

flac: prop ctab 1 ftab 2 i 147 170 j 1 18

flac: table 1 0,8.33e6 0,5e6

flac: table 2 0,30 0,27.5

flac: group 'Rock:Potash' notnull i 147 170 j 20 37

flac: model ss notnull group 'Rock:Potash'

flac: m ss i 147 170 j 20 37

flac: prop density=2100.0 bulk=23.94E9 shear=6.82E9 i 147 170 j 20 37

flac: prop cohesion=8.33E6 friction=30 dilation=0.0 tension=1.49e6 i 147 170 j 20 37

flac: prop ctab 1 ftab 2 i 147 170 j 20 37

flac: table 1 0,8.33e6 0,5e6

flac: table 2 0,30 0,27.5

flac: group 'Rock:Halite' notnull i 1 72 j 1 8

flac: model ss notnull group 'Rock:Halite'

flac: m ss i 1 72 j 1 8

flac: prop density=2200.0 bulk=17.93E9 shear=9.25E9 i 1 72 j 1 8

flac: prop cohesion=10E6 friction=40 dilation=0.0 tension=1.63e6 i 1 72 j 1 8

flac: prop ctab 1 ftab 2 i 1 72 j 1 8

flac: table 1 0,10e6 0,9.4e6

flac: table 2 0,40 0,10

flac: group 'Rock:Halite' notnull i 74 145 j 1 8

flac: model ss notnull group 'Rock:Halite'

flac: m ss i 74 145 j 1 8

flac: prop density=2200.0 bulk=17.93E9 shear=9.25E9 i 74 145 j 1 8

flac: prop cohesion=10E6 friction=40 dilation=0.0 tension=1.63e6 i 74 145 j 1 8

flac: prop ctab 1 ftab 2 i 74 145 j 1 8

flac: table 1 0,10e6 0,9.4e6

flac: table 2 0,40 0,10

flac: ; Initial conditions

flac: ini syy -10.3e6 i 1 145 j 105 153

flac: ini syy -10.8e6 i 1 145 j 103 105

flac: ini syy -17.8e6 i 1 145 j 71 103

flac: ini syy -26.0e6 i 1 145 j 31 71

flac: ini syy -28.7e6 i 1 145 j 16 31

flac: ini syy -30.0e6 i 1 145 j 11 16

flac: ini syy -30.2e6 i 1 145 j 10 11

flac: ini syy -30.4e6 i 147 170 j 1 37

flac: ini syy -34.5e6 i 1 145 j 1 8

flac: ini sxx -2.6e6 i 1 145 j 105 153

flac: ini sxx -0.6e6 i 1 145 j 103 105

flac: ini sxx -1.5e6 i 1 145 j 71 103

flac: ini sxx -2e6 i 1 145 j 31 71

flac: ini sxx -2.2e6 i 1 145 j 16 31

flac: ini sxx -8.5e6 i 1 145 j 11 16

flac: ini sxx -15.4e6 i 1 145 j 10 11

flac: ini sxx -15.5e6 i 147 170 j 1 37

flac: ini sxx -17.6e6 i 1 145 j 1 8

flac: ini szz -2.6e6 i 1 145 j 105 153

flac: ini szz -0.6e6 i 1 145 j 103 105

flac: ini szz -1.5e6 i 1 145 j 71 103

flac: ini szz -2e6 i 1 145 j 31 71

flac: ini szz -2.2e6 i 1 145 j 16 31

flac: ini szz -8.5e6 i 1 145 j 11 16

flac: ini szz -15.4e6 i 1 145 j 10 11

flac: ini szz -15.5e6 i 147 170 j 1 37

flac: ini szz -17.6e6 i 1 145 j 1 8

flac: ; Assigning boundary conditions

flac: fix x i 1

flac: fix x i 146

flac: fix x y i 1 146 j 1

flac: ; Undrained analysis

flac: set flow=off

flac: water bulk = 2.2e9

flac: apply pp=9.3e6 i 1 73 j 31 71

flac: apply pp=9.3e6 i 74 146 j 31 71

flac: fix sat i 1 146 j 31 71

flac: ; apply gravity

flac: set grav=9.81

flac: ; Checking solving equilibrium state - histories

flac: his unbal

flac: his ydis i 1 j 154

flac: his ydis i 85 j 154

flac: his ydis i 145 j 154

flac: ; Assiging interface properties - glued interface

flac: interface 103 glued kn=2.0E10 ks=2.0E9

flac: interface 103 glued kn=2.0E10 ks=2.0E9

flac: solve

flac: model null i 165 j 1 14

flac: group 'null' i 165 j 1 14

flac: group delete 'null'

flac: model null i 166 j 1 14

flac: group 'null' i 166 j 1 14

flac: group delete 'null'

flac: model null i 167 j 1 14

flac: group 'null' i 167 j 1 14

flac: group delete 'null'

flac: model null i 170 j 1 14

flac: group 'null' i 170 j 1 14

flac: group delete 'null'

flac: model null i 147 j 20 33

flac: group 'null' i 147 j 20 33

flac: group delete 'null'

flac: model null i 148 j 20 33

flac: group 'null' i 148 j 20 33

flac: group delete 'null'

flac: history 5 ydisp i=61, j=9

flac: history 6 ydisp i=167, j=15

flac: history 7 ydisp i=73, j=9

flac: history 8 ydisp i=147, j=34

flac: history 9 ydisp i=85, j=154

flac: history 10 ydisp i=77, j=154

flac: history 11 ydisp i=1, j=154

flac: history 12 ydisp i=75, j=154

flac: history 13 ydisp i=92, j=154

flac: history 14 ydisp i=146, j=154

flac: step 140

B.2.2 Unsaturated structures

B.2.2.1 Unglued (i.e. real) fault

```
flac: !
flac: config cppudm
 Special FLAC configuration:
   cppudm-s allowed
flac: grid 170,153
flac: gen 0.0,0.0 0.0,191.0 800.0,191.0 800.0,0.0 i 1 73 j 1 9
flac: model elastic i=1,72 j=1,8
flac: gen 800.0,0.0 800.0,191.0 1400.0,191.0 1400.0,0.0 i 74 146 j 1 9
flac: model elastic i=74,145 j=1,8
flac: gen 0.0,191.0 0.0,200.0 800.0,200.0 800.0,191.0 i 147 171 j 1 19
flac: model elastic i=147,170 j=1,18
flac: gen 800.0,191.0 800.0,200.0 1400.0,200.0 1400.0,191.0 i 147 171 j 20 38
flac: model elastic i=147,170 j=20,37
flac: gen 0.0,200.0 0.0,1400.0 600.0,1400.0 800.0,200.0 i 1 73 j 10 154
flac: model elastic i=1,72 j=10,153
flac: gen 800.0,200.0 600.0,1400.0 1400.0,1400.0 1400.0,200.0 i 74 146 j 10 154
flac: model elastic i=74,145 j=10,153
flac: attach aside from 1 9 to 73 9 bside from 147 1 to 171 1
flac: attach aside from 147 19 to 171 19 bside from 1 10 to 73 10
flac: attach aside from 74 9 to 146 9 bside from 147 20 to 171 20
flac: attach aside from 147 38 to 171 38 bside from 74 10 to 146 10
flac: attach aside from 73,9 to 73,1 bside from 74,9 to 74,1
flac: attach aside from 171,19 to 171,1 bside from 147,38 to 147,20
flac: interface 103 aside from 73,154 to 73,10 bside from 74,154 to 74,10
```

flac: group 'Rock:Lias' notnull i 1 72 j 105 153

flac: model drucker group 'Rock:Lias'

flac: prop density=2600.0 bulk_mod=2.3E9 shear_mod=3.14E9 kshear=0.006e6 qdil=0.0 qvol=0.192 tension=0.98E6 group 'Rock:Lias'

flac: group 'Rock:Lias' notnull i 74 145 j 105 153

flac: model drucker group 'Rock:Lias'

flac: prop density=2600.0 bulk_mod=2.3E9 shear_mod=3.14E9 kshear=0.006e6 qdil=0.0 qvol=0.192 tension=0.98E6 group 'Rock:Lias'

flac: group 'Rock:Rheatic' notnull i 1 72 j 103 105

flac: model drucker group 'Rock:Rheatic'

flac: prop density=2500.0 bulk_mod=1.2E9 shear_mod=1.55e9 kshear=0.024e6 qdil=0.0 qvol=0.2 tension=1.06E6 group 'Rock:Rheatic'

flac: group 'Rock:Rheatic' notnull i 74 145 j 103 105

flac: model drucker group 'Rock:Rheatic'

flac: prop density=2500.0 bulk_mod=1.2E9 shear_mod=1.55e9 kshear=0.024e6 qdil=0.0 qvol=0.2 tension=1.06E6 group 'Rock:Rheatic'

flac: group 'Rock:Mercia mudstone' i 1 72 j 71 103

flac: model mohr group 'Rock:Mercia mudstone'

flac: prop density=2700.0 bulk=3.38E9 shear=3.94E9 cohesion=1500000.0 friction=10.25 dilation=0.0 tension=690000.0 group 'Rock:Mercia mudstone'

flac: group 'Rock:Mercia mudstone' i 74 145 j 71 103

flac: model mohr group 'Rock:Mercia mudstone'

flac: prop density=2700.0 bulk=3.38E9 shear=3.94E9 cohesion=1500000.0 friction=10.25 dilation=0.0 tension=690000.0 group 'Rock:Mercia mudstone'

flac: group 'Rock:Sherwood sandstone' i 1 72 j 31 71

flac: model mohr group 'Rock:Sherwood sandstone'

flac: prop density=2500.0 bulk=2.38E9 shear=3.15E9 cohesion=2750000.0 friction=11.25 dilation=0.0 tension=1300000.0 group 'Rock:Sherwood sandstone'

flac: group 'Rock:Sherwood sandstone' i 74 145 j 31 71

flac: model mohr group 'Rock:Sherwood sandstone'

flac: prop density=2500.0 bulk=2.38E9 shear=3.15E9 cohesion=2750000.0 friction=11.25 dilation=0.0 tension=1300000.0 group 'Rock:Sherwood sandstone'

flac: group 'Rock:Sherwood mudstone' i 1 72 j 16 31

flac: model mohr group 'Rock:Sherwood mudstone'

flac: prop density=2300.0 bulk=2.63E9 shear=3.18E9 cohesion=6500000.0 friction=11.0 dilation=0.0 tension=1720000.0 group 'Rock:Sherwood mudstone'

flac: group 'Rock:Sherwood mudstone' i 74 145 j 16 31

flac: model mohr group 'Rock:Sherwood mudstone'

flac: prop density=2300.0 bulk=2.63E9 shear=3.18E9 cohesion=6500000.0 friction=11.0 dilation=0.0 tension=1720000.0 group 'Rock:Sherwood mudstone'

flac: group 'Rock:Anhydrite' i 1 72 j 11 16

flac: model mohr group 'Rock:Anhydrite'

flac: prop density=2800.0 bulk=3.61E9 shear=2.71E9 cohesion=4250000.0 friction=10.75 dilation=0.0 tension=1520000.0 group 'Rock:Anhydrite'

flac: group 'Rock:Anhydrite' i 74 145 j 11 16

flac: model mohr group 'Rock:Anhydrite'

flac: prop density=2800.0 bulk=3.61E9 shear=2.71E9 cohesion=4250000.0 friction=10.75 dilation=0.0 tension=1520000.0 group 'Rock:Anhydrite'

flac: group 'Rock:Carnalite marl' notnull i 1 72 j 10 11

flac: model ss notnull group 'Rock:Carnalite marl'

flac: m ss i 1 72 j 10 11

flac: prop density=2300.0 bulk=1.56E9 shear=1.17E9 i 1 72 j 10 11

flac: prop cohesion=1.2E6 friction=14 dilation=0.0 tension=0.5e6 i 1 72 j 10 11

flac: prop ctab 1 ftab 2 i 1 72 j 10 11

flac: table 1 0,1.2e6 0,0.4e6

flac: table 2 0,14 0,7.2

flac: group 'Rock:Carnalite marl' notnull i 74 145 j 10 11

flac: model ss notnull group 'Rock:Carnalite marl'

flac: m ss i 74 145 j 10 11

flac: prop density=2300.0 bulk=1.56E9 shear=1.17E9 i 74 145 j 10 11

flac: prop cohesion=1.2E6 friction=14 dilation=0.0 tension=0.5e6 i 74 145 j 10 11

flac: prop ctab 1 ftab 2 i 74 145 j 10 11

flac: table 1 0,1.2e6 0,0.4e6

flac: table 2 0,14 0,7.2

flac: group 'Rock:Potash' notnull i 147 170 j 1 18

flac: model ss notnull group 'Rock:Potash'

flac: m ss i 147 170 j 1 18

flac: prop density=2100.0 bulk=23.94E9 shear=6.82E9 i 147 170 j 1 18

flac: prop cohesion=8.33E6 friction=30 dilation=0.0 tension=1.49e6 i 147 170 j 1 18

flac: prop ctab 1 ftab 2 i 147 170 j 1 18

flac: table 1 0,8.33e6 0,5e6

flac: table 2 0,30 0,27.5

flac: group 'Rock:Potash' notnull i 147 170 j 20 37

flac: model ss notnull group 'Rock:Potash'

flac: m ss i 147 170 j 20 37

flac: prop density=2100.0 bulk=23.94E9 shear=6.82E9 i 147 170 j 20 37

flac: prop cohesion=8.33E6 friction=30 dilation=0.0 tension=1.49e6 i 147 170 j 20 37

flac: prop ctab 1 ftab 2 i 147 170 j 20 37

flac: table 1 0,8.33e6 0,5e6

flac: table 2 0,30 0,27.5

flac: group 'Rock:Halite' notnull i 1 72 j 1 8

flac: model ss notnull group 'Rock:Halite'

flac: m ss i 1 72 j 1 8

flac: prop density=2200.0 bulk=17.93E9 shear=9.25E9 i 1 72 j 1 8

flac: prop cohesion=10E6 friction=40 dilation=0.0 tension=1.63e6 i 1 72 j 1 8

flac: prop ctab 1 ftab 2 i 1 72 j 1 8

flac: table 1 0,10e6 0,9.4e6

flac: table 2 0,40 0,10

flac: group 'Rock:Halite' notnull i 74 145 j 1 8

flac: model ss notnull group 'Rock:Halite'

flac: m ss i 74 145 j 1 8

flac: prop density=2200.0 bulk=17.93E9 shear=9.25E9 i 74 145 j 1 8

flac: prop cohesion=10E6 friction=40 dilation=0.0 tension=1.63e6 i 74 145 j 1 8

flac: prop ctab 1 ftab 2 i 74 145 j 1 8

flac: table 1 0,10e6 0,9.4e6

flac: table 2 0,40 0,10

flac: ; Initial conditions

flac: ini syy -10.3e6 i 1 145 j 105 153

flac: ini syy -10.8e6 i 1 145 j 103 105

flac: ini syy -17.8e6 i 1 145 j 71 103

flac: ini syy -26.0e6 i 1 145 j 31 71

flac: ini syy -28.7e6 i 1 145 j 16 31

flac: ini syy -30.0e6 i 1 145 j 11 16

flac: ini syy -30.2e6 i 1 145 j 10 11

flac: ini syy -30.4e6 i 147 170 j 1 37

flac: ini syy -34.5e6 i 1 145 j 1 8

flac: ini sxx -2.6e6 i 1 145 j 105 153

flac: ini sxx -0.6e6 i 1 145 j 103 105

flac: ini sxx -1.5e6 i 1 145 j 71 103

flac: ini sxx -2e6 i 1 145 j 31 71

flac: ini sxx -2.2e6 i 1 145 j 16 31

flac: ini sxx -8.5e6 i 1 145 j 11 16

flac: ini sxx -15.4e6 i 1 145 j 10 11

flac: ini sxx -15.5e6 i 147 170 j 1 37

flac: ini sxx -17.6e6 i 1 145 j 1 8

flac: ini szz -2.6e6 i 1 145 j 105 153

flac: ini szz -0.6e6 i 1 145 j 103 105

flac: ini szz -1.5e6 i 1 145 j 71 103

flac: ini szz -2e6 i 1 145 j 31 71

flac: ini szz -2.2e6 i 1 145 j 16 31

flac: ini szz -8.5e6 i 1 145 j 11 16

flac: ini szz -15.4e6 i 1 145 j 10 11

flac: ini szz -15.5e6 i 147 170 j 1 37

flac: ini szz -17.6e6 i 1 145 j 1 8

flac: ; Assigning boundary conditions

flac: fix x i 1

flac: fix x i 146

flac: fix x y i 1 146 j 1

flac: ; apply gravity

flac: set grav=9.81

flac: ; Checking solving equilibrium state - histories

flac: his unbal

flac: his ydis i 1 j 154

flac: his ydis i 85 j 154

flac: his ydis i 145 j 154

flac: ; Assiging interface properties - unbonded interface

flac: interface 103 unglued kn=2.0E10 ks=2.0E9 cohesion=400000.0 dilation=0.0 friction=28.0 tbond=0.0 bslip=Off

flac: interface 103 unglued kn=2.0E10 ks=2.0E9 cohesion=400000.0 dilation=0.0 friction=28.0 tbond=0.0 bslip=Off

flac: solve

flac: !

local> !auto=off

flac: !

flac: set plot giic

flac: !resetallplots

flac: model null i 165 j 1 14

flac: group 'null' i 165 j 1 14

flac: group delete 'null'

flac: model null i 166 j 1 14

flac: group 'null' i 166 j 1 14

flac: group delete 'null'

flac: model null i 167 j 1 14

flac: group 'null' i 167 j 1 14

flac: group delete 'null'

flac: model null i 170 j 1 14

flac: group 'null' i 170 j 1 14

flac: group delete 'null'

flac: model null i 147 j 20 33

flac: group 'null' i 147 j 20 33

flac: group delete 'null'

flac: model null i 148 j 20 33

flac: group 'null' i 148 j 20 33

flac: group delete 'null'

flac: history 5 ydisp i=61, j=9

flac: history 6 ydisp i=167, j=15

flac: history 7 ydisp i=73, j=9

flac: history 8 ydisp i=147, j=34

flac: history 9 ydisp i=85, j=154

flac: history 10 ydisp i=77, j=154

flac: history 11 ydisp i=1, j=154

flac: history 12 ydisp i=75, j=154

flac: history 13 ydisp i=92, j=154

flac: history 14 ydisp i=146, j=154

flac: step 140

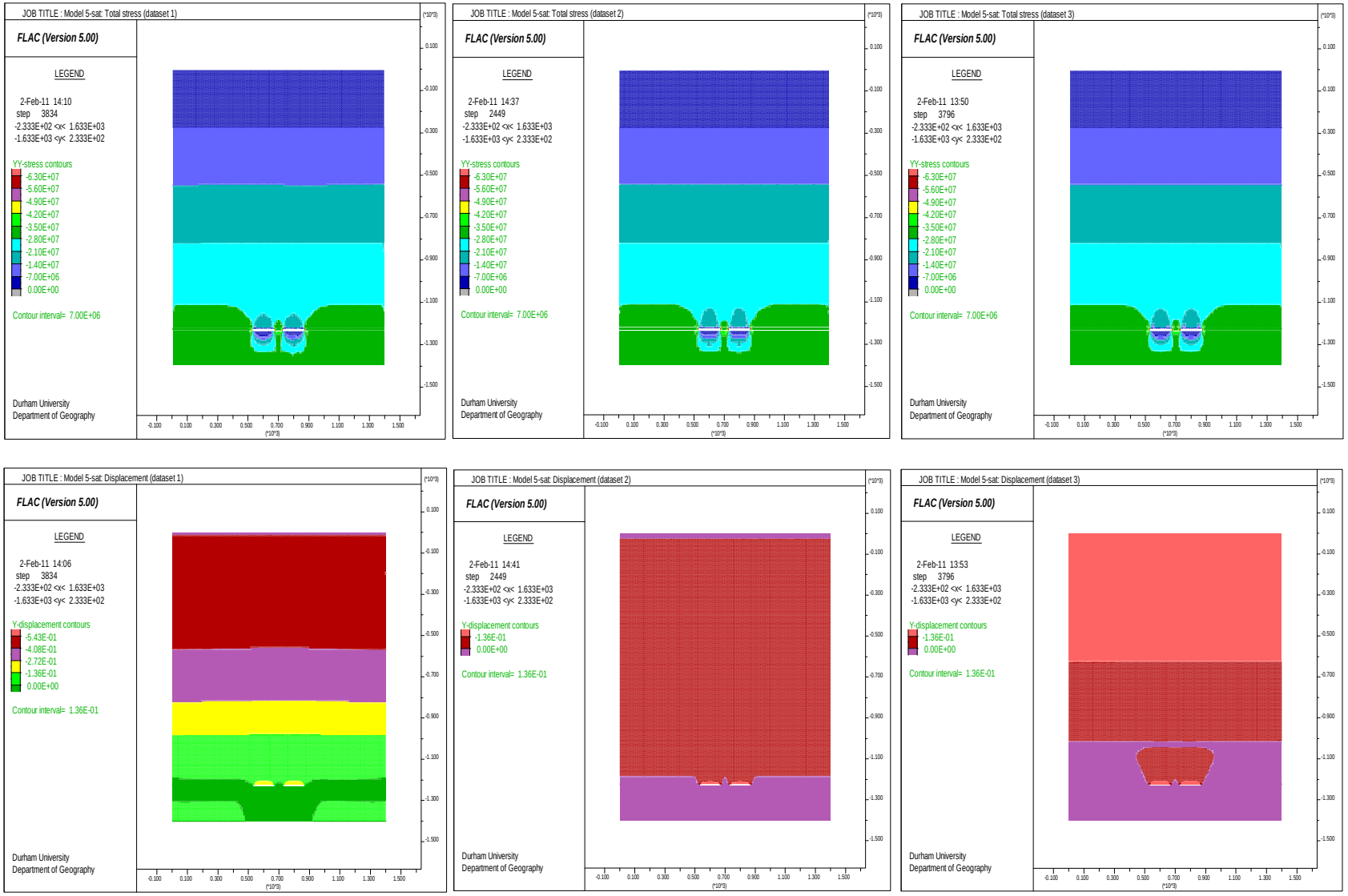

Figure A1.5 Patterns of total stress (top) and vertical displacement (bottom) for sensitivity analysis for model 5 using dataset 1 (left), dataset 2 (middle) and dataset 3 (right)

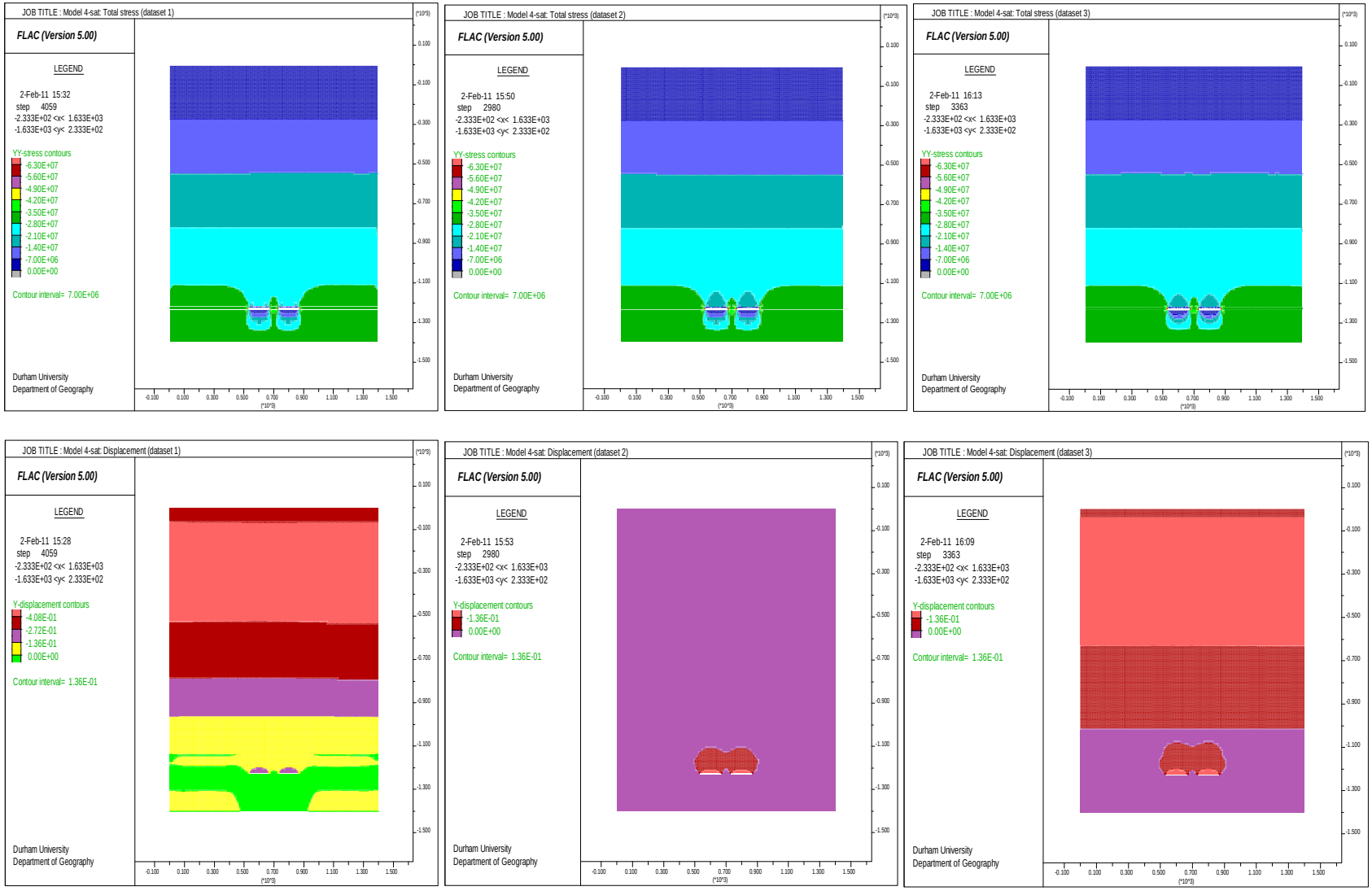

Figure A1.4 Patterns of total stress (top) and vertical displacement (bottom) for sensitivity analysis for model 4 using dataset 1 (left), dataset 2 (middle) and dataset 3 (right)

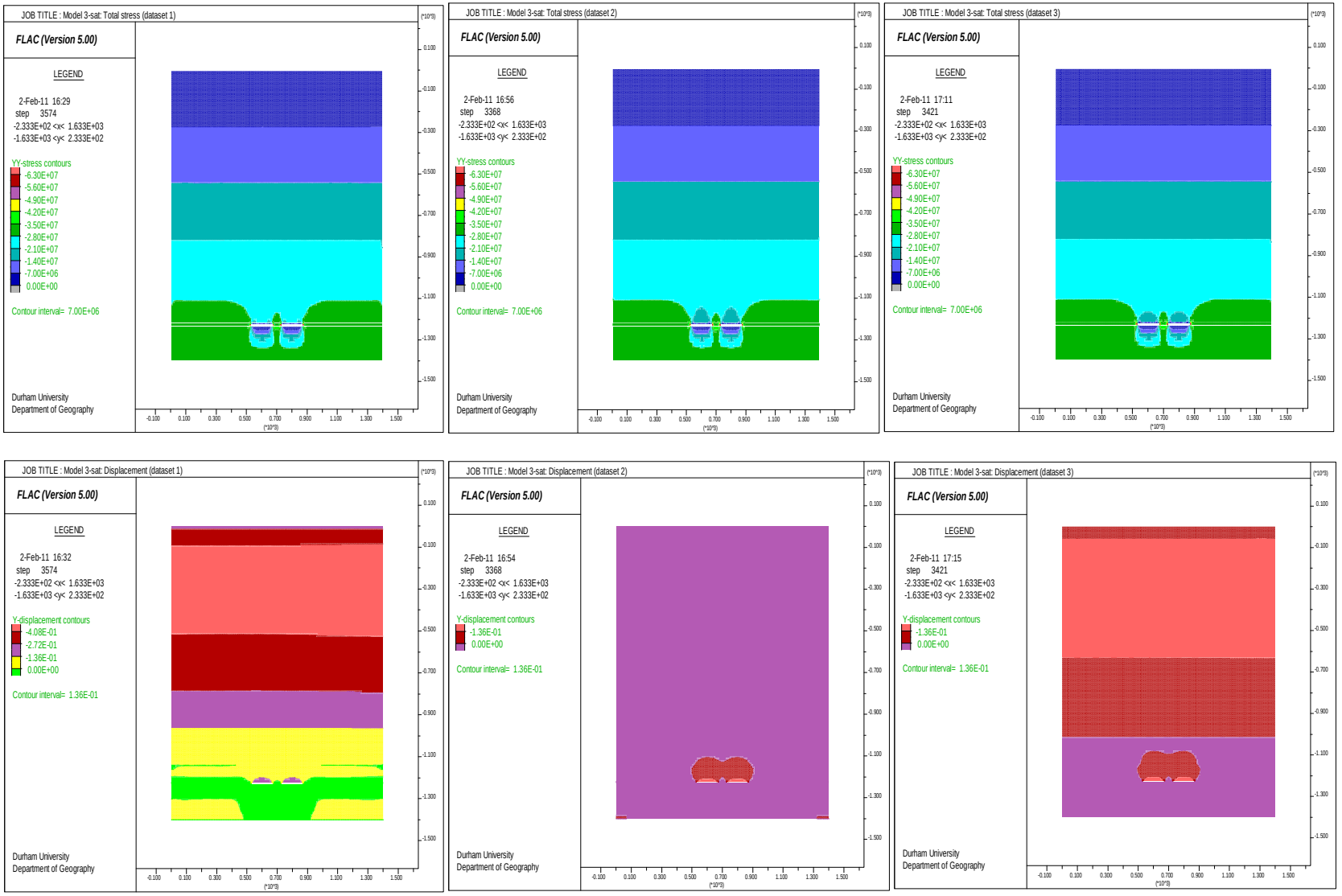

Figure A1.3 Patterns of total stress (top) and vertical displacement (bottom) for sensitivity analysis for model 3 using dataset 1 (left), dataset 2 (middle) and dataset 3 (right)

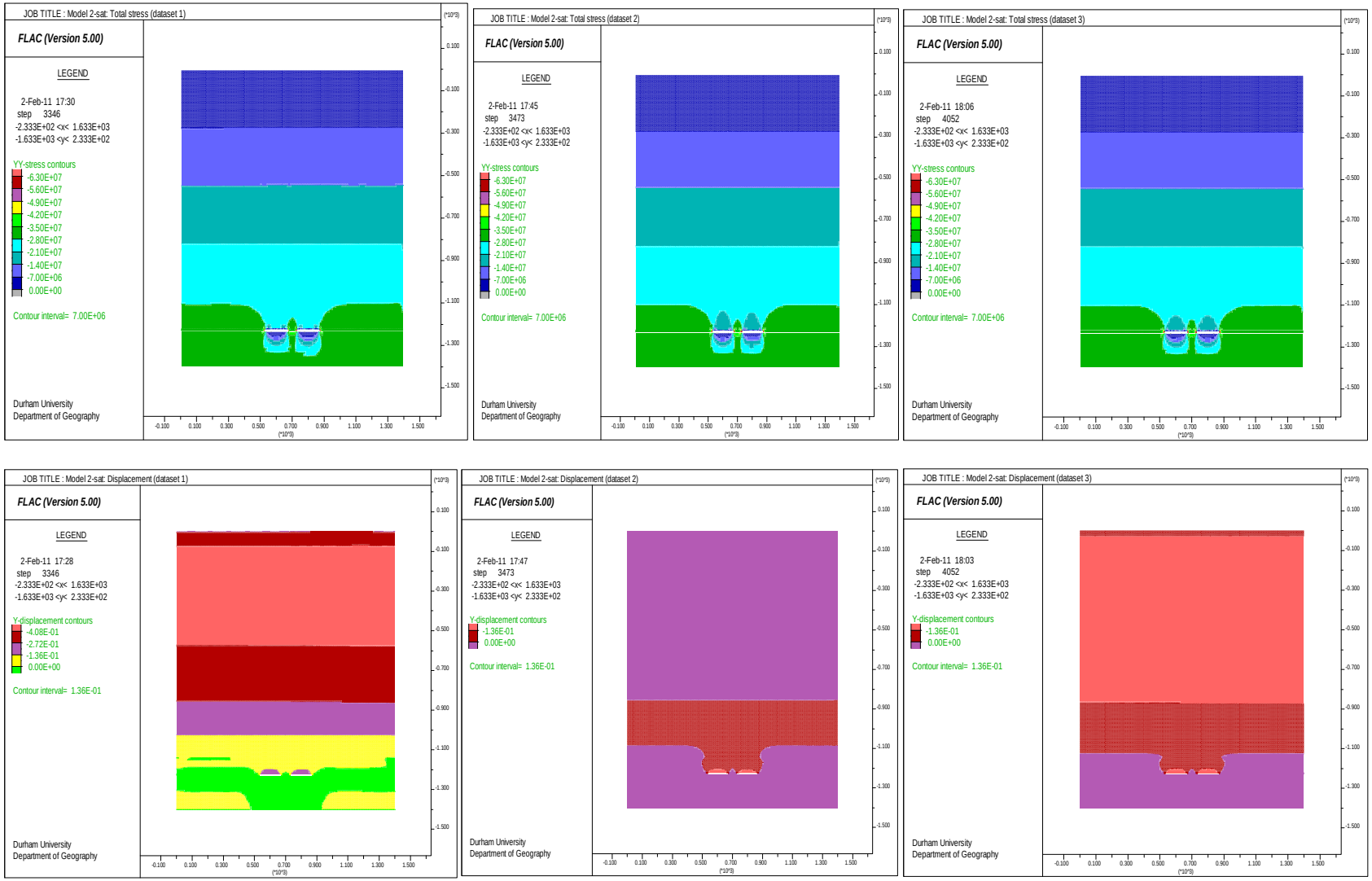

Figure A1.2 Patterns of total stress (top) and vertical displacement (bottom) for sensitivity analysis for model 2 using dataset 1 (left), dataset 2 (middle) and dataset 3 (right)

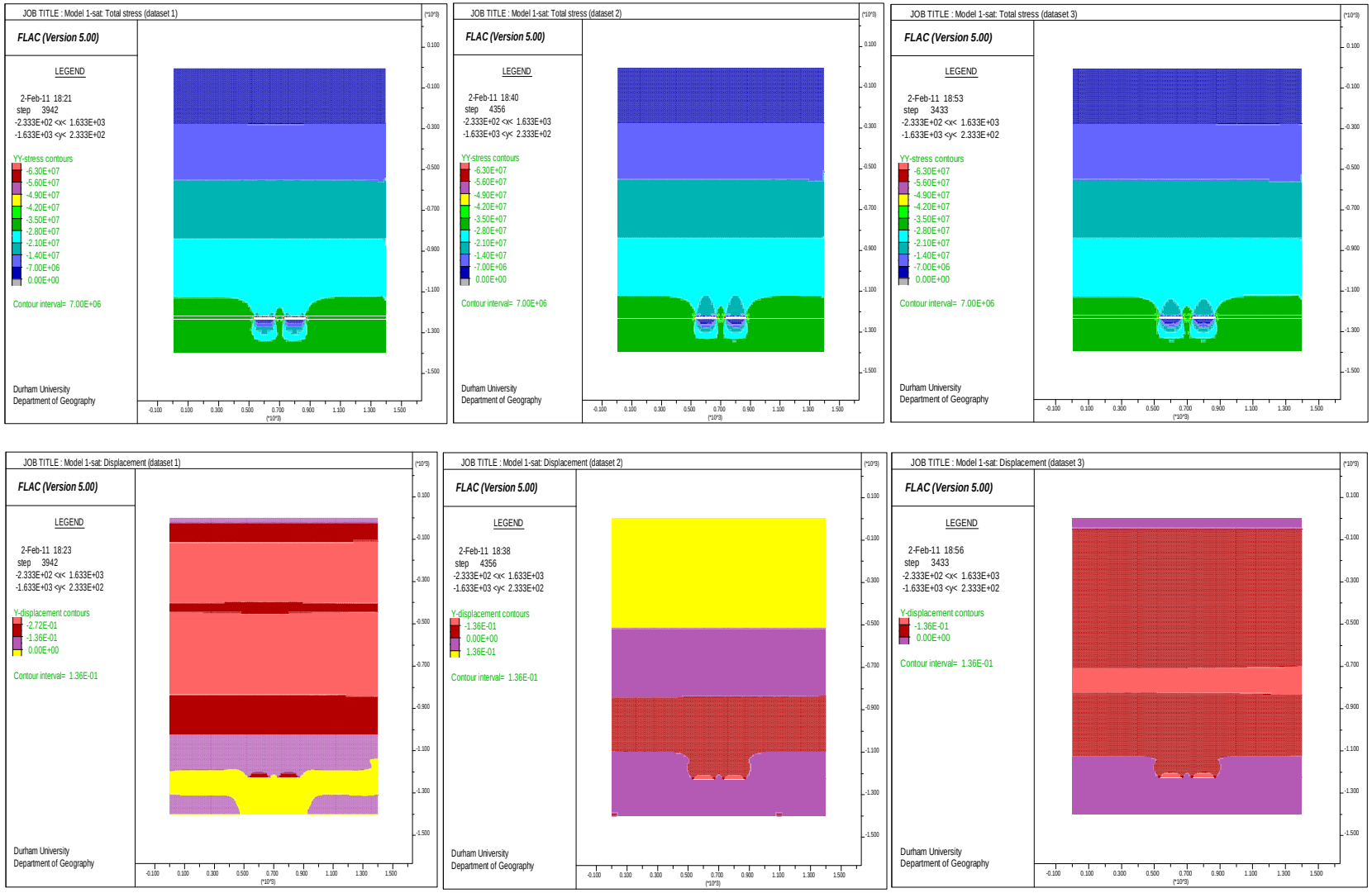

Figure A1.1 Patterns of total stress (top) and vertical displacement (bottom) for sensitivity analysis for model 1 using dataset 1 (left), dataset 2 (middle) and dataset 3 (right)